Ligation properties of N^4-phenylsemicarbazones towards transition metals: Synthesis and spectral studies

Thesis submitted to

Cochin University of Science and Technology

in partial fulfillment of the requirements

for the award of the degree of

Doctor of Philosophy

Under the Faculty of Science

By

ANNIE C.F.

Department of Applied Chemistry

Cochin University of Science and Technology
Kochi 682 022

January 2013

Ligation properties of N^4-phenylsemicarbazones towards transition metals: Synthesis and spectral studies

Ph. D. Thesis under the Faculty of Science

Author:

Annie C.F.
Research Fellow, Department of Applied Chemistry
Cochin University of Science and Technology
Kochi, India 682 022
E mail: anniecusat@yahoo.com

Research Advisor:

Dr. M. R. Prathapachandra Kurup
Professor
Department of Applied Chemistry
Cochin University of Science and Technology
Kochi, India 682 022
Email: mrp@cusat.ac.in

Department of Applied Chemistry,
Cochin University of Science and Technology
Kochi, India 682 022

January 2013

Front cover: Crystal structure of 2-hydroxy-4-methoxyacetophenone-N^4-phenylsemicarbazone monohydrate ($H_2ASC{\cdot}H_2O$)

Back cover: C–H $\cdots$ π interactions present in $H_2ASC{\cdot}H_2O$.

DEPARTMENT OF APPLIED CHEMISTRY
COCHIN UNIVERSITY OF SCIENCE AND TECHNOLOGY
KOCHI 682 022, INDIA

Dr. M.R. Prathapachandra Kurup
Professor

Phone Off. : 0484-2862423
Phone Res. : 0484-2576904
Telex : 885-5019 CUIN
Fax : 0484-2575804
Email : mrp@cusat.ac.in
mrp_k@yahoo.com

Certificate

This is to certify that the thesis entitled **"Ligation properties of N^4-phenylsemicarbazones towards transition metals: Synthesis and spectral studies"** submitted by Ms. Annie C.F., in partial fulfillment of the requirements for the degree of Doctor of Philosophy, to the Cochin University of Science and Technology, Kochi-22, is an authentic record of the original research work carried out by her under my guidance and supervision. The results embodied in this thesis, in full or in part, have not been submitted for the award of any other degree.

M.R. Prathapachandra Kurup
(Supervising guide)

Declaration

I hereby declare that the work presented in this thesis entitled **"Ligation properties of N^4-phenylsemicarbazones towards transition metals: Synthesis and spectral studies"** is entirely original and was carried out independently under the supervision of Prof. M. R. Prathapachandra Kurup, Department of Applied Chemistry, Cochin University of Science and Technology and has not been included in any other thesis submitted previously for the award of any other degree.

Annie C.F.

Kochi-22
02-01-2013

The LORD is the stronghold of my life.

(Psalms 27:1)

To my most beloved

Appan and Amma

Acknowledgement

At this turning point of my research it is my pleasure and privilege to remember each and everyone who helped me during this crucial period of my research work at the department of Applied Chemistry, CUSAT and I am really indebted to all those who have rendered timely help.

First and foremost let me bow my head before my ***Lord, Jesus Christ*** *for being my strength and source of wisdom.*

The person to whom I am most deeply grateful is my supervising guide Prof. M.R. Prathapachandra Kurup, a person with a unique set of personality characteristics, skills, abilities and competencies. His sincerity, simplicity, humble and noble behaviour, patience, dedication and enthusiasm to work, scholarly guidance; above all his positive outlook have been always a source of motivation for me. In hours of distress his words are really consoling. Sir, let me thank you from my innermost heart.

I would like to express my sincere gratitude to Prof. K.K. Mohammed Yusuff, my doctoral committee member, for his timely suggestions and support. I am very much obliged to Prof. K. Sreekumar, Head, Department of Applied chemistry CUSAT and Prof. K. Girish Kumar, Former Head for providing necessary facilities.

I remember with gratitude Prof. S. Sugunan and Dr. S. Prathapan for their valuable suggestions and positive criticism. I am really thankful for the cooperation received from all the Faculty members. At this stage I can not forget the services of the non-teaching staff of this Department.

I deeply acknowledge the heads of the institutions of SAIF Kochi, SAIF, CDRI, Lucknow, IISc Bangalore, IIT Bombay & Sri Ramakrishna Mission Vidyalaya College of Arts and science, Coimbatore for the services offered for my sample analyses. I am thankful to the UGC and the Govt. of Kerala for financial support in the form of Teacher fellowship.

It is a pleasure to remember all my senior researchers at this moment, with special mention to Dr. Seena E.B., Dr. U.L. Kala, Dr. Sheeja S.R., Dr. Reena T.A., Dr. Nancy Mathew, Dr. Neema Ani Mangalam, Dr. Laly K. and Dr. Renjusha S.

I owe much to my lab mates Jayakumar sir, Asokan sir, Roji, Jinsa, Bibitha & Nisha for all that they had been to me, with special regard to Eesan sir who offered much assistance in simulation work. I appreciate and remember with gratitude all research scholars of this department for their timely help.

It is very nice to have a person to share our joys and worries throughout. In its true sense I would like to say a special word of thanks to my colleague and friend, Jessy, my M.Phil and Ph.D mate, for the friendship and suggestions from the very beginning of my research. She is the one who really showed the way to our lab and helped in giving a good start in the new atmosphere.

I fondly remember my junior friends, Reshma, Ambili, Aiswarya, Sreejith, Mridula, Vineetha and Rakhi for creating a cordial environment in the lab and their whole-hearted support during the period.

I remember with gratitude Rev. Sr. Dr. Annie Kuriakose, our Principal, St. Joseph's college, Irinjalakuda for being inspirative, supportive and considerate in times of needs; also I am deeply grateful to my colleagues under the leadership of our dear Ms. Lissy, the Head of the Department, for the support and prayers offered to complete this thesis.

My loving Amma and Ammachi, deserve special mention for their constant prayers and I dedicate this thesis before the fond memories of my most beloved Appan and Appachan showering their blessings upon me from heaven. I express my extreme gratitude to all the loving families of my brothers and sisters and also the families of my in-laws.

My work would not have been completed and my dream not blossomed, unless my family was there with me with their whole hearted support. The love, patience, and adjustments from my husband Wilson, moral support from my loving son Ankith, who has been working in Goa, timely help from my dear daughter Annet…how can I value all these…

Finally I would like to thank everybody who has been, in one way or other, my motivating source and strength for the fulfilment of this thesis.

Annie C. F.

Preface

Hydrazine based compounds played a seminal role in the development of modern coordination chemistry and are considered to be among the most important stereochemical models in transition metal coordination chemistry due to their preparative accessibility and structural variety. Coordination compounds are found at key points in the development of inorganic biochemistry, catalysis and optical materials. They act as biological models for understanding the structures of biomolecules. Semicarbazones and their transition metal complexes are very promising compounds in this field and their crystal structures and spectral investigations are well desirable. This thesis is an attempt to explore the chelating behavior of some ONO donor semicarbazone systems.

The work embodied in this thesis was carried out by the author in the Department of Applied Chemistry during the period 2006-2012. The present work deals with the syntheses, spectral and structural characterization of some N^4-phenylsemicarbazones and their transition metal complexes. The thesis is divided into eight chapters. Chapter 1 deals with a general introduction of Schiff base, ligating modes of semicarbazones, their biological relevance and applications in nonlinear optics and analysis. The objectives of the present work, different analytical and spectroscopic techniques employed for the characterization of semicarbazones and their metal complexes are also included in this chapter. Chapter 2 provides the details regarding the syntheses of two new ONO donor semicarbazones and their characterization by elemental analysis, mass, IR, ^{1}H NMR and UV-Vis spectroscopy and single crystal X-ray diffraction studies. Chapters 3-8 describe the syntheses and characterization of oxovanadium(IV), manganese(II), cobalt(II/III), nickel(II), copper(II) and zinc(II) complexes derived from the semicarbazones under study. A brief summary and conclusion of the work is also included in the last part of the thesis.

Contents

.....ꕥ.....

Chapter 1

SEMICARBAZONES: LIGATING MODES, BIOLOGICAL POTENTIAL AND APPLICATIONS

Contents

1.1. General introduction

Coordination chemistry, the chemistry of metal complexes, is one of the most active areas of research in inorganic chemistry. The study of coordination chemistry originated from the ideas of two notable scientists Alfred Werner and Sophus Mads Jorgenson. The pioneering contribution of Werner to the study of coordination chemistry fetched him the Nobel Prize in Chemistry in 1913 [1]. Werner's basic ideas remain unchallenged even today. However the dawn of sophisticated physicochemical techniques has considerably enriched our understanding of the nature of the metal-ligand bond, the structure and stereochemistry of metal complexes and their stability. Research has come long way from the time of Werner and Jorgenson, and inorganic chemistry witnessed a great outflow of coordination compounds.

Nature makes extensive use of coordination compounds and their study is becoming increasingly important in biology as well as in chemistry. Many of the biologically active compounds are complexes and even the simpler types of complexes have served as model compounds in investigating bodily processes. The living system is partially supported by coordination compounds. Haemoglobin, an iron complex, carries oxygen to animal cells. Myoglobin, chlorophyll and cytochromes are some of the other important complex compounds in living systems. Mixed ligand complexes formed between metal ions and two different types of bioligands, namely Schiff bases and heteroaromatic nitrogen bases may be considered as models for substrate metal ion-enzyme interactions and other metal ion mediated biochemical interactions [2]. Schiff base complexes incorporating phenolic group as chelating moieties in the ligand are considered as models for executing important biological reactions and mimic the catalytic activities of metalloenzymes [3]. Their complexes are used as biological models for understanding the structures of biomolecules. They serve as models to mimic the activity of metalloproteins [4].

1.2. Semicarbazones

Semicarbazones are the condenzation products of semicarbazide with suitable aldehyde or ketone and are generally represented as $R^1R^2C{=}N{-}NH{-}CO{-}NH_2$ (Scheme 1.1)

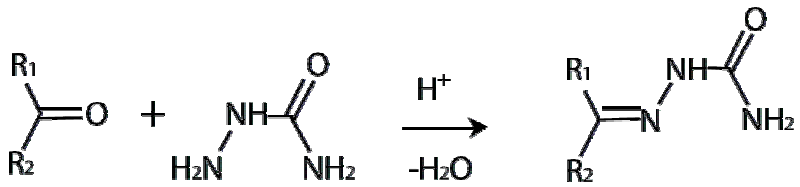

Scheme 1.1. Synthesis of semicarbazone.

According to IUPAC recommendations, semicarbazones may be named by adding the class name 'semicarbazone' after the name of the condensed aldehyde or ketone. It is usual also to include in this class, derivatives with substituents on the amide nitrogen. The numbering scheme shown in the Scheme 1.2 is in accordance with IUPAC system.

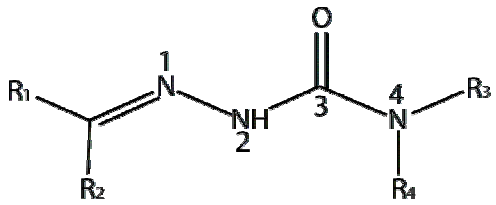

Scheme 1.2. Numbering scheme of the semicarbazone.

A review of *ca*. 70 semicarbazones included in the CSD (Cambridge Structural Database) [5] shows that in free unsubstituted semicarbazones, the C=N–NH–CO–NH_2 backbone is usually almost planar in the solid state, with the oxygen atom *trans* to the azomethine nitrogen atom, though there are exceptions [Scheme 1.3]. This *trans* arrangement places the amine and azomethine nitrogen atoms in relative positions suitable for intramolecular hydrogen bonding [6].

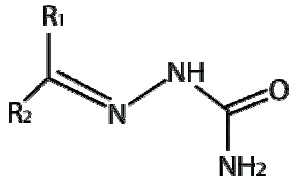

Scheme 1.3. Oxygen atom *trans* to the azomethine N atom.

The active grouping for chelation is shown below in Scheme 1.4.

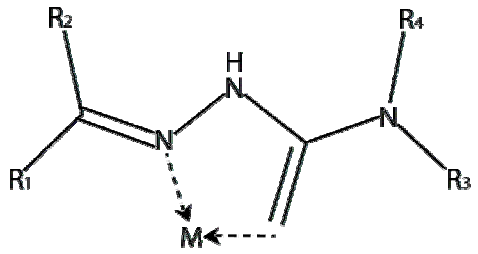

Scheme 1.4. Active grouping for chelation.

Semicarbazones are compounds with versatile structural features and can coordinate to the metal atom either as a neutral ligand or as a deprotonated anion due to their facile amido-iminol tautomerism, giving complexes in which semicarbazones behaves as chelating ligands (Scheme 1.5).

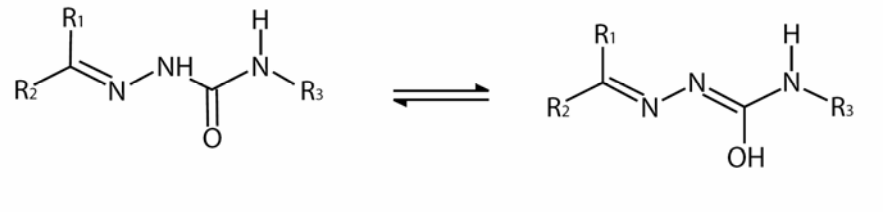

Amido (A) **Iminol (B)**

Scheme 1.5. Amido-iminol tautomerism in semicarbazones.

The amido form itself exists in *Z* and *E* isomers. In the *Z* form, as far as the azomethine bond is concerned the priority groups are on the same side, while in *E* isomer these groups are on the opposite side ($R_2 > R_1$) (Scheme 1.6).

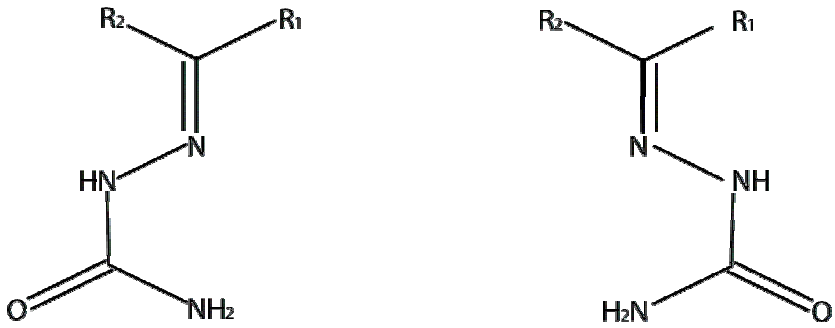

Z isomer *E* isomer

Scheme 1.6. *Z* and *E* isomers in semicarbazones.

1.3. Ligating modes of semicarbazones

Semicarbazones are promising ligands in coordination chemistry because of their excellent metal binding capability. The formation of a variety of metal complexes from these semicarbazones speaks for their spectacular progress in coordination and bioinorganic chemistry. They are among the most relevant nitrogen-oxygen donor ligands [7]. The coordinating ability of semicarbazones is attributed to the extended delocalization of electron density over the –NH–C(O) –NH–N= system, which is enhanced by the substitution at the N^4 position. The coordination possibilities deriving from many potential donor atoms in the semicarbazone backbone are increased if the substituents of the aldehyde or ketone include additional donor atoms. The π-delocalization and the configurational flexibility of their molecular chain can give rise to a great variety of coordination modes [5].

The coordination mode of semicarbazones is very sensitive towards minor variations in the experimental conditions, the nature of substituents on the carbonyl compound and the metal salt. Basuli *et al.* reported three

different coordination modes of the benzaldehyde semicarbazones with ruthenium metal; i) C, N, O-tricoordination ii) N, O-coordination forming a stable five membered chelate iii) an unusual four membered chelate as a N, O donor [8].

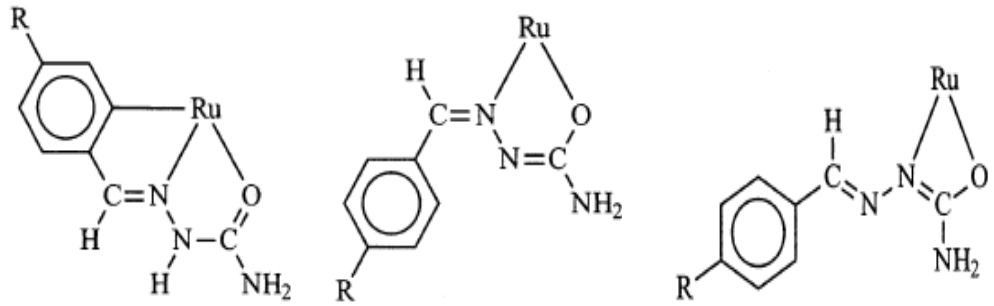

i) C, N, O-tricoordination ii) N, O-coordination iii) an unusual N, O coordination

The expected donor sites in simple semicarbazones are the amide oxygen and azomethine nitrogen. In addition to this, if the carbonyl part contains a ring with a hetero atom that can coordinate to the metal centre thus acting as a tridentate ligand. Due to tautomerism in semicarbazones, they can be either in the amido form or in the iminol form. The nitrogen in the thiazoline ring coordinates to the metal (Structure **I**) in which ligand is in the amido form and acts as a neutral tridentate O, N, N donor [9]. Anions present in the metal salt or ions like azide and thiocyanate can act as a bridging ligand forming a dimeric structure. In structure **II** nitrogen in the pyridine ring coordinates to the metal and the semicarbazone acts as a monoanionic tridentate O, N, N donor with the anion bridging the structure [10].

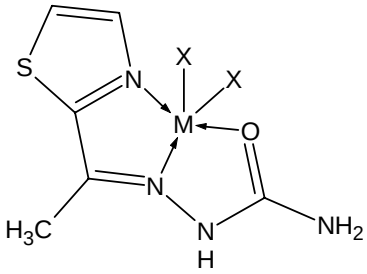

Structure I

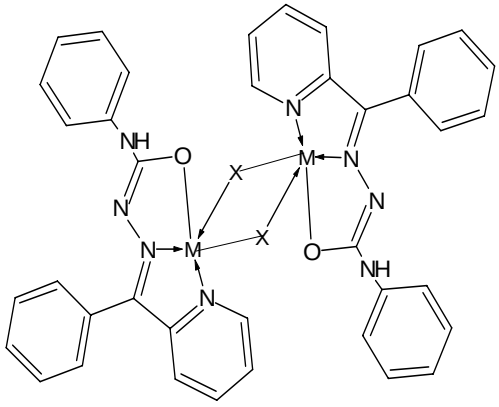

Structure II

If a phenolic –OH is present in the aldehyde/ketone part which is in suitable position for coordination, that can deprotonate and in structure **III** the phenolic –OH of salicylaldehyde deprotonates and the ligand exists in the amido form and acts as a monoanionic tridentate O, N, O donor [11] and in structure **IV** the phenolic and iminol –OH of 2-hydroxyacetophenone semicarbazone deprotonate and it acts as a dianionic tridentate O, N, O donor with the incorporation of heterocyclic base [12].

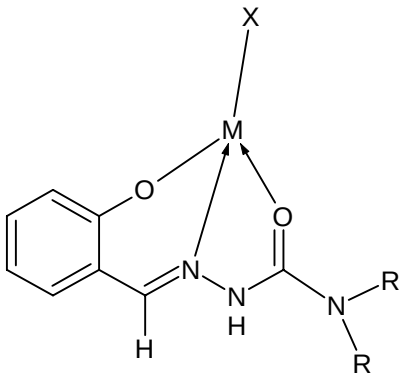

Structure III

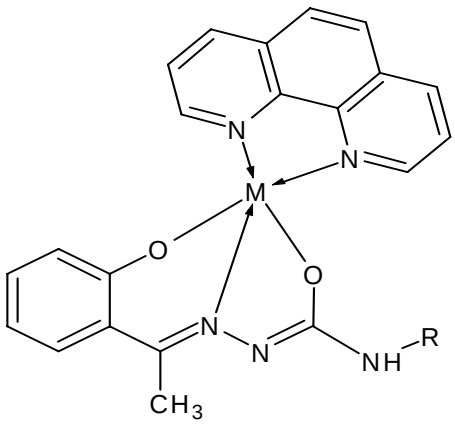

Structure IV

The actual ionization state is dependent upon the condition (pH of the medium) and the metal salts employed. In basic solution the amide oxygen gets deprotonated and coordinates to the metal centre in the enolic form whereas strongly acidic condition favors complexes with a neutral ligand [13,14].

Vidovic *et al*. reported a copper complex in which, phenolic oxygen of pyridoxal semicarbazone acts a bridge and connecting the metal centers to form a dimer (Structure **V**) [15]. In structure **VI**, acetone-N^4-phenylsemicarbazone acts as neutral bidentate N, O donor, forming six coordinated metal complex with anions [16].

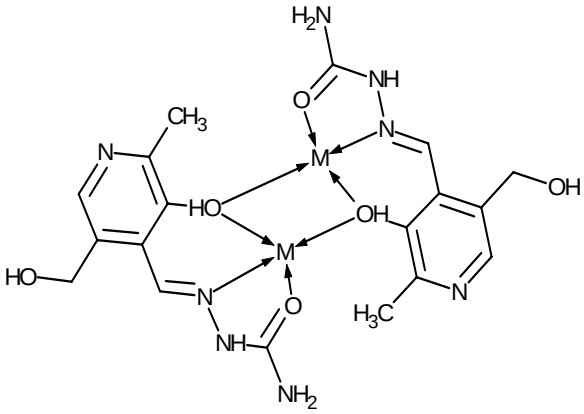

Structure V

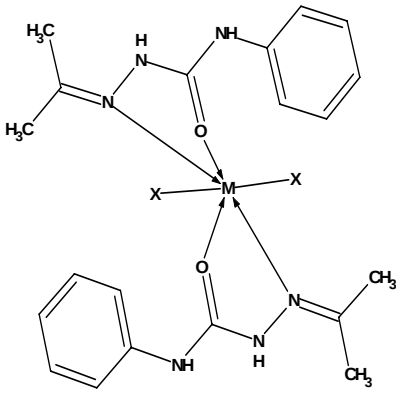

Structure VI

1.4. Biological potential of semicarbazones and their metal complexes

Semicarbazones are well known due to their wide spectrum of biological potential. The literature survey revealed that semicarbazones had been emerged as compounds with broad range of bioactivities including anticonvulsant, antitubercular, anticancer and even anti-HIV. The great advantage of semicarbazone derivatives over their thiosemicarbazone analogues is their

lower toxicity. Curcumin semicarbazone was synthesized by Dutta *et al*. and was examined for its antioxidant, antiproliferative and antiradical activity and compared with those of curcumin. It is found that curcumin semicarbazone is more active than curcumin with respect to its antioxidant and antiproliferative activity [17]. Vanillin semicarbazone is a potent anticancer agent [18]. Naphthaquinone semicarbazone is more active in the inhibition of cell proliferation than naphthaquinone thiosemicarbazone [19].

Epilepsy is a common disorder of the central nervous system. The conventional antiepileptic drugs are not ideal as they can be associated with chronic and adverse side effects. So the search for new anticonvulsant drugs continues to be an active area of investigation in medicinal chemistry. Aryl semicarbazones have recently acquired an important place as anticonvulsants [20]. A variety of 5-nitrofuryl semicarbazones and 5-nitrothiophenesemicarbazones were evaluated *in vivo* for their antitrypanosomal activity [21]. Ahsan *et al.* reported that the thioureido derivatives of 4-aminoacetophenone aryl semicarbazone showed maximum protection against HIV [22]. Domagk *et al*. reported for the first time the anti-tubercular activities of metal thiosemicarbazones and semicarbazones [23].

The interaction of simple vanadium species with ligand groups bearing pharmacological activity, particularly those with antitumoral, antimicrobial and insulin-mimetic properties, is of growing interest [24]. It has been demonstrated that the insulin effects of promoting glucose uptake and inhibiting lipolysis can be duplicated by vanadium. Insulin is a protein which is not orally active. But vanadium complexes can be orally administered, potentially eliminating or reducing the need for daily insulin injections [25]. Bastos *et al*. have reported the insulin -like activity of oxovanadium(IV) and

(V) complexes of acetylpyridine derived semicarbazones [26]. A series of copper(II) and zinc(II) complexes of 2-hydroxyacetophenone semicarbazone have been prepared and evaluated as superoxide dismutase (SOD) mimetics and the obtained results indicate that Cu(II) complexes exhibited the most potent SOD like activities [27].

1.5. Semicarbazones in nonlinear optics

Research in the field of organic NLO materials has gained momentum in the recent past on account of the interesting applications in photonic and electro optic devices. The large nonlinear optical effect found in some organic crystals make the materials attractive for applications in frequency conversion [28]. The organic molecular materials have emerged as a new class of promising nonlinear optical materials because of their superior qualities over inorganic systems. Among the nonlinear phenomena, frequency doubling, frequency mixing and electro-optic modulation are important in the fields of optical image storage and optical communications [29]. Organic nonlinear optical materials are often formed by weak van der Waals and hydrogen bonds and hence possess high degree of delocalization. An organic molecule should have high second order hyperpolarizability (β) to exhibit large NLO properties. The hyperpolarizability can be enhanced by increasing intramolecular charge transfer interaction by extending the π-conjugated system [30]. Basically, semicarbazone family crystals exhibit nonlinear optical behavior. Single crystals of semicarbazones of acetophenone, benzophenone, *p*-anisaldehyde and 4-hydroxy 3-methoxyacetophenone are potential organic NLO materials and they had a wide transparency window in the entire visible region, making them ideal candidates for NLO device applications [31-34].

1.6. Semicarbazones in analysis

Semicarbazones have applications in analytical field also. Some of the semicarbazones produce highly colored complexes with metal ions. These complexes have been proposed as analytical reagents that can be used in selective and sensitive determination of metal ions [35]. Semicarbazones are widely used as spectrophotometric agents for the analysis of metal ions. Janwadkar *et al*. reported spectrophotometric methods for the determination of Mo(VI) and Fe(III) ions using 2,5-dihydroxyacetophenone semicarbazone as an extractive reagent [36,37]. Salicylaldehyde semicarbazone and 2,4-dihydroxybenzaldehyde semicarbazone have been used for the spectrofluorimetric determination of a number of metal ions. Semicarbazones can be readily hydrolysed to give the original carbonyl compound and hence are often useful for identification and isolation of carbonyl compounds. They are also used as protected carbonyl compounds in synthesis [38].

1.7. Scope and objectives of the present work

Semicarbazones and their transition metal complexes have been receiving considerable attention because of their biological relevance and applications in the field of analysis and in the field of organic NLO materials. Their structural diversity also attracted inorganic chemists. A good deal of work has been reported on the synthesis and structural investigation of semicarbazones and their complexes. This is due partially to their capability of acting as multidentate, NO, NNO, ONO and ONNO donors with the formation of either mono or bi or polynuclear complexes. Their chemistry and pharmacological applications have been extensively investigated.

Appreciable biological applications as well as diverse stereochemistry of their metal complexes prompted us to synthesize two new tridentate ONO donor N^4-phenyl semicarbazones derived from 2-hydroxy-4-methoxyacetophenone and 2-hydroxy-4-methoxybenzophenone and their transition metal complexes. These ketones were selected since they can provide a further binding site from phenolic –OH and can thus increase the denticity. Introduction of heterocyclic bases like 1,10-phenanthroline, 2,2′-bipyridine, 4,4′-dimethyl- 2,2′-bipyridine and 4-picoline and some pseudohalides like azide and thiocyanate ion can result in mixed ligand metal chelates with different geometries in coordination compounds.

The objectives of our present work includes

- To synthesize ONO donor semicarbazones by the condenzation of 2-hydroxy-4-methoxyacetophenone and 2-hydroxy-4-methoxybenzophenone with N^4-phenylsemicarbazide.
- To characterize the synthesized N^4-phenylsemicarbazones by different physicochemical techniques.
- To synthesize some transition metal complexes using these semicarbazones and some mixed ligand metal chelates by incorporating heterocyclic bases and some pseudohalides as coligands.
- To characterize the metal complexes by elemental analyses, thermogravimetry and different spectroscopic techniques like IR, UV-Vis, NMR and EPR spectroscopy.
- To study the magnetic properties of the complexes prepared.

- To investigate the electrochemical behavior of the complexes by cyclic voltammetry.
- To establish the structure of the compounds by single crystal X-ray diffraction.

In the present study, oxovanadium(IV), manganese(II), cobalt (II/III), nickel(II), copper(II) and zinc(II) complexes of 2-hydroxy-4-methoxyacetophenone-N^4-phenylsemicarbazone (H_2ASC) and 2-hydroxy-4-methoxybenzophenone-N^4-phenylsemicarbazone (H_2BSC) were synthesized and characterized.

1.8. Characterization techniques

The physicochemical methods adopted for characterizing the synthesized compounds are discussed below.

1.8.1. Elemental analyses

Microanalysis for carbon, hydrogen and nitrogen in the synthesized N^4-phenylsemicarbazones and their metal complexes and sulfur in complexes **19** and **25** were carried out using Vario EL III CHNS analyzer at the Sophisticated Analytical Instrument Facility (SAIF), Kochi, India and also at SAIF, CDRI, Lucknow.

1.8.2. Conductivity measurements

The molar conductivities of the complexes in DMF (10^{-3} M) solutions were measured at 298 K with a Systronic model 303 direct-reading conductivity bridge at the Department of Applied Chemistry, CUSAT, Kochi, India.

1.8.3. Magnetic susceptibility measurements

The magnetic susceptibility measurements of the complexes were carried out on powdered samples at 298 K using a Sherwood Scientific Magnetic Susceptibility Balance (M.S.B) MK1 using $HgCo(SCN)_4$ as calibrant at the Department of Applied Chemistry, CUSAT, Kochi, India and the diamagnetic contribution to the susceptibility was estimated through Pascal's constants.

1.8.4. Mass spectroscopy

Mass spectra of the semicarbazones 2-hydroxy-4-methoxyacetophenone-N^4-phenylsemicarbazone monohydrate ($H_2ASC{\cdot}H_2O$) and 2-hydroxy-4-methoxybenzophenone-N^4-phenylsemicarbazone (H_2BSC) were recorded on a WATERS 3100 Mass Detector, designed for routine UPLC/MS analyses at the Department of Applied Chemistry, CUSAT, Kochi, India.

1.8.5. Infrared spectroscopy

The IR spectra were recorded on a JASCO FT/IR-4100 Fourier Transform Infrared spectrometer using KBr pellets in the range 4000-400 cm^{-1} at the Department of Applied Chemistry, CUSAT, Kochi, India and also on a Thermo Nicolet AVATAR 370 DTGS model FT-IR Spectrophotometer with KBr pellets and ATR technique at the SAIF, Kochi, India.

1.8.6. Electronic spectroscopy

Electronic spectra were recorded in acetonitrile/DMF solutions on a Spectro UV-Vis Double Beam UVD-3500 spectrometer in the 200-900 nm range at the Department of Applied Chemistry, CUSAT, Kochi, India.

1.8.7. NMR spectroscopy

^{1}H NMR spectrum of the synthesized 2-hydroxy-4-methoxyacetophenone-N^4-phenylsemicarbazone monohydrate ($H_2ASC{\cdot}H_2O$) was recorded in $CDCl_3$ and 2-hydroxy-4-methoxybenzophenone-N^4-phenylsemicarbazone (H_2BSC) was recorded in DMSO-d_6 as solvent on a Bruker AMX 400 Spectrometer with TMS as standard at the Sophisticated Instruments Facility, Indian Institute of Science, Bangalore, India.

1.8.8. EPR spectroscopy

The EPR spectra of the complexes, both in the polycrystalline state at 298 K and in DMF at 77 K, were recorded on a Varian E-112 X-band EPR spectrometer using TCNE as the standard (g=2.00277), with 100 kHz modulation frequency, modulation amplitude 2 G and microwave frequency 9.4 GHz at the SAIF, IIT Bombay, India.

1.8.9. Cyclic voltammetry

Cyclic voltammograms were recorded on a CHI 608 D electrochemical analyzer at Sri Ramakrishna Mission Vidyalaya College of Arts and Science, Coimbatore, India with a three electrode compartment consisting of platinum disc working electrode, platinum wire counter electrode and Ag/Ag^+ reference electrode. Tetraethylammonium phosphate was the supporting electrolyte. The voltammogram is run between the potentials of +2 and -2 V at a scan speed of 100 mV/s.

1.8.10. Thermogravimetric analyses

TG-DTA-DTG analyses of the complexes were carried out under nitrogen at a heating rate of 10 °C min^{-1} in the range 50-1000 °C using a

Perkin Elmer Pyris Diamond TG/DTA analyzer at the Department of Applied Chemistry, CUSAT, Kochi, India.

1.8.11. X-ray crystallography

Single crystal X-ray crystallographic measurements of 2-hydroxy-4-methoxyacetophenone-N^4-phenylsemicarbazone monohydrate ($H_2ASC{\cdot}H_2O$) and 2-hydroxy-4-methoxybenzophenone-N^4-phenylsemicarbazone (H_2BSC) were carried out by mounting on a Bruker SMART APEX diffractometer, equipped with a graphite crystal, incident-beam monochromator, and a fine focus sealed tube with Mo Kα (λ=0.71073 Å) as the X-ray source. The unit cell dimensions were measured and the data collections were performed at 296(2) K. Bruker SMART software was used for data acquisition and Bruker SAINT software for data integration [39]. Absorption corrections were carried out using SADABS based on Laue symmetry using equivalent reflections [40]. The structure was solved by direct methods and refined by full matrix least-squares calculations with the SHELXL-97 software package [41]. The graphics tools used were ORTEP-3 [42] and DIAMOND version 3.2g [43]. All non-hydrogen atoms were refined anisotropically. All the H atoms on carbon of this compound were placed in these calculated positions, guided by difference Fourier maps and refined isotropically.

References

[1] J.E. Huheey, E.A. Keiter, R.L. Keiter, Inorganic Chemistry, Principles of Structure and Reactivity, 4th ed., Harper Collins College Publishers, New York, 1993.

[2] R.N. Patel, Indian J. Chem. 48A (2009) 173.

[3] A.A. Khandar, S.A. Hosseini-Yazdi, S.A. Zarei, U.M. Rabie Inorg. Chim. Acta 358 (2005) 3211.

[4] D.M. Boghaei, S. Motebi, Tetrahedron 58 (2002) 5357.

[5] J.S. Casas, M.S. Garcia-Tasende, J. Sordo, Coord. Chem. Rev. 209 (2000) 197.

[6] D. Chattopadhyay, S.K. Mazumdar, T. Banerjee, W.S. Sheldrick, Acta Crystallogr. Sect. C 45 (1989) 814.

[7] B.A. Gingrass, R.W. Hornal, C.H. Baylay, Can. J. Chem. 38 (1960) 712.

[8] F. Basuli, S.M. Peng, S. Bhattacharya, Inorg. Chem. 36 (1997) 5645.

[9] F.J. Barros-Garcia, F. Luna-Giles, M.A. Maldonado-Rogado, E. Vinuelas-Zahinos, Polyhedron 24 (2005) 2972.

[10] M.R.P. Kurup, B. Varghese, M. Sithambaresan, S. Krishnan, S.R. Sheeja, E. Suresh, Polyhedron 30 (2011) 70.

[11] P.F. Lee, C.-T. Yang, D. Fan, J.J. Vittal, J.D. Ranford, Polyhedron 22 (2003) 2781.

[12] U.L. Kala, S. Suma, M.R.P. Kurup, S. Krishnan, R.P. John, Polyhedron 26 (2007) 1427.

[13] M.F. Iskander, T.E. Khalil, R. Werner, W. Haase, I. Svoboda, H. Fuess, Polyhedron 19 (2000) 949.

[14] B. Samanta, J. Chakraborty, S. Shit, S.R. Batten, P. Jensen, J.D. Masuda, S. Mitra, Inorg. Chim. Acta 360 (2007) 2471.

[15] D. Vidovic, A. Radulovic, V. Jevtovic, Polyhedron 30 (2011) 16.

[16] V.L. Siji, M.R. Sudarsanakumar, S. Suma, Polyhedron 29 (2010) 2035.

[17] S. Dutta, S. Padhye, K. Indira Priyadarsini, C. Newton, Bioorg. Med. Chem. Lett. 15 (2005) 2738

[18] S.M.M. Ali, M.A.K. Azad, M. Jesmin, S. Ahsan, M.M. Rahman, J.A. Khanam, M.N. Islam, S.M.S. Shahriar, Asian Pacific Journal of Tropical Biomedicine (2012) 438

[19] Z. Afrasiabi, E. Sinn, W. Lin, Y. Ma, C. Campana, S. Padhye, J. Inorg. Biochem. 99 (2005) 1526.

[20] J.R. Dimmock, R.N. Puthucode, J. Tuchek, G.B. Baker, C.N. Hinko, C.L. Steinmiller, J.P. Stables, Drug Dev. Res. 46 (1999) 112.

[21] H. Cerecetto, R.D. Maio, M. Gonzalez, M. Risso, G. Sagrera, G. Seoane, A. Denicola, G. Peluffo, C. Quijano, A.O.M. Stoppani, M. Paulino, C. Olea- Azar, M.A. Basombrio, Eur. J. Med. Chem. 35 (2000) 343.

[22] M.J. Ahsan, J.G. Samy, H. Khalilullah, Md.S. Nomani, Der Pharmacia Sinica 2 (6) (2011) 107.

[23] G. Domagk, R. Behnisch, F. Meitzsch, H. Schmidt, Naturwissenschaften 33 (1946) 315.

[24] P. Noblia, M. Vieites, B.S. Parajon-Costa, E.J. Baran, H. Cerecetto, P. Draper, M. Gonzalez, O.E. Piro, E.E. Castellano, A. Azqueta, A.L. Cerain, A. Monge-Vega, D. Gambino, J. Inorg. Biochem. 99 (2005) 443.

[25] K.H. Thompson, C. Orvig, J. Inorg. Biochem. 100 (2006) 1925.

[26] A.M.B. Bastos, J.G. da Silva, P.I. da S. Maia, V.M. Deflon, A.A. Batista, A.V.M. Ferreira, L.M. Botion, E. Niquet, H. Beraldo, Polyhedron 27 (2008) 1787.

[27] M. Safavi, A. Foroumadi, M. Nakhjiri, M. Abdollahi, A. Shafiee, H. Ilkhani, M.R Ganjali, S.J. Hosseinimehr, S. Emami, Bioorg. Med. Chem. Lett. 20 (2010) 3070.

[28] C. Maloney, W. Blau, J. Opt. Soc. Am. B 14 (1987) 1035.

[29] L. Zhengedong, W. Baichange, S. Genbo, J. Cryst. Growth 178 (1997) 539.

[30] R.A. Kuijts, G.L.J. Hesselink, Chem. Phys. Lett. 156 (1989) 209.

[31] N. Vijayan, R. Ramesh Babu, R. Gopalakrishnan, S. Dhanuskodi, P. Ramasamy, J. Cryst. Growth 233 (2001) 863.

[32] N. Vijayan, R. Ramesh Babu, R. Gopalakrishnan, S. Dhanuskodi, P. Ramasamy, J. Cryst. Growth 236 (2002) 407.

[33] S. Janarthanan, Y.C. Rajan, P.R. Umarani, D. Jayaraman, D. Premanand, S. Pandi, Indian Journal of Science and Technology, 3 (2010) 885.

[34] S. Janarthanan, Y.C. Rajan, P.R. Umarani, S. Selvakumar, S. Pandi, Physica B 406 (2011) 135.

[35] T. Atalay, E.G. Akgemci, Tr. J. Chem. 22 (1998) 123.

[36] R.S. Lokhande, S.P. Janwadkar, S. Pitale, S. Kulkarni, S. Patil, Int. J. Chem. Tech. Res. 3 (2011) 1765.

[37] R.S. Lokhande, S.P. Janwadkar, S. Pitale, S. Kulkarni, S. Patil, IJPWR. 2 (2011).

[38] R.B. Singh, B.S. Garg, R.P. Singh, Talanta 25 (1978) 619.

[39] SMART and SAINT, Area Detector Software Package and SAX Area Detector Integration Program, Bruker Analytical X-ray; Madison, WI, USA, 1997.

[40] SADABS, Area Detector Absorption Correction Program; Bruker Analytical X-ray; Madison, WI, 1997.

[41] G.M. Sheldrick, SHELXTL-PLUS, Crystal Structure Analysis Package; Bruker Analytical X-ray, Madison, WI, USA, 1997.

[42] L.J. Farrugia, J. Appl. Cryst. 30 (1997) 565.

[43] K. Brandenburg, Diamond Version 3.2g, Crystal Impact GbR, Bonn, Germany, 2010.

.....ꕥ.....

Chapter 2

SYNTHESES, SPECTRAL STUDIES AND CRYSTAL STRUCTURES OF N^4-PHENYLSEMICARBAZONES

Contents

2.1. Introduction

Semicarbazones are very promising ligands in coordination chemistry and are among the most relevant nitrogen-oxygen donor ligands. A good deal of work has been reported on the syntheses and structural investigation of semicarbazones and their complexes [1,2]. This is due partially to their capability of acting as NO, ONO, NNO and ONNO donors with the formation of either mono or bi or polynuclear complexes [3,4].

Semicarbazones as well as their derivative analogues with potential biological activity are the focus of extensive investigation. Specifically the semicarbazones have been screened for their antifungal, antibacterial and anticonvulsant activities [5-8]. Some studies on anticonvulsant activity of semicarbazones validate the hypothesis that presence of an aryl group near the semicarbazone moiety is essential for anticonvulsant activity. A number of arylsemicarbazones were devoid of sedative hypnotic activity with less neurotoxicity [9].

Interestingly, the activity of these substances might be stimulated by coordination to some metal ions. Particularly, nickel(II) complexes with semicarbazone ligands show antibacterial activities [10], and copper(II) complexes containing semicarbazone have also displayed biological properties. Moreover, in recent years a considerable amount of work has been done on the coordination chemistry of copper(II) with semicarbazones, to model the physical and chemical behavior of biological copper systems [11].

Keeping in view the above points and by considering the biological potential of semicarbazones we have synthesized two N^4-phenylsubstituted semicarbazones. The two ketones selected here are having a phenolic group which provides further binding site for metal cations and they behave as diprotic chelating ligands. Both are ONO donor ligands forming terdentate chelates with transition metal ions bonding through phenolic oxygen, amido oxygen and azomethine nitrogen atoms.

Our work includes the following two semicarbazone systems

1) 2-Hydroxy-4-methoxyacetophenone-N^4-phenylsemicarbazone (H_2ASC)
2) 2-Hydroxy-4-methoxybenzophenone-N^4-phenylsemicarbazone (H_2BSC)

This chapter deals with the synthesis, spectral and structural characterization of the above two N^4-phenylsemicarbazones and their structural formulae and numbering scheme are given in Fig. 2.1.

Molecular formula: $C_{16}H_{17}N_3O_3$
Formula weight : 299.32

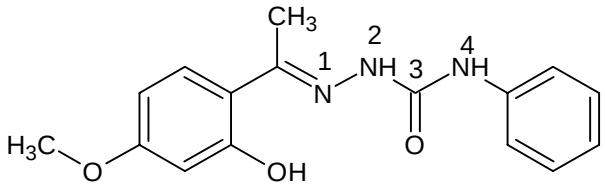

2-Hydroxy-4-methoxyacetophenone-N^4-phenylsemicarbazone (H_2ASC)

Molecular formula: $C_{21}H_{19}N_3O_3$
Formula weight : 361.39

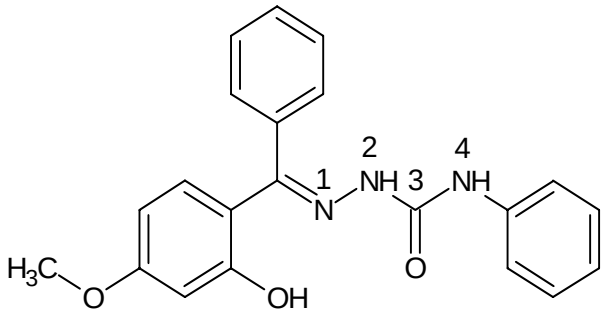

2-Hydroxy-4-methoxybenzophenone -N^4-phenylsemicarbazone (H_2BSC)

Fig. 2.1. Structure and numbering scheme of the semicarbazones.

2.2. 2-Hydroxy-4-methoxyacetophenone-N^4-phenylsemicarbazone monohydrate (H_2ASC·H_2O)

2.2.1. Experimental

2.2.1.1. Materials

2-Hydroxy-4-methoxyacetophenone (Sigma-Aldrich), *N*^{4}-phenylsemicarbazide (Sigma-Aldrich) were of Analar grade and were used as received. The solvent ethanol (Merck) was used without further purification.

2.2.1.2. Synthesis

2-Hydroxy-4-methoxyacetophenone-N^4-phenylsemicarbazone monohydrate ($H_2ASC{\cdot}H_2O$) was prepared by the adaptation of a method reported earlier [12]. N^4-phenylsemicarbazide (0.302 g, 2 mmol) was dissolved in warm ethanol (25 mL). To this solution added an ethanolic solution (25 mL) of 2-hydroxyl-4-methoxyacetophenone (0.332 g, 2 mmol) and the resulting solution was boiled under reflux for 4 h. after adding a few drops of glacial acetic acid. There was no immediate formation of the product. Then the reaction mixture was kept aside for slow evaporation at room temperature. After two days the yellow crystalline precipitate formed was filtered, washed with ethanol, followed by ether and dried over P_4O_{10} in *vacuo* (Scheme 2.1). XRD quality single crystals of this compound were grown from its solution in ethanol. The purity of the semicarbazone was checked by melting point determination and elemental analyses.

Melting point = 170 ^oC; Yield: 70%.

Elemental Anal. Found (calcd)

% : C: 60.44 (60.56); H: 6.13 (6.03); N: 13.63 (13.24).

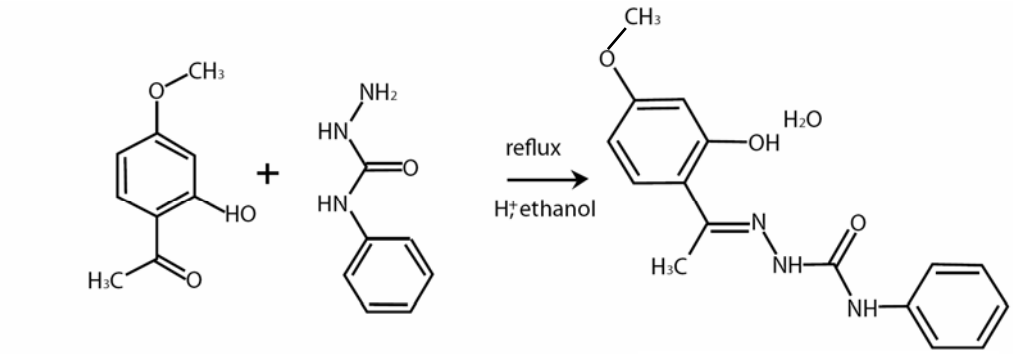

2-Hydroxy-4-methoxyacetophenone | N^4 - phenylsemicarbazide | 2-Hydroxy-4-methoxyacetophenone – N^4-Phenylsemicarbazone monohydrate

Scheme 2.1.

2.2.1.3. Characterization of 2-hydroxy-4-methoxyacetophenone-N^4-phenylsemicarbazone monohydrate ($H_2ASC{\cdot}H_2O$)

The prepared 2-hydroxy-4-methoxyacetophenone-N^4-phenylsemicarbazone monohydrate ($H_2ASC{\cdot}H_2O$) was characterized by elemental analyses, mass, ^1H NMR, IR and electronic spectra. Mass spectrum was recorded on a WATERS 3100 Mass detector. The ^1H NMR spectrum was recorded using Bruker DRX 500 Spectrometer, with $CDCl_3$ as solvent and TMS as standard at the Sophisticated Instruments Facility, Indian Institute of Science, Bangalore, India. Infrared spectrum was recorded on a JASCO FT-IR-4100 Fourier Transform Infrared spectrometer in the range 4000-400 cm^{-1} using KBr pellets at the Department of Applied Chemistry, CUSAT, Kochi, India. Electronic spectrum was recorded on a Spectro UV-Vis Double Beam UVD-3500 spectrometer in the range 200-900 nm at the Department of Applied Chemistry, CUSAT, Kochi, India. Elemental analyses were carried out using a Vario EL III CHNS analyzer at SAIF, Kochi, India and also at SAIF, CDRI, Lucknow. Single crystals of this compound were grown from its solution in ethanol and its structure was determined by X-ray diffraction studies at SAIF, Kochi, India, mounting on a Bruker SMART APEX diffractometer.

2.2.1.3.1. *Elemental analyses*

C, H, N analyses of the $H_2ASC{\cdot}H_2O$ are given in Section 2.2.1.2.

2.2.1.3.2. *Mass spectrum*

A mass spectrum is obtained by converting components of a sample into rapidly moving gaseous ions and resolving them on the basis of their mass to charge ratios. Here the mass spectrum was recorded by using the

WATERS 3100 Mass Detector, designed for routine UPLC/MS analyses. It is an analytical technique used to measure the mass to charge ratio of charged particles by electron spray ionization (ESI) MS mode. In this the organic molecules are bombarded with high energy electrons and quantitatively record the result as a spectrum of positive ion fragments. The most intense peak in the spectrum called the base peak is assigned a value of 100% and the intensities of other peaks including the parent peak are reported as % of the base peak. Mass spectrum is a plot of m/z of positive ion fragments verses their relative abundance. Here for the ligand $H_2ASC{\cdot}H_2O$ the (M+1) peak at 300.2 amu (Fig. 2.2) confirms the proposed formula.

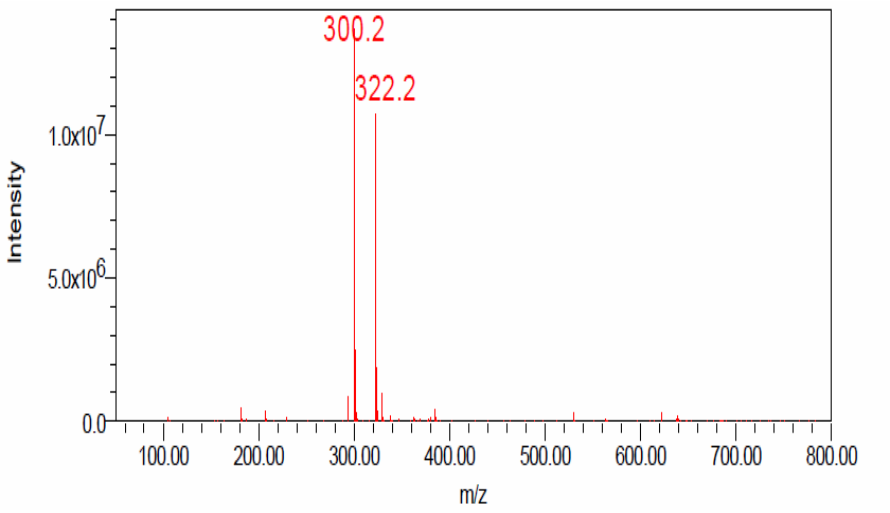

Fig. 2.2. Mass spectrum of H_2ASC showing (M+1) peak.

2.2.1.3.3. *^{1}H NMR spectrum*

Proton magnetic resonance spectroscopy is a helpful tool for the identification of organic compounds in conjunction with other spectrometric informations. The ^{1}H NMR spectrum of an organic compound provides useful information about the number of different types of hydrogens present in the molecule and their electronic environment. The areas underneath each signal are in the same ratio as the number of hydrogen atoms causing each signal.

^{1}H NMR spectrum of the synthesized 2-hydroxy-4-methoxyacetophenone-N^4-phenylsemicarbazone monohydrate ($H_2ASC{\cdot}H_2O$) was recorded in $CDCl_3$ on a Bruker AMX 400 Spectrometer with TMS as standard and the spectrum is given in Fig. 2.3.1. For $H_2ASC{\cdot}H_2O$, a sharp singlet, which integrate as one hydrogen at 11.334 ppm is assigned to the phenolic OH proton. The observed downfield shift of this proton is due to its hydrogen bonding to the azomethine nitrogen atom (N1). The signals at 8.405 and 7.421 ppm observed along with the aromatic multiplets, each having a peak area corresponds to one are assigned to ^{4}NH and ^{2}NH protons, respectively. The downfield value of ^{4}NH proton is due to the deshielding effect of the phenyl group. The hydrogen bonding interaction of these NH protons with oxygen atom of lattice water present in the molecule has an adding effect for these downfield shifts. Hydrogen bonding decreases the electron density around the proton and thus moves the proton absorption to a lower field [13]. Absence of any coupling interactions by protons on neighboring atoms render singlet peaks for these imine and phenolic protons.

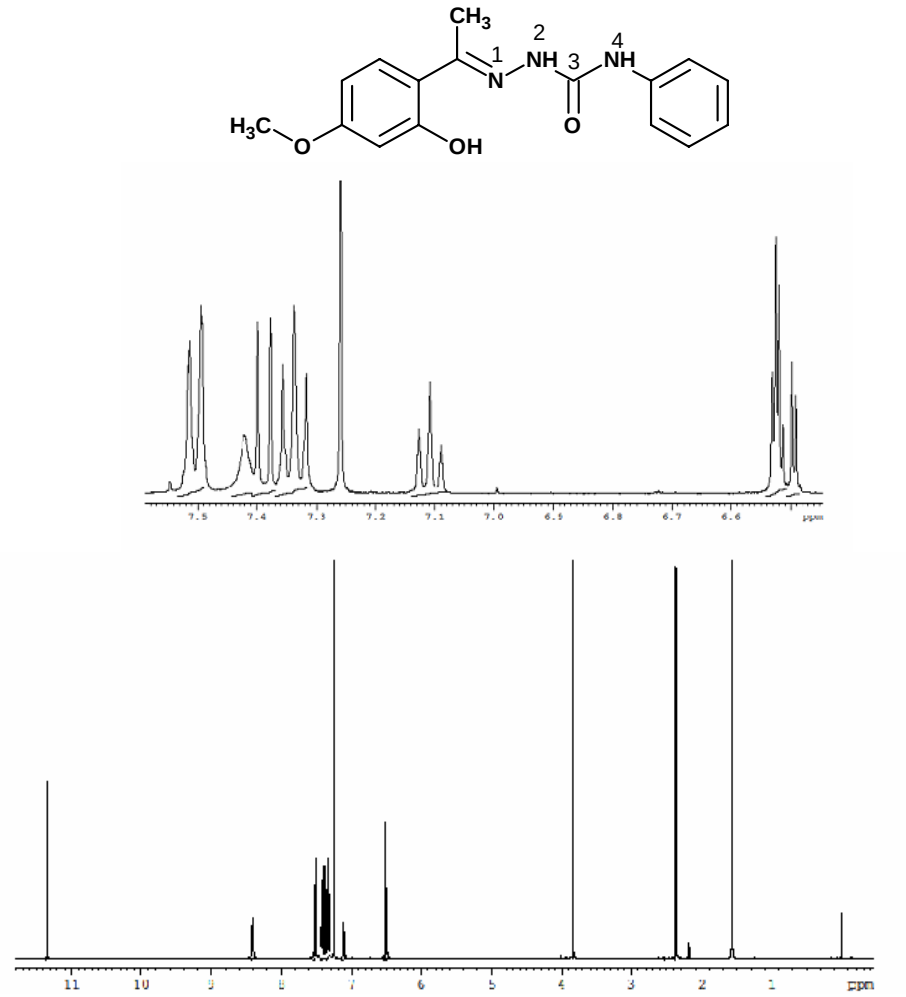

Fig. 2.3.1. ^{1}H NMR spectrum of $H_2ASC{\cdot}H_2O$.

A sharp singlet at 3.833 ppm which integrates as three hydrogens is assigned to methoxy protons. A singlet peak at 2.359 ppm is assigned to the methyl group, while the multiplet peaks between 6.492 and 7.156 ppm are due to the aromatic protons present in the molecule.

Upon D_2O exchange the signals due to imine and phenolic protons disappeared, suggesting that these protons are easily exchangeable and confirmed the above assignments (Fig. 2.3.2).

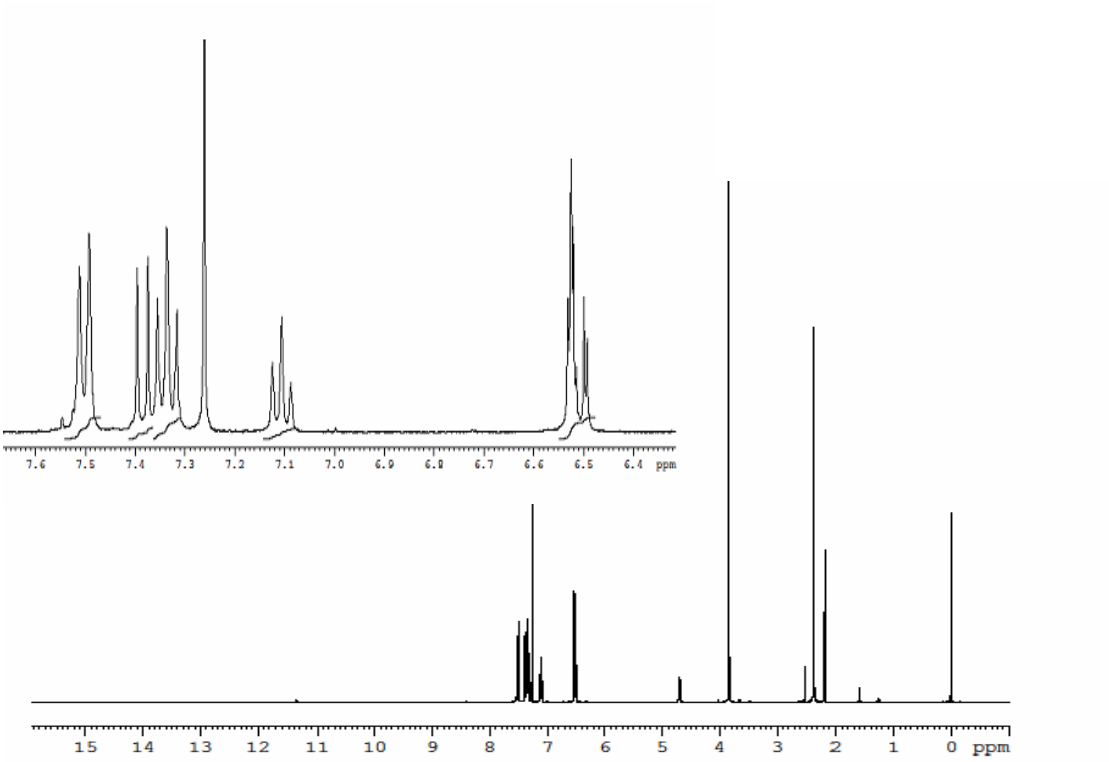

Fig. 2.3.2. ^{1}H NMR spectrum of $H_2ASC{\cdot}H_2O$-D_2O exchange.

2.2.1.3.4. *Infrared spectrum*

Infrared spectrum was recorded on a JASCO FT-IR4100 spectrometer in the range 4000-400 cm^{-1} using KBr pellets and is shown in Fig. 2.4. The characteristic IR bands of the semicarbazone provide significant information regarding the various functional groups present in them.

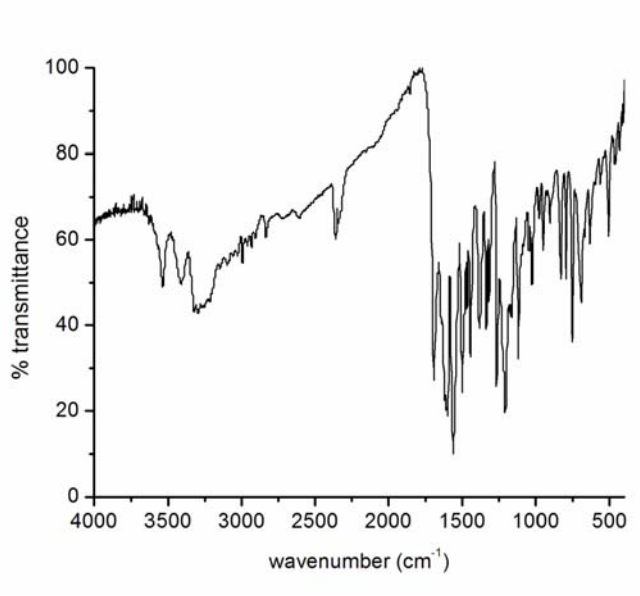

Fig. 2.4. IR spectrum of $H_2ASC{\cdot}H_2O$.

The observed IR frequency of the carbonyl group of the semicarbazones *ca*. 1692 cm^{-1} (in KBr), are abnormally high as compared to those of amides and urea [14]. This shift of IR frequency can be explained by the combined inductive effect of nitrogen atoms, which would pull the π cloud of carbonyl closer to the carbon, diminishing the polar character of the C=O [15]. The presence of a sharp band at 1692 cm^{-1} is assigned to *ν*(C=O) stretching vibration which proves the existence of amido form in the solid state and the crystal structure confirms this assignment. Medium bands observed at 3295 and 3408 cm^{-1} are assigned to the $\nu(N^2H)$ and $\nu(N^4H)$ of the imino group of H_2ASC. A prominent band at 1619 cm^{-1} due to azomethine *ν*(C=N) linkage is observed in the spectrum indicating the condenzation of phenylsemicarbazide and the ketone moiety, and it is in agreement with earlier reports of N^4-substituted semicarbazones [16]. The IR spectral band observed at 1020 cm^{-1} correspond to *ν*(N–N) [17]. The broad

absorption bands in the range 3331–3210 cm^{-1} is due to the ν(O–H) stretching mode of lattice water present and the decrease in the value is due to the involvement of intermolecular hydrogen bonding [13,18]. The sharp band at 3535 cm^{-1} is due to the O–H stretching mode of phenolic oxygen.

2.2.1.3.5. *Electronic spectrum*

The electronic spectrum of the compound was recorded in acetonitrile solution on a Spectro UV–Vis Double Beam UVD–3500 spectrometer in the range 50000–25000 cm^{-1} and it is presented in Fig. 2.5.

Generally π–π* transitions are observed in the 32000–44000 cm^{-1} region and the n–π* transitions are observed in the region of 32000–29000 cm^{-1} [19]. For the compound H_2ASC the bands in the range 31780-41750 cm^{-1} are attributed to the π-π* and n-π* transitions of the benzene ring, imine and carbonyl groups present in the semicarbazone moiety.

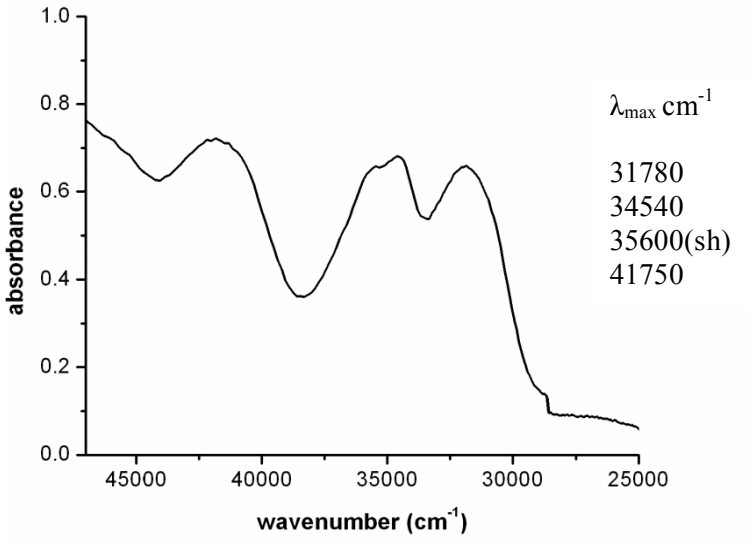

Fig. 2.5. Electronic spectrum of H_2ASC.

2.2.1.3.6. *X–ray crystallography*

Single crystals of the ligand $H_2ASC{\cdot}H_2O$ suitable for X–ray diffraction were obtained from its ethanolic solution. A yellow colored block shaped crystal with approximate dimensions of 0.50 x 0.30 x 0.25 mm^3 was selected for collecting the data. It was mounted on a Bruker SMART APEX diffractometer, equipped with a graphite crystal, incident-beam monochromator, and a fine focus sealed tube with Mo Kα (λ=0.71073 Å) as the X-ray source. The crystallographic data along with the details of structure solution refinements are given in Table 2.1. The unit cell dimensions were measured and the data collections were performed at 296(2) K. Bruker SMART software was used for data acquisition and Bruker SAINT software for data integration [20]. Absorption corrections were carried out using SADABS based on Laue symmetry using equivalent reflections [21]. The structure was solved by direct methods and refined by full matrix least-squares calculations with the SHELXL-97 software package [22]. The graphics tool used was DIAMOND version 3.2g [23]. All non-hydrogen atoms were refined anisotropically. All H atoms on C were placed in calculated positions, guided by difference maps, with C–H bond distances 0.93–0.96 Å. H atoms were assigned as *U*iso = 1.2Ueq. H1A and H1B atoms of O1S were located from difference Fourier maps and restrained using DFIX and DANG instructions with O–H = 0.86 (2) and H···H = 1.36(2) Å respectively. N2–H2N, N3–H3 and O2–H2′ atoms were located from difference maps and restrained using DFIX instructions with bond distance of 0.88(1). The molecular structure of $H_2ASC{\cdot}H_2O$ with the atom numbering scheme is given in Fig. 2.6. The selected bond lengths and angles are given in Table 2.2 and torsional angles in Table 2.3.

Table 2.1. Crystal data and structure refinement for $H_2ASC{\cdot}H_2O$.

Empirical formula	$C_{16}H_{19}N_3O_4$
Formula weight	317.34
Temperature	296(2) K
Wavelength	0.71073 Å
Crystal system	Monoclinic
Space group	$P2_1/c$
Unit cell dimensions	a = 12.4020(18) Å α = 90°.
	b = 13.7808(19) Å β = 96.813(7)°.
	c = 9.3919(10) Å γ = 90°.
Volume	1593.8(4) $Å^3$
Z	4
Calculated density	1.322 Mg/m^3
Absorption coefficient	0.097 mm^{-1}
F(000)	72.0
Crystal size	0.50 x 0.30 x 0.25 mm
Theta range for data collection	2.64 to 25.00°.
Limiting indices	$-14\leq h\leq 14$, $-15\leq k\leq 16$, $-11\leq l\leq 11$
Reflections collected / unique	12097 / 2811 [R(int) = 0.0834]
Completeness to theta = 25.	99. 9%
Absorption correction	Semi–empirical from equivalents
Max. and min. transmission	0.9782 and 0.968
Refinement method	Full–matrix least–squares on F^2
Data / restraints / parameters	2809 / 3 / 219
Goodness–of–fit on F^2	1.025
Final R indices [I>2sigma(I)]	$R_1 = 0.0525$, $wR_2 = 0.104$
R indices (all data)	$R_1 = 0.0836$, $wR_2 = 0.1714$
Largest diff. peak and hole	0.216 and –0.173 e. $Å^{-3}$

$R_1 = \Sigma||F_o| - |F_c|| / \Sigma|F_o|$

$wR_2 = [\Sigma w(F_o^2-F_c^2)^2 / \Sigma w(F_o^2)^2]^{1/2}$

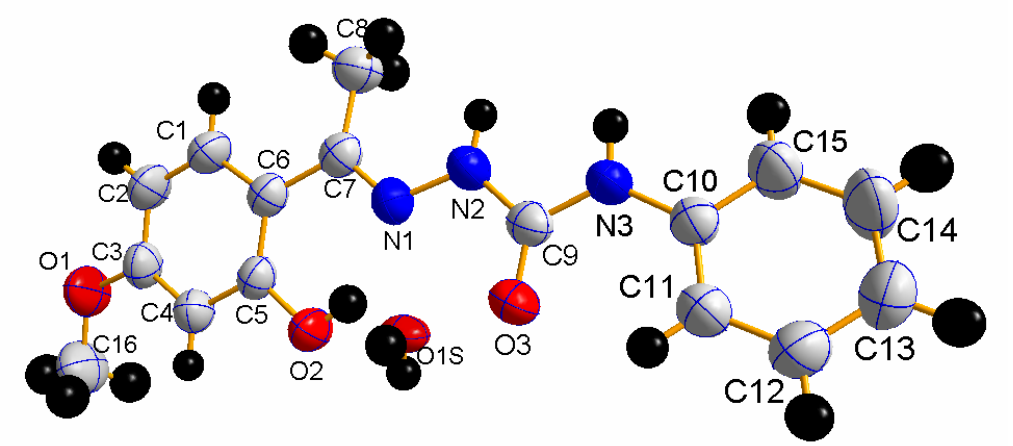

Fig. 2.6. The molecular structure of $H_2ASC{\cdot}H_2O$ along with the atom numbering scheme.

Table 2.2. Selected bond lengths [Å] and angles [°] for $H_2ASC{\cdot}H_2O$.

N(1)–N(2)	1.359(3)	N(1)–C(7)–C(6)	115.4(2)
N(2)–C(9)	1.361(3)	O(3)–C(9)–N(2)	122.5(2)
O(3)–C(9)	1.212(3)	C(7)–N(1)–N(2)	119.7(2)
N(3)–C(9)	1.347(3)	N(1)–N(2)–C(9)	117.18(19)
N(3)–C(10)	1.398(3)	C(6)–C(7)–C(8)	121.5(2)
C(6)–C(7)	1.462(3)	O(3)–C(9)–N(3)	125.2(2)
N(1)–C(7)	1.289(3)	N(3)–C(9)–N(2)	112.3(2)
		N(1)–C(7)–C(8)	123.0(2)

Table 2.3. Selected torsion angles [°] for $H_2ASC{\cdot}H_2O$.

C(7)–N(1)–N(2)–C(9)	–177.36(18)
C(5)–C(6)–C(7)–N(1)	–8.6(3)
O(2)–C(5)–C(6)–C(7)	3.3(3)
C(9)–N(3)–C(10)–C(11)	–17.1(4)
N(1)–N(2)–C(9)–N(3)	–178.66(17)
N(2)–N(1)–C(7)–C(6)	178.58(17)
N(1)–N(2)–(C9)–(O3)	–0.2(3)

The compound $H_2ASC{\cdot}H_2O$ is crystallized into a monoclinic space group $P2_1/c$. The phenyl ring is almost coplanar with the central semicarbazone moiety with maximum deviation of -0.060(3) Å for the C1 atom. The two aromatic rings are twisted with dihedral angle of 22.8(13)°. The molecule is almost planar with a dihedral angle of 22.8(13)° between the rings 1 and 2 formed by the atoms C1, C2, C3, C4, C5, C6 and C10, C11, C12, C13, C14, C15 respectively. The torsion angles of 178.58(17)° and –178.66(17)° corresponding to C6–C7–N1–N2 and N1–N2–C9–N3 moieties confirm the *E* configuration of the compound with respect to the C7–N1 and N2–C9 bonds [24]. According to the crystal structure the compound exists in the amido form with N1 and O3 in the *Z* configuration with respect to N2–C9 as evidenced from the torsion angle of –0.2(3)° for the N1–N2–C9–O3 moiety. The amido form in the solid state is evidenced by the observed bond length of 1.212 Å for C9–O3 which is very close to the formal C=O bond length 1.21 Å [25]. The N1–N2 1.359(3) Å and C9–N2 1.361(3) Å bond distances are intermediate between the ideal values of corresponding single [N–N: 1.45 Å and C–N: 1.47 Å] and double bonds [N=N:1.25 Å and C=N 1. 28 Å], giving evidence for an extended π delocalization along the semicarbazone chain [26].

The phenolic -OH and azomethine N1 are in *cis* configuration as evidenced from torsion angles of –8.6(3)° and 3.3 (3)° for C5–C6–C7–N1 and O2–C5–C6–C7 moieties respectively. This facilitates intramolecular hydrogen bonding of OH to N1 [27]. The packing diagram arrangements of the molecules along the b axis is shown in Fig. 2.7.

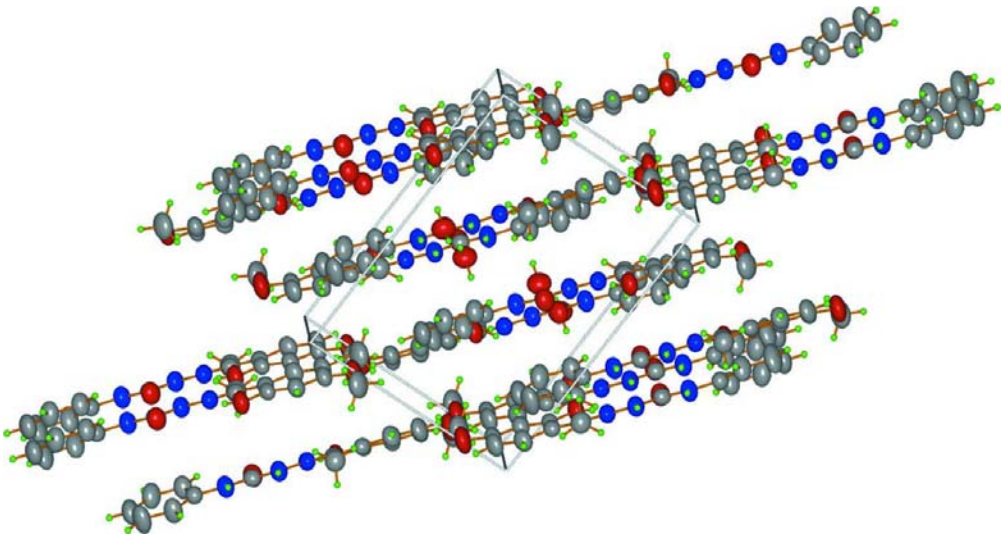

Fig. 2.7. Packing diagram of $H_2ASC{\cdot}H_2O$ showing the parallel arrangement of the molecules along the 'b' axis.

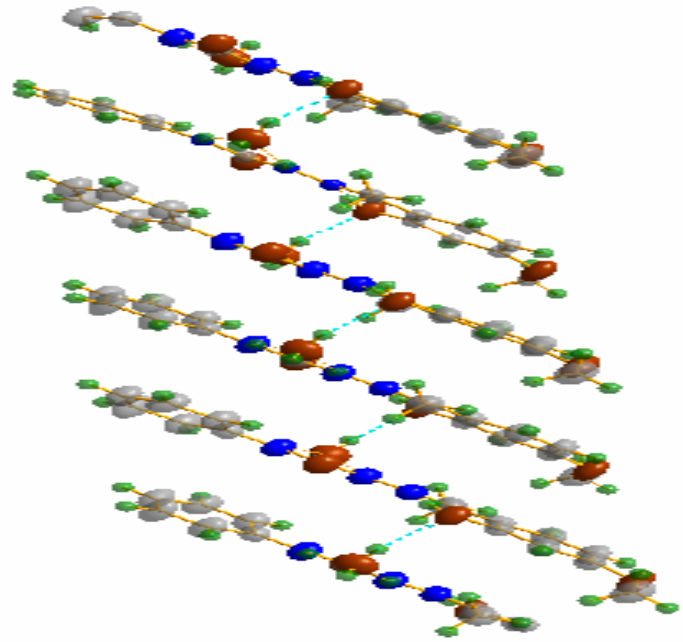

Fig. 2.8. Supramolecular chain stabilized by hydrogen bonding between the semicarbazone and the lattice water molecule.

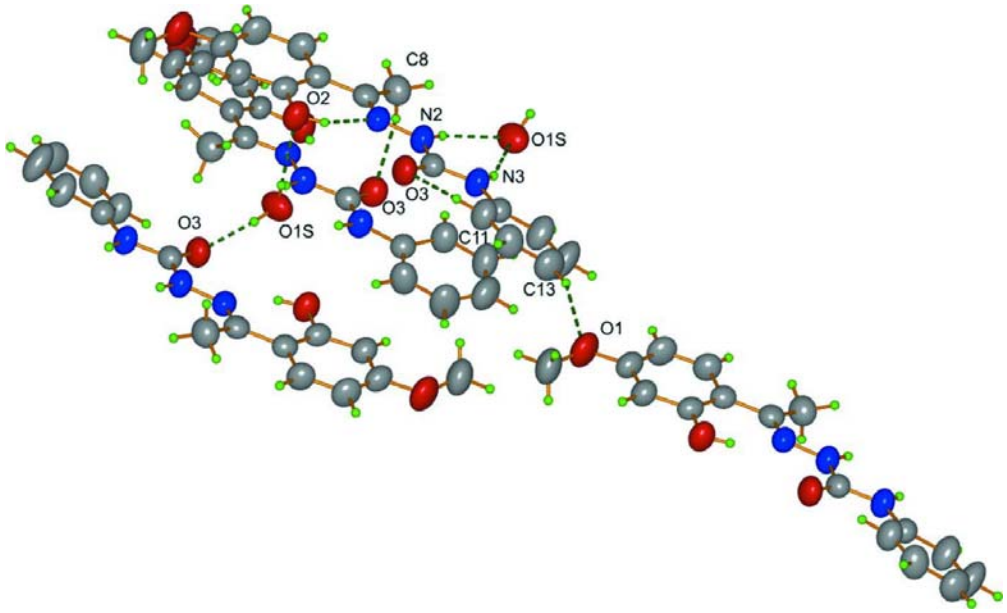

Fig. 2.9. Three dimensional supramolecular hydrogen bonding network in the crystal structure of $H_2ASC \cdot H_2O$.

An important feature of the crystal packing is the formation of supramolecular chain mediated by a network of hydrogen bonds (Fig. 2.8). The water molecule present in the crystal lattice interconnects adjacent molecules through hydrogen bonds. The two protons in the water molecule form hydrogen bonds with amide oxygen and phenolic oxygen of different semicarbazone moieties. The oxygen in the water molecule also forms hydrogen bonds with N(2)–H(2^1) and N(3)–H(3) protons of third semicarbazone molecule. The supramolecular chain stabilized by hydrogen bonding is shown in Fig. 2.9. The interaction parameters are given in Table 2.4.

Table 2.4. Interaction parameters of $H_2ASC{\cdot}H_2O$.

Hydrogen bonds and angles for $H_2ASC{\cdot}H_2O$ [Å, °]				
D–H ···A	**d(D–H)**	**d(H···A)**	**d(D···A)**	**<(DHA)**
O(2)–H(2A)···N(1)	0.82	1.81	2.526(2)	145.7
N(2)–H(2')···O(1S)^{i}	0.86	2.12	2.900(3)	150.6
N(3)–H(3)···O(1S)^{i}	0.86	2.11	2.922(3)	156.9
O(1S)–H(1A)···O(2)	0.852(18)	2.13(2)	2.925(3)	156(3)
O(1S)–H(1B···O(3)^{ii}	0.837(18)	1.895(18)	2.730(3)	174(3)
C8–H8C ···O(3)^{iii}	0.96	2.51	3.457(3)	167
C11–H11C ···O(3)	0.93	2.31	2.881(3)	119
C13–H13C ···O(1)^{iv}	0.93	2.60	3.489(3)	160

Symmetry codes: (i) x, –y+1/2, z–1/2 (ii) –x+1, –y+1, –z+1 (iii) x, -y+1/2, z+1/2 (iv) x+1, y, z-1

C–H···π interactions			
X–H(I)···Cg(J)	**H···Cg (Å)**	**X–H···Cg(°)**	**X···Cg (Å)**
C(8) –H(8A)···Cg(1)^{v}	2.91	124	3.543(3)
C(16)–H(16C)···Cg(1)^{vi}	2.80	148	3.645(3)

Equivalent position code: v= x,-y-1/2,z-3/2; vi= –x,– y+1, -z+1
Cg(1) = C(1), C(2), C(3), C(4), C(5), C(6)

The C–H···π interactions observed C(8)–H(8A)···Cg(1) at a distance of 2.91 Å and C(16)–H(16C)···Cg(1) at a distance of 2.80 Å reinforce the packing in adjacent layers of unit cell and is shown in Fig. 2.10.

However, no significant π···π interactions are found in the packing.

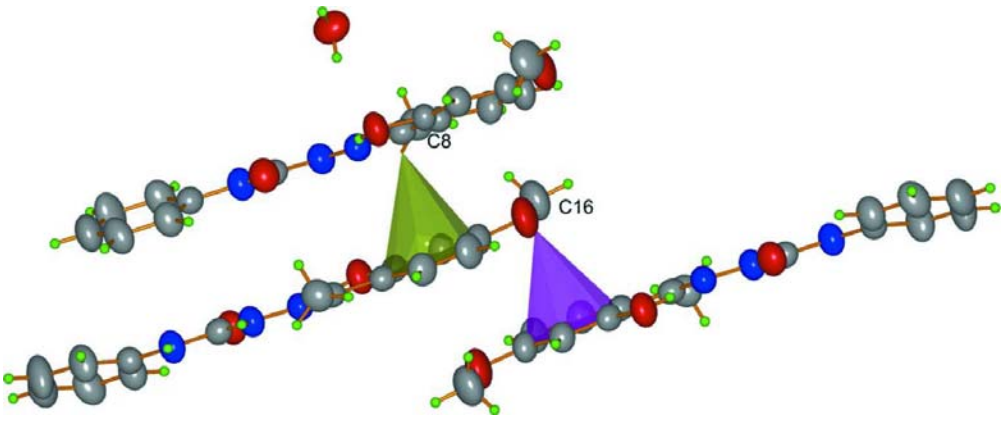

Fig. 2.10. C–H··· π interactions present in the compound $H_2ASC{\cdot}H_2O$.

2.3. 2-Hydroxy-4-methoxybenzophenone-N^4-phenylsemicarbazone (H_2BSC)

2.3.1. Experimental

2.3.1.1. Materials

N^4-phenylsemicarbazide (Sigma-Aldrich), 2-hydroxy-4-methoxybenzophenone (Sigma-Aldrich) were of analar grade and were used as received. Methanol (Merck) was used without further purification.

2.3.1.2. Synthesis

2-Hydroxy-4-methoxybenzophenone-N^4-phenylsemicarbazone (H_2BSC) was synthesized by a similar method to that of $H_2ASC{\cdot}H_2O$. To a warm methanolic solution of N^4-phenylsemicarbazide (0.302 g, 2 mmol) (25 mL), a methanolic solution (25 mL) of 2-hydroxy-4-methoxybenzophenone (0.4566 g, 2 mmol) was added and the resulting solution was boiled under reflux for 2 h. after adding 3 drops of conc. HCl. On slow evaporation at room temperature colorless crystals were separated out (Scheme 2). It was filtered and washed with methanol and ether. Single crystals of the

compound for X-ray analysis were obtained from its solution in methanol and also from its solution in 1:1 (v/v) mixture of methanol and DMF. The purity of the semicarbazone was checked by melting point determination and elemental analyses.

Melting point = 225 ^{o}C; Yield: 76%.

Elemental Anal. Found (calcd) % : C: 69.68 (69.79); H: 5.72 (5.30);

N: 11.93 (11.63).

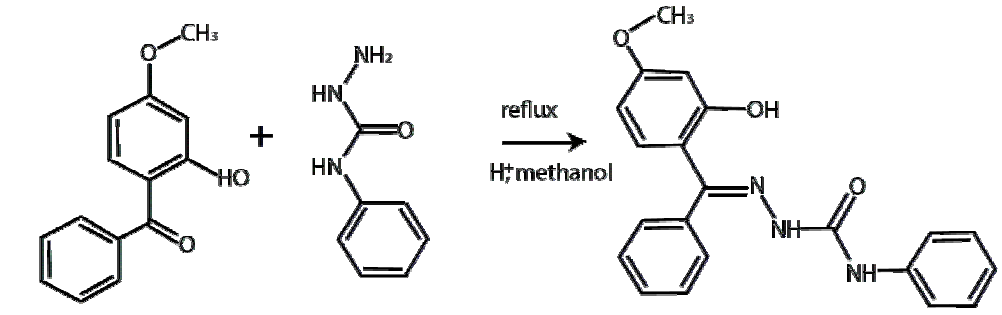

2-Hydroxy-4-methoxybenzophenone | N^4 - phenylsemicarbazide | 2-Hydroxy-4-methoxybenzophenone – N^4-phenylsemicarbazone

Scheme 2.2.

2.3.1.3. Characterization of 2-hydroxy-4-methoxybenzophenone-N^4-phenylsemicarbazone (H_2BSC)

The ligand 2-hydroxy-4-methoxybenzophenone-N^4-phenylsemicarbazone (H_2BSC) was characterized by using the same techniques as described in section 2.2.2.

2.3.1.3.1. *Elemental analyses*

C, H, N analyses of the ligand H_2BSC are given in Section 2.3.1.2.

2.3.1.3.2. *Mass spectrum*

Mass spectrum of H_2BSC was recorded by using the WATERS 3100 Mass Detector, designed for routine UPLC/MS analyses. The ESI mass spectrum of the semicarbazone shows the parent ion peak at 362.3 for (M+1) peak. This is consistent with the stoichiometry of the compound. The mass spectrum is shown in Fig. 2.11.

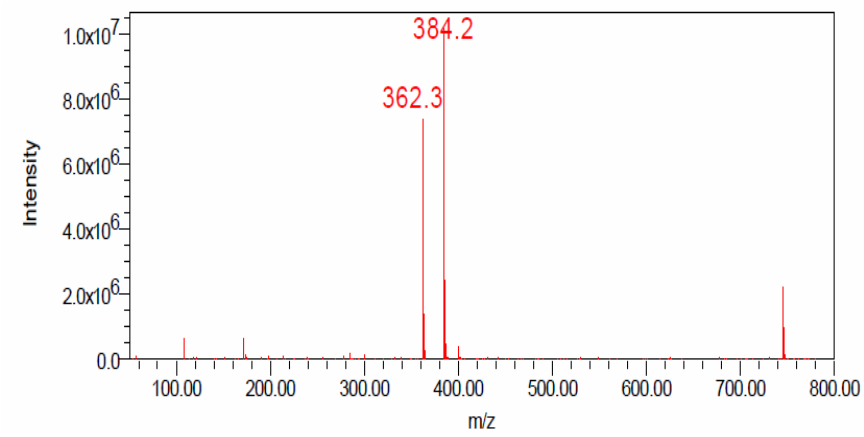

Fig. 2.11. Mass spectrum of H_2BSC showing (M+1) peak.

2.3.1.3.3. *^1H NMR spectrum*

^1H NMR spectrum of 2-hydroxy-4-methoxybenzophenone-N^4-phenylsemicarbazone (H_2BSC) was recorded in DMSO-d_6 as solvent on a Bruker AMX 400 Spectrometer with TMS as standard.

The ^1H NMR spectrum of the compound H_2BSC is shown in Fig. 2.12.1. Here the sharp singlet in the very downfield region of the spectrum at 12.94 ppm with a peak area corresponds to one is assigned to phenolic OH proton. The high δ value of this OH proton is due to its attachment to the azomethine nitrogen atom N1 through hydrogen bonding. The signals at 9.105 and 9.034

ppm each having a peak area corresponds to one are attributed to ^{4}NH and ^{2}NH protons, respectively. A signal due to methoxy protons is appeared as a singlet at 3.899 ppm with an area integral of three whereas the multiplets between 6.33 and 7.672 ppm are all due to the aromatic protons of the phenyl rings.

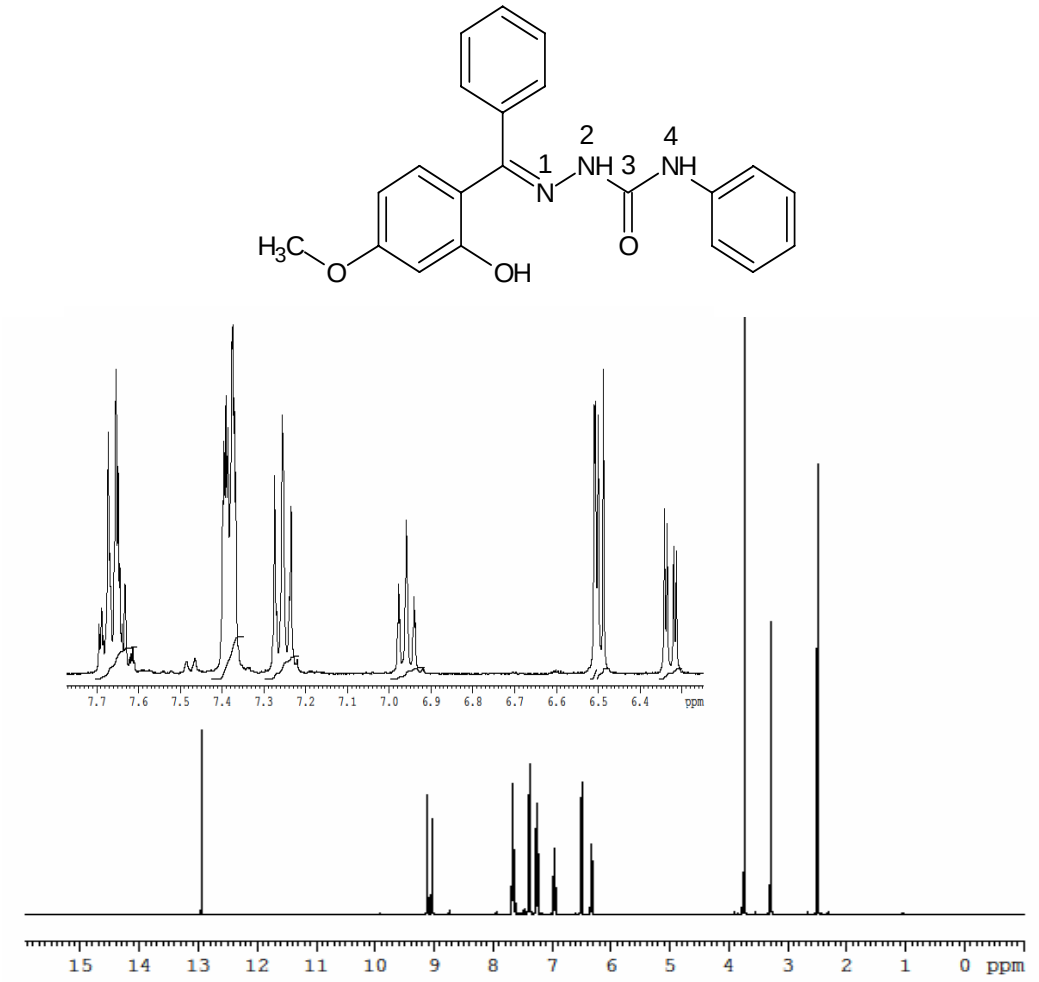

Fig. 2.12.1. ^{1}H NMR spectrum of H_2BSC.

Upon D_2O exchange the signals due to phenolic and imine protons were disappeared confirming the above assignments (Fig 2.12.2).

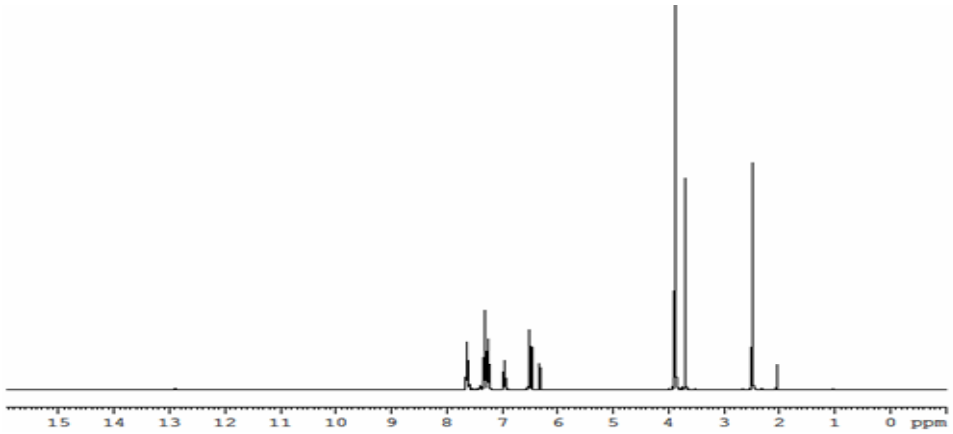

Fig. 2.12.2. ^{1}H NMR spectrum of H_2BSC on D_2O exchange.

2.3.1.3.4. *Infrared spectrum*

Infrared spectrum was recorded on a JASCO FT-IR-5300 spectrometer in the range 4000-400 cm^{-1} using KBr pellets (Fig. 2.13).

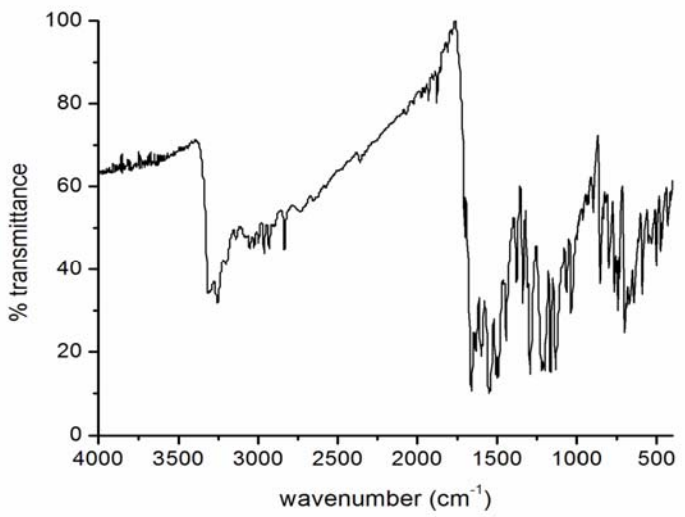

Fig. 2.13. IR spectrum of H_2BSC.

The bands of diagnostic importance and their tentative assignments are as follows. The presence of a sharp band at 1662 cm^{-1} is assigned to ν(C=O) stretching vibration which reveals the existence of amido form in the solid

state and the crystal structure confirms this assignment. Medium bands observed at 3145 and 3249 cm^{-1} are assigned to the $\nu(N^2H)$ and $\nu(N^4H)$ of the imino group of H_2BSC. A prominent band at 1631 cm^{-1} is attributed to azomethine ν(C=N) linkage. The IR spectral band observed at 1059 cm^{-1} corresponds to ν(N–N) [28]. The sharp band at 3316 cm^{-1} is due to the O–H stretching mode of phenolic oxygen.

2.3.1.3.5. *Electronic spectrum*

The electronic spectrum of the compound was recorded in acetonitrile solution on a Spectro UV–Vis Double Beam UVD–3500 spectrometer in the range 200–900 nm and it is presented in Fig. 2.14. and the bands in the range 31330-41680 cm^{-1} are attributed to the π-π* and n-π* transitions and are shown below.

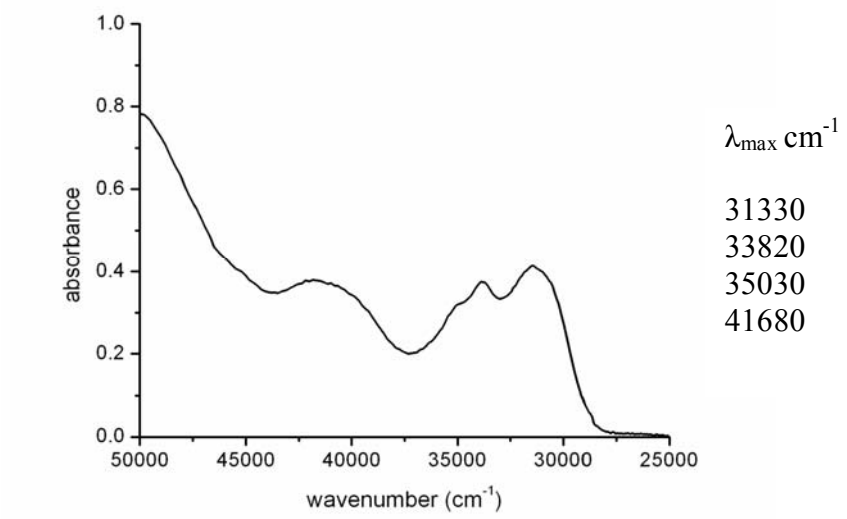

Fig. 2.14. Electronic spectrum of H_2BSC.

2.3.1.3.6. *X–ray crystallography*

Two types of colorless block shaped single crystals of the ligand H_2BSC suitable for X–ray diffraction studies were obtained; one from its solution in

methanol and the other from its solution in 1:1(v/v) mixture of methanol and DMF. The one obtained from its methanolic solution crystallizes in orthorhombic $P2_1/c$ and the other one in monoclinic $P2_1/c$. The single crystal grown from a mixture of methanol and DMF has one molecule of DMF as solvent of crystallization.

2.3.1.3.6a. *Crystal structure of H_2BSC*

A single crystal with approximate dimensions of 0.32 x 0.20 x 0.20 mm was selected from its methanolic solution for collecting the data. The details are given in Section 2.2.1.3.6. The molecular structure of H_2BSC with the atom numbering scheme is given in Fig. 2.15.

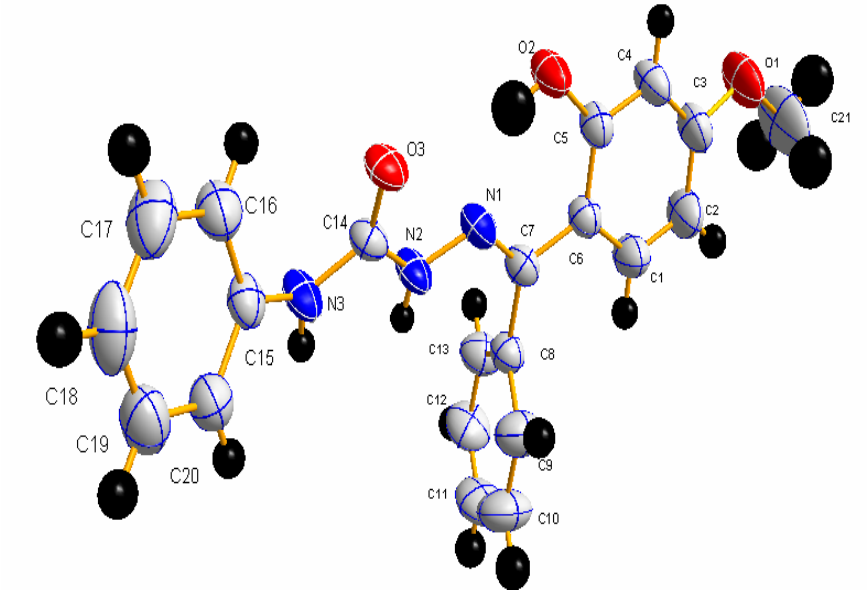

Fig. 2.15. The molecular structure of H_2BSC along with the atom numbering scheme.

The crystallographic data and structure refinement parameters of the compound are given in Table 2.5 and the selected bond lengths and angles are given in Table 2.6 and torsional angles in Table 2.7.

Table 2.5. Crystal data and structure refinement for H_2BSC.

Empirical formula	$C_{21}H_{19}N_3O_3$
Formula weight	361.39
Temperature	296(2) K
Wavelength	0.71073 Å
Crystal system	Orthorhombic
Space group	$P2_1/c$
Unit cell dimensions	a = 20.0062(11) Å α = 90°
	b = 10.0203(7) Å β = 90°
	c = 9.3643(5) Å γ = 90°
Volume	1877.22(19) $Å^3$
Z	4
Calculated density	1.279 Mg/ m^3
Absorption coefficient	0.087 mm^{-1}
F(000)	760.0
Crystal size	0.32 x 0.20 x 0.20 mm^3
Theta range for data collection	2.88 to 28.00°.
Limiting indices	$-18 \le h <= 26$, $10 \le k \le 13$, $12 \le l \le 10$
Reflections collected / unique	6467 / 4549 [R(int) = 0.0268]
Completeness to theta = 28.00	71.9%
Absorption correction	Semi–empirical from equivalents
Max. and min. transmission	0.9838 and 0.9743
Refinement method	Full–matrix least–squares on F^2
Data / restraints / parameters	3267 / 3 / 258
Goodness–of–fit on F^2	0. 802
Final R indices [I>2sigma(I)]	R_1 = 0.0468, wR_2 = 0.0893
R indices (all data)	R_1 = 0.1118, wR_2 = 0.1034
Extinction coefficient	0.0071(14)
Largest diff. peak and hole	0.146 and –0.106 e. $Å^{-3}$

$R_1 = \Sigma||F_o| - |F_c|| / \Sigma|F_o|$

$wR_2 = [\Sigma w(F_o^2-F_c^2)^2 / \Sigma w(F_o^2)^2]^{1/2}$

Table 2.6. Bond lengths [Å] and angles [°]for H_2BSC.

N(1)–C(7)	1. 291(2)	C(14)–N(2)–N(1)	118.43(14)
O(3)–C(14)	1.227(2)	C(7)–N(1)–N(2)	118.55(14)
N(1)–N(2)	1.3698(19)	N(1)–C(7)–C(6)	117.82(15)
N(2)–C(14)	1.364 (2)	N(1)–C(7)–C(8)	122.68(14)
N(3)–C(14)	1.356(2)	C(6)–C(7)–C(8)	119.44(16)
N(3) –C(15)	1.413(2)	O(3)–C(14)–N(3)	124.44(18)
C(6)–C(7)	1.467(2)	O(3)–C(14)–N(2)	122.99(15)
		N(3)–C(14)–N(2)	112.55(15)

Table 2.7. Torsion angles [°] for H_2BSC.

N(2)–N(1)–C(7)–C(6)	177.02(15)
C(5)–C(6)–C(7)–N(1)	–8.7(3)
N(1)–N(2)–C(14)–O(3)	0.3(3)
N(1)–N(2)–C(14)–N(3)	–178.22(15)
C(14)–N(3)–C(15)–C(16)	42.5(3)
O2–C5–C6–C7	1.9(3)

The compound H_2BSC is crystallized into an orthorhombic space group $P2_1/c$. The molecule is almost planar with a dihedral angle of 28.75(11)^o with respect to the terminal rings formed by the atoms C1, C2, C3, C4, C5, C6 and C15, C16, C17, C18, C19, C20 respectively. The other phenyl ring of benzophenone formed by the atoms C7, C8, C9, C10, C11 and C12 is almost perpendicular to the first with a dihedral angle of 81.15(11)^o. The torsion angles of 177.02(15)° and (–178.22)(15)° corresponding to C6–C7–N1–N2 and N1–N2–C14–N3 moieties confirm the *E* configuration of the compound with respect to the C7–N1 and N2–C14 bonds. The C7–N1 bond distance 1.291(2) Å is appreciably close to that of C=N double bond (1.28 Å), proving

the azomethine bond formation. The amido form in the solid state is evidenced by the observed bond length of 1.227 Å for C14–O3 which is very close to the formal C=O bond length 1.21 Å [25]. The torsion angle of –0.3(3)^{o} for the N1–N2–C14–O3 moiety indicates that the amido oxygen is positioned *cis* to the azomethine nitrogen atom N1. The hydrazine carboxamide moiety adopts an extended conjugation with electron delocalization throughout the N3–C14–O3–N2–N1 chain as cleared from the bond distances of 1.3698(19) Å, 1.364(2) Å and 1.227 Å for N1–N2, C14–N2 and C14–O3 respectively. Fig. 2.16 shows unit cell packing diagram of H_2BSC viewed along the 'c' axis.

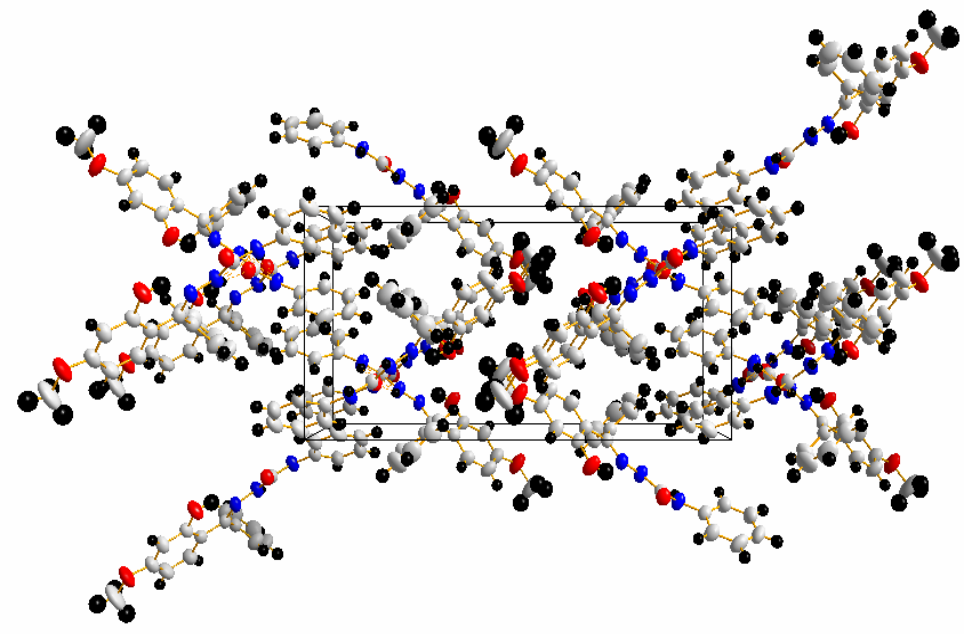

Fig. 2.16. Unit cell packing diagram of H_2BSC viewed along the 'c' axis.

The packing of the molecules in the crystal lattice is stabilized by π···π stacking interactions, π–ring interactions and hydrogen bonding interactions. A strong π···π stacking interaction is present between Cg(3)···Cg(3)^{c} (c = –x, 2–y, –z)

at an average distance of 3.8953(13) Å (Fig. 2.17). Some weak π···π interactions, present, viz. Cg(1)···Cg(2)[a] (a= x, ½–y, ½+z) and Cg(1)···Cg(2)[b] (b= x, ½–y, –½+z) at an average distance of 4.6417(13) and 4.6718(13) respectively also contribute stability to the unit cell packing. In addition C(14)–O(4)···Cg(2)[d] (d= x, 3/2–y, –½+z) interaction is also observed with O4···Cg distance of 3.4432(17) Å.

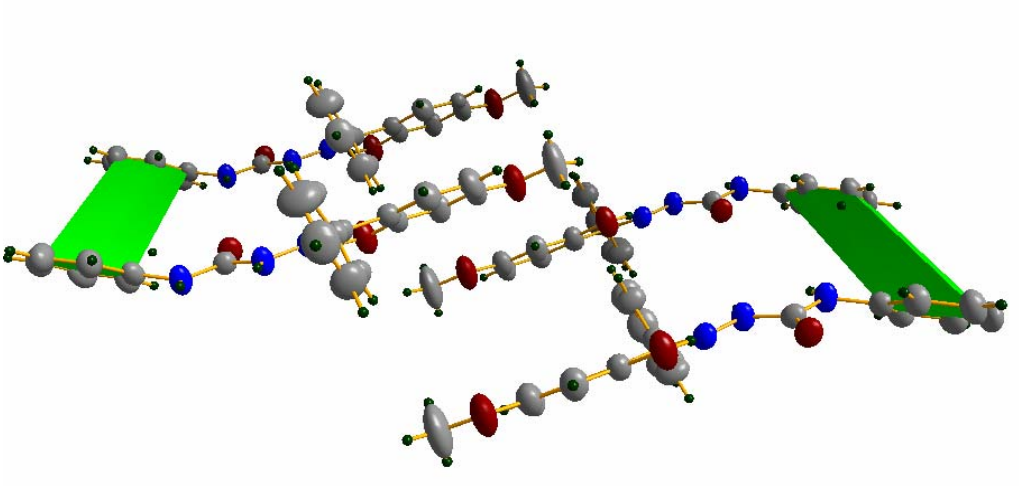

Fig. 2.17. π···π interactions present in H_2BSC.

The phenolic -OH and azomethine N1 are in *cis* configuration as evidenced from the torsion angles of –8.7(3)° and 1.9(3)° for C5–C6–C7–N1 and O2–C5–C6–C7 moieties respectively facilitating intramolecular hydrogen bond. The two prominent intermolecular hydrogen bondings N2–H2N···O3 and N3–H3···O3 both at a distance of 2.940 Å stabilize the crystal packing (Fig. 2.18). The important interaction parameters of H_2BSC are given in Table 2.8.

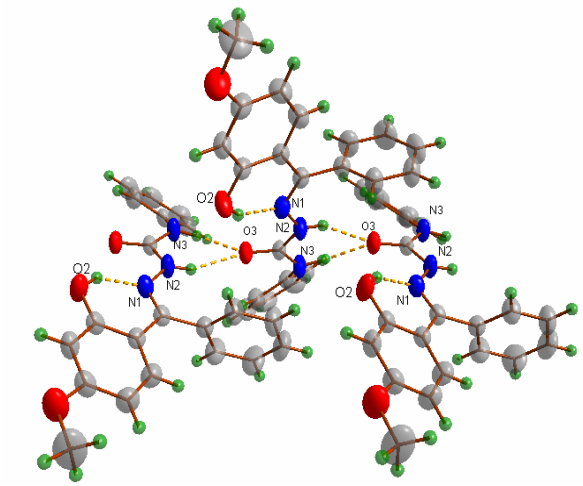

Fig. 2.18. Intermolecular and intramolecular hydrogen bonding in H_2BSC.

Table 2. 8 Interaction parameters of H_2BSC.

Hydrogen bonds and angles for H_2BSC [Å, °]

D–H	d(D–H)	d(H···A)	D–H···A	d(D···A)	A
N2–H2N	0.821	2.187	152.51	2.940	O3 [x, –y+3/2, z–1/2]
N3–H3	0.879	2.104	158.40	2.940	O3 [x, –y+3/2, z–1/2]
O2–H2'	0.900	1.798	142.03	2.568	N1

Short ring interactions

Cg(I)···Cg(J)	Cg···Cg (Å)	α°	β°
Cg(1)···Cg(2)[a]	4.6418 (13)	32.44(11)	22.48
Cg(2)···Cg(1)[b]	4.6417(13)	32.44(11)	11. 49
Cg(3)···Cg(3)[c]	3.8953(13)	0	29.11

Equivalent position code:

a= x, ½–y, ½+z; b= x, ½–y, –½+z; c= –x, 2–y, –z
Cg(1) = C(1), C(2), C(3), C(4), C(5), C(6)
Cg(2) = C(8), C(9), C(10), C(11), C(12), C(13)
Cg(3) = C(15), C(16), C(17), C(18), C(19), C(20)
α° = Dihedral angle between planes I and J(°)
β = Angle between Cg(I)–Cg(J) vector and normal to the plane I

π –ring interactions

Y–X(I)···Cg(J)	X···Cg (Å)	Y–X···Cg (°)	Y···Cg (Å)
C(14)–O(4)···Cg(2)[d]	3.4432(17)	95.51(11)	3.765

Equivalent position code:

d= x, 3/2–y, –½+z

2.3.1.3.6b. *Crystal structure of H_2BSC·DMF*

For the semicarbazone H_2BSC, the single crystal obtained from its solution of 1:1(v/v) mixture of methanol and DMF is different from that obtained from its methanolic solution. It is crystallized in monoclinic space group $P2_1/c$. Its approximate dimensions are 0.35 x 0.30 x 0.25 mm. A molecule of DMF is also present in its lattice. The experimental details are given in section 2.2.1.3.6. For refinement all H atoms on C were placed in calculated positions, guided by difference Fourier maps, with C–H bond distances of 0.93–0.97 A. H atoms were assigned as *U*iso=1.2Ueq (1.5 for Me). N2–H2′, N3–H3′ and O1–H1 H atoms were located from difference maps and restrained using *DFIX* instructions. All the C, N and O atoms of the dimethylformamide molecule are disordered over two sites A and B with relative occupancies of 0.637(4) and 0.363(4) respectively. The molecular structure of H_2BSC·DMF with the atom numbering scheme is given in Fig. 2.19.

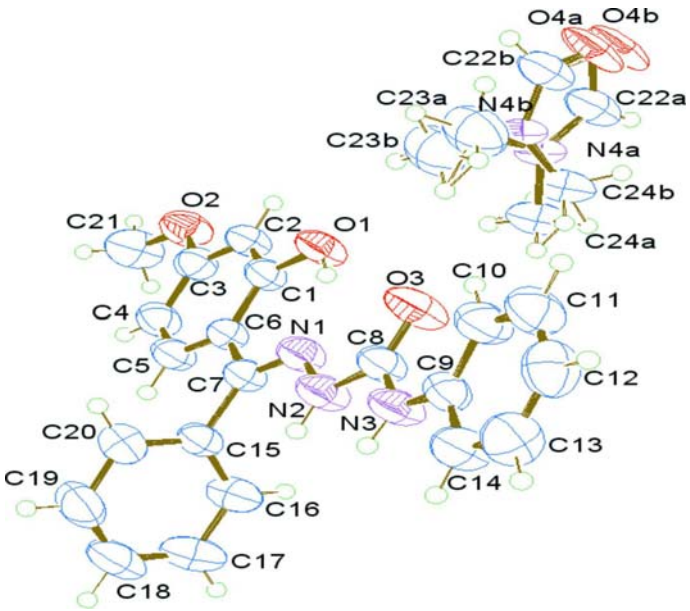

Fig. 2.19. The molecular structure of H_2BSC·DMF,showing the disordered DMF solvent molecule along with the atom numbering scheme.

The crystallographic data and structure refinement parameters of the compound are given in Table 2.9 and the selected bond lengths and angles are given in Table 2.10 and torsional angles in Table 2.11.

Table 2.9. Crystal data and structure refinement for $H_2BSC{\cdot}DMF$.

Empirical formula	$C_{24}H_{25.68}N_4O_4$
Formula weight	434.16
Temperature	296(2) K
Wavelength	0.71073 Å
Crystal system	Monoclinic
Space group	$P2_1/c$
Unit cell dimensions	a = 13.1155(7) Å alpha = 90°
	b = 16.9619(11) Å beta = 105.509(3)°
	c = 10.7399(5) Å gamma = 90°
Volume	2302.2(2) $Å^3$
Z	4
Calculated density	1.253 Mg/m^3
Absorption coefficient	0.087 mm^{-1}
F(000)	918.7
Crystal size	0.35 x 0.30 x 0.25 mm
Theta range for data collection	2.31 to 25.00°.
Limiting indices	$-15 \le h \le 15$, $-19 \le k \le 20$, $-12 \le l \le 12$
Reflections collected / unique	17398 / 4066 [R(int) = 0.0688]
Completeness to theta = 25.00	99.9%
Absorption correction	Semi–empirical from equivalents
Max. and min. transmission	0.9790 and 0.9707
Refinement method	Full–matrix least–squares on F^2
Data / restraints / parameters	4061 / 7 / 315
Goodness–of–fit on F^2	1.029
Final R indices [I>2sigma(I)]	$R_1 = 0.0584$, $wR_2 = 0.1571$
R indices (all data)	$R_1 = 0.0803$, $wR_2 = 0.1785$
Extinction coefficient	0.0084(18)
Largest diff. peak and hole	0.287 and –0.284 e. $Å^{-3}$

$R_1 = \Sigma||F_o| - |F_c|| / \Sigma|F_o|$

$wR_2 = [\Sigma w(F_o^2-F_c^2)^2 / \Sigma w(F_o^2)^2]^{1/2}$

The C8–O3 bond length of 1.208(3) Å indicates the molecule exists in the amido form in the solid state. The N1–C7 bond length of 1.292(3) Å confirms its significant double bond character. The values of the N1–N2 and N2–C8 bond distances of 1.363(3) Å and 1.378(3) Å respectively are greater than the value for a double bond and less than the value for a single bond which indicate appreciable delocalization of π–electron density over the semicarbazone chain. The molecule is synperiplanar with a dihedral angle of 14.43(12) between rings 1 and 2 (ring 1–C1, C2, C3, C4, C5, C6 and ring 2–C9, C10, C11, C12, C13, C14) and the molecule exists in *E* configuration with respect to C7–N1 bond. The torsion angle values, 179.54(19)^o and 175.9(2)^o corresponding to C6–C7–N1–N2 and N1–N2–C8–N3 moieties confirm the *E* configuration of the compound with respect to the C7–N1 and N2–C8 bonds. The torsion angle of -3.8(3)^o for the N1–N2–C8–O3 moiety indicates that the amido oxygen is positioned *cis* to the azomethine nitrogen atom N1.

The torsion angles of -1.6(3)^o and -1.2(3)^o for O1–C1–C6–C7 and C(1)–C(6)–C(7) N(1) moieties respectively confirm the *cis* configuration of phenolic -OH and azomethine nitrogen atom N1 and it favors intramolecular hydrogen bonding. The packing diagram of the unit cell viewed along the c axis is shown in Fig. 2.20.

Table 2.10. Bond lengths [Å] and angles [°] for H_2BSC·DMF.

O(3)–C(14)	1.227(2)	C(7)–N(1)–N(2)	119.65(17)
N(1)–C(7)	1.292(3	C(8)–N(2)–N(1)	117.48(18)
N(1)–N(2)	1.363(3)	N(1)–C(7)–C(6)	117.09(18)
N(2)–C(8)	1.378 (3)	N(1)–C(7)–C(15)	122.51(19)
N(3)–C(8)	1.356(3)	C(6)–C(7)–C(15)	120.39(17)
N(3)–C(8)	1.356(3)	O(3)–C(8)–N(3)	125.7(2)
C(6)–C(7)	1.465(3)	O(3)–C(8)–N(2)	122.2(2)
		N(3)–C(8)–N(2)	112.09(18)

Table 2.11. Torsion angles [°] for $H_2BSC \cdot DMF$.

C(7)–N(1)–N(2)–C(8)	–174.9(2)
N(2)–N(1)–C(7)–C(6)	–179.54(19)
N(2)–N(1)–C(7)–C(15)	0.3(3)
N(1)–N(2)–C(8)–O(3)	–3.8(4)
N(1)–N(2)–C(8)–N(3)	175.9(2)
O(1)–C(1)–C(6)–C(7)	–1.6(3)

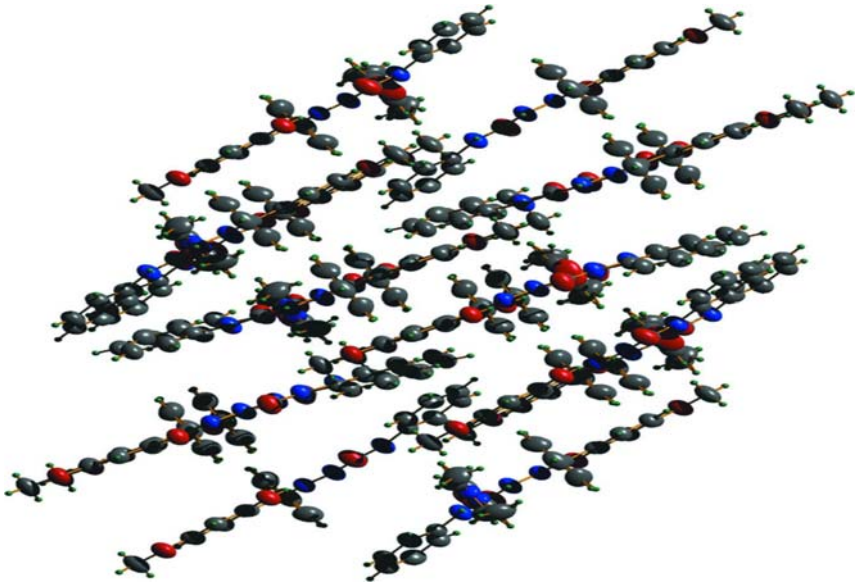

Fig. 2.20. A view of the unit cell along *c* axis.

Table 2.12. Interaction parameters of H_2BSC·DMF.

Hydrogen bonding [Å, °].

D–H···A	d(D–H)	d(H···A)	d(D···A)	<(DHA)
N(3)–H(3'···O(4)#1	0.846(17)	2.014(18)	2.838(3)	164(3)
N(2)–H(2')···O(4)#1	0.867(17)	2.19(2)	2.940(3)	145(3)
O(1)–H(1)···N(1)	0.886(18)	1.78(2)	2.565(2)	147(3)

Symmetry transformations used to generate equivalent atoms:

#1 x, y, z–1

Short ring interactions

Cg(I)···Cg(J)	**Cg···Cg (Å)**	**α°**	**β°**
Cg(1)···Cg(1)[a]	3.6561(13)	0	13.84
Cg(2)···Cg(2)[b]	4.8933(15)	24.34(12)	35.33
Cg(2)···Cg(1)[c]	4.8932(13)	24.34(12)	51.43
Cg(3)···Cg(1)[d]	4.9747(13)	88.60(12)	59.31

Equivalent position code:

a=1– x, 1–y, 1–z; b= x, ½–y, –½+z; c= –x, 2–y, –z

Cg(1) = C(1), C(2), C(3), C(4), C(5), C(6)

Cg(2) = C(8), C(9), C(10), C(11), C(12), C(13)

Cg(3) = C(15), C(16), C(17), C(18), C(19), C(20)

α = Dihedral angle between planes I and J (°)

β = Angle between Cg(I)–Cg(J) vector and normal to the plane I

π–ring interactions

Y–X(I)···Cg(J)	**X···Cg (Å)**	**Y–X···Cg (°)**	**Y···Cg (Å)**
C(14)–O(4)···Cg(2)[d]	3.4432(17)	95.51(11)	3.765

Equivalent position code:

d= x, 3/2–y, –½+z

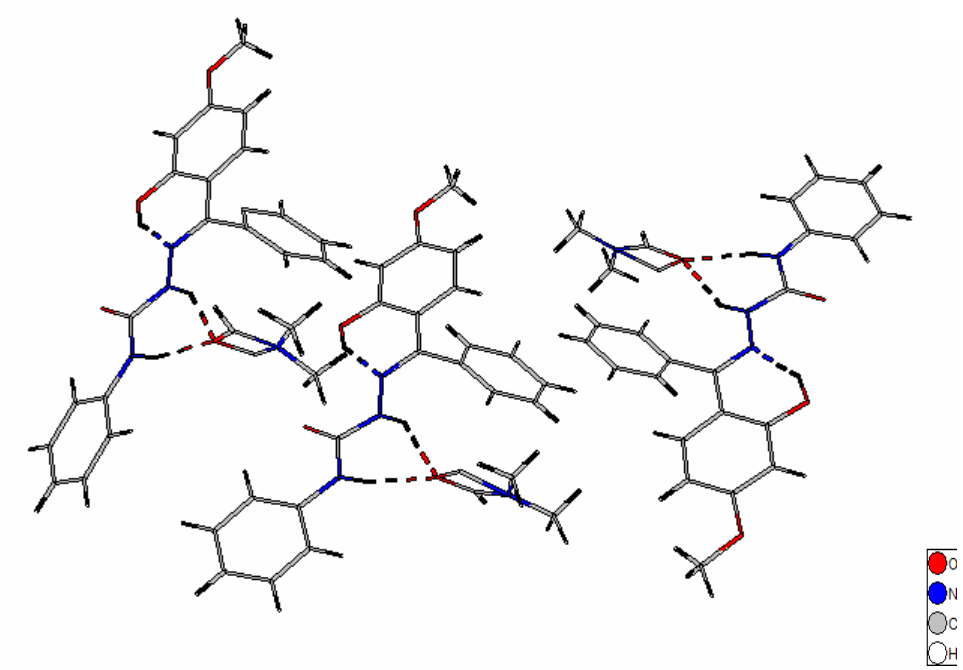

Fig. 2.21. Unit cell packing with intermolecular hydrogen bonding.

A prominent π-π interaction is observed between Cg(1)···Cg(1)^{a} at a distance of 3.6561(13) Å. Other short ring interactions are weak as they correspond to distances greater than 4 Å. An appreciable π–ring interaction is observed between C(14)–O(4)···Cg(2)^{d} at a O4···Cg distance of 3.4432(17) Å. The oxygen atom of dimethylformamide forms two hydrogen bonds with N(3)–H(3') and N(2)–H(2') with H(3')–O(4) distance of 2.838(3) Å and H(2')–O(4) distance of 2.940(3) Å respectively and is shown in Fig. 2.21.

Single crystal XRD studies of the three N^4-phenylsemicarbazones show that they adopt *E* configuration with respect to azomethine bond and exist in amido form with C=O bond length very close to the formal value of 1.21 Å. In each case the phenolic OH and azomethine N1 are in *cis* configuration facilitating intramolecular hydrogen bonding of OH to N1. 2-Hydroxy-4-

methoxyacetophenone-N^4-phenylsemicarbazone monohydrate ($H_2ASC{\cdot}H_2O$) is crystallized into a monoclinic space group $P2_1/c$, while 2-hydroxy-4-methoxybenzophenone-N^4-phenylsemicarbazone (H_2BSC) in an orthorhombic crystal system with a space group $P2_1/c$. The same compound H_2BSC is crystallized in monoclinic space group $P2_1/c$ from its solution of 1:1 (v/v) mixture of methanol and DMF with a molecule of DMF in its lattice. All the C, N and O atoms of the dimethylformamide molecule are disordered over two sites A and B with relative occupancies of 0.637(4) and 0.363(4) respectively. The packing of the molecules in the crystal lattice is stabilized by π···π stacking interactions, π–ring interactions and hydrogen bonding interactions. An important feature of the crystal packing in $H_2ASC{\cdot}H_2O$ is the formation of supramolecular structure mediated by a network of hydrogen bonds involving water molecule present in its lattice.

References

[1] Y. Kumar, S.P. Tolani, Croat. Chem. Acta 62 (1989) 73.

[2] B.K. Rai, K. Kumer, Y.P. Srivastava, Asian J. Chem. 17 (2005) 1773.

[3] V.M. Leovac, L.S. Jovanovic, V. Divjakovic, A. Pervec, I. Lebnan, T.R. Ambruster, Polyhedron 26 (2007) 49.

[4] H. Beraldo, D. Gambino, Mini-Review Med. Chem. 4 (2004) 31.

[5] N.Z. Kenezevic, V.M. Leovac, V.S. Jevtovic, S. Grguric-Sipka, T.J. Sabo, Inorg. Chem. Commun. 6 (2003) 561.

[6] P. Yogeeswari, D. Sriram, V. Veena, R. Kavya, K. Rakhra, J.V. Ragavendran, S. Mehta, R. Thirumurugan, J.P. Stables, Biomed. Pharmacother. 59 (2005) 51.

[7] J.R. Dimmock, R.N. Puthucode, J.M. Smith, M. Hetherington, J. W. Quail, U. Pugazhenthi, T. Lechler, J.P. Stables, J. Med. Chem. 39 (1996) 3984.

[8] A. Navneet, M. Pradeep, J. Zhejiang Univ SCI. 6B (7) (2005) 617.

[9] M. Shalini, P. Yogeeswari, D. Sriram, J.P. Stables, Biomed. Pharmacother. 63 (2009) 187.

[10] N.C. Kasuga, K. Sekino, C. Koumo, N. Shimada, M. Ishikawa, K. Nomiya, J. Inorg. Biochem. 84 (2001) 55.

[11] J.C. Magna, J. Vargas, R. Latorse, A. Alvarado, G. Mena, Coord. Chem. Rev. 119 (1992) 67.

[12] A. Sreekanth, U.L. Kala, C.R. Nayar, M.R.P. Kurup, Polyhedron 3 (2004) 41.

[13] R.M. Silverstein, G.C. Bassler, T.C. Morrill, Spectrometric Identification of Organic Compounds, 4th Ed., Wiley, New York (1981).

[14] T.S. Wang, Appl. Spectrosc. 22 (1968) 167.

[15] V.M. Kolb, J.W. Stupar, T.E. Janota, W.L. Duax, J. Org. Chem. 54 (1989) 2341.

[16] U.L. Kala, S. Suma, M.R.P. Kurup, S. Krishnan, R.P. John, Polyhedron 26 (2007) 1427.

[17] P.F. Rapheal, E. Manoj, M.R.P. Kurup, Polyhedron 26 (2007) 5088.

[18] M. Kuriakose, M.R.P. Kurup, E. Suresh, Polyhedron 26 (2007) 2713.

[19] W. Kemp. Organic Spectroscopy, 3rd Ed., Macmillan, Hampshire (1996).

[20] SMART and SAINT, Area Detector Software Package and SAX Area Detector Integration Program, Bruker Analytical X-ray; Madison, WI, USA, 1997.

[21] SADABS, Area Detector Absorption Correction Program; Bruker Analytical X-ray; Madison, WI, 1997.

[22] G.M. Sheldrick, SHELXTL-PLUS,Crystal Structure Analysis Package; Bruker Analytical X-ray, Madison, WI, USA, 1997.

[23] K. Brandenburg, Diamond Version 3.2g, Crystal Impact GbR, Bonn, Germany, 2010.

[24] J. March, Advanced Organic Chemisty, Reactions, Mechanisms and Structure, 4th Ed., Wiley, New York, 1992.

[25] F.H. Allen, O. Kennard, D.G. Watson, l. Brammer, A.G. Orpen, R. Taylor, J. Chem. Soc., Perkin Trans. 2 (1987) S1.

[26] T.A. Reena, E.B. Seena, M.R.P. Kurup, Polyhedron 27 (2008) 1825.

[27] M. Sithambaresan, M.R.P. Kurup, Acta Cryst. E 67 (2011) o2972.

[28] D.X. West, A.M. Stark, G.A. Bain, A.E. Liberta, Trans. Met. Chem. 21 (1996).

…..ꕥ…..

Chapter 3

SYNTHESES AND SPECTRAL CHARACTERIZATION OF OXIDOVANADIUM(IV) COMPLEXES OF N^4-PHENYLSEMICARBAZONES

Contents

3.1. Introduction

Vanadium is a pervasive element of biological systems, being widely distributed across the food supply. It has been estimated to comprise about 136 ppm of the earth's crustal rocks. It is the fifth most abundant transition metal after Fe, Ti, Mn and Zr. This element 23, first claimed to have been discovered by A.M. del Rio in 1801, then rediscovered by N.G. Sefström in 1830, was named vanadium after Vanadis, the Scandinavian goddess of beauty, because of the richness and variety of colors in its compounds. While vanadium is widely spread with a natural abundance of ~0.014% there are few concentrated deposits and pure vanadium is rare due to its reactivity towards oxygen. Although vanadium can possess formal oxidation states from +5 to -1, the most stable under normal conditions is +4, with +3 and +2 states also having many well-characterized compounds.

The +4 oxidation state is most notable for the uniquely stable VO^{2+} (vanadyl) ion which retains its identity throughout a wide variety of reactions and forms many complexes. Many of compounds containing the VO^{2+} unit

are blue to green, form stable complexes with *F*, *Cl*, *O*, and *N* donor semicarbazones and can be cationic, neutral, or anionic. Most often, these compounds are 5 coordinate and are almost always square pyramidal while in the case of hexacoordinated complexes octahedral geometry predominates.

Recent studies indicate that vanadium, which is proposed to be one of essential trace elements in animals and humans, relates to both glucose and lipid metabolisms. Oxidovanadium(IV) and vanadate(V) are the main species present in solution under physiological conditions. The physiological effects are in many cases a consequence of good complexation behavior of VO^{2+}, and the chemical similarity of phosphate and vanadate. The coordination chemistry of vanadium has received considerable attention since the discovery of vanadium in enzymes like bromoperoxidases and azotobactervinelandii [1].

Medicinal applications of vanadium compounds have focused on their in *vitro* and in *vivo* activity in the treatment of insulin deficiency [2]. Vanadium complexes of semicarbazones of low molecular weight could in principle be useful as potential biomimetic drugs. Vanadium coordination compounds are much safer as antidiabetic agents than inorganic vanadium salts [3]. Besides the antidiabetic effects for which it is now so well known, vanadium compounds also exhibit a number of therapeutic effects including antitumor [2-5], anti-inflammatory [3] and antibacterial [6] activities.

This chapter deals with the syntheses and spectral characterization of mononuclear and binuclear oxidovanadium(IV) complexes with two new ONO donor semicarbazones, 2-hydroxy-4-methoxyacetophenone-N^4-phenylsemicarbazone (H_2ASC), 2-hydroxy-4-methoxybenzophenone-N^4-phenylsemicarbazone (H_2BSC) and some heterocyclic compounds like 1,10-

phenanthroline, 2,2′-bipyridine, 4,4′-dimethyl-2,2′-bipyridine and 4-picoline as coligands.

3.2. Experimental

3.2.1. Materials

2-Hydroxy-4-methoxyacetophenone (Sigma-Aldrich), 2-hydroxy-4-methoxybenzophenone (Sigma-Aldrich), N^4-phenylsemicarbazide (Sigma-Aldrich), vanadyl sulphate monohydrate (Aldrich), 1,10-phenanthroline (Ranchem), 2,2′-bipyridine (Qualigens), 4,4′-dimethyl-2,2′-bipyridine (Qualigens), and 4-picoline (BDH) were of analar grade and were used as received. Solvent used was methanol.

3.2.2. Syntheses of semicarbazones

2-Hydroxy-4-methoxyacetophenone-N^4-phenylsemicarbazone monohydrate ($H_2ASC{\cdot}H_2O$) and 2-hydroxy-4-methoxybenzophenone-N^4-phenylsemicarbazone (H_2BSC) were synthesized as described in Chapter 2.

3.2.3. Syntheses of VO(IV) complexes of 2-hydroxy-4-methoxyacetophenone-N^4-phenylsemicarbazone (H_2ASC)

3.2.3.1. *$[VO(ASC)]_2{\cdot}2H_2O$ (1)*

The complex **1** was prepared by refluxing a methanolic solution of $H_2ASC{\cdot}H_2O$ (0.317 g, 1 mmol) and an aqueous solution of vanadyl sulfate (0.163 g, 1 mmol) for 5 h. The resulting solution was allowed to evaporate at room temperature and the yellow colored product formed was filtered, washed with methanol, followed by ether and dried over P_4O_{10} in *vacuo*.

Elemental Anal. Found (Calcd.) (%): C: 49.91 (50.27); H: 4.60 (4.48); N: 10.70 (10.99)

3.2.3.2. *[VO(ASC)(bipy)]·2H$_2$O (2)*

An aqueous solution of vanadyl sulfate (0.163 g, 1 mmol) was added to a hot methanolic solution of $H_2ASC·H_2O$ (0.317 g, 1 mmol) and 2,2′-bipyridine (0.156 g, 1 mmol) and refluxed for 4 h. The reddish brown solution was allowed to stand at room temperature and after slow evaporation the yellowish brown complex formed was filtered, washed with methanol and then ether and dried over P_4O_{10} in *vacuo.*

Elemental Anal. Found (Calcd.) (%): C: 56.70 (56.12); H: 4.90 (4.89); N: 12.3 (12.59)

3.2.3.3. *[VO(ASC)(dmbipy)]·3H$_2$O (3)*

The complex **3** was synthesized by adding an aqueous solution of vanadyl sulfate (0.163 g, 1 mmol) to a hot methanolic solution of $H_2ASC·H_2O$ (0.317 g, 1 mmol) and the base 4,4′-dimethyl-2,2′-bipyridine (0.156 g, 1 mmol) and refluxing the solution for 6 h. The complex formed was collected, washed with methanol and ether and dried over P_4O_{10} in *vacuo*.

Elemental Anal. Found (Calcd.) (%): C: 55.22 (55.81); H: 4.90 (5.52); N: 11.30 (11.62)

3.2.4. Syntheses of VO(IV) complexes of 2-hydroxy-4-methoxybenzophenone-N^4-phenylsemicarbazone

3.2.4.1. *[VO(BSC)]$_2$·2H$_2$O (4)*

A hot solution of H_2BSC (0.361 g, 1 mmol) in 20 ml of methanol was treated with an aqueous solution of vanadyl sulfate (0.163 g, 1 mmol) and was refluxed for 5 h. The resulting brown solution was allowed to stand at room temperature and after slow evaporation the yellow complex was separated out.

It was filtered, washed with methanol followed by ether and dried over P_4O_{10} in *vacuo*.

Elemental Anal. Found (Calcd.) (%): C: 55.01 (54.55); H: 4.56 (4.58); N: 9.03 (9.09)

3.2.4.2. *[VO(BSC)(phen)]·2H$_2$O (5)*

Methanolic solutions of H_2BSC (0.361 g, 1 mmol) and 1,10-phenanthroline (0.198 g, 1 mmol) and an aqueous solution of vanadyl sulfate (0.163 g, 1 mmol) were mixed and the resulting mixture was refluxed for 4 h. The dark yellow colored complex separated out was filtered, washed with methanol followed by ether and dried over P_4O_{10} in *vacuo*.

Elemental Anal. Found (Calcd.) (%): C: 61.78 (61.68); H: 4.80 (4.55); N: 10.75 (10.90)

3.2.4.3. *[VO(BSC)(dmbipy)]·2H$_2$O (6)*

To a methanolic solution of H_2BSC (0.361 g, 1 mmol), an aqueous solution of vanadyl sulfate (0.163 g, 1 mmol) was added. 4,4′-Dimethyl-2,2′-bipyridine (0.184 g, 1 mmol) was also added to it. The resulting mixture was refluxed for 4 h. The complex formed was green in color. It was filtered, washed with methanol, followed by ether and dried over P_4O_{10} in *vacuo.*

Elemental Anal. Found (Calcd.) (%): C: 61.82 (61.30); H: 4.73 (5.14); N: 10.53 (10.83)

3.2.4.4. *[VO(BSC)(pic)]·0.5H$_2$O (7)*

A hot methanolic solution of H_2BSC (0.361 g, 1 mmol**)** was mixed with 4-picoline (0.186 g, 1 mmol) and an aqueous solution of vanadyl sulfate (0.163 g, 1 mmol) was added to it. The resulting mixture was refluxed for 4 h.

The yellow product formed was filtered, washed with methanol followed by ether and dried over P_4O_{10} in *vacuo*.

Elemental Anal. Found (Calcd.) (%): C: 61.63 (61.37); H: 5.20 (4.77); N: 10.56 (10.60)

3.3. Results and discussion

The oxidovanadium(IV) complexes of N^4-phenylsemicarbazones **1** and **4** were synthesized by refluxing methanolic solutions of the respective semicarbazone and vanadyl sulphate monohydrate in 1:1 ratio. The complexes **2**, **3**, **5**, **6** and **7** were synthesized by refluxing the methanolic solution of semicarbazone, vanadyl sulfate monohydrate and heterocyclic bases in 1:1:1 ratio. Out of the seven complexes prepared complexes **1** and **4** are binuclear, while the remaining five are mononuclear metal chelates. All the complexes are yellow in color except **6**, which is green in color. They are soluble in solvents like DMSO, DMF and CH_3CN. In all the complexes synthesized the semicarbazones coordinated to the metal centre in the iminol form and act as dideprotonated tridentate semicarbazones. The synthesized compounds are characterized by the following physico-chemical methods.

3.3.1. Elemental analyses

Elemental (C, H, N) analyses of all complexes were carried out using a Vario EL III CHNS analyzer at SAIF, Kochi, India and the values were given in Sections 3.2.3 and 3.2.4.

3.3.2. Molar conductivity

The conductivity measurements were made at 298 K with a systronic model 303 direct reading conductivity bridge in DMF (10^{-3} M) solutions and

the observed values were found to be less than 12 ohm^{-1} cm^2 mol^{-1} which is very much less than the value of 65-90 ohm^{-1} cm^2 mol^{-1} reported for a 1:1 electrolyte in the same solvent [7]. This confirmed the nonelectrolytic nature of the complexes.

3.3.3. Magnetic susceptibility

Magnetic moments of the complexes were calculated from the magnetic susceptibility measurements at room temperature. Complexes **1** and **4** showed μ_{eff} 1.20 BM and 1.27 BM respectively and this subnormal values are due to the strong antiferromagnetic exchange, suggesting dimeric nature to these complexes [8]. All other complexes exhibited magnetic moments having slight deviations from the spin only value for a d^1 system. All the complexes contain the VO^{2+} unit in which vanadium is in +4 oxidation state. The magnetic moment and molar conductivity values of the complexes are given in Table 3.1.

Table 3.1. Molar conductivities and magnetic susceptibilities of VO(IV) complexes.

Compound	λ_m^*	μ_{eff} (B.M.)
$[VO(ASC)]_2 \cdot 2H_2O$ (**1**)	8	1.20
$[VO(ASC)(bipy)] \cdot 2H_2O$ (**2**)	11	1.67
$[VO(ASC)(dmbipy)] \cdot 3H_2O$ (**3**)	6.5	1.77
$[VO(BSC)]_2 \cdot 3H_2O$ (**4**)	2.8	1.27
$[VO(BSC)(phen)] \cdot 2H_2O$ (**5**)	4.5	1.65
$[VO(BSC)(dmbipy)] \cdot 2H_2O$ (**6**)	3.0	1.74
$[VO(BSC)(pic)] \cdot 0.5H_2O$ (**7**)	9	1.78

*Molar conductivity (in mho cm^2 mol^{-1}) taken in 10^{-3} M DMF solution.

3.3.4. Infrared spectra

The IR spectra of the seven vanadium complexes were recorded in the 4000-400 cm^{-1} range with KBr pellets. The shift of characteristic IR bands of the complexes from the metal free phenyl semicarbazones provide significant indications regarding the ligating behavior to the metal centre. By coordination, shifts of the ν(C=N), ν(C=O) and the phenolic ν(C–O) bands were observed for the complexes. They are consistent with the tridentate coordination of the phenyl semicarbazones through the enolic oxygen atom, the azomethine nitrogen atom and the phenolic oxygen atom [9]. Some IR spectra are shown in Figs. 3.1-3.3.

The bands at 3295 and 3145 cm^{-1} due to ν(N^2H), 1692 and 1662 cm^{-1} due to ν(C=O) for the semicarbazones $H_2ASC{\cdot}H_2O$ and H_2BSC respectively disappeared on complexation indicating the involvement of the carbonyl oxygen in bonding as enolate form. The presence of a new band in the region 1540-1571 cm^{-1}due to the newly formed ν(C=N) bond confirms this statement. The shift of ν(C=N) of the semicarbazones at 1619 and 1631 cm^{-1} to lower wavenumbers in the metal complexes in the region (1574-1615 cm^{-1}) indicates the coordination of azomethine nitrogen to the metal [10]. The positive shift of the characteristic ligand bands due to ν(N–N) in the spectra of complexes in the range 1055-1109 cm^{-1} is owing to the increase in double bond character, counterbalancing the electron density via donation to the metal [11]. The azomethine nitrogen coordination is further evidenced by the presence of new bands in the range 415-440 cm^{-1} assignable to ν(V–N) for the complexes [12]. The sharp bands at 3535 and 3316 cm^{-1} for $H_2ASC{\cdot}H_2O$ and H_2BSC respectively assigned to the phenolic –OH groups disappeared and it gives evidence for the coordination in its deprotonated form [13]. This causes ν(C–O) to shift to lower

frequencies and a new band in the range 510-550 cm^{-1}, assigned to ν(V–O) is found in complexes [14]. Furthermore, the compounds containing the vanadyl unit have a characteristic strong V=O stretching band. For these complexes a strong band is observed in the range 935-965 cm^{-1} due to terminal V= O stretching and this is close to the usual range (960 ± 50 cm^{-1}) observed for the majority of oxidovanadium (IV) complexes [15]. In addition to this a prominent band is observed at *ca.* 896 and at 846 cm^{-1} for the binuclear complexes **1** and **4** respectively due to the V–O–V bridge vibrations [16,17]. Since IR spectra are rich with bands tentative assignments of vibrational bands were made and are listed in Table 3.2.

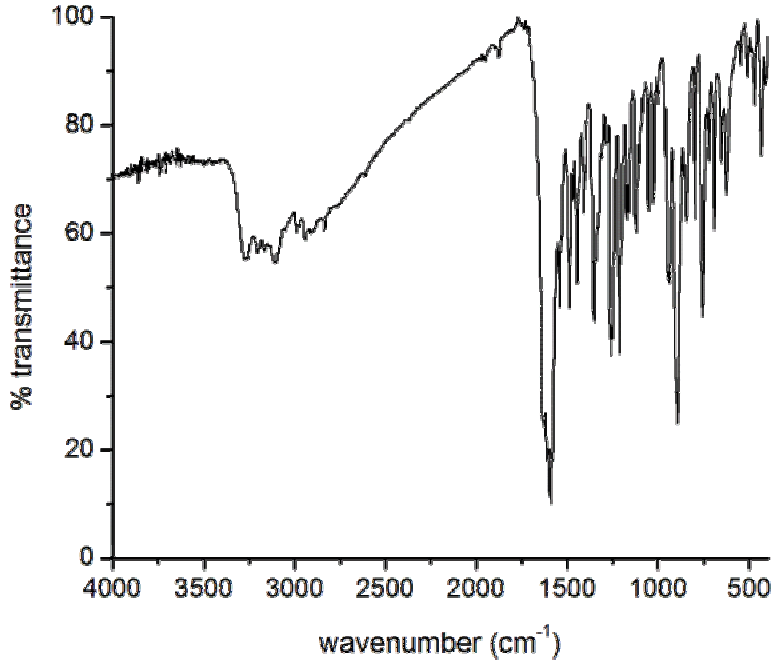

Fig. 3.1. IR spectrum of $[VO(ASC)]_2 \cdot 2H_2O$ (1).

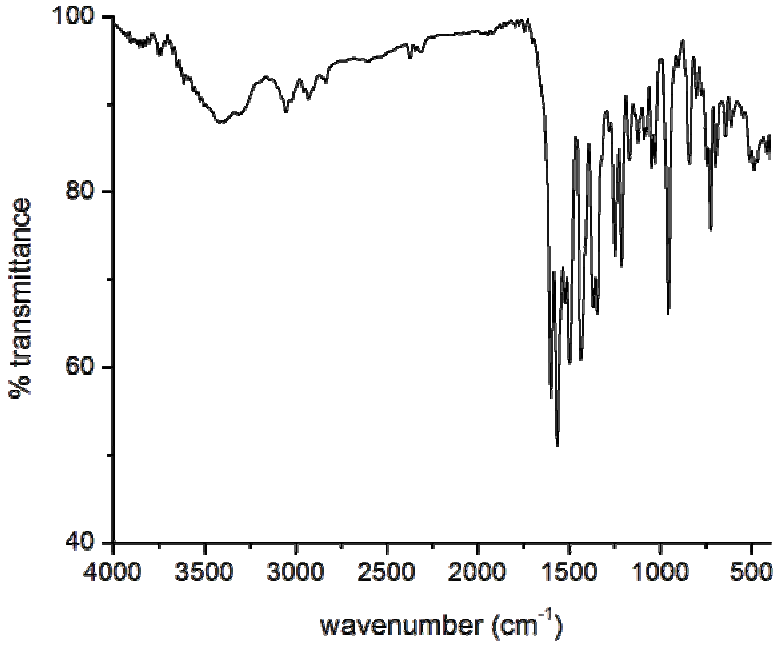

Fig. 3.2. IR spectrum of [VO(BSC)(phen)]·2H_2O (5).

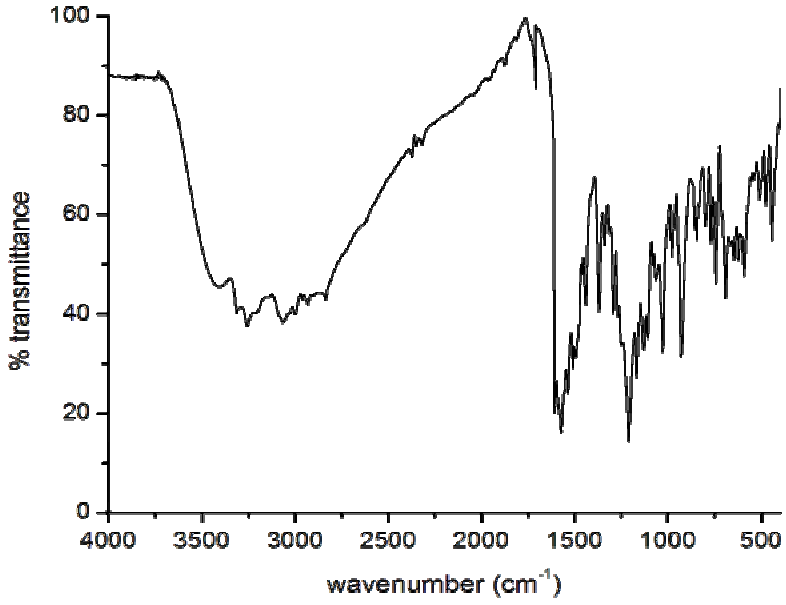

Fig. 3.3. IR spectrum of [VO(BSC)(pic)]·0.5H_2O (7).

Table 3.2 Selected IR bands (cm^{-1}) with tentative assignments of VO(IV) complexes.

Compound	ν(C=O)	ν(C=N)	ν(C=N)[a]	ν(N–N)	ν(C–O)	ν(N^2–H)	ν(V=O)	ν(V–O)	ν(V–N)
$H_2ASC\cdot H_2O$	1692	1619	----	1020	1270	3295	-----		
$[VO(ASC)]_2\cdot 2H_2O$ (**1**)	----	1591	1542	1055	1255	-----	944	550	432
$[VO(ASC)(bipy)]\cdot 2H_2O$ (**2**)	----	1604	1530	1089	1263	-----	965	545	433
$[VO(ASC)(dmbipy)]\cdot 3H_2O$ (**3**)	----	1574	1540	1109	1246	-----	956	548	439
H_2BSC	1662	1631	----	1059	1292	3145	-----		
$[VO(BSC)]_2\cdot 2H_2O$ (**4**)	----	1615	1539	1065	1226	-----	932	510	415
$[VO(BSC)(phen)]\cdot 2H_2O$ (**5**)	----	1598	1563	1082	1245	-----	962	514	418
$[VO(BSC)(dmbipy)]\cdot 2H_2O$ (**6**)	----	1602	1566	1090	1244	-----	953	518	422
$[VO(BSC)(pic)]\cdot 0.5H_2O$ (**7**)	----	1609	1571	1065	1210	-----	935	515	429

[a] Newly formed C=N

3.3.5. Electronic spectra

The electronic spectral bands of H_2ASC and H_2BSC and their vanadyl complexes are presented in Table 3.3. For complexes **1**, **3**, **4**, **5** and **7** spectra were recorded in acetonitrile solutions and for complexes **2** and **6** in DMF solutions. The bands in the range 41750-31330 cm^{-1} attributed to the n-π* and π-π* transitions for semicarbazones suffered some shift upon complexation and they are observed in between 31050-44230 cm^{-1}. The high energy bands in the region 27630-24750 cm^{-1} are attributed to ligand to metal charge transfer (LMCT) transitions and their broadness can be explained due to the combination of O→V and N→V LMCT transitions [18]. The UV spectra of all the complexes are given in Figs. 3.4-3.7. along with the spectra of corresponding semicarbazones.

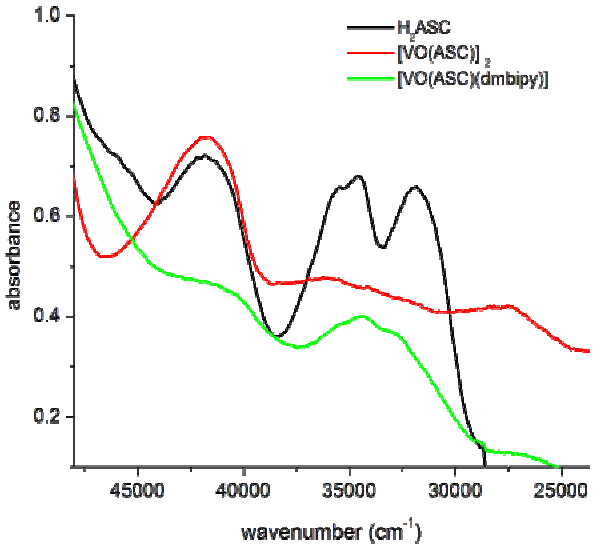

Fig. 3.4. UV spectra of H_2ASC, $[VO(ASC)]_2$ and [VO(ASC)(dmbipy)].

Table 3.3. Electronic spectral assignments (cm^{-1}) of N^4-phenylsemicarbazones and their VO(IV) complexes.

Compound	Solvent	Intraligand transitions	LMCT	*d-d*
H_2ASC	CH_3CN	31780, 34540, 35600(sh), 41750	----	----
H_2ASC	DMF	31590, 34250, 35300	----	----
[VO(ASC)]$_2$·2H_2O (**1**)	CH_3CN	31050(sh), 34080(sh), 35670, 41610	27630	18600 11600
[VO(ASC)(bipy)]·2H_2O (**2**)	DMF	33610(sh), 34550(sh), 37220	26790	----
[VO(ASC)(dmbipy)]·3H_2O (**3**)	CH_3CN	32260(sh), 34270, 35770(sh), 41380	26740	16280 12250
H_2BSC	CH_3CN	31330, 33820, 35030, 41680	----	----
H_2BSC	DMF	31030, 32070 (sh), 33610, 34890	----	----
[VO(BSC)]$_2$·2H_2O (**4**)	CH_3CN	31780(sh), 32310(sh), 34300, 41180	26810	17550 12500
[VO(BSC)(phen)]·2H_2O (**5**)	CH_3CN	31100(sh), 34230(sh), 37050, 44230	24750	18800 12000
[VO(BSC)(dmbipy)]·2H_2O (**6**)	DMF	31080, 33640, 34870, 37810	25840	----
[VO(BSC)(pic)]·0.5H_2O (7)	CH_3CN	31430, 33860, 34950(sh), 40780	25780	----

sh= shoulder

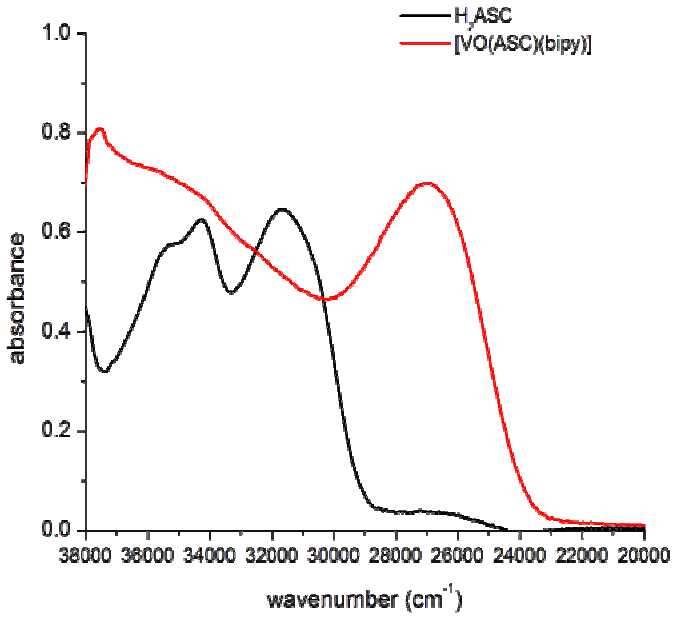

Fig. 3.5. UV spectra of H_2ASC and [VO(ASC)(bipy)].

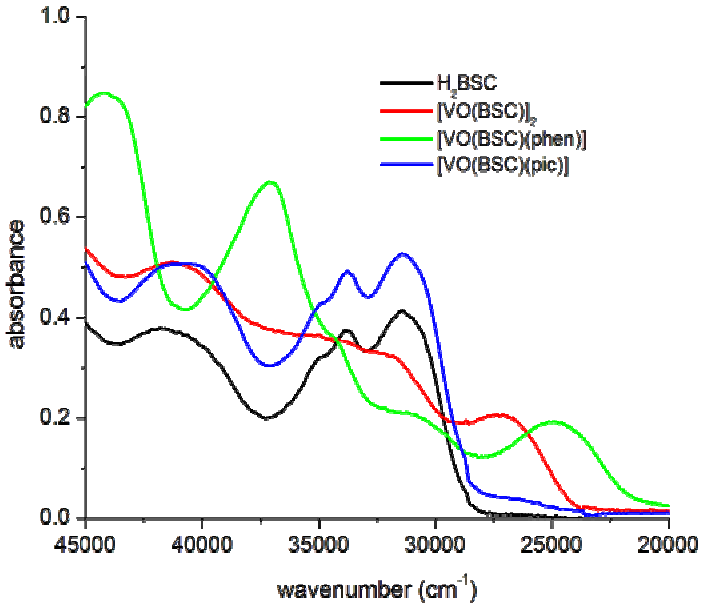

Fig. 3.6. UV spectra of H_2BSC, $[VO(BSC)]_2$, [VO(BSC)(phen)] and [VO(BSC)(pic)].

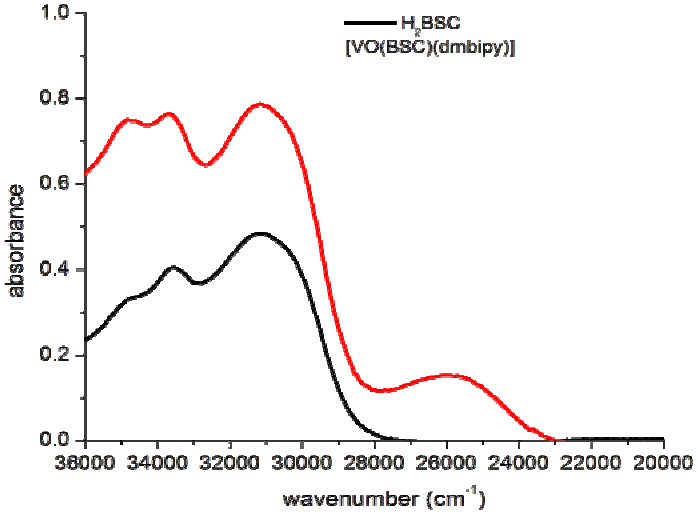

Fig. 3.7. UV spectra of H_2BSC and [VO(BSC)(dmbipy)].

Ballhausen and Gray (BG scheme) have provided a convenient energy level scheme for VO(IV) type complexes. In general most of the oxidovanadium complexes show three low intensity bands in the 12000-24000 cm^{-1} range. in the visible region, with various semicarbazones arising from the tetragonal compression caused by V=O bond, which results in further splitting of d orbitals and give rise to three spin allowed transitions, assigned to $^2E \leftarrow {}^2B_2$ (ν_1) ($d_{xy} \rightarrow d_{xz}, d_{yz}$), $^2B_1 \leftarrow {}^2B_2$ (ν_2) ($d_{xy} \rightarrow d_{x^2-y^2}$), $^2A_1 \leftarrow {}^2B_2$ (ν_3) ($d_{xy} \rightarrow d_{z^2}$) [19]. Since the ^2E and $^2B_1$ levels are very close in energy and may cross and result a weak broad band. In our present investigation complexes **1, 4** and **5** showed two weak *d-d* bands, while in compound **3** two distinct *d-d* bands due to ν_1 and ν_2 are observed. Generally the third band is not observed and is thought to be buried beneath the low energy tail of the much more intense charge transfer bands [20].

The two bands at 11600 and 18600 cm^{-1} for the complex **1** are due to the ν_1 and ν_2 transitions, while in **4** these transitions are observed at 12500 and

17550 cm^{-1} respectively. In compound **3** the distinct energy bands at 12250 and 16280 cm^{-1} are corresponding to ν_1 and ν_2 transitions. In complex **5** these *d-d* bands are at *ca*. 18800 and 12000 cm^{-1} [21]. In all other complexes the expected *d-d* bands are not observed and are probably obscured by the intense LMCT absorptions. The observed electronic spectra of the complexes in DMF, in the region 22000-11000 cm^{-1} are presented in Figs. 3.8.1-3.8.4.

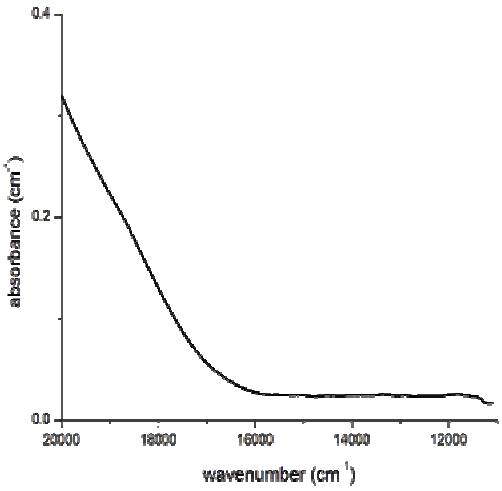

Fig. 3.8.1. $[VO(ASC)]_2$

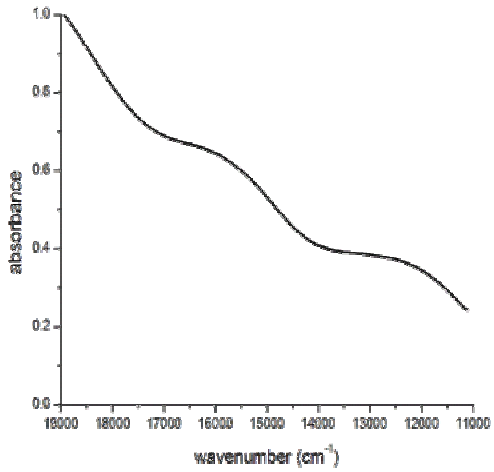

Fig. 3.8.2. [VO(ASC)(dmbipy)]

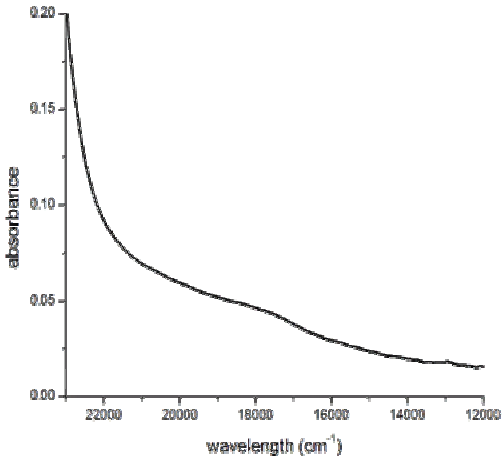

Fig. 3.8.3. $[VO(BSC)]_2$

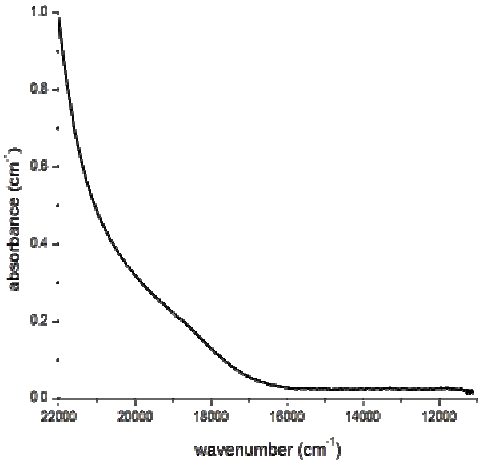

Fig.3.8.4. [VO(BSC)(phen)]

Fig. 3.8. Visible spectra of VO(IV) complexes.

3.3.6. Electron paramagnetic resonance spectra

Electron paramagnetic resonance is a branch of absorption spectroscopy in which radiation of microwave frequency is absorbed by a molecule or ion having unpaired electron(s). Thus it is a convenient and effective way to probe the electronic structure of paramagnetic molecules.

The oxidation state of the central vanadium atom in the complexes was confirmed by the measurements of EPR spectroscopy. In vanadyl complexes vanadium is in +4 oxidation state with d^1 configuration and they are EPR active. Complexes containing the VO_2^+ unit in which vanadium is in +5 oxidation state with d^0 configuration are EPR silent. All seven complexes synthesized were EPR active and contain VO^{2+} unit. For the case of vanadium(IV) the nuclear spin $I = 7/2$ and eight and fifteen hyperfine lines are expected for mononuclear and binuclear complexes respectively, separated by the hyperfine coupling constant, A.

EPR spectra of all the oxidovanadium complexes were recorded in polycrystalline state at 298 K and in DMF solution at 77 K using TCNE as the standard with 100 kHz modulation frequency, modulation amplitude 1 G and 9.4 GHz microwave frequency. The spectral parameters are summarized in Table 3.4. The EPR spectra of complexes **(2- 5)** in the solid state at 298 K are isotropic in nature and hence only one g value, arising due to dipolar interactions and enhanced spin-lattice relaxation. Compounds **1**, **6** and **7** gave axial spectra in the polycrystalline state in which that of **7** is poorly resolved and difficult to interpret. $A_{||}$ complexes in DMF solution at 77 K displayed well resolved axial anisotropy with two sets of eight line pattern with $g_{||} < g_{\perp}$ and $A_{||} > A_{\perp}$ relationship, characteristic of an axially compressed

d^1_{xy} configuration [22,23]. The absence of any ligand nitrogen superhyperfine lines on the vanadium line is an explicit indication of the sole electron lying in the d_{xy} orbital $^2B_2$ ground state, localized on metal, thus excluding the possibility of its direct interaction with the semicarbazones [24,25].

Some of the EPR spectra are simulated and the experimental and simulated best fits are presented. The spectrum of the compound **1** is axial both in polycrystalline state at 298 K and in frozen DMF at 77 K. The spectrum in polycrystalline state is presented in Fig. 3.9.

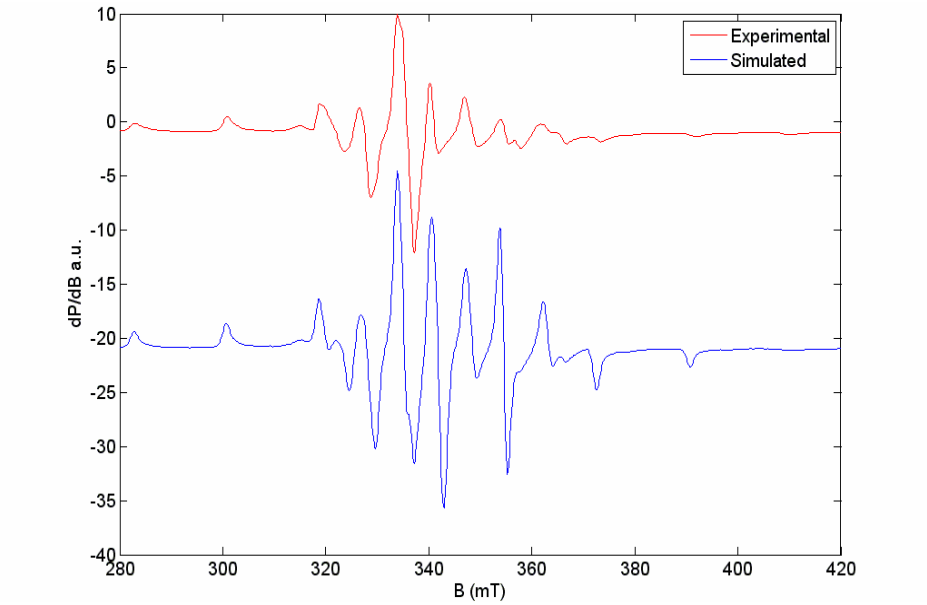

Fig. 3.9. The EPR spectrum of $[VO(ASC)]_2 \cdot 2H_2O$ (1) in polycrystalline state at 298 K.

It exhibits well resolved axial anisotropy with two sets of eight line pattern, characteristic of an unpaired electron being coupled to the vanadium nuclear spin (^{51}V, I=7/2) with anisotropic hyperfine parameters $g_{\|}$=1.962 and $g_{\perp}$=1.980 and $A_{\|}$ = 169×10^{-4} cm^{-1}, $A_{\perp}$ = 55×10^{-4} cm^{-1}. In the case of

binuclear complexes, a half field signal is expected due to forbidden $\Delta M_s = \pm 2$ transition. But in this compound half field is absent, indicating that the spin-spin interaction of this compound is not so significant such that each unpaired electron virtually interact with only one vanadium centre [26]. The spectrum in frozen DMF at 77 K is presented in Fig. 3.10. Here also the spectrum displays well resolved axial anisotropy with $g_{\|}$ = 1.951 and $g_{\perp}$ = 1.980 and $A_{\|}$ = 164×10^{-4} cm^{-1}, $A_{\perp}$ = 52×10^{-4} cm^{-1}.

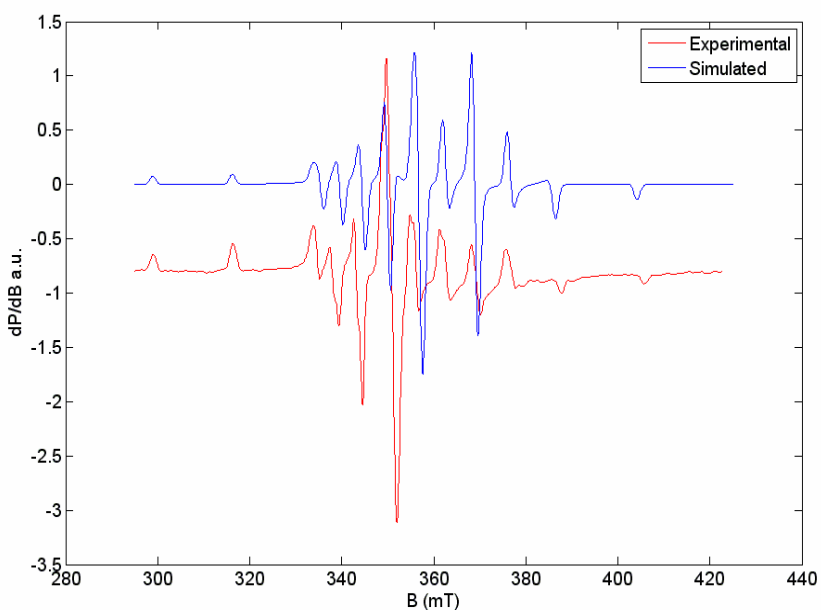

Fig. 3.10. The EPR spectrum of [VO(ASC)]$_2$ in DMF at 77 K.

The spectrum of compound **2** in polycrystalline state is isotropic with g_{iso} = 1.977 (Fig. 3.11) and in frozen DMF at 77 K it displays a well resolved axial anisotropy (Fig. 3.12) with two sets of eight- line pattern with anisotropic hyperfine parameters $g_{\|}$ = 1.914 and $g_{\perp}$ =1.975 and $A_{\|}$ = 171×10^{-4} cm^{-1}, $A_{\perp}$ = 68×10-4 cm^{-1}.

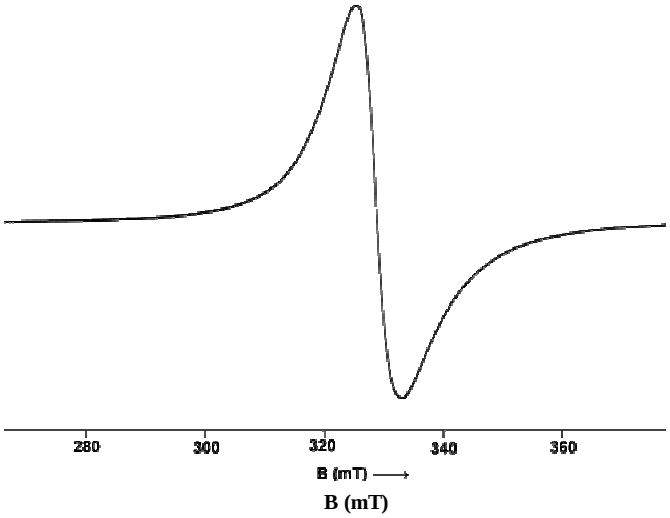

Fig. 3.11. EPR spectrum of [VO(ASC)(bipy)]·2H_2O (2) in polycrystalline state at 298 K.

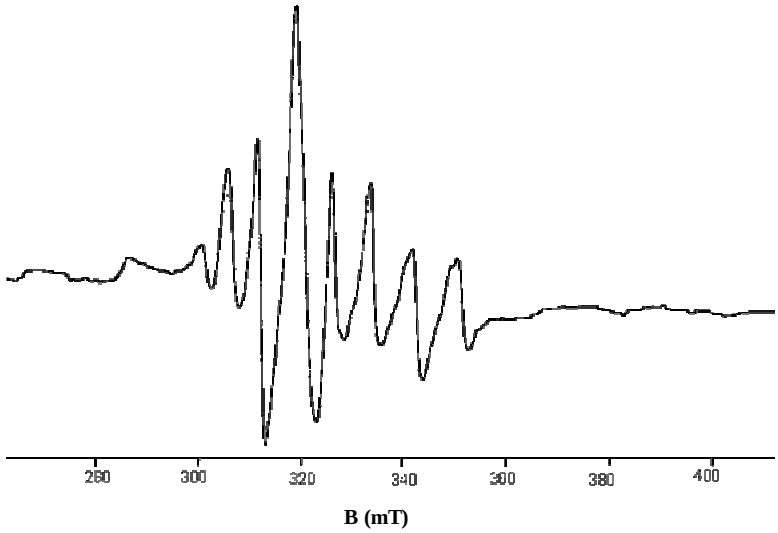

Fig. 3.12. EPR spectrum of [VO(ASC)(bipy)] in DMF 77 K.

Compound **3** exhibits an isotropic spectrum, with g_{iso} 1.975 (Fig. 3.13). The anisotropic EPR spectrum obtained for this compound in frozen DMF is depicted in Fig. 3.14. For this compound $g_{\|} = 1.945$ and $g_{\perp} = 1.979$, $A_{\|} = 152\times10^{-4}$ cm^{-1} and $A_{\perp} = 52\times10^{-4}$ cm^{-1}. The $g_{\|} < g_{\perp}$ and $A_{\|} > A_{\perp}$ relationships are consistent

with an axially compressed octahedral geometry around the vanadium(IV) centre with the unpaired electron in the d_{xy} orbital.

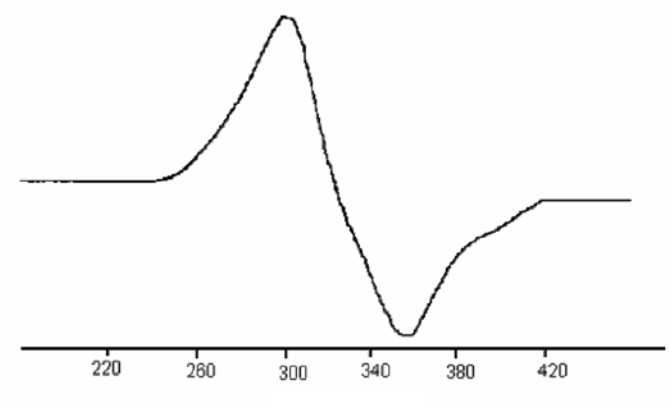

Fig. 3.13. EPR spectrum of [VO(ASC)(dmbipy)]·3H$_2$O (3) in polycrystalline state at 298 K.

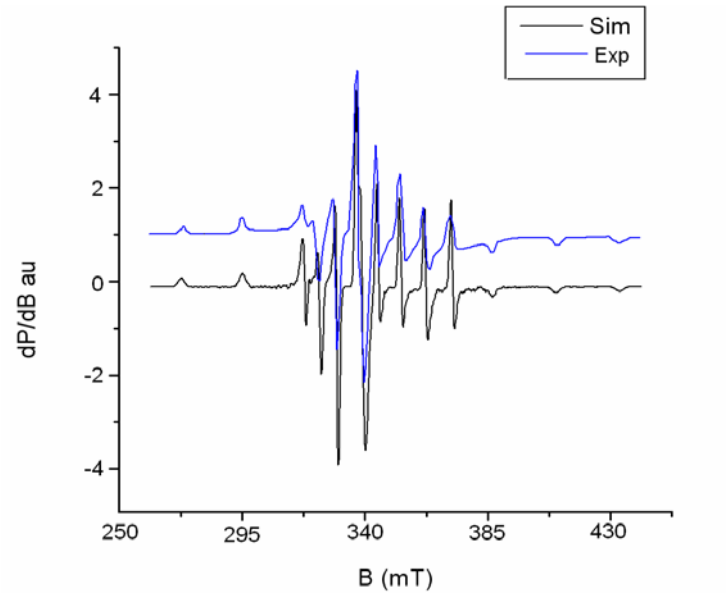

Fig. 3.14. EPR spectrum of [VO(ASC)(dmbipy)] in DMF at 77 K.

The X-band EPR spectrum of compound **4** in polycrystalline state at 298 K exhibits an isotropic spectrum with g_{iso} 1.976 (Fig. 3.15) and its spectrum in DMF is depicted in Fig. 3.16. Here also it exhibits well resolved

axial anisotropy with two sets of eight-line pattern with $g_{\parallel} = 1.945$ and $g_{\perp} = 1.984$, $A_{\parallel} = 153 \times 10^{-4}$ cm^{-1} and $A_{\perp} = 50 \times 10^{-4}$ cm^{-1}. Though the compound 4 is a binuclear complex, the expected half field signal due to $\Delta Ms = \pm 2$ transition is not observed. It is probably due to insignificant spin-spin interaction [26].

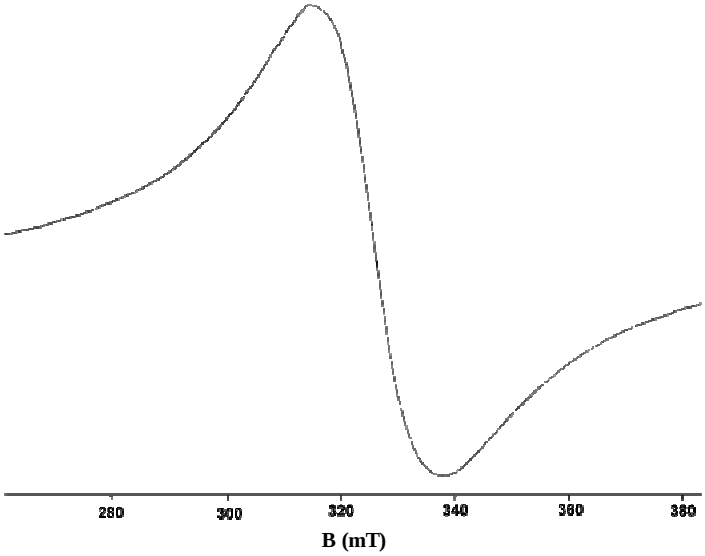

Fig. 3.15. EPR spectrum of $[VO(BSC)]_2 \cdot 2H_2O$ (4) in polycrystalline state at 298 K.

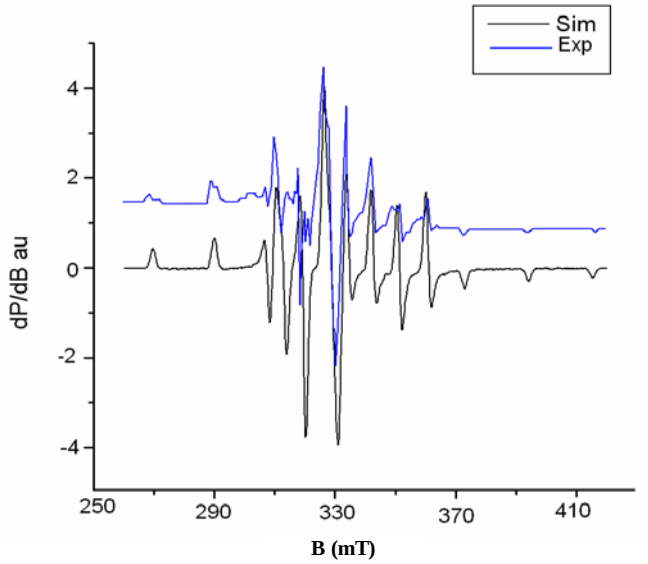

Fig. 3.16. EPR spectrum of $[VO(BSC)]_2$ in DMF at 77 K.

The compound [VO(BSC)(phen)]·2H_2O (**5**) in polycrystalline state at 298 K displayed an isotropic spectrum with g_{iso} 1.978 (Fig. 3.17) and in DMF at 77 K an axial spectrum with two sets of *g* and *A* values is observed and is depicted in Fig. 3.18.

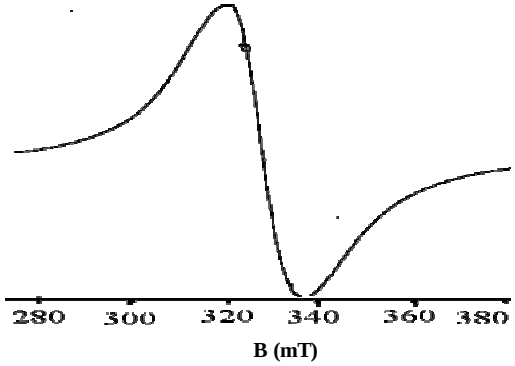

Fig. 3.17. EPR spectrum of [VO(BSC)(phen)]·2H_2O (5) in polycrystalline state at 298 K.

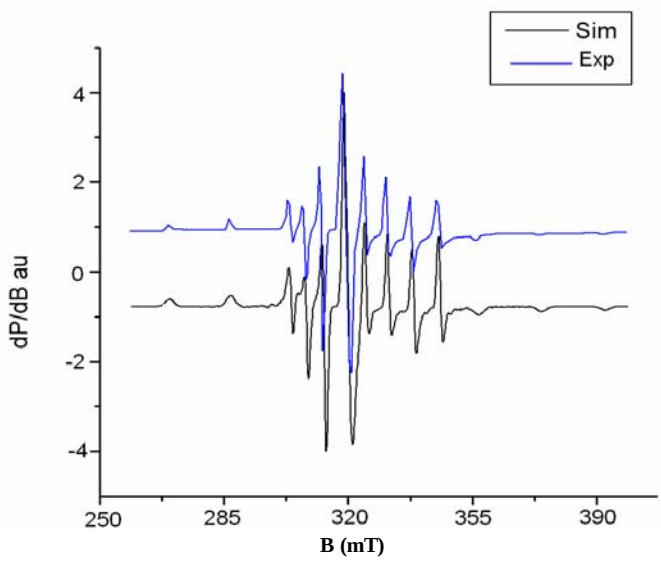

Fig. 3.18. EPR spectrum of [VO(BSC)(phen)] in DMF at 77 K.

In polycrystalline state at 298 K, EPR spectrum of compound **6** is axial with $g_{\|}$ = 1.945 and $g_{\perp}$ = 1.987 (Fig. 3.19). The spectrum shows two sets of eight-line pattern, but not well resolved.

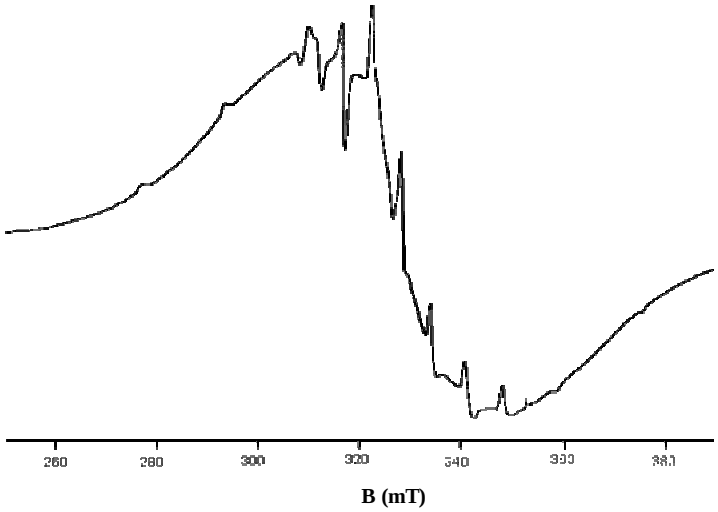

Fig. 3.19. EPR spectrum of [VO(BSC)(dmbipy)]·2H_2O (6) in polycrystalline state at 298 K.

But a well resolved axial spectrum is obtained in frozen DMF at 77 K. The calculated anisotropic hyperfine parameters are as follows, $g_{\|}$= 1.955 and $g_{\perp}$ = 1.987, $A_{\|}$ = 147 ×10^{-4} cm^{-1} and $A_{\perp}$ = 51 ×10^{-4} cm^{-1} (Fig. 3.20).

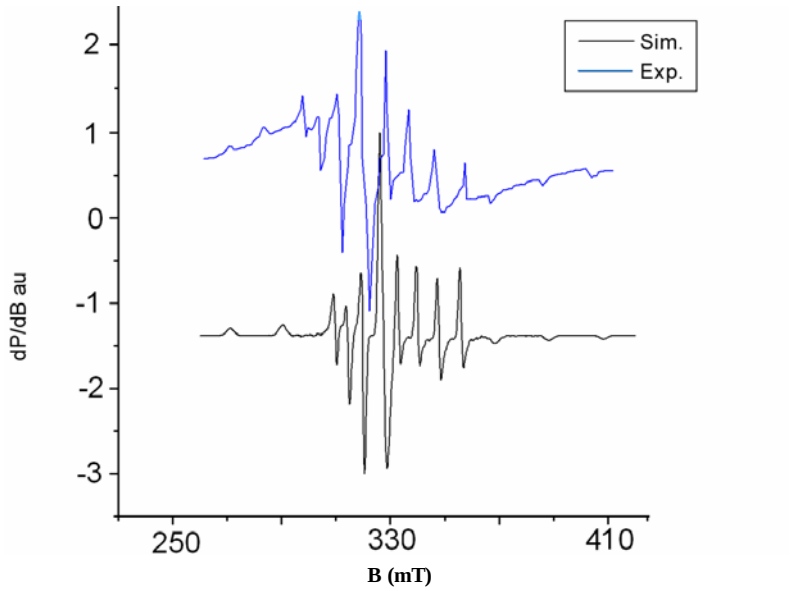

Fig. 3.20. EPR spectrum of [VO(BSC)(dmbipy)] in DMF at 77 K.

The EPR spectrum of the complex **7** in polycrystalline state is poorly resolved and was difficult to interpret. But the solution spectrum in frozen DMF shows well resolved axial anisotropy (Fig. 3.20) with hyperfine parameters $g_{\|} = 1.945$ and $g_{\perp} = 1.988$, $A_{\|} = 156\times10^{-4}$ cm^{-1} and $A_{\perp} = 58\times10^{-4}$ cm^{-1}.

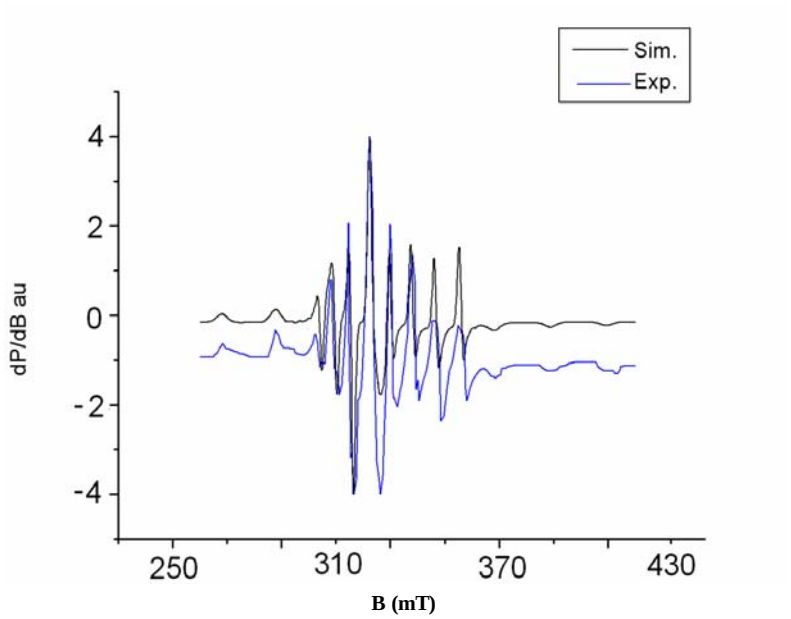

Fig. 3.21 EPR spectrum of [VO(BSC)(pic)] in DMF at 77 K.

In all these complexes the anisotropic parameters are related with isotropic parameters by the equations, $A_{av} = {}^1/_3(A_{\|} + 2A_{\perp})$ and $g_{av} = {}^1/_3(g_{\|} + 2g_{\perp})$ [27]. The values obtained for g_{av} are near to the g_{iso} values obtained from the polycrystalline spectra, suggest that the molecules retain their structural identity in solution.

The EPR parameters $g_{\|}$, $g_{\perp}$, $A_{\|}$ and $A_{\perp}$ and energies of *d–d* transitions were used to evaluate the molecular orbital coefficients α^2 and β^2 for the complexes by using the following equations:

$$\alpha^2 = \frac{(2.0023 - g_{\parallel})E_{d-d}}{8\lambda\beta^2}$$

$$\beta^2 = \frac{7}{6}\left[\left(\frac{-A_{\parallel}}{P}\right)+\left(\frac{A_{\perp}}{P}\right)+\left(g_{\parallel}-\frac{5}{14}g_{\perp}\right)-\frac{9}{14}g_e\right]$$

where P = 128 x 10^{-4} cm^{-1}, λ = 135 cm^{-1} and $E_{d\text{-}d}$ is the energy of *d-d* transition.

A less than unity value of α^2 is an indication of increasing covalency, while that of β^2 does not found to vary significantly, from the most often observed value of 1.0 for most of the complexes. This is expected as the bonding ability of the ligand decreases with increasing distortion from the planar geometry [28]. EPR spectral data for VO(IV) complexes are presented in Table 3.4.

Table 3.4. EPR spectral data for VO(IV) complexes.

Compound	Polycrystalline state (298 K)	DMF solution (77 K)							
	(g_{iso})	$g_{\parallel}$	$g_{\perp}$	g_{av}	$A_{\parallel}$ [a]	$A_{\perp}$ [a]	A_{av} [a]	α^2	β^2
[VO(ASC)]$_2$·2H$_2$O (**1**)	1.962/1.980 ($g_{\parallel}$ / $g_{\perp}$)	1.951	1.980	1.970	164	52	89	0.824	1.07
[VO(ASC)(bipy)]·2H$_2$O (**2**)	1.977	1.914	1.975	1.955	171	68	102	-----	1.030
[VO(ASC)(dmbipy)]·3H$_2$O (**3**)	1.975	1.945	1.979	1.967	152	52	86	0.891	0.969
[VO(BSC)]$_2$.3H$_2$O (**4**)	1.976	1.945	1.984	1.972	153	50	85	0.932	0.998
[VO(BSC)(phen)]·2H$_2$O (**5**)	1.978	1.955	1.987	1.976	146	51	82	0.899	0.915
[VO(BSC)(dmbipy)]·2H$_2$O (**6**)	1.945/1.987 ($g_{\parallel}$ / $g_{\perp}$)	1.955	1.988	1.976	147	51	83	------	0.924
[VO(BSC)(pic)]·0.5H$_2$O (**7**)	-------	1.945	1.988	1.974	156	58	91	------	0.954

[a] Expressed in units of cm^{-1} multiplied by a factor of 10^{-4}.

3.3.7. Thermogravimetric analyses

Thermal methods are based upon the measurement of the dynamic relationship between temperature and some property of a system such as mass, heat of reaction or volume. In thermogravimetric analysis, the mass of sample is recorded continuously as its temperature is increased linearly from ambient to as high as 1200 °C. A plot of mass as a function of temperature (a thermogram) provides both qualitative and quantitative information.

The thermal behavior of all the complexes was investigated by TG-DTG measurements. Decomposition was carried out by heating the sample from 50 °C to 1000 °C with a heating rate of 10 °C /min. in an inert atmosphere of nitrogen. It was observed that the hydrated complexes lose water molecules of hydration in the first step, followed by decomposition of ligand molecules in the subsequent steps. Analyses show that the weight losses for lattice water are observed below 200 °C [29] and weight losses due to coordinated water molecules are in the range of 200-350 °C [30]. In all the complexes the weight loss is observed between 60-190 °C suggesting the presence of water molecules outside the coordination sphere. The weight loss data in % composition with temperature was recorded and some thermograms are presented in Figs. 3.22-3.24. The decomposition was not seen to be completed even upto 1000 °C and vanadium pentoxide has been inferred to be the ultimate pyrolysis product [31].

The TGA curve for the complex **5** displays the first stage of decomposition in the temperature range of 60-190 °C in two steps due to the loss of two molecules of water with 2.6% of the total weight of the complex (calcd. 2.97%). The weight losses due to the decomposition of ligand and the heterocyclic base, phenanthroline were found to take place over 250 °C.

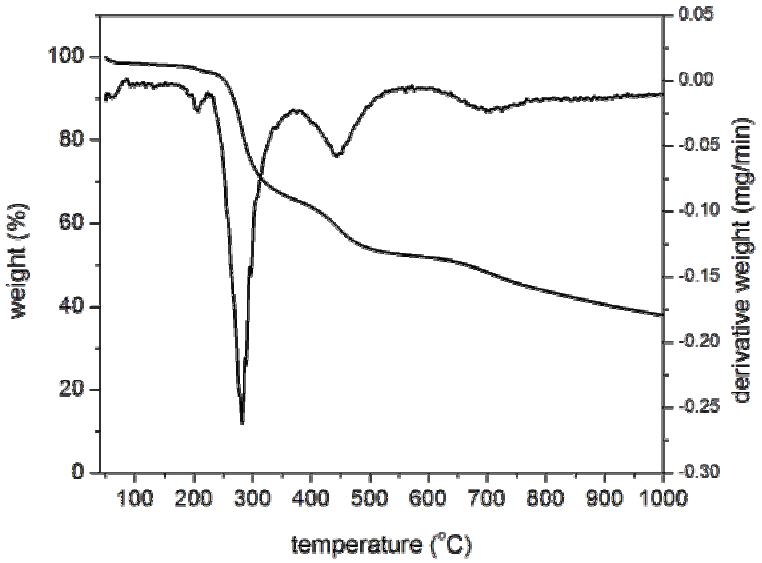

Fig. 3.22. Thermogram of the compound [VO(BSC)(phen)]·2H$_2$O (5).

In compound **6** a weight loss of 4.9% is observed at about 125 °C (calcd 5.5%) due to the loss of two molecules of water from its lattice. Further degradation of the complex takes place in three steps over 200 °C.

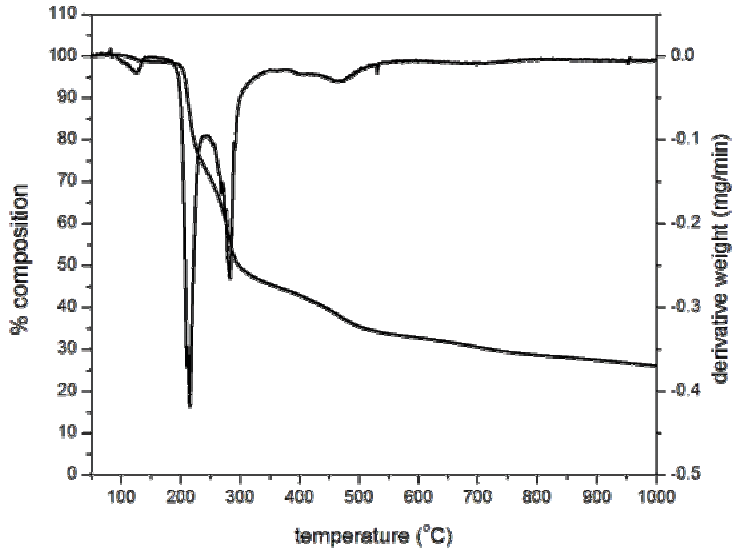

Fig. 3.23. Thermogram of the compound [VO(BSC)(dmbipy)]·2H$_2$O (6).

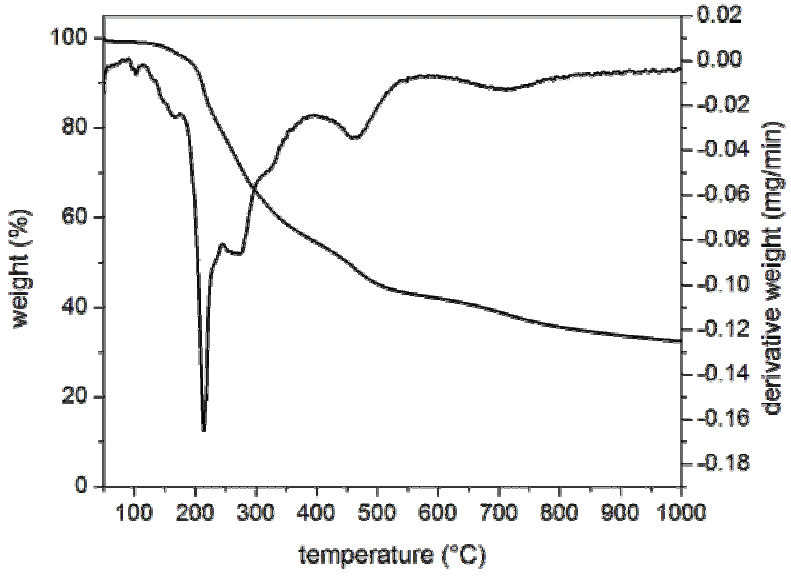

Fig. 3.24. Thermogram of the compound [VO(BSC)(pic)]·0.5H_2O (7).

In compound **7** the first stage of decomposition is observed in the range 90 -160 °C which is due to the loss of 0.5 molecule of water with 1.88% of the total weight of the complex (calcd. 1.70%) and it confirms the presence of lattice water. Beyond 200 °C a gradual weight loss occurs due to the thermal degradation of the ligand and heterocyclic base.

Based on the above physico-chemical methods, proposed structures for some compounds are given below. Water molecules are omitted. Out of the seven oxidovanadium complexes prepared two are dimers and the remaining five are mixed ligand metal chelates incorporating heterocyclic bases. In all the complexes semicarbazones exist in iminol form and act as dideprotonated ONO donor semicarbazones.

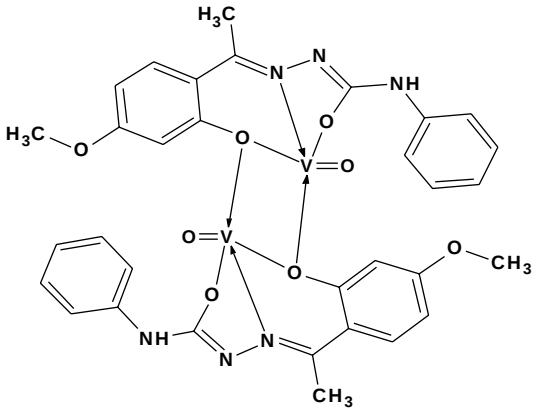

[VO(ASC)]$_2$·2H$_2$O (1)

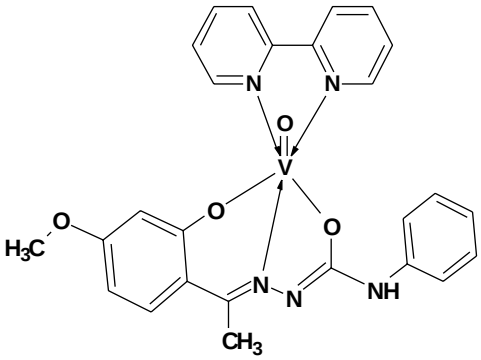

[VO(ASC)(bipy)]·2H$_2$O (2)

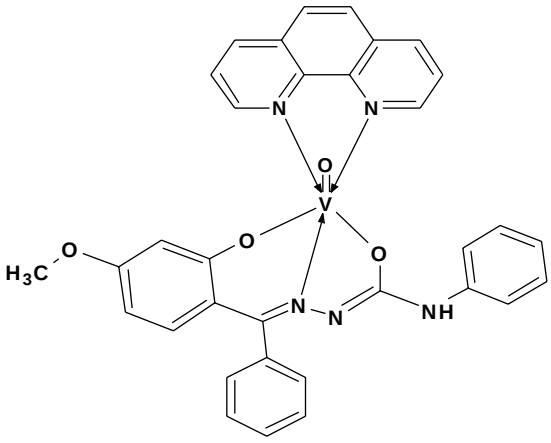

[VO(BSC)(phen)]·2H$_2$O (5)

References

[1] C.J. Carrano, C.M. Nunn, R. Quan, J.A. Bonadies, V.L. Pecoraro, Inorg. Chem. 29 (1990) 941.

[2] D. Rehder, Inorg. Chem. Commun. 6 (2003) 604.

[3] S. Ahmad, A.A. Isab, S. Ali, A.R. Al-Arfaj, Polyhedron 25 (2006) 1633.

[4] M.J. Clarke, F. Zhu, D.R. Frasca, Chem. Rev. 99 (1999) 2511.

[5] M.R. Maurya, A. Kumar, M. Abid, A. Azam, Inorg. Chim. Acta 359 (2006) 2439.

[6] P.I. da S. Maia, V. M. Deflon, E. J. de Souza. E. Garcia, G. F. de Sousa, A.A. Batista, A.T. de Figueiredo, E. Niquet, Transit. Met. Chem. 30 (2005) 404.

[7] W.J. Geary, Coord. Chem. Rev. 7 (1971) 81.

[8] S.N. Chol, Y.I. Kim, Y.B. Shim. H.S. Choo, Y.J. Kim, Bull. Korean Chem. Soc. 10 (1989) 138.

[9] P. Noblia, E.J. Baran, L.Otero, P. Draper, H. Cerecetto, M. Gonzalez, O.E. Piro, E.E. Castellano, T. Inohara, Y. Adachi, H. Sakurai, D. Gambino, Eur. J. Inorg. Chem. 45 (2004) 322.

[10] N. Kanoongo, R.V.Singh, J.P. Tandon, Synth. React. Inorg. Met-Org. Chem. 17 (1987) 837.

[11] M.R.P Kurup, B. Varghese, M. Sithambaresan, S. Krishnan, S.R. Sheeja, E. Suresh, Polyhedron 30 (2011) 76.

[12] P.B. Sreeja, M.R.P. Kurup, Spectrochim. Acta A61 (2004) 331.

[13] M.A.Ali, D.A. Chowdhary, M. Nazimuddin, Inorg. Chim. Acta 7 (1973) 179.

[14] T. Ma, T. Kojima, Y. Matsuda, Polyhedron 19 (2000) 1167.

[15] A. Syamal, K.S. Kale, Inorg. Chem. 18 (1979) 992.

[16] M. Kuriakose, M.R.P. Kurup, E. Suresh, Polyhedron 26 (2007) 2713.

[17] S.K. Dutta, S.B. Kumar, S. Bhattacharyya, E.R.T. Tiekink, M. Chaudhury, Inorg. Chem. 36 (1997) 4954.

[18] L. Sacconi, M. Ciampolini, G.P Speroni, J. Am. Chem. Soc. 87 (1965) 3102.

[19] C.J. Ballhausen, H.B. Gray, Inorg. Chem. 1 (1962) 111.

[20] E. Garriba, G. Micerra, A. Panzanelli, Inorg. Chem. 42 (2003) 3981.

[21] T. Ghosh, S. Bhattacharya, A. Das, G. Mukherjee, M.G.B. Drew, Inorg. Chim. Acta 358 (2005) 989.

[22] D. Collison, B. Gahan, C.D. Garner, F.E. Mabbs, J. Chem. Soc., Dalton Trans. (1980) 667.

[23] P.R. Klich, A.T. Daniher, P.R. Challen, D.D. McConville, W.J. Youngs, Inorg. Chem. 35 (1996) 347.

[24] F.A. Walker, R.L. Carlin, P.H. Rieger, J. Chem. Phys. 45 (1996) 4181.

[25] H. Kon, E. Sharpless, J. Chem. Phys. 42 (1965) 906.

[26] S.K. Dutta, E.R.T. Tiekink, M. Chaudhury, Polyhedron 16 (1997) 1863.

[27] D. Rehder, Bioinorganic Vanadium Chemistry, Wiely, Chichester, (2008).

[28] N. Raman, Y.P. Raja, A. Kulandaisamy, Proc. Indian Acad. Sci. (Chem. Sci.) 113 (2001) 183.

[29] S. Kavlak, H. Kaplan Can, Z.M.O. Rzaev, A. Guner, J. Appl. Polym. Sci. 100 (2006) 3926.

[30] W. Jingping, H. Qiuxia, N. Jingyang, J. Coord. Chem. 57 (2004) 33.

[31] M. Asadi, M.H. Ghatee, S. Torabi, K. Mohammadi, F. Moosavi, J. Chem. Sci. 122 (2010) 539.

Chapter 4

SYNTHESES AND SPECTRAL CHARACTERIZATION OF MANGANESE(II) COMPLEXES OF N^4-PHENYLSEMICARBAZONES

Contents

4.1. Introduction

Manganese is an essential trace nutrient in all forms of life. In biology, manganese(II) ions function as cofactor for a large variety of enzymes with many functions. The classes of enzymes that have manganese cofactors are very broad and include oxidoreductase, transferases, hydrolases, isomerases etc. The best known manganese containing polypeptides may be arginase, the diphtheria toxin, and Mn-containing superoxide dismutase (Mn-SOD). Manganese enzymes are particularly essential in detoxification of superoxide free radicals in organisms that must deal with elemental oxygen. Manganese is also important in photosynthetic oxygen evolution in chloroplasts in plants. The oxygen evolving complex (OEC) is a part of photosystem II and it is responsible for the terminal photooxidation of water during the light reaction of photosynthesis, and has a metalloenzyme core containing four atoms of manganese [1]. Manganese overexposure is most frequently associated with manganism, a rare neurological disorder associated with excessive manganese ingestion or inhalation.

Manganese metal has a well established importance in the field of biology and medicine. Ruminants manganese is present in the serum of blood as manganese(III) β-globulin and in erythrocytes as manganese porphyrin ring.

The common oxidation states of manganese are +2, +3, +4, +6 and +7. The most stable oxidation state is +2, which has a pale pink colour and it is the state used in living organisms for essential functions. Other states are toxic for the human body. Manganese is an essential trace element, forming the active sites of a number of metalloproteins. In these metalloproteins, manganese can exist in any of the five oxidation states or in the mixed valence states [2]. Manganese and its compounds are widely used in analytical chemistry, metallurgical processes and paint & pigments industry. The complexes of manganese(II) play an excellent role in catalytic property [3,4].

This chapter is focused on the characterization of manganese(II) complexes of two ONO donor N^4-phenylsemicarbazones including three mixed ligand metal chelates incorporating heterocyclic base 1,10-phenanthroline as coligand.

4.2. Experimental

4.2.1. Materials

Manganese(II) acetate tetrahydrate (Merck), manganese(II) chloride tetrahydrate (Merck), manganese(II) perchlorate hexahydrate (Aldrich) and 1,10-phenanthroline (Ranchem) were commercial products of higher grade and used without further purification. Solvent used was ethanol.

4.2.2. Syntheses of semicarbazones

The semicarbazones $H_2ASC{\cdot}H_2O$ and H_2BSC were synthesized as described in Chapter 2.

4.2.3. Syntheses of Mn(II) complexes of 2-hydroxy-4-methoxyacetophenone-N^4-phenylsemicarbazone (H_2ASC)

4.2.3.1. *[Mn(HASC)(OAc)] (8)*

Manganese(II) acetate tetrahydrate (0.245 g, 1 mmol) in ethanol was added to the ethanolic solution of $H_2ASC{\cdot}H_2O$ (0.317 g, 1 mmol) and refluxed for 4 h. The light yellow colored compound formed was filtered, washed with ethanol followed by ether and dried over P_4O_{10} in *vacuo*.

Elemental Anal. Found (Calcd.) (%): C: 51.88 (52.44); H: 4.78 (4.64); N: 10.05 (10.19)

4.2.3.2. *$[Mn(H_2ASC)(H_2O)]Cl_2$ (9)*

A hot ethanolic solution of $H_2ASC{\cdot}H_2O$ (0.317 g, 1 mmol) was refluxed with an ethanolic solution of manganese(II) chloride tetrahydrate (0.198 g, 1 mmol) and 2 mL of DMF for 4 h. The resulting solution was allowed to stand at room temperature and after slow evaporation the flesh colored complex formed was filtered, washed with ethanol followed by ether and dried over P_4O_{10} in *vacuo*.

Elemental Anal. Found (Calcd.) (%): C: 43.14 (43.36); H: 3.94 (4.32); N: 10.02 (9.48)

4.2.3.3. *$[Mn(HASC)(phen)]ClO_4$ (10)*

A mixture of ethanolic solutions of $H_2ASC{\cdot}H_2O$ (0.317 g, 1 mmol) and manganese(II) perchlorate hexahydrate (0.362 g, 1 mmol) was refluxed with

1,10-phenanthroline (0.198 g, I mmol) for 4 h. The complex formed was collected, washed with ethanol and ether and dried over P_4O_{10} in *vacuo*.

Elemental Anal. Found (Calcd.) (%): C: 52.72 (53.14); H: 3.88 (3.82); N: 11.02 (11.07)

4.2.4. Syntheses of Mn(II) complexes of 2-hydroxy-4-methoxybenzophenone-N^4-phenylsemicarbazone (H_2BSC)

4.2.4.1. *[Mn(HBSC)$_2$] (11)*

A hot solution of H_2BSC (0.361 g, 1 mmol) in ethanol was treated with an ethanolic solution of manganese(II) acetate tetrahydrate (0.124 g, 0.5 mmol) and was refluxed for 4 h. A pale yellow complex was separated out. It was filtered, washed with ethanol followed by ether and dried over P_4O_{10} in *vacuo*.

Elemental Anal. Found (Calcd.) (%): C: 64.67 (65.03); H: 4.53 (4.68); N: 10.44 (10.83)

4.2.4.2. *[Mn(HBSC)Cl]$_2$·2EtOH (12)*

H_2BSC (0.361 g, 1 mmol) was dissolved in 20 mL ethanol and refluxed with an ethanolic solution of manganese(II) chloride tetrahydrate (0.198 g, 1 mmol) and 2 mL of DMF for 3 h. The solution turned into yellow. Keeping overnight for cooling, the yellow product formed was filtered, washed with ethanol followed by ether and dried over P_4O_{10} in *vacuo*.

Elemental Anal. Found (Calcd.) (%): C: 55.45 (55.60); H: 4.95 (4.87); N: 8.47 (8.46)

4.2.4.3. *[Mn(HBSC)(phen)]ClO$_4$·H$_2$O (13)*

To a solution of H_2BSC (0.361 g, 1 mmol) in ethanol, an ethanolic solution of manganese(II) perchlorate hexahydrate (0.362 g, 1 mmol) was added

followed by 1,10-phenanthroline (0.198 g, 1 mmol) in ethanol. The resulting solution was refluxed for 4 h. The yellow product formed was filtered, washed with ethanol followed by ether and dried over P_4O_{10} in *vacuo*.

Elemental Anal. Found (Calcd.) (%): C: 55.67 (55.59); H: 4.40 (3.96); N: 10.24 (9.83)

4.2.4.4. *[Mn(HBSC)(phen)(OAc)] (14)*

Ethanolic solutions of H_2BSC (0.361 g, 1 mmol), manganese(II) acetate tetrahydrate (0.245 g, 1 mmol) and 1,10-phenanthroline (0.198 g, 1 mmol) were mixed and refluxed for 4 h. A yellow complex was separated out. It was filtered, washed with ethanol followed by ether and dried over P_4O_{10} in *vacuo*.

Elemental Anal. Found (Calcd.) (%): C: 64.92 (64.22); H: 4.72 (4.47); N: 11.21 (10.70)

Caution! Perchlorate salts of metal complexes with organic ligands are potentially explosive. So they should be synthesized in small quantities and handled with due caution.

4.3. Results and discussion

All the complexes were synthesized by refluxing ethanolic solutions of the semicarbazone and corresponding metal salts in 1:1 ratio, while in complex **11** it is in 2:1. Out of the seven complexes prepared, complex **12** is supposed to be a dimer as evidenced from its EPR and the remaining six are mononuclear metal chelates. In complexes **10**, **13** and **14** heterocyclic base 1,10-phenanthroline is incorporated. All the complexes are yellow in color and are soluble in solvents like DMSO and DMF. Complexes **8**, **10**, **11** and **14** are only slightly soluble in acetonitrile, while others are readily soluble. In all the

complexes synthesized the semicarbazone exists in the amido form. In complex **9,** the semicarbazone is in the neutral form, while in all others it behaves as an monoanionic one. The synthesized compounds are characterized by the following physico-chemical methods.

4.3.1. Elemental analyses

Elemental (C,H,N) analyses of all samples were carried out using a Vario EL III CHN analyzer at SAIF, Kochi, India and the values were given in Sections 4.2.3 and 4.2.4.

4.3.2. Molar conductivity

The molar conductivities of the complexes in DMF (10^{-3} M) solutions were measured at 298 K with a Systronic model 303 direct reading conductivity bridge. For complexes **8, 11, 12** and **14,** the observed values were less than 20 ohm^{-1} cm^2 mol^{-1} which are very much less than the value of 65-90 ohm^{-1} cm^2 mol^{-1}reported for a 1:1 electrolyte in the same solvent. This confirmed the nonelectrolytic nature of the complexes. For complex **9,** the observed value of 146 ohm^{-1} cm^2 mol^{-1} is in tune with a 2:1 electrolyte. The values found for perchlorate salts **10** and **13** were 65 ohm^{-1} cm^2 mol^{-1} and 76 ohm^{-1} cm^2 mol^{-1} respectively, which are indicative of 1:1 electrolytes [5]. This gives evidence that the perchlorate ion is present outside the coordination sphere.

4.3.3. Magnetic susceptibility

Magnetic moments of the complexes were calculated from the magnetic susceptibility measurements at room temperature. Diamagnetic corrections were applied using Pascal's constants. The magnetic moments are found to be

in the range of 5.17-6.1 B.M. and are consistent with high spin d^5 system with manganese in the +2 oxidation state [6]. Though the complex **12** seems to be a dimer as evidenced from its EPR, magnetic susceptibility measurement does not give any indication of significant exchange interactions between adjacent metal centers [7]. It is found that μ_{eff} value for this complex is slightly lower when compared to other complexes. The magnetic moment and molar conductivity values of the complexes are given in Table 4.1.

Table 4.1. Molar conductivities and magnetic moments of Mn(II) complexes.

Compound	λ_m*	μ_{eff} (B.M.)
[Mn(HASC)(OAc)] (**8**)	10	5.65
$[Mn(H_2ASC)(H_2O)]Cl_2$ (**9**)	146	6.1
$[Mn(HASC)(phen)]ClO_4$ (**10**)	65	5.31
$[Mn(HBSC)_2]$ (**11**)	15	5.24
$[Mn(HBSC)Cl]_2 \cdot 2EtOH$ (**12**)	13	5.17
$[Mn(HBSC)(phen)]ClO_4 \cdot H_2O$ (**13**)	76	5.39
[Mn(HBSC)(OAc)(phen)] (**14**)	9	5.53

*Molar conductivity (mho cm^2 mol^{-1}) taken in 10^{-3} M DMF solution.

4.3.4. Infrared spectra

The prominent infrared data of semicarbazones and their Mn(II) complexes are presented in Table 4.2. IR spectra of the seven manganese complexes were recorded in the range 4000-400 cm^{-1} with KBr pellets.

The ν(C=O) bands in the region 1636-1657 cm^{-1} for the manganese complexes of the semicarbazone $H_2ASC \cdot H_2O$ and 1640-1652 cm^{-1} for the complexes of the semicarbazone H_2BSC, showing shift to lower wavenumbers from the corresponding ν(C=O) of semicarbazones (1692 and 1662 cm^{-1}) confirm

that the carbonyl oxygen is coordinated to the metal ion, so that in all the manganese(II) complexes semicarbazones exist in the amido form [8,9]. The medium bands at *ca*. 3295 and 3145 cm^{-1} assigned to $\nu(^2N–H)$ are not disappearing, but shifted slightly in the complexes, indicative of the existence of semicarbazones in the amido form in all complexes. In the IR spectra of the semicarbazones, sharp bands observed at 1619 and 1631 cm^{-1} were assigned to the ν(C=N) for $H_2ASC·H_2O$ and H_2BSC respectively. These bands were shifted to lower wavenumbers in all the complexes by 15-27 cm^{-1} indicating the coordination of azomethine nitrogen to the metal ion centre [10,11]. This shift to lower frequency is attributed to the conjugation of the *p*-orbital on the double bond with the *d*-orbital on the metal ion owing to reduction of the force constant. The involvement of this nitrogen in bonding is also supported by a shift in ν(N–N) to higher frequencies in the range 1047-1109 cm^{-1} [12]. This is further substantiated by the presence of new bands in the range 409-429 cm^{-1} assignable to ν(Mn–N) [13]. The characteristic phenolic ν(O–H) modes due to the presence of a hydroxy group at ortho position in the semicarbazone were observed at 3535 and 3316 cm^{-1} respectively for $H_2ASC·H_2O$ and H_2BSC and bands at 1270 and 1292 cm^{-1} were assigned to ν(C–O) bands of phenolate groups in the spectra of ligands. In all the complexes under study except in compound **9**, this ν(O–H) band disappeared suggesting the coordination by the phenolic oxygen after deprotonation and correspondingly ν(C–O) mode decreases by 22-27 cm^{-1} for the complexes of H_2ASC and for the complexes of H_2BSC it experiences a lower shift by 23-54 cm^{-1}. But in complex **9**, only a shift to this ν(O–H) band (3535 → 3426 cm^{-1}) indicating phenolic oxygen is not getting deprotonated and exists as neutral tridentate ONO donor ligand. The appearance of a non-ligand band in the range 448-469 cm^{-1} in the

complexes due to ν(Mn–O) further substantiate this [14]. Thus the IR spectral results provide strong evidences for the complexation of semicarbazones with metal ions in tridentate mode.

We can distinguish the nature of the linkage of the acetate anion in the complex depending upon the mode of coordination of the anion. The spectrum of the complex [Mn(HASC)(OAc)] (**8**) exhibits relatively strong bands at 1569 and 1316 cm^{-1} and [Mn(HBSC)(phen)(OAc)] (**14**) displays bands at 1570 and 1323 cm^{-1}. The bands at 1569 and 1570 cm^{-1} are assignable to asymmetric streching and the bands at 1316 and 1323 cm^{-1} are assignable to symmetric streching [15,16] indicating monodentate nature of the acetato group.

The perchlorate salt **10** shows a single broad band at 1110 cm^{-1} assignable to $\nu_3(ClO_4)$ and a band at 626 cm^{-1} assignable to $\nu_4(ClO_4)$, indicating the presence of ionic perchlorate [17]. The other perchlorate salt **13** displays strong band at 1095 and 625 cm^{-1}. In the perchlorate salt **13**, the ν_3 and ν_4 bands of the perchlorate group appear at 1090 and 625 cm^{-1} respectively. For both these perchlorate salts weak bands at 963 and 958 cm^{-1} may be due to $\nu_1(ClO_4)$ suggesting that ionic perchlorate is distorted from tetrahedral symmetry possibly due to lattice effects or hydrogen bonding by the NH functions of the coordinated ligand [18]. This along with unsplit ν_3 and ν_4 bands show exclusive presence of non-coordinated perchlorate group [19]. The band at 3353 cm^{-1} corresponds to that of lattice ethanol in compound **12** and the band at 3452 cm^{-1} in compound **13** is due to water molecule present in its lattice [15]. The bands due to heterocyclic base, phenanthroline are observed at 1426, 839 and 753 cm^{-1} for complex **10** and at 1419, 841 and 724 cm^{-1} for complex **13** [20]. The IR spectra of the complexes are shown in Figs. 4.1- 4.7.

Table 4.2. The important IR frequencies (cm^{-1}) of semicarbazones and their Mn(II) complexes.

Compound	ν(C=O)	ν(C=N)	ν(N–N)	ν(C–O)	ν(^{2}N–H)	ν(Mn–N)	ν(Mn–O)
$H_2ASC\cdot H_2O$	1692	1619	1020	1270	3295	----	-----
[Mn(HASC)(OAc)] (8)	1657	1604	1093	1244	3240	413	469
$[Mn(H_2ASC)(H_2O)]Cl_2$ (9)	1636	1594	1054	1243	3063	409	461
$[Mn(HASC)(phen)]ClO_4$ (10)	1651	1598	1047	1248	3052	424	466
H_2BSC	1662	1631	1059	1292	3145	-----	---
$[Mn(HBSC)_2]$. (11)	1652	1605	1065	1244	3091	420	448
$[Mn(HBSC)Cl]_2\cdot 2EtOH$ (12)	1641	1604	1103	1246	3140	429	469
$[Mn(HBSC)(phen)]ClO_4\cdot H_2O$ (13)	1640	1597	11	1269	3063	416	449
[Mn(HBSC)(phen)(OAc)] (14)	1651	1604	1109	1238	3276	411	458

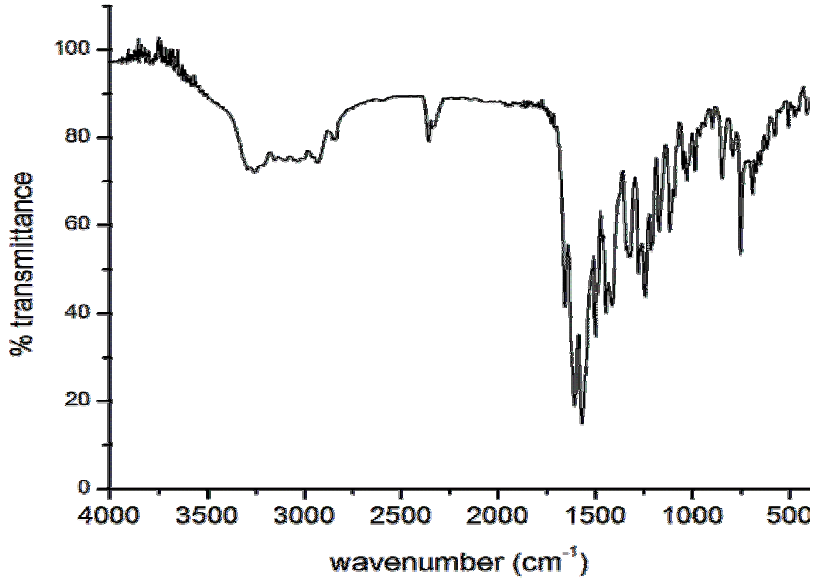

Fig. 4.1. IR spectrum of [Mn(HASC)(OAc)] (8).

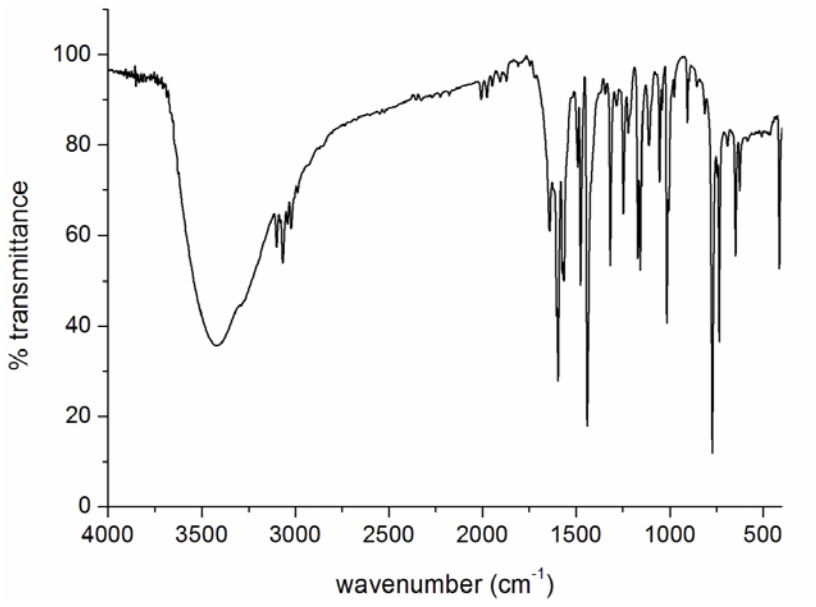

Fig. 4.2. IR spectrum of [Mn(H_2ASC)(H_2O)]Cl_2 (9).

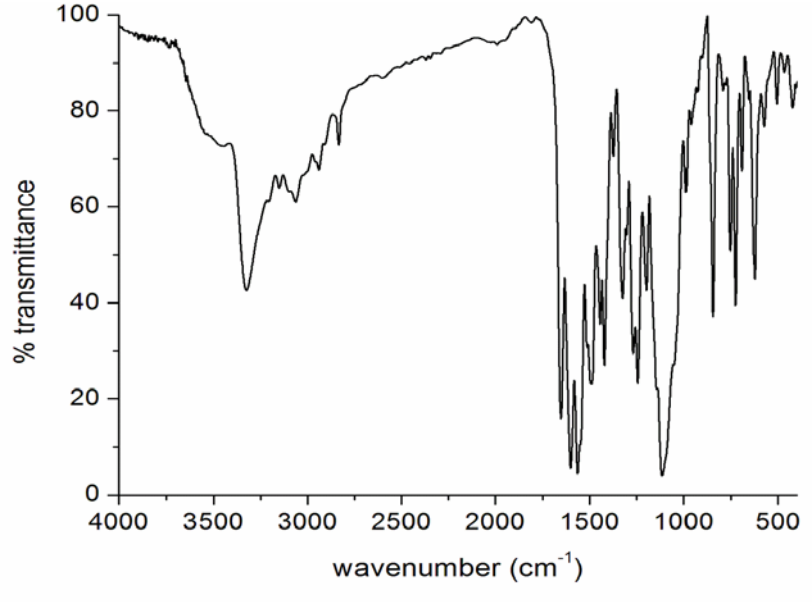

Fig. 4.3. IR spectrum of $[Mn(HASC)(phen)]ClO_4$ (10).

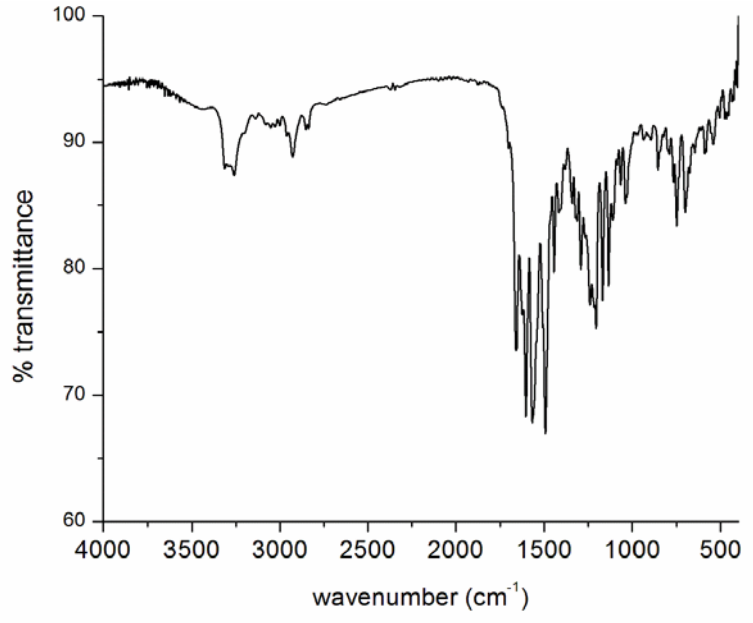

Fig. 4.4. IR spectrum of $[Mn(HBSC)_2]$ (11).

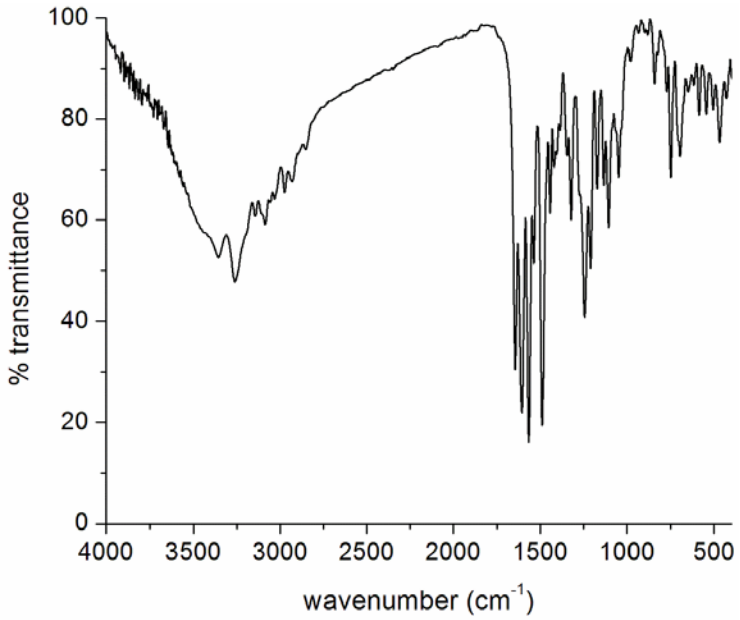

Fig. 4.5. IR spectrum of $[Mn(HBSC)Cl]_2 \cdot 2EtOH$ (12).

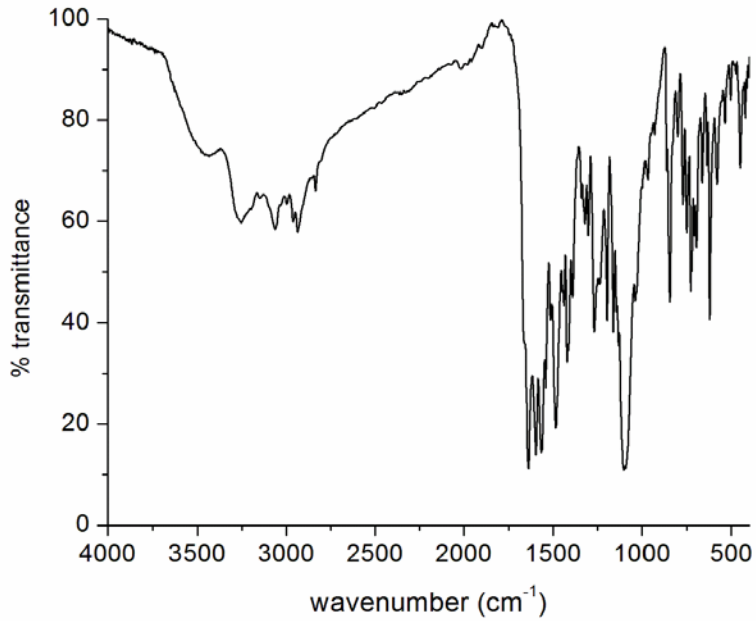

Fig. 4.6. IR spectrum of $[Mn(HBSC)(phen)]ClO_4 \cdot H_2O$ (13).

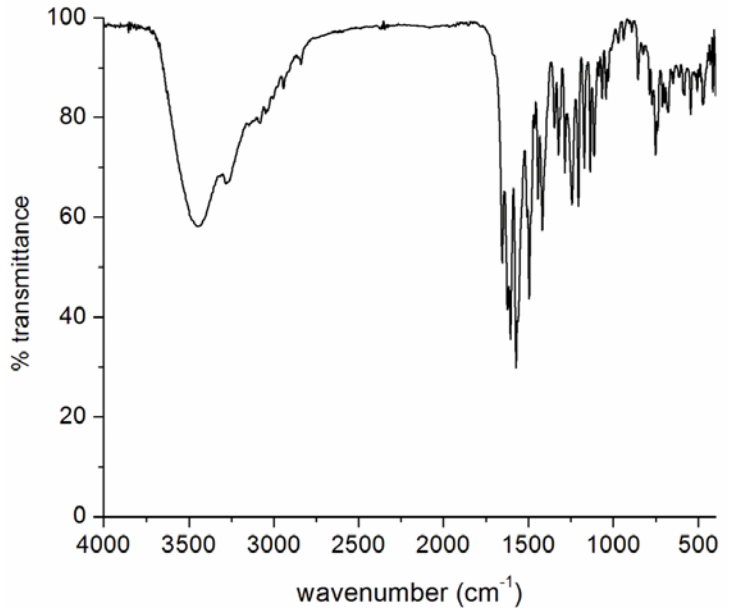

Fig. 4.7. IR spectrum of [Mn(HBSC)(phen)(OAc)] (14).

4.3.5. Electronic spectra

In the high spin octahedrally coordinated Mn(II) complexes, the lowest configuration $(t_{2g})^3(e_g)^2$ gives rise to the ground state $^6A_{1g}$. Since this is the only sextet level present, all the absorption bands must, therefore, be spin forbidden transitions. Thus for octahedral manganese(II) complexes *d-d* transitions are doubly forbidden, spin as well as parity. This rule never applies to tetrahedral complexes. However some forbidden transitions can occur to the quartet excited states with extremely low molar extinction coefficient values and they are assigned to $^4T_{1g}$ (^4G) $\leftarrow$ $^6A_{1g}$, ^4E_g, $^4A_{1g}$ (^4G) $\leftarrow$ $^6A_{1g}$, ^4E_g (^4D) $\leftarrow$ $^6A_{1g}$ and $^4T_{1g}$(^4P) $\leftarrow$ $^6A_{1g}$,. The reason for observing some transitions is that the symmetry centre is transiently destroyed by vibrations of the molecules or ions. For tetrahedral complexes the absorption bands are assigned to the transitions: $^4T_{2g}$ (^4G) $\leftarrow$ $^6A_{1g}$, $^4T_{2g}$ (^4D) $\leftarrow$ $^6A_{1g}$, $^4A_{2g}$ (^4F) $\leftarrow$ $^6A_{1g}$ [21]. The

electronic spectra were recorded in DMF for the complexes **8**, **10** (Fig. 4.8), **11** and **14** (Fig**.** 4.10) and in acetonitrile for the complexes **9** (Fig**.** 4.9), **12** and **13** (Fig**.** 4.11). The charge transfer band for complex **9** is also shown in Fig. 4.9. The electronic spectral assignments of the complexes along with semicarbazones are presented in Table 4.3.

Table 4.3. Electronic spectral assignments (cm^{-1}) of N^4-phenylsemicarbazones and their Mn(II) complexes

Compound	Solvent	Intraligand transitions	LMCT	*d-d*
H_2ASC	CH_3CN	31780, 34540, 35600(sh), 41750	---	------
H_2ASC	DMF	31590, 34250, 35300	----	-----
[Mn(HASC)(OAc)] (**8**)	DMF	31550, 34330	25050	18590
$[Mn(H_2ASC)(H_2O)]Cl_2$ (**9**)	CH_3CN	34160, 41270	26250	18480
$[Mn(HASC)(phen)]ClO_4$ (**10**)	DMF	31360, 33390(sh), 36350(sh)	25320	18600
H_2BSC	CH_3CN	31330, 33820, 35030, 41680	-----	-----
H_2BSC	DMF	31030, 32070 (sh), 33610, 34890	-----	-----
$[Mn(HBSC)_2]$ (**11**)	DMF	31120, 33560, 34800 (sh)	25400	18160
$[Mn(HBSC)Cl]_2 \cdot 2EtOH$ (**12**)	CH_3CN	31530, 33700, 35250 (sh), 40640	26320	18450
$[Mn(HBSC)(phen)]ClO_4 \cdot H_2O$ (**13**)	CH_3CN	34080, 37130, 43850	25840	18310
[Mn(HBSC)(phen)(OAc)] (**14**)	DMF	31430, 33860, 34950(sh), 40780	25780	18750

sh = shoulder

Transitions associated with semicarbazones suffered some shifts upon complexation, indicating coordination. Because of the coordination *via* oxygen atom of C=O, the C=O bond gets weakened and conjugation system is enhanced after the formation of the complex [22]. Charge transfer bands are observed in the range 25000-26320 cm^{-1}. The electronic spectra in the visible region were recorded in DMF for all the complexes. Only broad bands due to *d-d* transitions are observed in the range 17000-21000 cm^{-1} and the spectra are

shown in Figs. 4.12.1-4.12.7. The very weak bands at *ca*.18000 cm^{-1} are assigned to $^4T_{1g} \leftarrow {}^6A_{1g}$,. The high intense charge transition tailing into the visible region, mask the weak *d-d* absorptions of Mn(II) complexes.

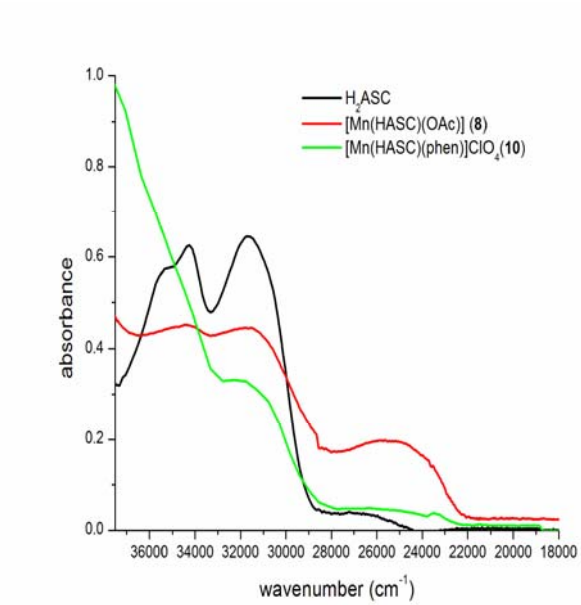

Fig. 4.8. UV spectra of H_2ASC, [Mn(HASC)(OAc)] and [Mn(HASC) (phen)]ClO_4

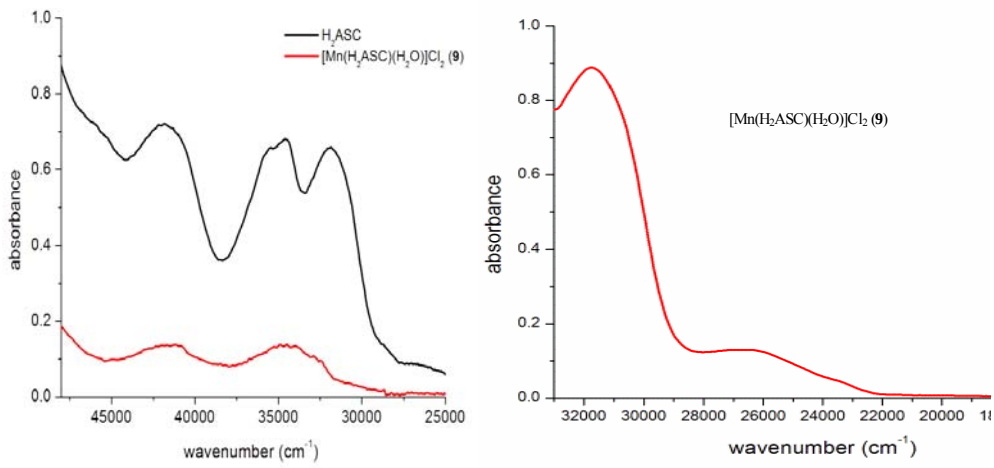

Fig. 4.9. UV spectra of H_2ASC and [Mn(H_2ASC)(H_2O)]Cl_2.

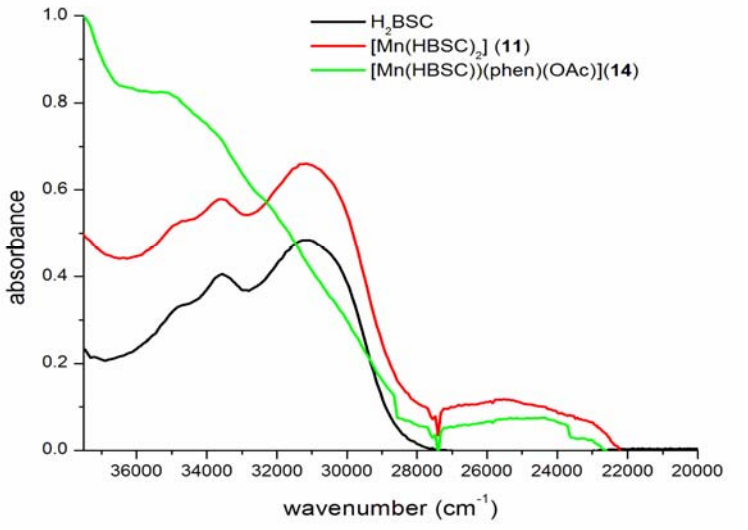

Fig. 4.10. UV spectra of $H_2ASC{\cdot}H_2O$, $[Mn(HBSC)_2]$ and [Mn(HBSC)(phen)(OAc)].

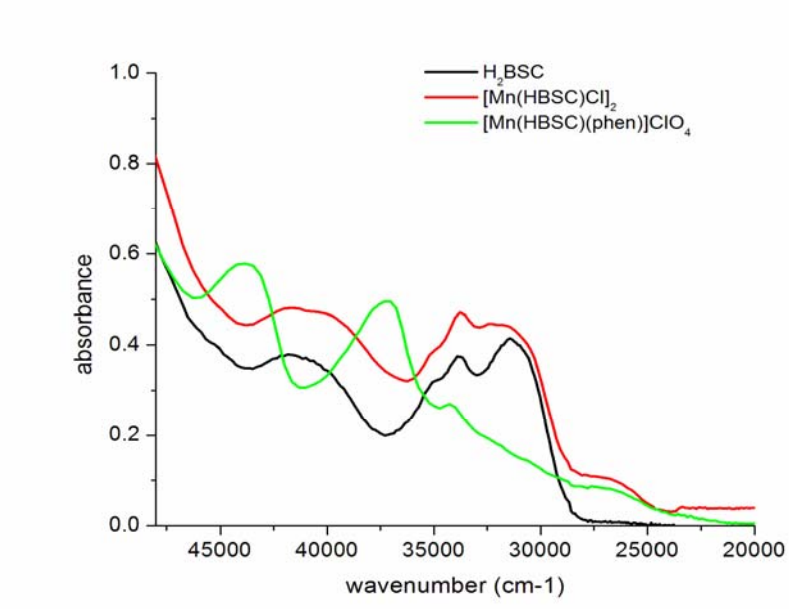

Fig. 4.11. UV spectra of H_2BSC, $[Mn(HBSC)Cl]_2$ and $[Mn(HBSC)(phen)]ClO_4$.

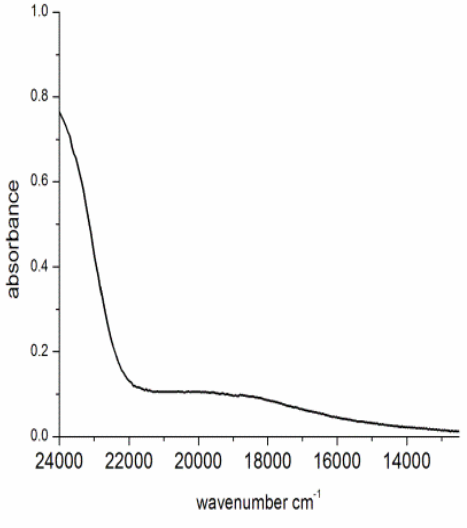

Fig. 4.12.1. [Mn(HASC)(OAc)]

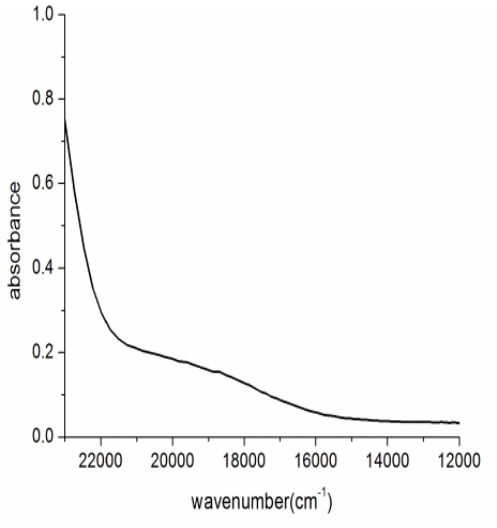

Fig. 4.12.2. [Mn(H_2ASC)(H_2O)]Cl_2

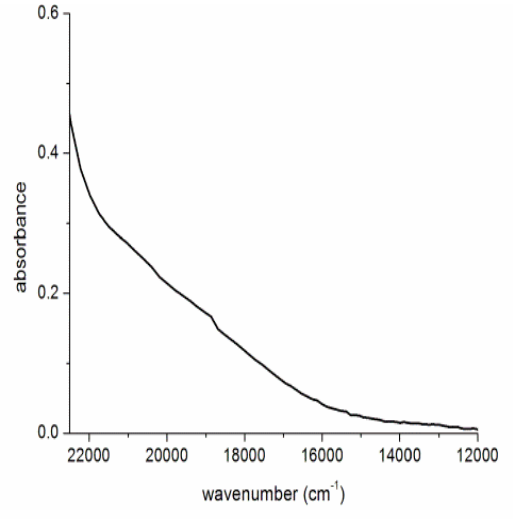

Fig. 4.12.3. [Mn(HASC)(phen)]ClO_4

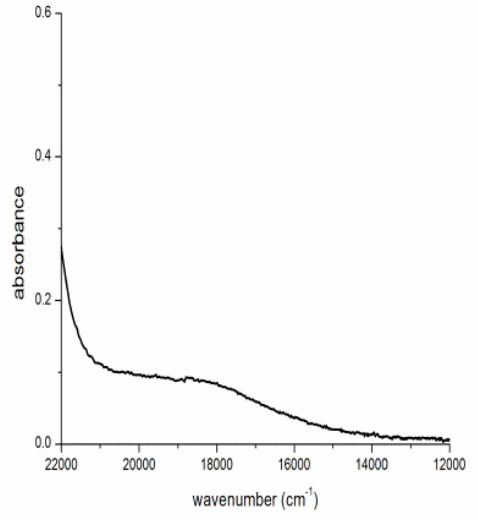

Fig. 4.12.4. [Mn(HBSC)$_2$]

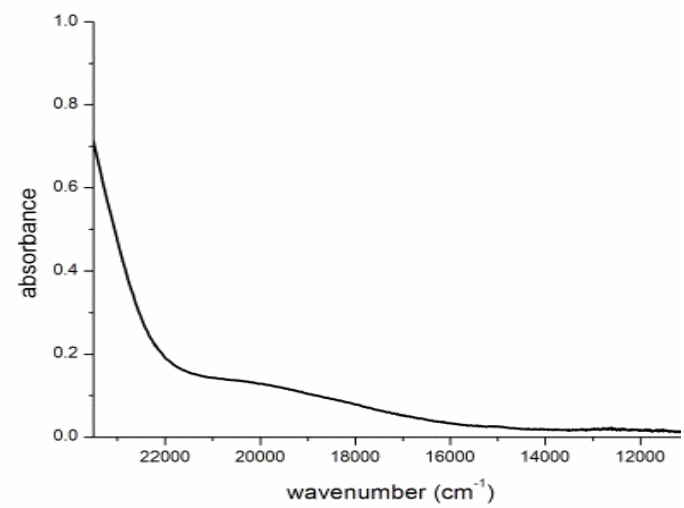

Fig. 4.12.5. $[Mn(HBSC)Cl]_2$

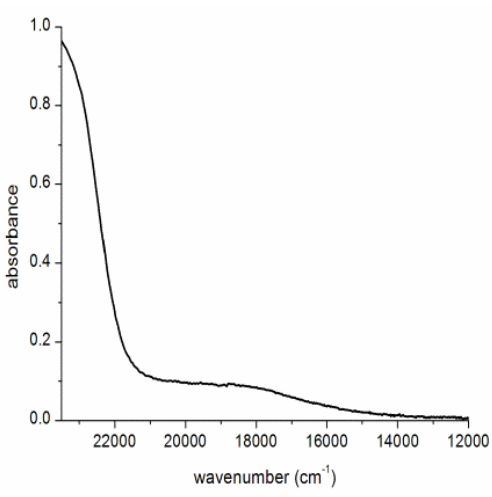

Fig. 4.12.6. $[Mn(HBSC)(phen)]ClO_4$

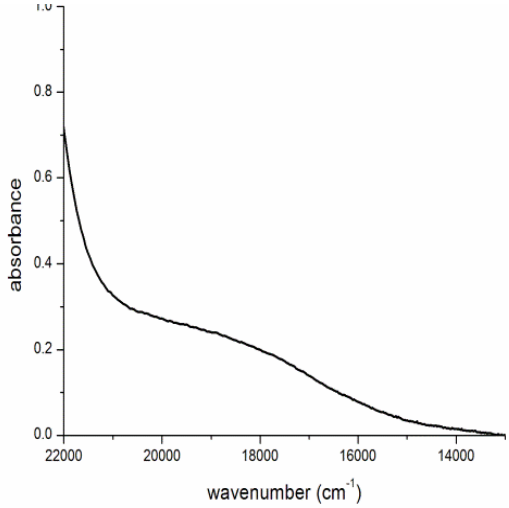

Fig. 4.12.7. [Mn(HBSC)(phen)(OAc)]

Fig. 4.12. Visible spectra of Mn(II) complexes.

4.3.6. Electron paramagnetic resonance spectra

An EPR spectrum is readily detected even for large zero-field splitting, because d^5 is an odd electron system whose ground state is Kramer's doublets

(±5/2, ±3/2, ±1/2) and whose degeneracy is completely removed by a magnetic field, producing six levels. As a result of this splitting, five transitions are expected where $\Delta m_s = \pm 1$ (m = electron spin quantum number). The EPR spectra of Mn(II) may be described by the spin Hamiltonian

$$\hat{H} = g\beta BS + D[S_z^2 - S(S+1)/3] + E(S_x^2 - S_y^2)$$

where B - magnetic field vector, g - spectroscopic splitting factor, β - Bohr magneton, D - axial zero field splitting parameter, E - rhombic zero field splitting parameter and S - electron spin vector [23].

If both D and E are very small compared with $g\beta BS$, five EPR transitions should be obtained corresponding to $\Delta m_s = \pm 1$, with a g value of 2.0. However, in the case when D is comparable to hv, the Mn^{2+} system exhibits tetragonal spectrum with two g values, *ie*. $g \approx 2$ and 6 [24]. Ligand fields of lower symmetry are often characterized by a rhombic signal at g = 4.3, but this is typically observed for relatively strong field ligands.

The X-band EPR spectra of the manganese complexes were recorded in polycrystalline state at 298 K and in frozen DMF at 77 K. The broad signal in the polycrystalline EPR spectra of Mn(II) complexes is attributed to dipolar interactions and random orientation of the Mn^{2+} ions, which is temperature dependent [25]. All the Mn(II) complexes, under study, show isotropic EPR spectra, when recorded in polycrystalline state. In DMF solution, Mn(II) complexes give EPR spectra containing six lines, arising due to the hyperfine interaction between the unpaired electron with the ^{55}Mn nuclear spin (I = 5/2). Some of the EPR spectra are simulated using EasySpin and the experimental (red) and simulated (blue) best fits are included.

EPR spectrum obtained for the complex [Mn(HASC)(OAc)] (**8**) was broad with a *g* value of 2.738 having peak to peak separation ΔB_{pp}=102 mT (Fig. 4.13).

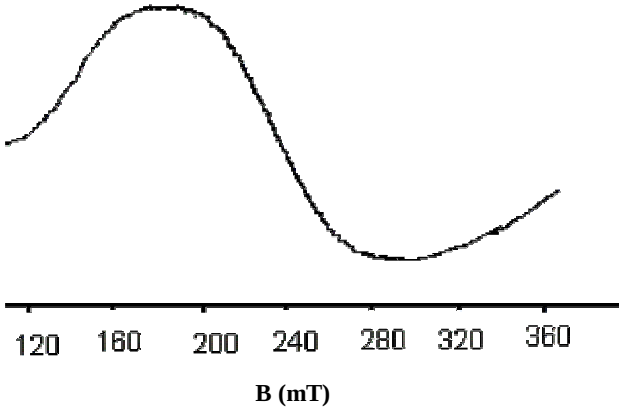

Fig. 4.13. EPR spectrum of [Mn(HASC)(OAc)] (8) in polycrystalline state at 298 K.

But in frozen DMF at 77 K, a hyperfine sextet is observed due to electron spin-nuclear spin coupling with g_{iso}= 2.001 and hyperfine coupling constant A_{iso} = 88x10^{-4} cm^{-1} (Fig. 4.14). The observed *g* value is very close to the free electron spin value of 2.0023 which is consistent with the typical manganese(II) system, and also suggestive of the absence of spin orbit coupling in the ground state. In addition to this, the mixing of the nuclear hyperfine levels with the zero field splitting factor produces low intensity forbidden lines with an average spacing of 2.7 mT, corresponding to $\Delta m_I = \pm 1$ lying between each of the two main hyperfine lines [26].

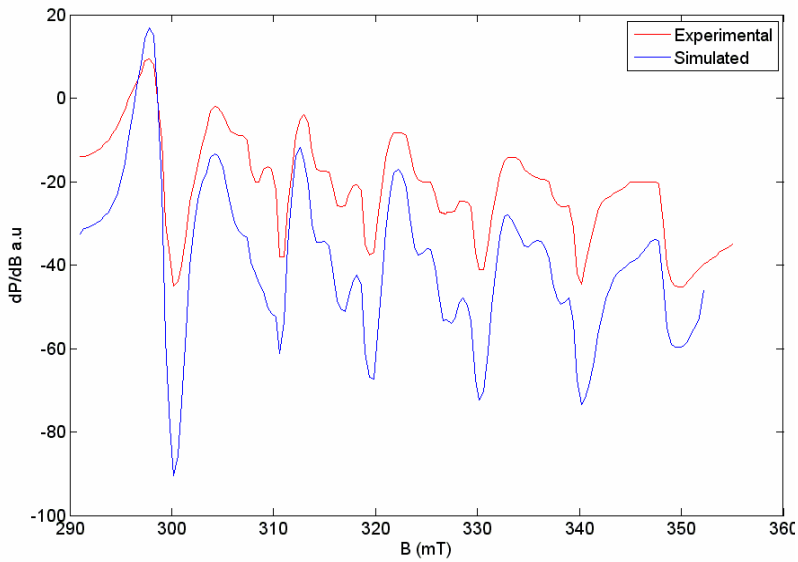

Fig. 4.14. EPR spectrum of [Mn(HASC)(OAc)] (8) in DMF at 77 K.

For compound **9**, the EPR spectrum in polycrystalline state shows the *g* value of 2.009 having peak to peak separation ΔB_{pp}= 44 mT (Fig. 4.15) and in frozen DMF at 77 K it displayed a hyperfine sextet with g_{iso} = 2.014 and A_{iso} = 91x10^{-4} cm^{-1} (Fig. 4.16).

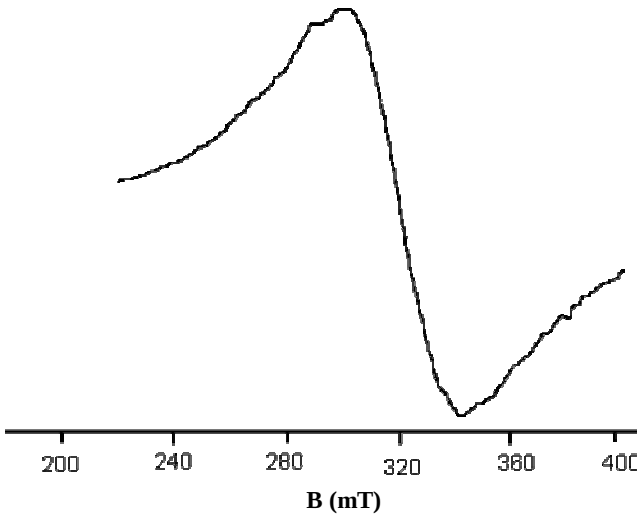

Fig. 4.15. EPR spectrum of [Mn(H_2ASC)(H_2O)]Cl_2 (9) in polycrystalline state at 298 K.

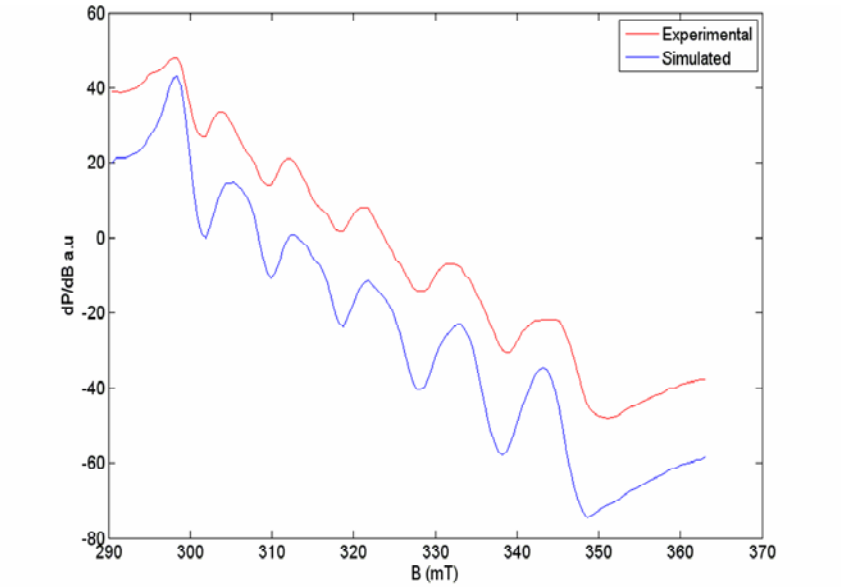

Fig. 4.16. EPR spectrum of $[Mn(H_2ASC)(H_2O)]Cl_2$ (9) in DMF at 77 K.

In polycrystalline state, compound **10** exhibited a broad signal with a *g* value of 2.639 having peak to peak separation ΔB_{pp} = 44 mT and it is shown in Fig. 4.17.

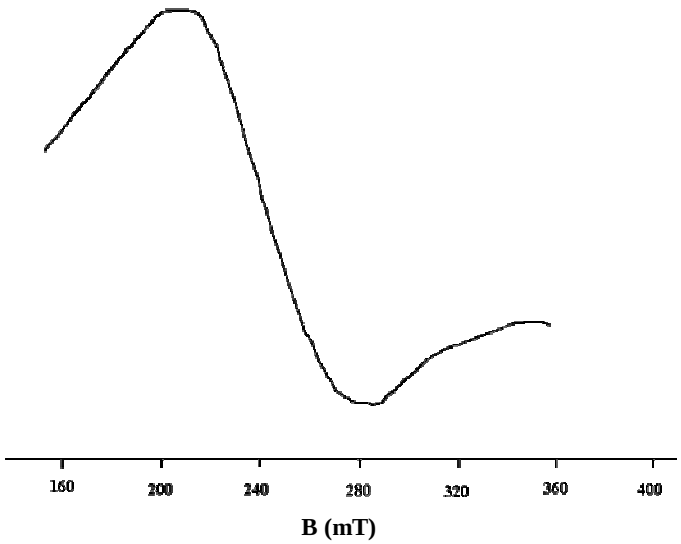

Fig. 4.17. EPR spectrum of $[Mn(HASC)(phen)]ClO_4$ (10) in polycrystalline state at 298 K.

But in frozen DMF the spectrum has four signals with *g* values (*g* = 1.997, 2.536, 3.092, 4.060), out of which one signal showed hyperfine sextet with A_{iso} = 85x10^{-4} cm^{-1} (Fig. 4.18). These different signals arise due to zero field splitting and Kramers degeneracy.

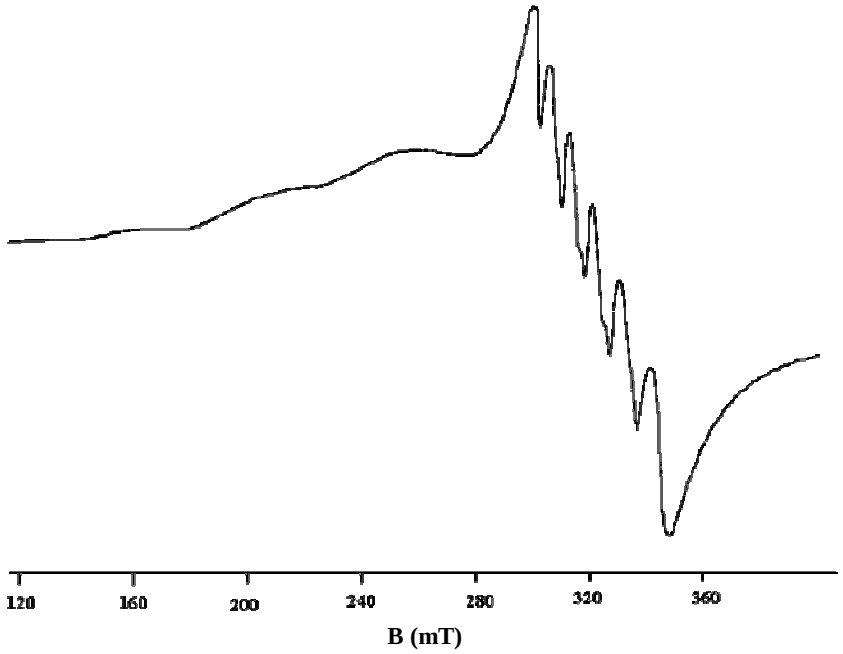

Fig. 4.18. EPR spectrum of [Mn(HASC)(phen)]ClO_4 (10) in DMF at 77 K.

Compound **11** showed two broad signals in the polycrystalline state at 298 K with *g* values of 2.501 and 1.996 with no hyperfine splitting (Fig. 4.19).

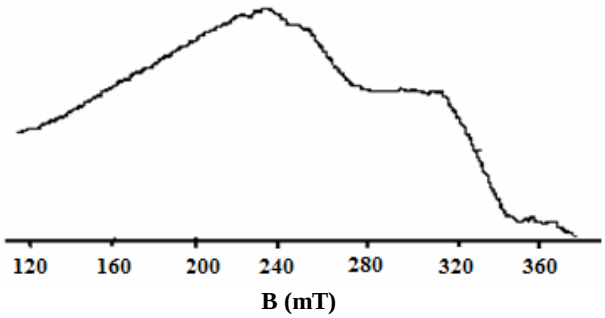

Fig. 4.19. EPR spectrum of [Mn(HBSC)$_2$] (11) in polycrystalline state at 298 K.

However when recorded in frozen DMF at 77 K, the spectrum displayed a hyperfine sextet with g value centered on 2.001 and hyperfine coupling constant A_{iso} = 89x10^{-4} cm^{-1}. In addition to this, a pair of forbidden lines are also observed in between each of the two main hyperfine levels (Fig. 4.20) with a spacing of 3 mT [26].

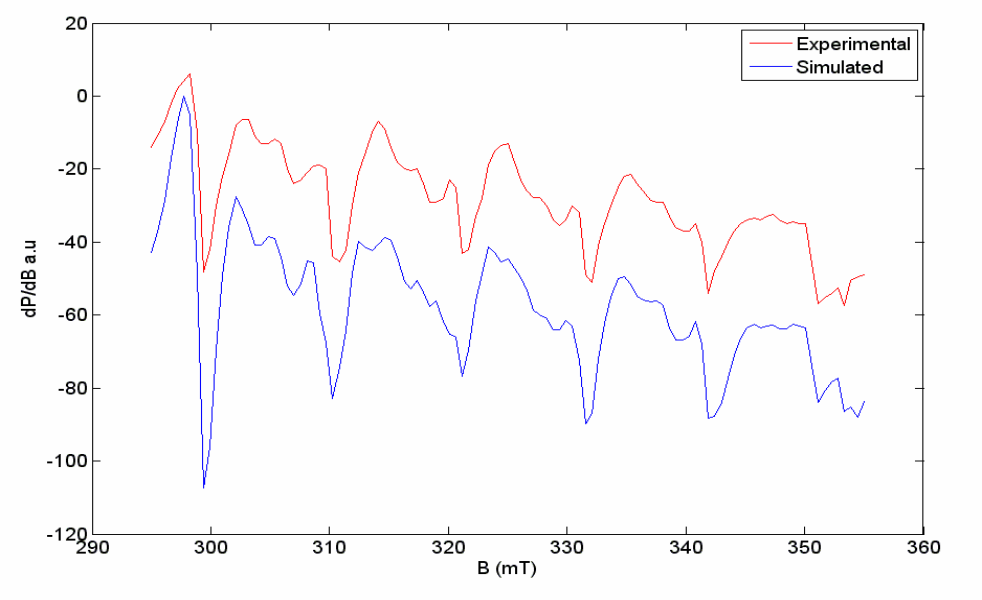

Fig. 4.20. EPR spectrum [Mn(HBSC)$_2$] (11) in DMF at 77 K.

The complex [Mn(HBSC)Cl]$_2$·2EtOH (**12**) displayed an isotropic spectrum with eleven lines in polycrystalline state at 298 K (Fig. 4.21). Binuclear Mn(II) centres are often identified by observation of a characteristic 11-line hyperfine factor in EPR spectra [27]. Here the g_{iso} value is 2.059 and A_{iso} = 78 x10^{-4} cm^{-1}. The probable structure is shown at the end of this chapter.

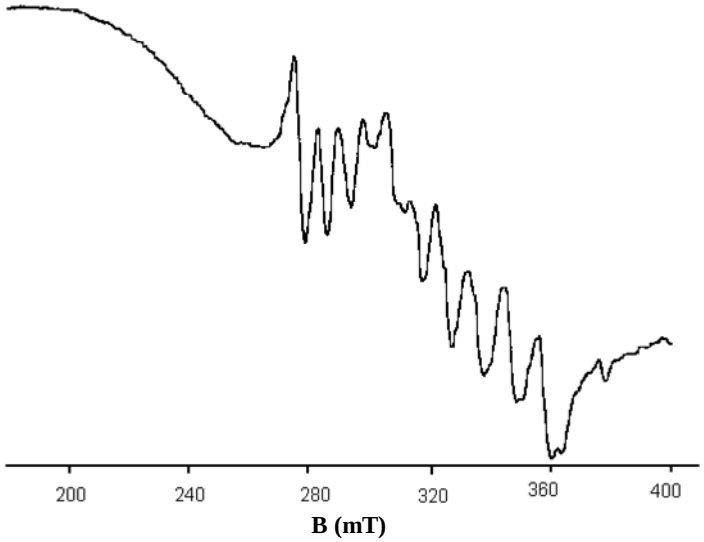

Fig. 4.21. EPR spectrum of $[Mn(HBSC)Cl]_2 \cdot 2EtOH$ (12) in polycrystalline state at 298 K.

In frozen DMF similar spectrum as reported above, as in the cases of other complexes with six hyperfine splittings, is obtained with g_{iso}= 2.001 and A_{iso} = 91 x10^{-4} cm^{-1} (Fig. 4.22)

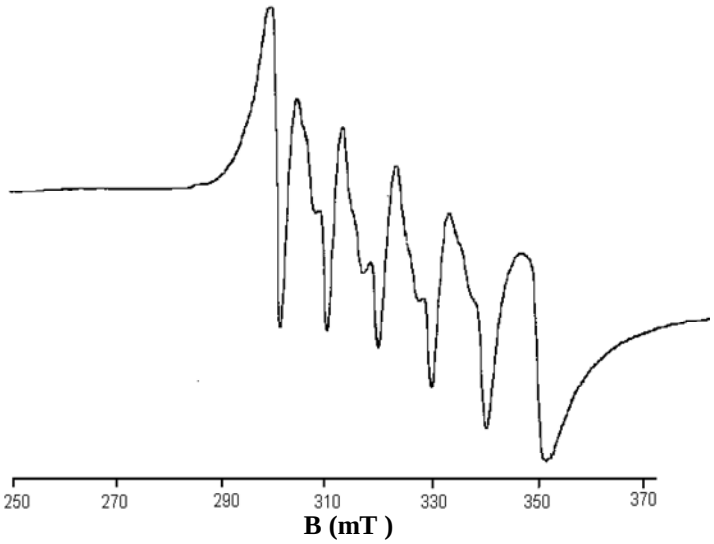

Fig. 4.22. EPR spectrum of $[Mn(HBSC)Cl]_2$ in DMF at 77 K.

The solid state EPR spectrum of compound **13** was characterized by three signals with corresponding g values of 3.059, 2.545 and 2.008 (Fig. 4.23). Its solution spectrum was a hyperfine sextet with g_{iso} = 1.997 A_{iso} = 92 x10^{-4} cm^{-1} (Fig. 4.24).

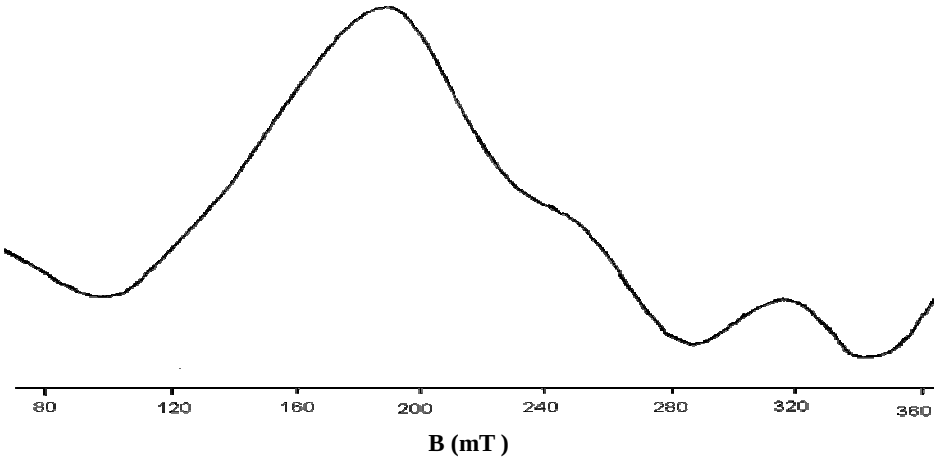

Fig. 4.23. EPR spectrum of [Mn(HBSC)(phen)]ClO_4·H_2O (13) in polycrystalline state at 298 K.

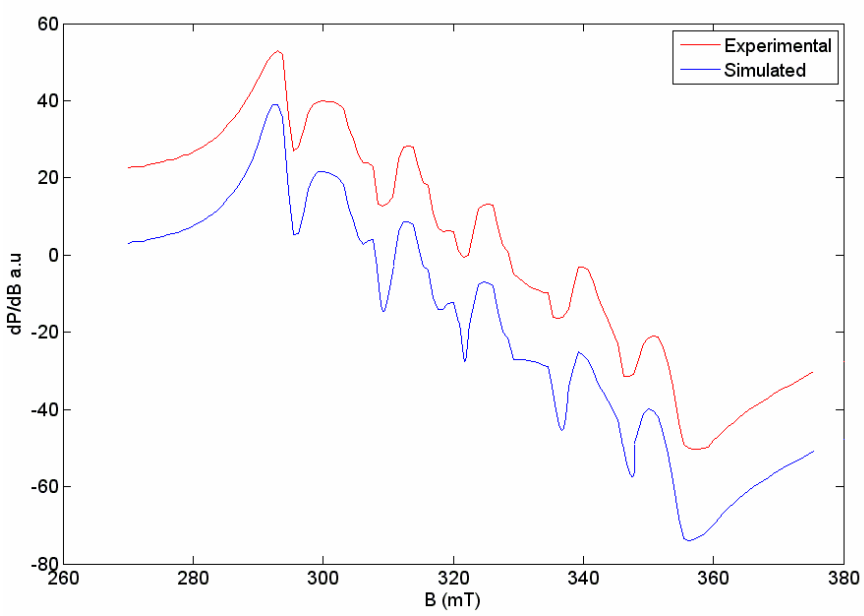

Fig. 4.24. EPR spectrum of [Mn(HBSC)(phen)]ClO_4 in DMF at 77 K.

EPR spectrum of [Mn(HBSC)(phen)(OAc)] (**14**) in polycrystalline state gave a signal with *g* value of 2.007 and without any resolved hyperfine splitting (Fig. 4.25), but the frozen solution spectrum was a well resolved hyperfine sextet with g_{iso} = 2.001 and A_{iso} = 90 x10^{-4} cm^{-1} (Fig. 4.26).

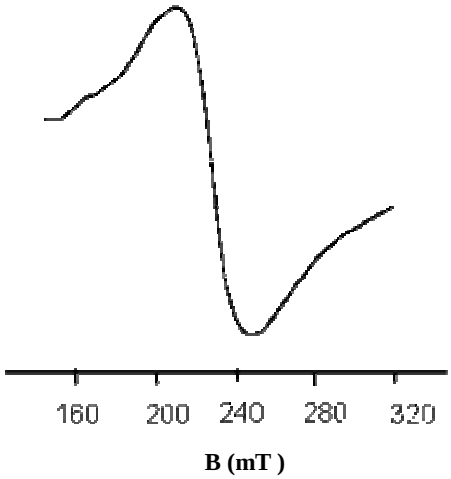

Fig. 4.25. EPR spectrum of [Mn(HBSC)(phen)(OAc)] (14) in polycrystalline state at 298 K.

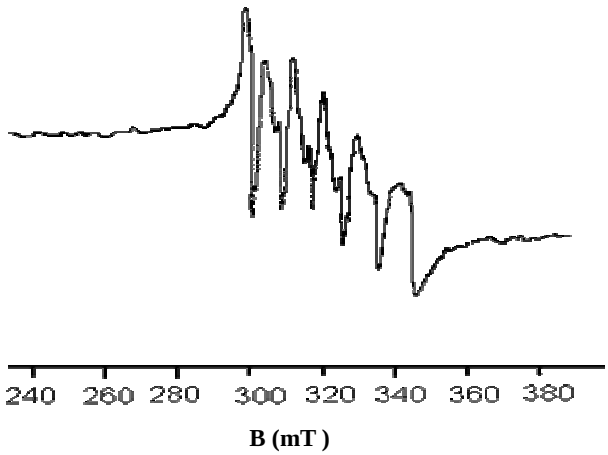

Fig. 4.26. EPR spectrum of [Mn(HBSC)(phen)(OAc)] (14) in DMF at 77 K.

In all the complexes reported above, the A_{iso} values are somewhat lower than pure ionic compounds which reflects the covalent nature of the metal-ligand bond in the complexes [28]. EPR spectral data for Mn(II) complexes including axial zero field splitting parameter *D*, rhombic zero field splitting parameter *E*, obtained from simulated spectra for some complexes and their *E*/*D* ratios are presented in Table 4.4. *E*/*D* ratios of compounds **11** and **13** are consistent with the reported values of distorted octahedral and five coordinated Mn(II) complexes [29]. However these ratios are widely different for tetra coordinate compounds **8** and **9**. No definite conclusion can be drawn for the geometry in the absence of crystal structure.

Table 4.4. EPR spectral data for Mn(II) complexes.

Compound	g Values		*D* (MHz)	*E* (MHz)	*E/D*
	Polycrystalline at 298 K	DMF at 77 K			
[Mn(HASC)(OAc)] **(8)**	2.738	2.001	470	140	0.297
$[Mn(H_2ASC)(H_2O)]Cl_2$ **(9)**	2.009	1.998	210	90	0.428
$[Mn(HASC)(phen)]ClO_4$ **(10)**	2.639	1.997, 2.536, 3.092, 4.060	----	----	----
$[Mn(HBSC)_2]$ **(11)**	2.501, 1.996	2.001	420	120	0.285
$[Mn(HBSC)Cl]_2 \cdot 2EtOH$ **(12)**	2.059	2.001	----	----	----
$[Mn(HBSC)(phen)]ClO_4 \cdot H_2O$ **(13)**	3.059, 2.545, 2.008	1.997	410	110	0.268
[Mn(HBSC)(phen)OAc)] (**14**)	2.007	2.001	----	----	----

4.3.7. Thermogravimetric analyses

Thermogravimetric analyses were obtained to give information concerning the thermal stability of the complexes. TGA studies for all the complexes except the perchlorate salts **10** and **13** were carried out in the temperature range 50-1000 °C. Perchlorate salts are potentially explosive. The results show that there is no indication of lattice water in complexes **8**, **9**, **11** and **14** and they are stable upto 300 °C [30]. For the complex **12,** a weight

loss of 9.3% is observed due to the loss of two molecules of ethanol in the temperature range 167-198 °C (cald. 9.2%). The second stage of decomposition is observed around 360 °C with a weight loss of 44.5% and may be assignable to the removal of ligand and the chlorine atom (cald. 44%). Some thermograms are presented in Figs. 4.27 and 4.28.

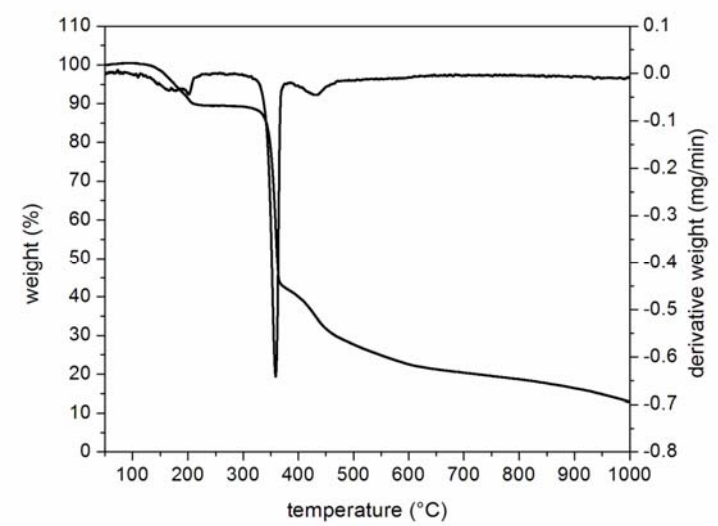

Fig. 4.27. Thermogram of $[Mn(HBSc)Cl]_2 \cdot 2EtOH$ (12).

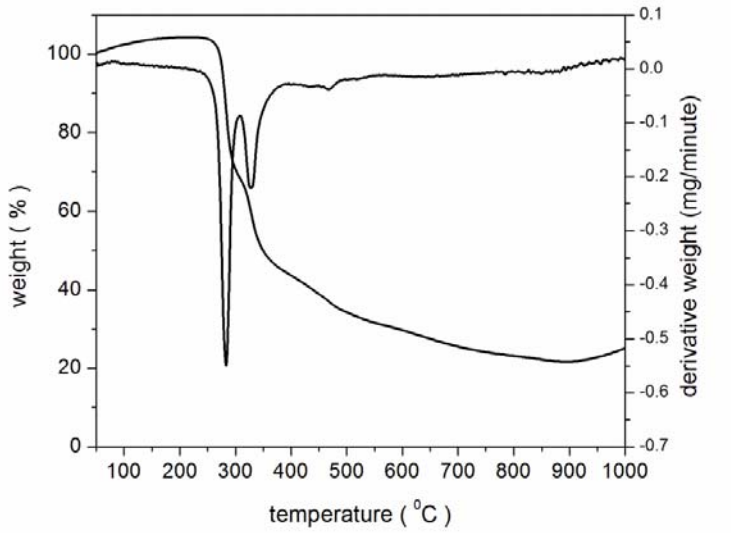

Fig. 4.28. Thermogram of [Mn(HBSc)(phen)(OAc)](14).

4.3.8. Cyclic voltammetry

In cyclic voltammetry, the potential of a small, stationary working electrode is changed linearly with time starting from a potential where no electrode reaction occurs and moving to potentials where reduction or oxidation of a solute (the material being studied) occurs. After traversing the potential region in which one or more electrode reactions take place, the direction of the linear sweep is reversed and the electrode reactions of intermediates and products, formed during the forward scan, often can be detected. A supporting electrolyte is present to repress migration of charged reactants and products. Here the redox properties of six Mn(II) complexes were investigated with the help of cyclic voltammetry (CV) using DMF solutions of the complexes in the potential range +2 to -2 V at a scan speed of 100 mV/s. Cyclic voltammograms were recorded on a CHI 608 D electrochemical analyzer with a three electrode compartment consisting of platinum disc working electrode, platinum wire counter electrode and Ag/Ag^+ reference electrode. Tetraethylammonium phosphate was the supporting electrolyte.

Generally the electrochemical properties of the complexes depend on a number of factors such as chelate ring size, substitution pattern in the chelate ring, charge type and coordination number [31,32].

The Mn(II) complexes are electroactive with respect to the metal centre and exhibited two redox processes in all the cases [33]. The first set of reduction waves are observed in the region of 0.146 to 0.385 V and the second set is occurred in the -1.529 to -0.129 V region. The corresponding oxidation responses are observed in the reverse scan. Two cyclic voltammograms are shown in Figs. 4.29 and 4.30. The two reduction peaks in the forward scan correspond to Mn(II)/Mn(I) and Mn(I)/Mn(0) reduction processes. The

corresponding oxidation responses are observed in the reverse scan. The cyclic voltammetric data for Mn(II) complexes are presented in Table 4.5.

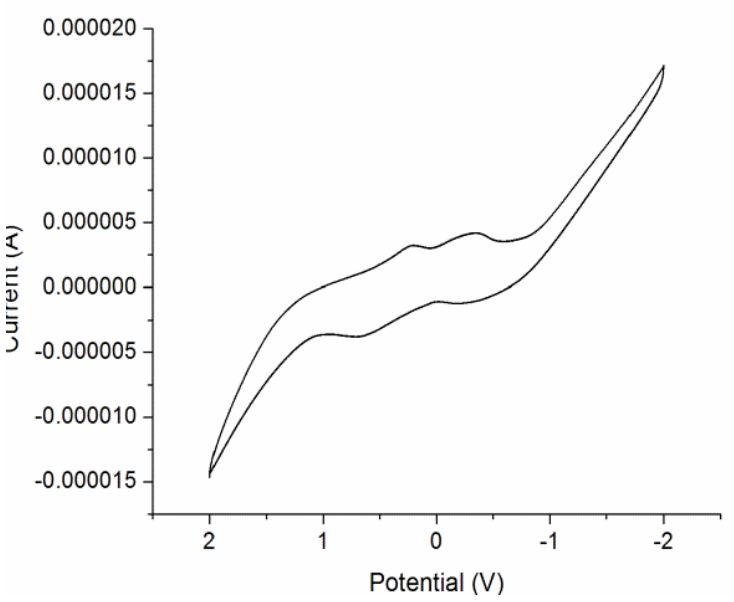

Fig. 4.29. Cyclic voltammogram of [Mn(HASC)(phen)]ClO_4 (10).

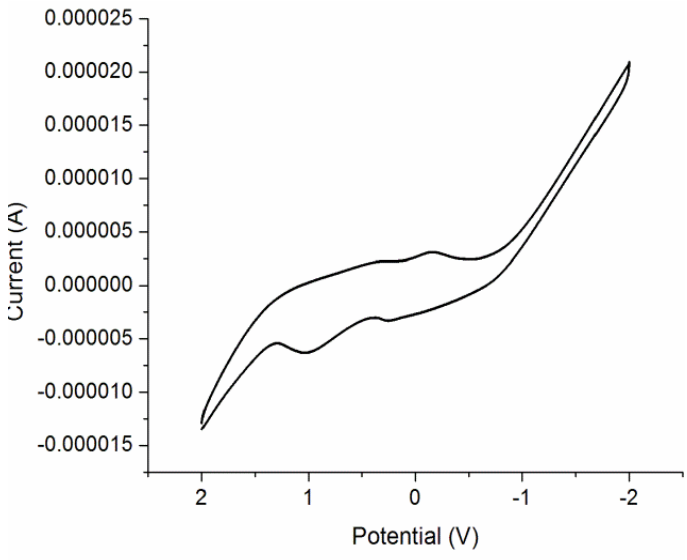

Fig. 4.30. Cyclic voltammogram of [Mn(HBSC)(phen)(OAc)] (14).

Table 4.5. Electrochemical data of the Mn(II) complexes in DMF.

Compound	Epc (V)	Ipc (μA)	Epa (V)	Ipa (μA)
[Mn(HASC)(OAc)] (**8**)	0.293	4.51	0.661	-6.5
	-1.529	20.32	-0.351	-3.03
$[Mn(H_2ASC)(H_2O)]Cl_2$ (**9**)	0.182	6.89	0.680	-5.15
	-0.553	9.10	-0.332	-3.69
$[Mn(HASC)(phen)]ClO_4$ (**10**)	0.231	3.19	0.652	-3.91
	-0.320	4.25	-0.378	0.89
$[Mn(HBSC)Cl]_2 \cdot 2EtOH$ (**12**)	0.201	4.12	0.717	-6.74
	-0.442	5.40	1.146	-9.02
$[Mn(HBSC)(phen)]ClO_4 \cdot H_2O$ (**13**)	0.146	8.43	0.036	-4.93
	-0.351	6.03	0.772	-7.70
[Mn(HBSC)(phen)(OAc)] (**14**)	0.385	1.98	0.238	-3.63
	-0.129	3.15	0.975	-6.55

On the basis of the physico-chemical measurements discussed above, the tentative structures proposed for some Mn(II) complexes are presented below. In all complexes the semicarbazones exist in the amido form, and act as ONO donor ligands. In complex **[**$Mn(H_2ASC)(H_2O)]Cl_2$ (**9**) semicarbazone acts as a neutral ligand, while in all others they act as monoanionic tridentate ones. Ethanol molecules are omitted in compound **12**.

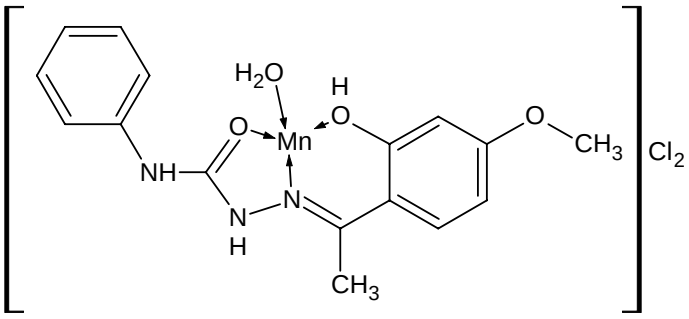

[Mn(H$_2$ASC)(H$_2$O)]Cl$_2$ (9)

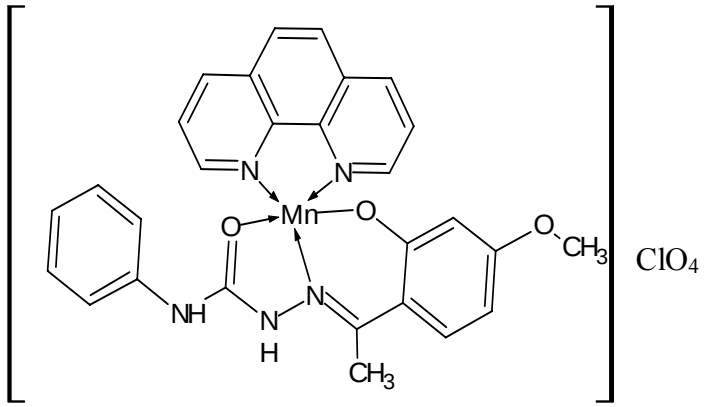

[Mn(HASC)(phen)]ClO$_4$ (10)

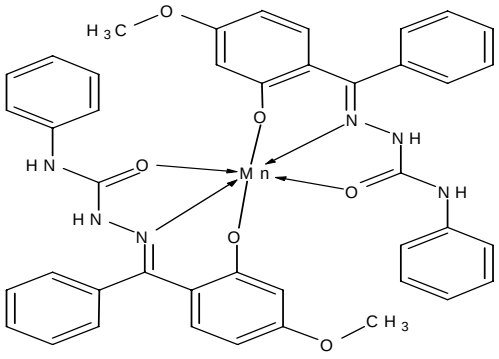

[Mn(HBSC)$_2$] (11)

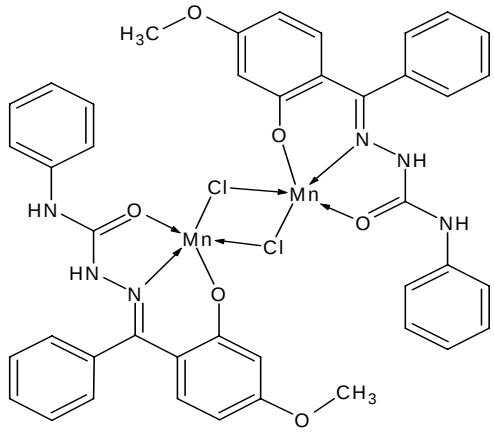

[Mn(HBSC)Cl]$_2$·2EtOH (12)

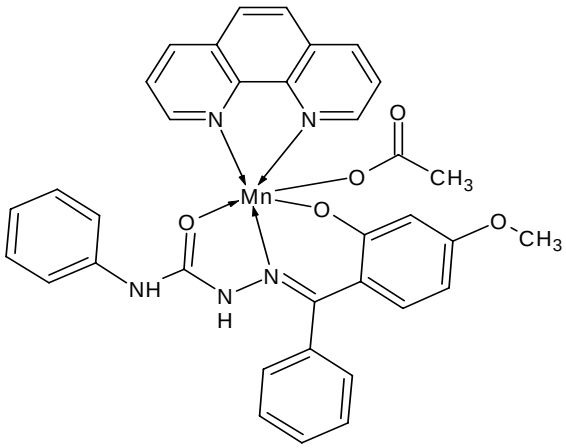

[Mn(HBSC)(phen)(OAc)] (14)

References

[1] M. Maneiro, M.R. Bermejo, M. Fondo, A.M. Gonzalez, J. Sanmartin, J.C. Garcia- Monteagudo, R.G. Pritchard, A.M. Tyryshkin, Polyhedron 20 (2001) 711.

[2] A. Sreekanth, M. Joseph, H.-K. Fun, M.R.P. Kurup, Polyhedron 25 (2006) 1408.

[3] H.N. Tang, L.F. Wang, R.D. Yang, Transit. Met. Chem. 28 (2003) 395.

[4] R.I. Kureshy, N.H. Khan, S.H.R. Abdi, P. Iyer, S.T. Patel, Polyhedron 18 (1999) 1773.

[5] W.J. Geary, Coord. Chem. Rev. 7 (1971) 81.

[6] D.F. Xiang, C.Y. Duan, X.S. Tan, Q.W. Hang, W.X. Tang, J. Chem. Soc., Dalton Trans. (1998) 1201.

[7] M. Devereux, M. McCann, V. Leon, R. Kelly, D. OSheaa, V. Mckee, Polyhedron 22 (2003) 3187.

[8] B. Murukan, S.K. Bhageerethi, M. Kochukittan, J. Coord. Chem. 60 (2007) 1607.

[9] G. Cerchiaro, P.L. Saboya, A.M.C. Ferreira, D.M. Tomazela, M.N. Eberlin, Transit. Met. Chem., 29 (2004) 495.

[10] R.P. John, A. Sreekanth, M.R.P. Kurup, S.M. Mobin, Polyhedron 21 (2002) 2515.

[11] M. Joseph, A. Sreekanth, V. Suni, M.R.P. Kurup, Spectrochim. Acta Part A 64 (2006) 637.

[12] P.B. Sreeja, M.R.P. Kurup, Polyhedron 23 (2004) 575.

[13] P.F. Rapheal, E. Manoj, M.R.P. Kurup, Polyhedron 26 (2007) 5088.

[14] A. Hatzidumitrious, C.A. Bolos, Polyhedron 17 (1998) 1779.

[15] K. Nakamoto, Infrared and Raman Spectra of Inorganic and Coordination Compounds, Wiley Interscience, New York (1986) 60.

[16] V.L. Siji, M.R. Sudarsanakumar, S. Suma, Polyhedron 29 (2010) 2035.

[17] S. Renjusha, M.R.P. Kurup, Polyhedron 27 (2008) 3294.

[18] A.M. Bond, R.L. Martin, Coord. Chem. Rev. 54 (1984) 23.

[19] E. Manoj, M.R.P. Kurup, A. Punnoose, Spectrochim. Acta Part A 72 (2009) 474.

[20] B.A. Reddy, J. Biomed. Sci. Res. 1 (2009) 27.

[21] A.B.P. Lever, Inorganic Electronic Spectroscopy, 2nd Edition, Elsevier Amsterdam, 1984.

[22] L. Latheef, M.R.P. Kurup, Polyhedron 27 (2008) 35.

[23] D.J.E. Ingram, Spectroscopy at Radio and Microwave Frequencies, 2nd Ed., Butterworth, London (1967).

[24] C. Mantel, C. Baffert, I. Romero, A. Deronzier, J. Pe´caut, M.N. Collomb, C. Duboc, Inorg. Chem. 43 (2004) 6455.

[25] S. Chandra, L. K. Gupta, Spectrochim. Acta Part A 61 (2005) 2549.

[26] B. Bleany, R.S. Rubins, Proc. Phys. Soc. London 77 (1961) 103.

[27] A.P. Golombek, M.P. Hendrich, J. Magn. Reson. 165 (2003) 33.

[28] V. Philip, V.Suni, M.R.P. Kurup, M. Nethaji, Spectrochim. Acta Part A 64 (2006) 171.

[29] S. Sasi, M. Sithambaresan, M.R.P. Kurup, H.-K. Fun, Polyhedron 29 (2010) 2643.

[30] G.A. Nazri, C. Julien, Solid State Ionics 80 (1995) 271.

[31] P. Bindu, M.R.P. Kurup, T.R. Satyakeerty, Polyhedron 18 (1998) 321.

[32] R.P. John, A. Sreekanth, V. Rajakannan, T.A. Ajith, M.R.P. Kurup, Polyhedron 23 (2004) 2549.

[33] D.K. Ajayakumar, A.P. Sangamesh, S.B. Prema, Int. J. Electrochem. Sci., 4 (2009) 717.

Chapter 5

SYNTHESES AND SPECTRAL CHARACTERIZATION OF COBALT(II/III) COMPLEXES OF N^4-PHENYLSEMICARBAZONES

Contents

5.1. Introduction

Cobalt is a ferromagnetic metal. Pure cobalt is not found in nature, but compounds of cobalt are common. Common oxidation states of cobalt include +2 and +3, although compounds with oxidation states ranging from -3 to +4 are also known. Co(II) complexes has a d^7 configuration and are very stable and difficult to oxidize. In contrast, in many cases during complexation, Co(II) is readily oxidized to Co(III) because the crystal field stabilization energy of Co(III) with a d^6 configuration is higher than Co(II) with a d^7 configuration. The synthesis and reactivity of cobalt complexes of Schiff base ligands have played an important role in the development of coordination chemistry [1].

Cobalt is an essential trace dietary mineral for all the animals, as the active centre of coenzymes called cobalamins, the most common example of which is vitamin B_{12}. Vitamin B_{12} is an organometallic compound found in nature and is the only vitamin that contains a metal atom. The cobalt complexes of tetradentate Schiff base ligands have been extensively used to

mimic cobalamin (B_{12}) coenzymes [2,3], dioxygen carriers and oxygen activators [4,5]. Although less common than other metalloproteins, cobaltoproteins are known aside from B_{12}. Cobaltocene is a structural analog to ferrocene where cobalt substitutes for iron. Cobaltocene is sensitive to oxidation much more than ferrocene. Cobalt carbonyl is a catalyst in carbonylation reactions.

This chapter deals with the syntheses and characterization of Co(II/III) complexes of N^4-phenylsemicarbazones including mixed ligand metal chelates incorporating heterocyclic bases and some pseudohalogens like azide and thiocyanate as coligands.

5.2. Experimental

5.2.1. Materials

Cobalt(II) acetate tetrahydrate (Nice Chemicals Pvt Ltd), 1,10-phenanthroline (Ranchem), 2,2′-bipyridine (Qualigens) and 4,4′-dimethyl 2,2′-bipyridine (Qualigens), potassium thiocyanate (Merck), 4-picoline (BDH) and sodium azide (Reidel-De Haen) were of Analar grade and were used as supplied and solvent used was methanol.

5.2.2. Syntheses of semicarbazones

Details regarding the syntheses of $H_2ASC{\cdot}H_2O$ and H_2BSC are described in Chapter 2.

5.2.3. Syntheses of cobalt complexes of 2-hydroxy-4-methoxyacetophenone-N^4-phenylsemicarbazone

5.2.3.1. *$[Co(HASC)_2]{\cdot}3H_2O$ (15)*

To a hot methanolic solution of $H_2ASC{\cdot}H_2O$ (0.317 g, 1 mmol), a solution of cobalt(II) acetate tetrahydrate (0.125 g, 0.5 mmol) in methanol was

added. The mixture was stirred for 4 h. and was kept overnight at room temperature. The brown colored compound formed was filtered, washed with methanol and ether. It was then dried over P_4O_{10} in *vacuo*.

Elemental Anal. Found (Calcd.) (%): C: 54.26 (54.16); H: 5.90 (5.40); N: 11.39 (11.84)

5.2.3.2. *[Co(ASC)phen(N_3)] (16)*

A hot solution of $H_2ASC{\cdot}H_2O$ (0.317 g, 1 mmol) in methanol was mixed with methanolic solutions of 1 mmol each of cobalt(II) acetate tetrahydrate (0.249 g) and phenanthroline (0.198 g). The resulting mixture was stirred with sodium azide (0.065 g, 1 mmol) for 4 h. and was kept at room temperature. The compound formed was filtered, washed with methanol and ether. It was then dried in *vacuo* over P_4O_{10}.

Elemental Anal. Found (Calcd.) (%): C: 57.45 (57.24); H: 4.12 (4.12); N: 19.61 (19.07)

5.2.3.3. *[Co(ASC)bipy(N_3)] (17)*

Methanolic solutions of 1 mmol each of $H_2ASC{\cdot}H_2O$ (0.317 g), cobalt(II) acetate tetrahydrate (0.249 g) and 2,2′-bipyridine (0.156 g) were mixed and the resulting solution was stirred for 2 h. To this sodium azide (0.065 g, 1 mmol) was added and stirred for two more hours. The compound formed was filtered, washed with methanol followed by ether. It was then dried over P_4O_{10} in *vacuo*.

Elemental Anal. Found (Calcd.) (%): C: 56.05 (56.22); H: 4.26 (4.36); N: 20.14 (20.17)

5.2.3.4. *[Co(ASC)dmbipy(N_3)] (18)*

This complex was prepared by stirring $H_2ASC{\cdot}H_2O$ (0.317 g, 1 mmol), cobalt(II) acetate tetrahydrate (0.249 g) and 4,4′-dimethyl 2,2′-bipyridine (0.184 g) in 1:1:1 ratio for 2 h. Then sodium azide (0.065 g) in methanolic medium was added in parts to the above mixture and continued stirring for another 2 h. and kept overnight at room temperature. The compound formed was filtered, washed with methanol and ether. It was then dried over P_4O_{10} in *vacuo*.

Elemental Anal. Found (Calcd.) (%): C: 57.76 (57.73); H: 4.99 (4.67); N: 19.83 (19.24)

5.2.3.5. *[Co(ASC)phen(NCS)]·2H_2O (19)*

To a methanolic solution of $H_2ASC{\cdot}H_2O$ (0.317 g, 1 mmol), solutions of 1,10-phenanthroline (0.198 g, 1 mmol) and cobalt(II) acetate tetrahydrate (0.249 g, 1 mol) in methanol were added with constant stirring and the resulting solution was stirred for 4 h. Then a solution of potassium thiocyanate (0.097 g, 1 mmol) in methanol was added to the above mixture and continued stirring for another 1 h. and allowed to cool at room temperature. The compound formed was filtered, washed with methanol and ether. It was then dried over P_4O_{10} in *vacuo*.

Elemental Anal. Found (Calcd.) (%): C: 54.73 (55.24); H: 3.91 (4.32); N: 13.34 (13.33); S: 4.98 (5.09)

5.2.3.6. *[Co(ASC)pic(N_3)] (20)*

An equimolar mixture of $H_2ASC{\cdot}H_2O$ (0.317 g, 1 mmol), 4-picoline (0.198 g, 1 mmol) and cobalt(II) acetate tetrahydrate (0.249 g, 1 mmol) is stirred for 3 h. To this solution sodium azide (0.065 g, 1 mmol) in methanolic medium was added in drops and continued stirring for one more hour. The

compound formed was filtered, washed with methanol and ether. It was then dried over P_4O_{10} in *vacuo*.

Elemental Anal. Found (Calcd.) (%): C: 54.14 (53.77); H: 4.18 (4.51); N: 20.41 (19.95)

5.2.4. Syntheses of Co(II/III) complexes of 2-hydroxy-4-methoxybenzophenone-N⁴-phenylsemicarbazone

5.2.4.1. *[Co(HBSC)$_2$] (21)*

To a hot methanolic solution of H_2BSC (0.361 g, 1 mmol), a methanolic solution of cobalt(II) acetate tetrahydrate (0.125 g, 0.5 mmol) was added. The mixture was stirred for 4 h. and kept at room temperature. The brown colored compound formed was filtered, washed with methanol and ether. It was then dried over P_4O_{10} in *vacuo*.

Elemental Anal. Found (Calcd.) (%): C: 64.17 (64.70); H: 4.49 (4.65); N: 11.44 (10.78)

5.2.4.2. *[Co(BSC)phen(N$_3$)]·2H$_2$O (22)*

To a hot solution of 1 mmol of H_2BSC (0.361 g) in methanol, methanolic solutions of 1 mmol each of cobalt(II) acetate tetrahydrate (0.249 g) and phenanthroline (0.198 g) were added with constant stirring. The resulting mixture was stirred further with sodium azide (0.065 g, 1 mmol) for 4 h. and was allowed to cool at room temperature. The compound formed was filtered, washed with methanol and ether. It was then dried over P_4O_{10} in *vacuo*.

Elemental Anal. Found (Calcd.) (%): C: 58.84 (58.58); H: 4.03 (4.32); N: 16.46 (16.56)

5.2.4.3. *[Co(BSC)bipy(N_3)] (23)*

Methanolic solutions of H_2BSC (0.361 g, 1 mmol), cobalt(II) acetate tetrahydrate (0.249 g, 1 mmol) and 2,2′-bipyridine (0.156 g, 1 mmol) in the ratio 1:1:1 were mixed and stirred for 2 h. The resulting solution was stirred for 2 h. more with sodium azide (0.065 g). The compound formed was filtered, washed with methanol followed by ether. It was then dried over P_4O_{10} in *vacuo*.

Elemental Anal. Found (Calcd.) (%):C: 59.96 (60.39); H: 4.70 (4.09); N: 18.21 (18.18)

5.2.4.4. *[Co(BSC)dmbipy(N_3)] (24)*

This complex was synthesized by stirring 1:1:1:1 ratio of H_2BSC (0.361 g), cobalt(II) acetate tetrahydrate (0.249 g), 4,4′-dimethyl 2,2′-bipyridine (0.184 g) and sodium azide (0.065 g) in methanolic medium for 4 h. and keeping overnight at room temperature. The compound formed was filtered, washed with methanol and ether. It was then dried over P_4O_{10} in *vacuo*.

Elemental Anal. Found (Calcd.) (%): C: 59.82 (59.82); H: 4.89 (4.72); N: 16.91 (17.2)

5.2.4.5. *[Co(HBSC)$_2$(NCS)] (25)*

Solutions of H_2BSC (0.361 g, 1 mmol), potassium thiocyanate (0.097 g, 1 mmol), and cobalt(II) acetate tetrahydrate (0.249 g, 1 mmol) in methanol were mixed and stirred for 4 h. The resulting solution was allowed to cool at room temperature. The compound formed was filtered, washed with methanol and ether. It was then dried over P_4O_{10} in *vacuo*.

Elemental Anal. Found (Calcd.) (%): C: 61.67 (61.65); H: 4.27 (4.33); N: 11.58 (11.70); S: 3.23 (3.83)

5.2.4.6. *[Co(BSC)phen(OAc)]·1.5H_2O (26)*

To a hot methanolic solution of H_2BSC (0.361 g, 1 mmol), methanolic solutions of 1 mmol each of cobalt(II) acetate tetrahydrate (0.249 g) and phenanthroline (0.198 g) were added. The resulting mixture was refluxed for 4 h. and was allowed to cool at room temperature. The compound formed was filtered, washed with methanol and ether. It was then dried over P_4O_{10} in *vacuo*.

Elemental Anal. Found (Calcd.) (%): C: 61.52 (61.41); H: 4.90 (4.56); N: 10.27 (10.23)

5.2.4.7. *[Co(BSC)dmbipy(OAc)]·3H_2O (27)*

Methanolic solutions of H_2BSC (0.361 g, 1 mmol), cobalt(II) acetate tetrahydrate (0.249 g, 1 mmol) and 4,4′-dimethyl-2,2′-bipyridine (0.184 g, 1 mmol) were mixed in 1:1:1 ratio and refluxed for 4 h. and kept overnight at room temperature. The compound formed was filtered, washed with methanol and ether. It was then dried over P_4O_{10} in *vacuo*.

Elemental Anal. Found (Calcd.) (%): C: 58.78 (58.74); H: 5.73 (5.35); N: 10.29 (9.79)

5.2.4.8. *[Co(BSC)pic]·3H_2O (28)*

This complex was prepared by stirring equimolar mixture of H_2BSC (0.361 g, 1 mmol), 4-picoline (0.186 g, 1 mmol) and cobalt(II) acetate tetrahydrate (0.249 g, 1 mmol) in methanolic medium for 4 h. The compound formed was

filtered, washed with methanol and ether. It was then dried over P_4O_{10} in *vacuo*.

Elemental Anal. Found (Calcd.) (%):C: 57.21 (57.35); H: 5.21 (5.35); N: 10.21 (9.91)

Caution! Azide complexes of metals with organic ligands are potentially explosive. So they should be synthesized and handled with due caution.

5.3. Results and discussion

Out of the fourteen complexes of Co(II/III) complexes presented here, compounds **15** and **21** have been synthesized by refluxing methanolic solutions of the semicarbazones and cobalt acetate in 2:1 ratio and in all other compounds it is in 1:1 ratio. Some mixed ligand metal chelates incorporating heterocyclic bases and some pseudohalogens like azide and thiocyanate as coligands are included in this group. All the complexes are brown in color and are soluble in solvents like DMSO, DMF and acetonitrile. In compounds **15**, **21** and **28** cobalt is in +2 oxidation state and found to be paramagnetic. All other complexes synthesized are diamagnetic confirming the oxidation of Co(II) to Co(III) during syntheses. In compounds **15**, **21** and **25** semicarbazones are in the amido form and in all others they are in the iminol form. The synthesized compounds are characterized by the following physico-chemical methods.

5.3.1. Elemental analyses

Elemental (C, H, N, S) analyses of all samples were tabulated in Sections 5.2.3 and 5.2.4. The observed C, H, N, S values showed that all the

complexes are analytically pure and in consistent with the stochiometry of the formulae suggested.

5.3.2. Molar conductivity

For all the complexes the molar conductance values observed in 10^{-3} M DMF solutions are in the range 2-18 ohm^{-1} cm^2 mol^{-1}. These low values indicate their non-conductive nature so that the pseudohalogens, azide and thiocyanate are present inside the coordination sphere and get coordinated with the metal ion [6].

5.3.3. Magnetic susceptibility

The magnetic moments of the complexes were calculated from the magnetic susceptibility measurements at room temperature. All complexes except **15**, **21** and **28** are found to be diamagnetic which confirms the oxidation of Co(II) to Co(III) during synthesis as has been reported previously with N^4-substituted semicarbazones, showing that it has no unpaired electrons with a spin paired octahedral configuration [7].

The magnetic moment values are of great significance in a structural context in the case of Co(II) complexes. Magnetic moments of tetrahedral, octahedral and square planar complexes differ significantly and therefore structural type can be easily identified using magnetic data. The low spin square planar Co(II) complexes may have magnetic moment 2.9 B.M., arising from one unpaired electron plus an apparently large orbital contribution [8].

Both tetrahedral and high-spin octahedral Co(II) complexes possesses three unpaired electrons but may be distinguished by the magnitude of the deviation of μ_{eff} from the spin only value. The magnetic moment of tetrahedral

Co(II) complexes with an orbitally non-degenerate ground term is increased above the spin only value *via* contribution from higher orbitally degenerate terms and occurs in the range 4.4-4.8 B.M. [9,10]. In octahedral Co(II) complexes, the ground state is $^4T_{1g}$ is orbitally degenerate and this causes large orbital contribution to the magnetic moment and exhibit μ_{eff} in the range 4.8-5.6 B.M. [11]. The observed magnetic moments for the octahedral complexes **[**$Co(HASC)_2]\cdot 3H_2O$ **(15)** and $[Co(HBSC)_2]$ **(21)** are 4.80 B.M. and 4.73 B.M. respectively. These values are larger than the spin only value of high spin Co(II) (3.87 B.M.; μ_{SO} =$[4S(S+1)]^{½}$; S=3/2), but are close to that expected when the spin and orbital angular momenta exist independently (5.20 B.M.; μ_{LS}=$[L(L+1) +4S(S+1)]^{½}$; L=3, S=3/2). This suggests a contribution of the orbital angular momentum [12,13]. The compound $[Co(BSC)pic]\cdot 3H_2O$ **(28)** exhibited a magnetic moment of 2.25 B.M., which is much lower than that expected of four coordinate Co(II) tetrahedral complexes (4.4-4.8 B.M.). This suggests a possible tendency towards a square planar geometry in this complex [14].

5.3.4. Infrared spectra

IR spectra of the semicarbazones and the complexes have been recorded as KBr pellets. The characteristic IR bands of the complexes show significant changes when compared with those of the free ligands and these changes in the characteristic vibrational frequencies of the ligands upon complexation provided evidence for the mode of their binding to the metal ion.

The tentative assignments of the IR spectral bands of $H_2ASC\cdot H_2O$ and its cobalt(II/III) complexes useful for determining the ligand's mode of coordination are listed in Table 5.1. The characteristic $\nu(^2N–H)$ and ν(C=O)

observed at 3295 and 1692 cm^{-1} respectively for the free ligand, indicate the amido nature of the semicarbazone in the solid state [15]. In all the complexes synthesized except in **15**, these bands disappeared, providing a strong evidence for the ligand coordination around cobalt(III) ion in its deprotonated enolate form [16]. Correspondingly a new band has appeared in the region 1528-1539 cm^{-1} which is due to the stretching frequency of the newly formed C=N group on enolization. But in compound **15 (**Fig. 5.1), ν(^{2}N–H) and ν(C=O) bands do not disappear, but undergo some shift, indicating the amido form of the semicarbazone in the complex. The broad band around 3400 cm^{-1} observed in this complex indicates the presence of lattice water. The azomethine band observed at 1619 cm^{-1} in the spectrum of $H_2ASC{\cdot}H_2O$ is shifted to lower wavenumbers by 14-21 cm^{-1} in the case of complexes. This red shift indicates the participation of azomethine nitrogen in coordination. The ν(N–N) band is observed at 1020 cm^{-1} for $H_2ASC{\cdot}H_2O$. The increase in frequency of this band in the case of complexes (1028-1099 cm^{-1}) again confirms the coordination of azomethine nitrogen. This increase in ν(N–N) value is due to the increase in double bond character, off-setting the loss of electron density *via* donation to the metal. Medium bands around 457-496 cm^{-1} corresponding to ν(Co–N) further support azomethine nitrogen coordination [17]. The spectra of the complexes do not exhibit the band at 3535 cm^{-1} due to the –OH stretching mode of phenolic group present in the semicarbazone, indicating deprotonation during coordination. Weak bands in the region 713-735 cm^{-1} indicate the presence of a Co–O bond resulting from coordination of the phenolic oxygen. Besides, the shifting of the band due to the Ar–O bond to lower frequencies indicates the weakening of the Ar–O bond due to coordination [18], the shift is being from 1270 cm^{-1} to 1235-1248 cm^{-1} region in the complexes.

Table 5.1. The important IR frequencies (cm^{-1}) of $H_2ASC\cdot H_2O$ and Co(II/III) complexes.

Compound	ν(C=O)	ν(C=N)	ν(C=N)[a]	ν(N–N)	ν(C–O)	ν(Co–O)	ν (Co–N)
$H_2ASC\cdot H_2O$	1692	1619	----	1020	1270	----	----
$[Co(HASC)_2]\cdot 3H_2O$ (**15**)	1661	1599	----	1028	1235	532	476
$[Co(ASC)phen(N_3)]$ (**16**)	----	1605	1532	1096	1248	534	496
$[Co(ASC)bipy(N_3)]$ (**17**)	----	1603	1528	1093	1239	536	490
$[Co(ASC)dmbipy(N_3)]$ (**18**)	----	1605	1532	1099	1245	535	494
$[Co(ASC)phen(NCS)]\cdot 2H_2O$ (**19**)	----	1598	1539	1090	1243	531	457
$[Co(ASC)pic(N_3)]$ (**20**)	-----	1604	1530	1094	1242	529	492

[a] Newly formed C=N

The most interesting part of the spectra of all the complexes **16-20** is the region above 2000 cm^{-1}, where the absorptions due to pseudohalogens are observed.

The azido complexes **16, 17, 18** (Fig. 5.2-5.4) and **20** (Fig. 5.6) exhibited the antisymmetric ν(NNN) vibration as sharp bands at 2021, 2014, 2020 and 2016 respectively. The presence of terminal azido group in the coordination sphere is evident from these values. The slight lowering in values is assumed to be the result of its coordination with Co(III) ion [19]. The strong bands at 1349, 1374 and 1348 cm^{-1} are attributed to their ν_s(NNN) vibrations [20]. The δ(NNN) bands are observed at 588, 654 and 587 cm^{-1} for these complexes. The medium bands in the region 411-419 cm^{-1} are assigned to the ν(Co–N_{azido}) bands.

The pseudohalide thiocyanate ion is a typical ambidentate ligand involving two different terminal donor atoms, the sulfur and nitrogen atoms. It is a very interesting anion for it may coordinate to a metal through the sulfur (thio) or through nitrogen (isothio) or through both of these atoms (bridging). Infrared spectroscopy is very useful in elucidation of the type of bonding exists. The various criteria proposed for determining the mode of bonding have been discussed by Nakamoto [21]. The CN stretching frequencies are generally lower in N–bonded complexes (near and below 2050 cm^{-1}) than in S-bonded complexes (near 2100 cm^{-1}) and the bridging [M-NCS-M] complexes exhibits *ν*(CN) well above 2100 cm^{1}. The *ν*(CS) band for S-bonded complexes are found in the 720-690 cm^{-1} region. The N-bonded complexes exhibit a single sharp *δ*(NCS) near 480 cm^{1}, where as the S-bonded complexes show several weak bands near 421 cm^{-1}. However these frequencies are very sensitive to the overall structure of

the complexes, the nature of the central metal, nature of other ligands in the complex and steric consideration [22]. Here in the thiocyanato complex [Co(ASC)phen(NCS)]·2H_2O **(19)** (Fig. 5.5) in the 2000-2100 cm^{-1}, expected for the *ν*(CN) stretching of the thiocyanato group absorption, the occurrence of two sharp and strong bands at 2126 and 2065 cm^{-1}, indicates the presence of two different coordinated thiocyanato groups. Such a higher wavenumber of 2126 cm^{-1} is probably due to the presence of bridging thiocyanato group. But in the absence of crystal structure, it is impossible to draw definite conclusions. A broad band due to the presence of lattice water in the complex is seen at 3420 cm^{-1}, which is also evident from the thermogravimetric analysis. The IR data are in conformity with the previous reports dealing with complexes having similar ligand systems [7].

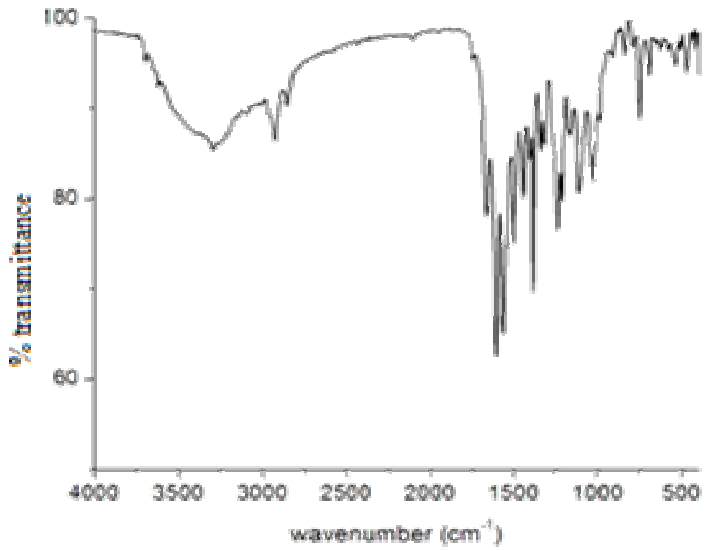

Fig. 5.1. IR spectrum of [Co(HASC)$_2$]·3H_2O (15).

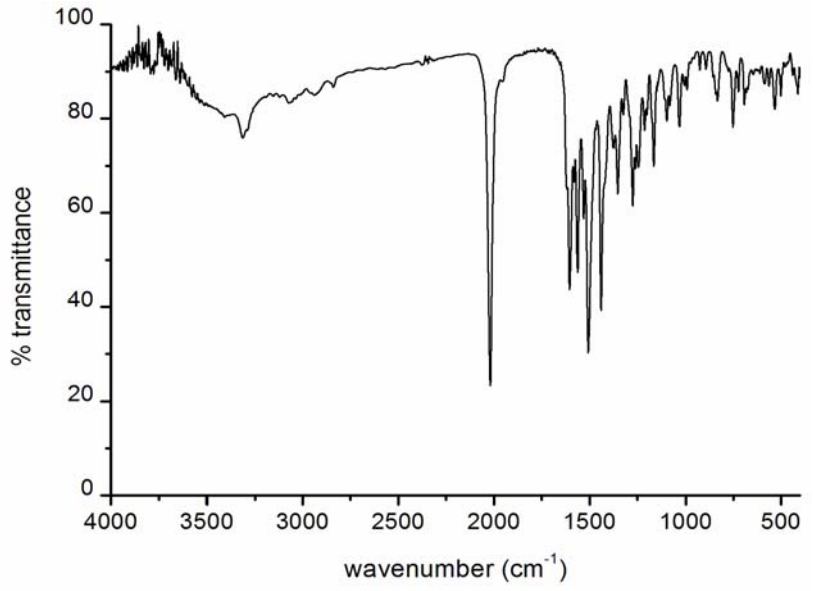

Fig. 5.2. IR spectrum of [Co(ASC)phen(N_3)] (16).

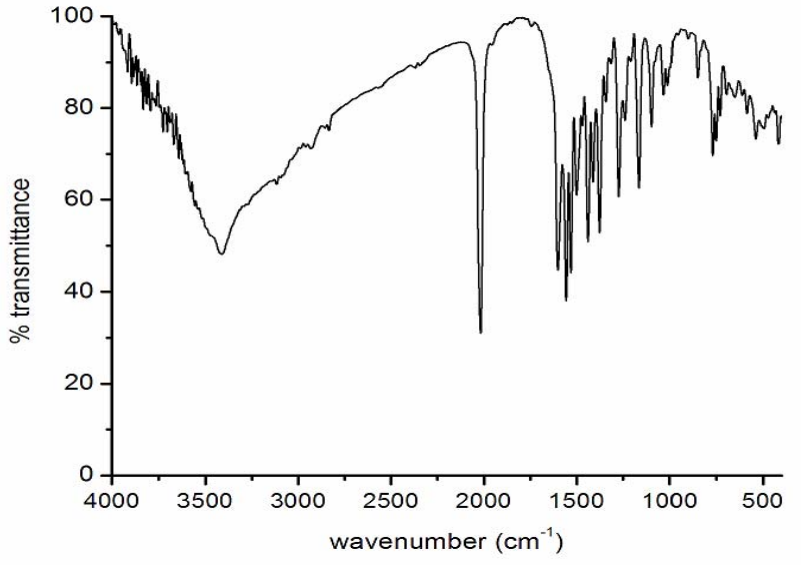

Fig. 5.3. IR spectrum of [Co(ASC)bipy(N_3)] (17).

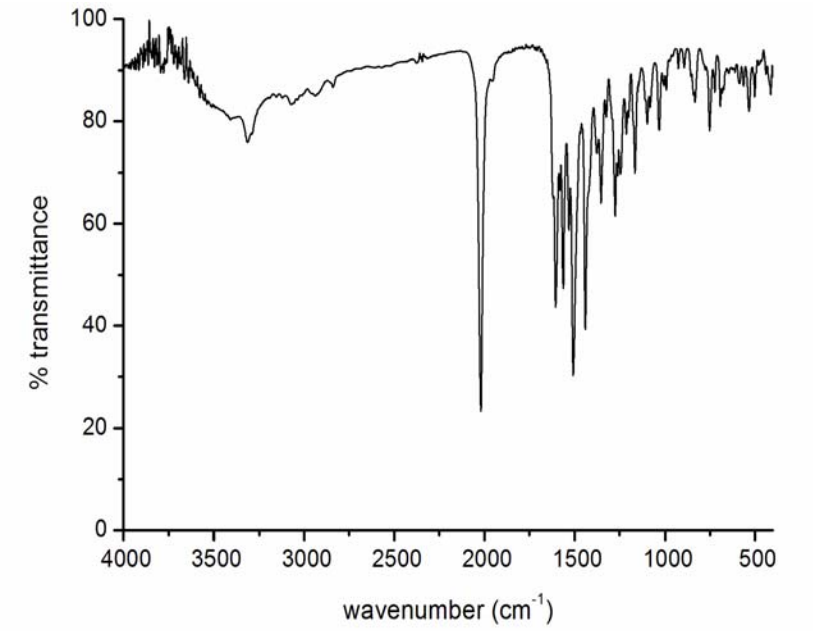

Fig. 5.4. IR spectrum of [Co(ASC)dmbipy(N_3)] (18).

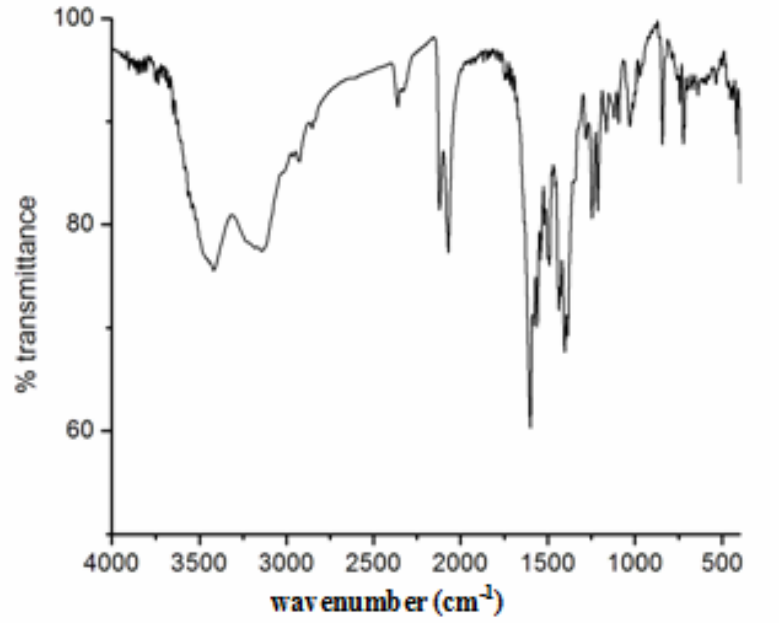

Fig. 5.5. IR spectrum of [Co(ASC)phen(NCS)]·2H_2O (19).

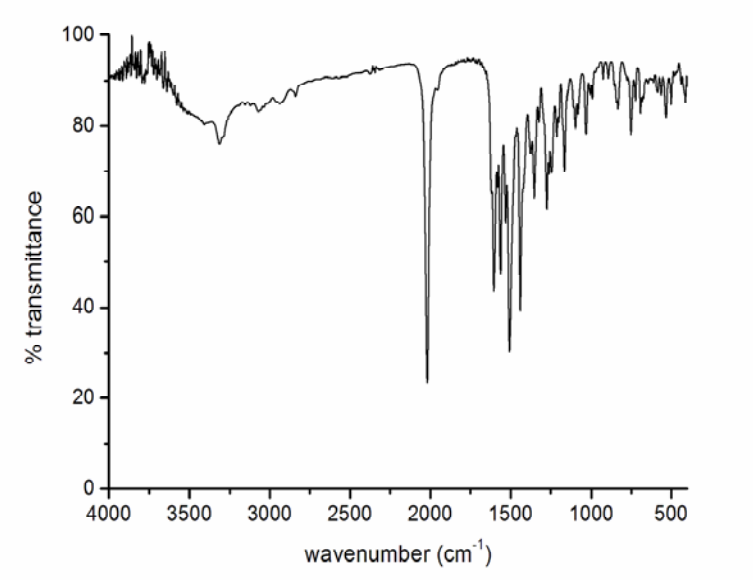

Fig. 5.6. IR spectrum of [Co(ASC)pic(N_3)] (20).

IR spectra of cobalt complexes of the semicarbazone H_2BSC showed similar dramatic changes as that of H_2ASC·H_2O for its complexes. The spectral assignments of the complexes are made, compared with that of the ligand and are tabulated in Table 5.2. The IR spectrum of H_2BSC shows a strong band at 1662 cm^{-1} attributed to ν(CO) and medium bands at 3145 and 3249 cm^{-1} assigned to $\nu(^2NH)$ and $\nu(^4NH)$ respectively. This suggests the amido form of semicarbazones in the solid state [23]. For the complexes [Co(HBSC)$_2$] (**21**) and **[**Co(HBSC)$_2$(NCS)] **(25)** these are shifted to lower frequencies indicating the ligand's existence in the amido form itself (Figs. 5.7 and 5.11) and coordination of the carbonyl oxygen atom to the central metal ion. But in all other complexes **22-24** and **26-28**, the bands due to the stretching vibrations of $\nu(^2NH)$ and ν(CO) are disappeared, giving evidence for the existence of semicarbazones in the iminol form. As a result of enolization we can observe the appearance of bands in the 1520-1555 cm^{-1} range due to the stretching vibrations of newly formed C=N

bond (Figs. 5.8- 5.10 and 5.12- 5.14). This is further confirmed by the new bands in the 493-519 cm^{-1} range due to the *ν*(Co–O) stretching vibrations. The IR spectral band observed at 1631 cm^{-1} is assigned to the ν(C=N) mode. The peak of this azomethine group was found in the lower frequency in the spectra of complexes which is an evidence of the bonding of azomethine nitrogen to the central cobalt ion [24]. Correspondingly the characteristic band of the semicarbazone at 1059 cm^{-1} due to *ν*(N–N) stretch undergoes a shift to higher wavenumbers upon complexation due to diminished repulsion between the lone pairs of adjacent nitrogen atoms. Further proof for the azomethine coordination is the presence of new band in the range 442-474 cm^{-1} which is assignable for *ν*(Co–N) for the complexes.

In the case of free phenyl semicarbazone the sharp band at 3316 cm^{-1} is due to the O–H stretching mode of phenolic oxygen. This band is found to be absent in all the complexes, indicating deprotonation of phenolic –OH and its coordination to the central metal ion [25]. Thus in complexes **22**, **23**, **24**, **26**, **27** and **28** semicarbazone acts as dideprotonated tridentate ligands, whereas in compounds **21** and **25** it acts as monodeprotonated tridentate one. In complexes **22**, **26**, **27** and **28** broad bands are seen *ca*. 3380 due to the presence of lattice water which is further confirmed from their thermogravimetric analyses.

Table 5.2. The important IR frequencies (cm^{-1}) of H_2BSC and Co(II/III) complexes.

Compound	ν(C=O)	ν(C=N)	ν(C=N)[a]	ν(N–N)	ν(C–O)	ν (Co–O)	ν (Co–N)
H_2BSC	1662	1631	----	1059	1294	----	----
[Co(HBSC)$_2$] (21)	1647	1605	----	1064	1238	497	449
[Co(BSC)phen(N_3)] ·2H_2O (22)	----	1606	1521	1071	1280	508	443
[Co(BSC)bipy(N_3)] (23)	----	1604	1555	1076	1259	524	444
[Co(BSC)dmbipy(N_3)] (24)	----	1606	1532	1092	1250	497	458
[Co(HBSC)$_2$(NCS)] (25)	1650	1605	----	1112	1254	519	442
[Co(BSC)phen(OAc)] ·1.5 H_2O (26)	----	1605	1520	1107	1240	515	474
[Co(BSC)dmbipy(OAc)] ·3H_2O (27)	----	1599	1543	1100	1259	497	451
[Co(BSC)pic] ·3H_2O (28)	----	1607	1529	1105	1256	493	463

[a] Newly formed C=N

The most peculiar feature for IR spectra of azido and thiocyanato complexes are observed in the region 2000-2100 cm^{-1}. In azido complexes **22**, **23** and **24** the strong and sharp bands observed at 2021, 2033 and 2035 cm^{-1} are assigned to the antisymmetric stretching modes and the bands at 1353, 1358 and 1349 cm^{-1} are due to symmetric stretching modes of azido group. The deformation modes of the azido ligand are observed as weak bands at 699, 696 and 700 cm^{-1} respectively for these compounds [26]. The presence of a single strong band at 2065 cm^{-1} is due to ν(CN) band of thiocyanato group. The ν(CS) of the NCS ligand at 744 cm^{-1} indicates the coordination through nitrogen atom of the terminal NCS ligand [27], the bending vibration of the NCS group is observed near 484 cm^{-1}. The intensity and band position indicate the coordination of the thiocyanate through the nitrogen atom of the NCS ligand.

The free acetate ion CH_3COO^- exhibits asymmetric and symmetric vibrations at 1578 and 1414 cm^{-1} respectively. It is reported that if it is covalently bonded to a metal as a unidentate ligand, the ν_{as} and ν_s are shifted to higher and lower frequencies respectively [21].

The very intense peak *ca*. 1600 cm^{-1} present in acetato complexes **26** and **27** are possibly due to the combination of ν(C=N) and ν_{as} (CH_3COO) stretching frequencies. Also these complexes displayed bands at 1363 and 1349 cm^{-1} may be due to the ν_s stretch of the acetate ion [28]. The difference between these two frequencies is of ~250 cm^{-1}, which is greater than that for uncoordinated acetate ion by ~143 cm^{-1} and that for bidentate acetate ion by ~217 cm^{-1}. It is strongly supported that both acetate ions are coordinated to the metal ion in a unidentate fashion [21,29]. Coordination of bases are indicated by the

presence of weak bands in the 410- 485 cm^{-1} region. The heterocyclic breathing are observed in the 740-1450 cm^{-1} region.

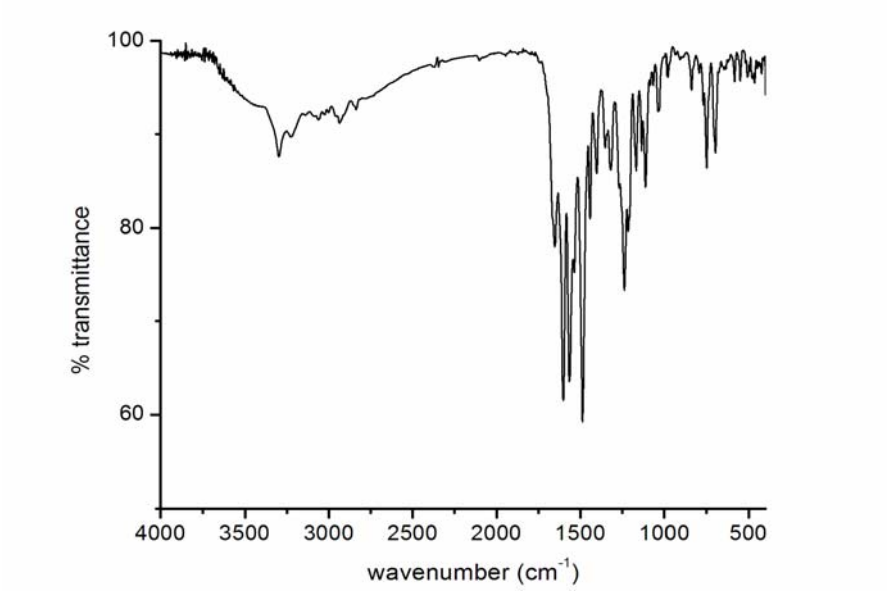

Fig. 5.7. IR spectrum of $[Co(HBSC)_2]$ (21).

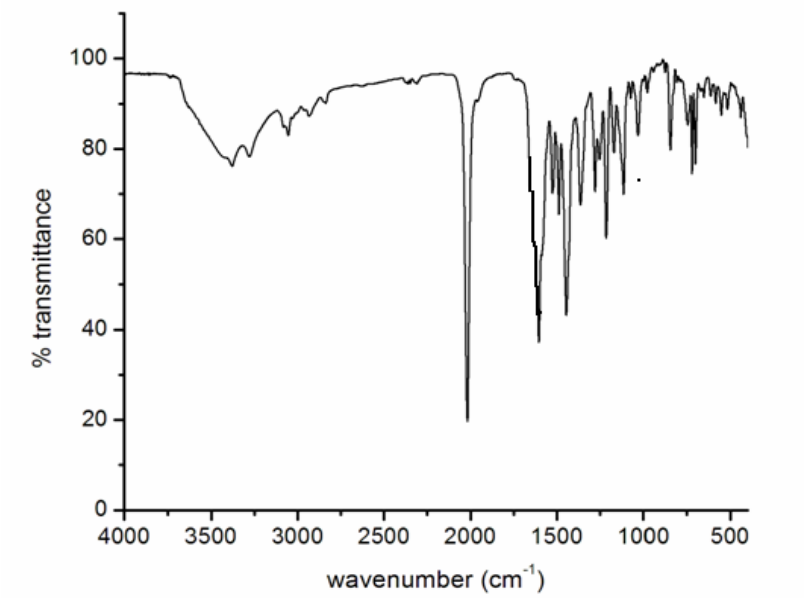

Fig. 5.8. IR spectrum of $[Co(BSC)phen(N_3)]\cdot 2H_2O$ (22).

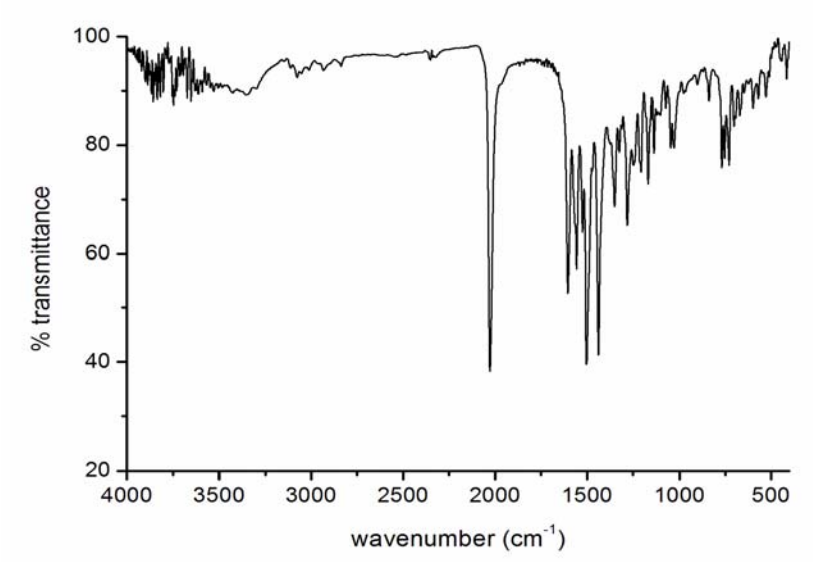

Fig. 5.9. IR spectrum of [Co(BSC)bipy(N_3)] (23).

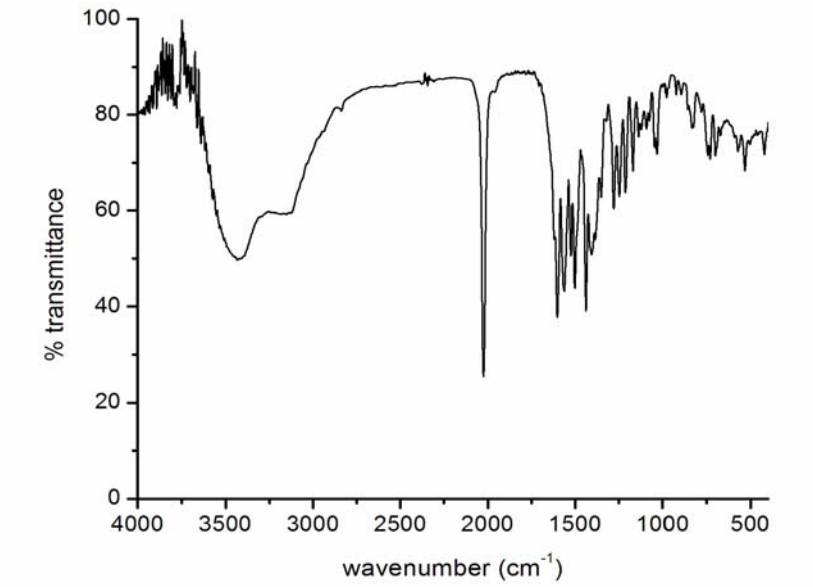

Fig. 5.10. IR spectrum of [Co(BSC)dmbipy(N_3)] (24).

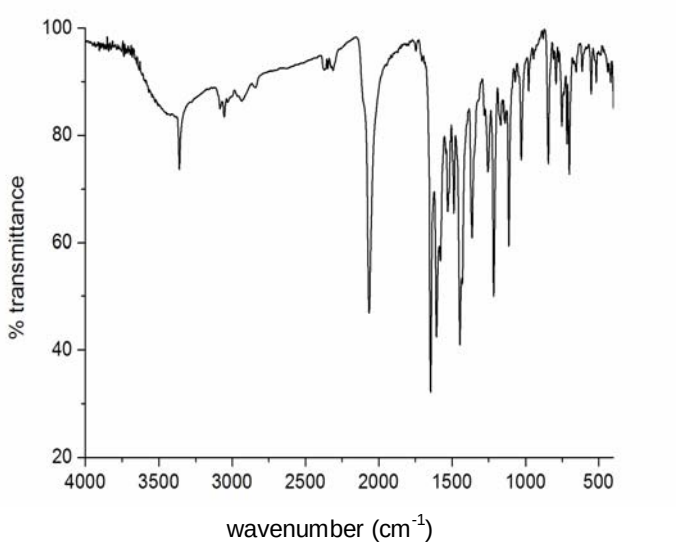

Fig. 5.11. IR spectrum of $[Co(HBSC)_2(NCS)]$ (25).

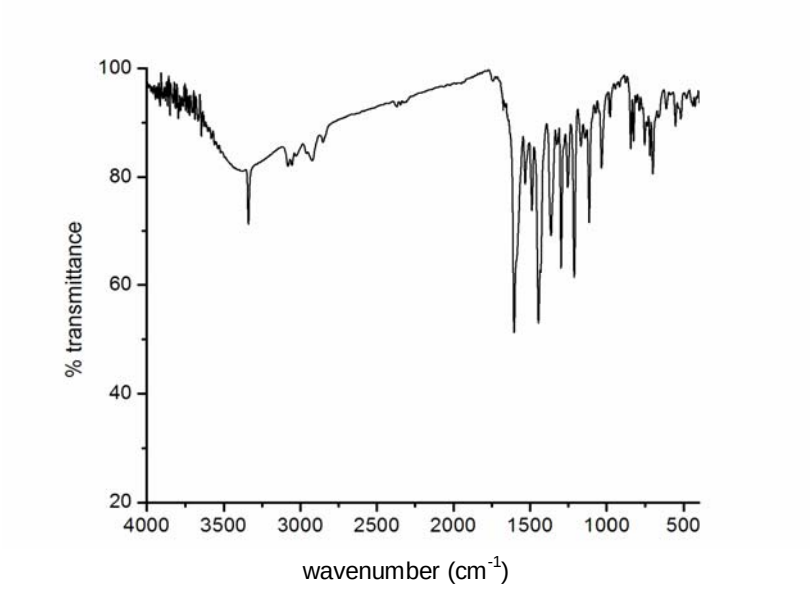

Fig. 5.12. IR spectrum of $[Co(BSC)phen(OAc)]\cdot 1.5H_2O$ (26).

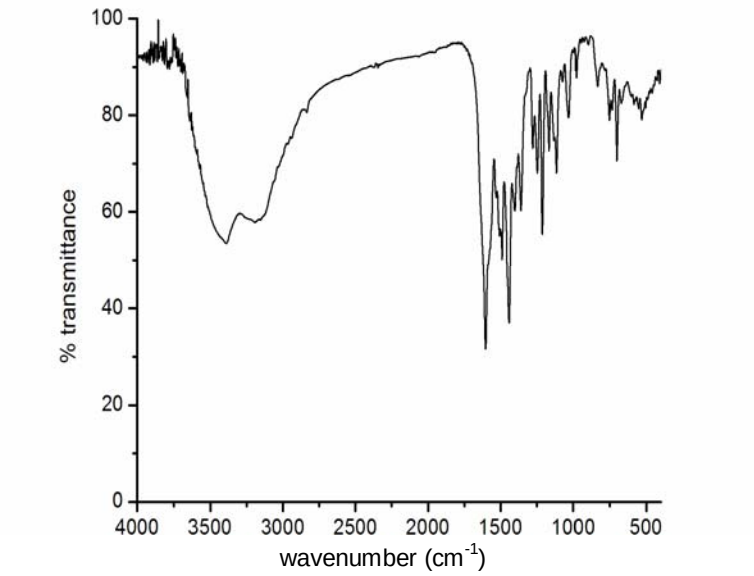

Fig. 5.13. IR spectrum of [Co(BSC)dmbipy(OAc)]·3H_2O (27).

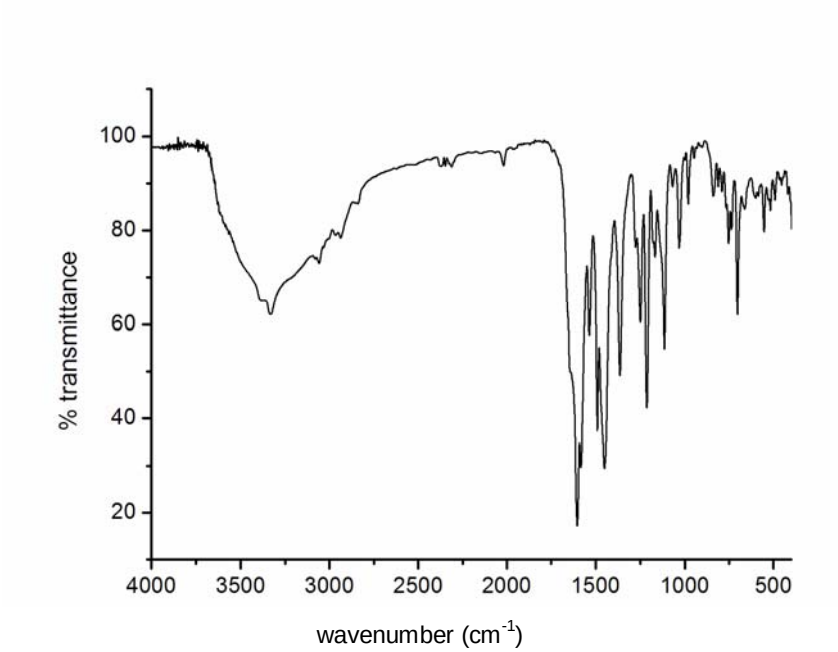

Fig. 5.14. IR spectrum of [Co(BSC)pic]·3H_2O (28).

5.3.5. Electronic spectra

The UV spectra of the semicarbazone H_2ASC and its complexes were recorded in acetonitrile and the spectral data are presented in Table 5.3. The semicarbazone H_2ASC shows bands in the range 31780–41750 cm^{-1} due to intraligand transitions. Upon complexation these bands are slightly shifted to the 30780-44250 cm^{-1} region. For all the complexes a broad band having two peaks is observed in the 25450-27000 cm^{-1} region which is assigned to the intramolecular charge transfer transitions combined with ν_2 ; ($^1T_{2g} \leftarrow {}^1A_{1g}$) [30,31]. The broadness is explained as the combination of O → Co and N → Co charge transfer bands (Fig 5.15).

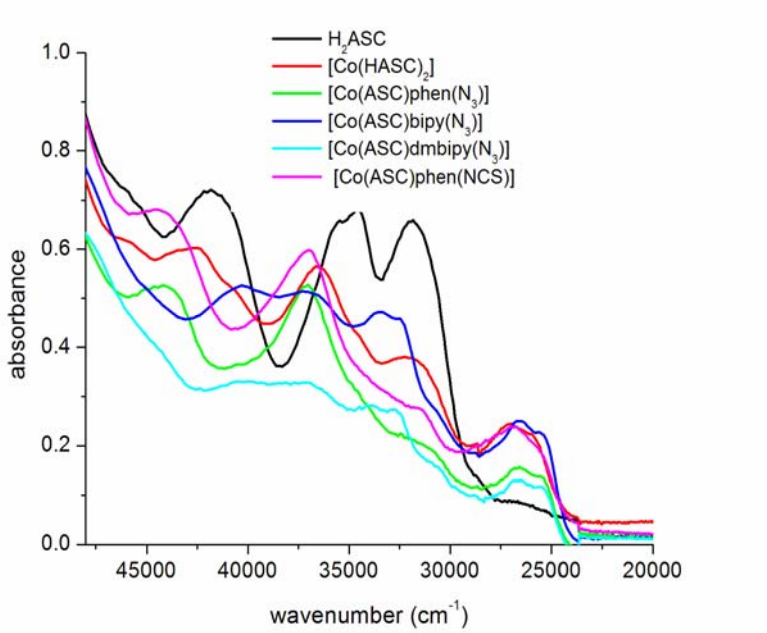

Fig. 5.15. UV spectra of H_2ASC and its Co(II/III) complexes.

The electronic spectra in the visible region were recorded in DMF for all the complexes. The electronic spectra of spin paired trivalent cobalt complexes of approximate O_h symmetry have the following assignments of *d-d*

bands: two spin allowed transitions at relatively low energies; $^1T_{1g} \leftarrow {}^1A_{1g}$ and $^1T_{2g} \leftarrow {}^1A_{1g}$. We have assigned for the complexes **16, 17** and **20**, these two spin allowed transitions, to be the bands in the 19420-20540 cm^{-1} region (ν_1; $^1T_{1g} \leftarrow {}^1A_{1g}$) (Figs. 5.17.2.-5.17.4) and 25450-25930 cm^{-1} region (ν_2; $^1T_{2g} \leftarrow {}^1A_{1g}$), found along with the charge transfer transitions. The band assigned to ν_2 is a combination band between it and charge transfer bands. There are two additional spin-forbidden transitions $^3T_{1g} \leftarrow {}^1A_{1g}$ and $^3T_{2g} \leftarrow {}^1A_{1g}$ at higher energies and these are usually complicated by the overlap of intraligand and charge transfer transitions. $^3T_{2g} \leftarrow {}^1A_{1g}$ is the most difficult to assign because this weak spin forbidden band is always at the onset of other high energy intense bands [32,33].

Table 5.3. Electronic spectral assignments (cm^{-1}) of H_2ASC and Co(II/III) complexes.

Compound	Intraligand transitions	LMCT	*d-d*
H_2ASC	31780, 34540, 35600 (sh), 41750	----	----
[Co(HASC)$_2$]·3H_2O (**15**)	31750, 36500, 40850 (sh), 42530	25930, 27000	18850
[Co(ASC)phen(N_3)] (**16**)	31100, 37080, 44140	25550, 26630	20360
[Co(ASC)bipy(N_3)] (**17**)	32400, 33470, 36970, 40310	25450, 26520	20540
[Co(ASC)dmbipy(N_3)] (**18**)	30780, 32720, 37130, 40370	25450, 26690	-----
[Co(ASC)phen(NCS)]·2H_2O (**19**)	31320, 37000, 44250	25770,26790	-----
[Co(ASC)pic(N_3)] (**20**)	31250, 36990, 42210	25530,26700	19420

From the magnetic susceptibility measurements it is assumed that the compounds **[**Co(HASC)$_2$]·3H_2O (**15**) and [Co(HBSC)$_2$] (**21**) have high spin octahedral configuration with cobalt in the +2 oxidation state. For a d^7 system, with the ground state term ^4F is split into three states in an octahedral crystal field. So in an octahedral geometry, Co^{2+} complexes usually show three bands corresponding to the spin allowed transitions $^4T_{2g}(F) \leftarrow {}^4T_{1g}(F)$ (ν_1), $^4A_{2g}(F) \leftarrow {}^4T_{1g}(F)$ (ν_2) and $^4T_{1g}(P) \leftarrow {}^4T_{1g}(F)$ (ν_3) transitions. The band observed at

18850, 18660 cm^{-1} respectively for compounds **15** and **21** (Figs. 5.17.1 & 5.17.5) can be assigned to $^4T_{1g}(P) \leftarrow {}^4T_{1g}(F)$ (ν_3) transitions. The other two bands are not well defined [34].

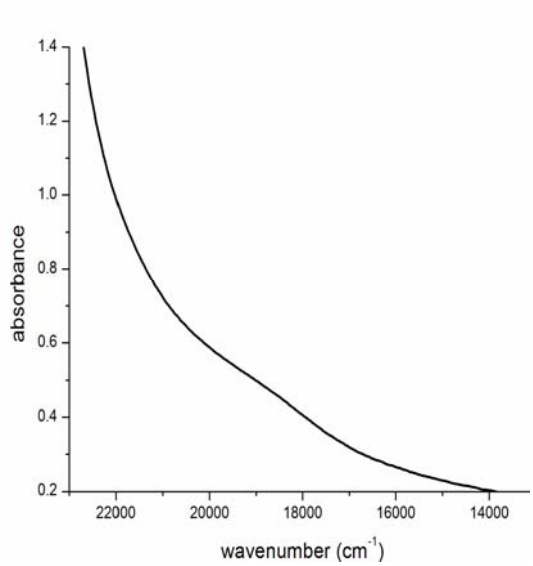

Fig. 5.17.1. [Co(HASC)$_2$]

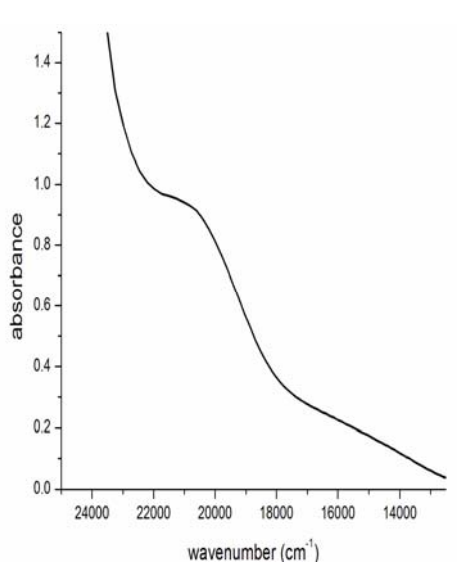

Fig. 5.17.2.[Co(ASC)phen(N$_3$)]

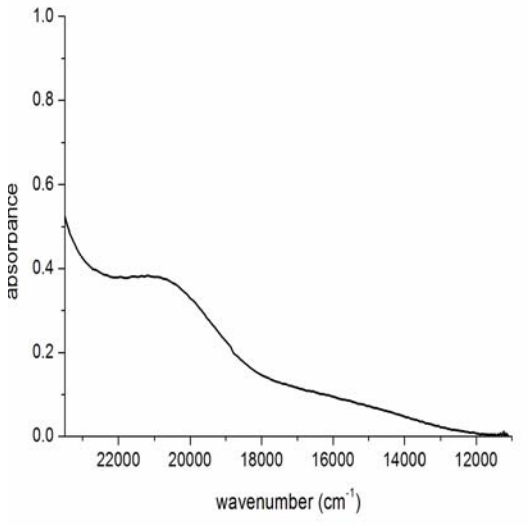

Fig. 5.17.3. [Co(ASC)bipy(N$_3$)]

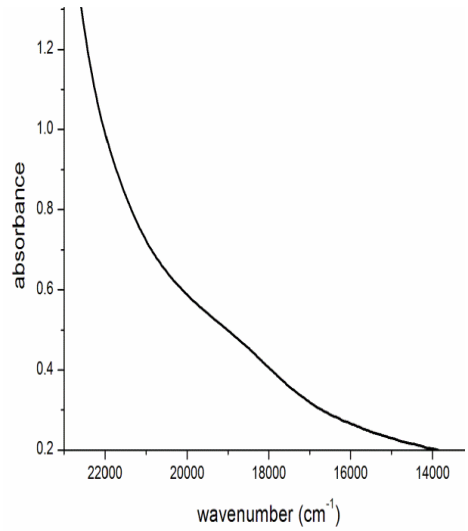

Fig. 5.17.4. [Co(ASC)pic(N$_3$)]

Fig. 5.17. Visible spectra of Co(II/III) complexes of H_2ASC.

For the low spin Co(III) complexes of H_2BSC (22-27) the bands observed in the 30170-43600 cm^{-1} region are intraligand transitions of the metal free ligand, suffered some shift due to complexation. For the free ligand these bands are in the 31330-41680 cm^{-1} region. The charge transfer transitions are occurred as a broad band in the range 25780-26740 cm^{-1}. For the compounds **23** and **24** additional peaks seen at 24920 and 25030 cm^{-1} can be attributed to the ν_2 ($^1T_{2g} \leftarrow {}^1A_{1g}$). Since $^1T_{2g} \leftarrow {}^1A_{1g}$ transition occurs at ca.25000 cm^{-1} for octahedral geometry, the bands assigned to charge transfer can be considered as a combination of LMCT and ν_2 (Fig. 5.16). The bands in the region 20820-21550 cm^{-1} are assigned to (ν_1; $^1T_{1g} \leftarrow {}^1A_{1g}$) transitions (Figs. 5.17.6. -5.17.10.). For compounds **18**, **19** and **22** we couldn't locate the *d-d* bands.

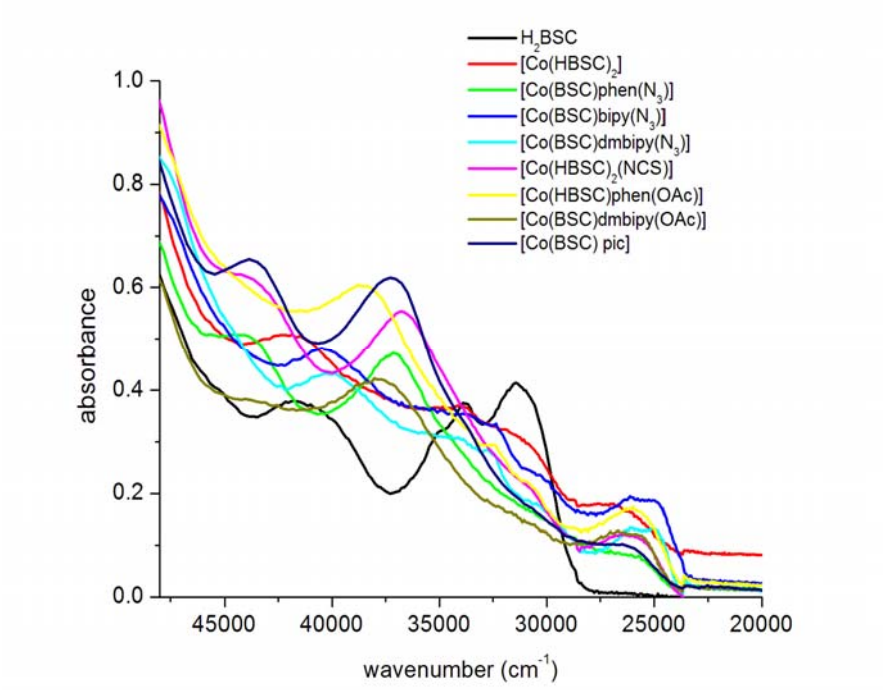

Fig. 5.16. UV spectra of H_2BSC and its Co(II/III) complexes.

Table 5.4. Electronic spectral assignments of H_2BSC and its Co(II/III) complexes (λ_{max} cm^{-1})

Compound	Intraligand transitions	LMCT	*d-d*
H_2BSC	31330, 33820, 35030, 41680	----	----
$[Co(HBSC)_2]$ (**21**)	31170, 33760, 41600	26740	18660
$[Co(BSC)phen(N_3)]\cdot 2H_2O$ (**22**)	36980, 43620	25780	----
$[Co(BSC)bipy(N_3)]$ (**23**)	30170, 32470, 33710, 40400	24920, 25960	20820
$[Co(BSC)dmbipy(N_3)]\cdot H_2O$ (**24**)	32520, 34030, 40070	25030, 25960	20880
$[Co(HBSC)_2NCS]$ (**25**)	30540 (sh), 36760 (sh), 43600	25920	21000
$[Co(BSC)phenOAc]\cdot 1.5H_2O$ (**26**)	30670, 32500, 38480	25990	21550
$[Co(BSC)dmbipy(OAc)]\cdot 3H_2O$ (**27**)	30580 (sh), 33700 (sh), 37230	25990	20900
$[Co(BSC)pic]\cdot 3H_2O$ (**28**)	30420 (sh), 37680, 43340	26150	20330, 16000 (w)

sh=shoulder w=weak

The compound **28** is probably square planar as evidenced from its μ_{eff} (2.25 B.M) value**.** The band observed at *ca*. 20330 cm^{-1} may be assigned to $^2A_{1g} \leftarrow {}^2B_{2g}$ transition. The band due to $^2E_g \leftarrow {}^2B_{2g}$ transition is not well resolved (Fig. 5.17.11.) [35].

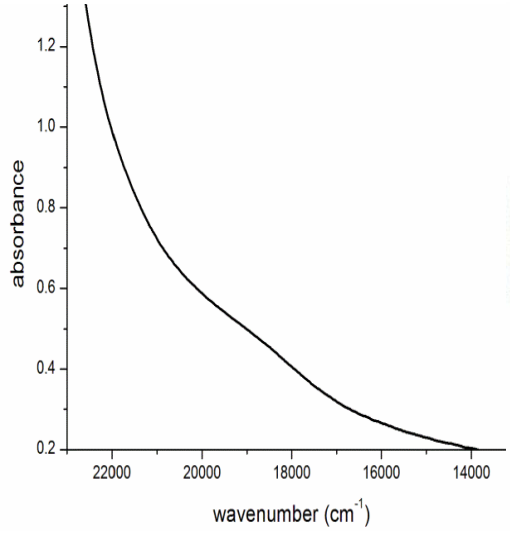

Fig. 5.17.5. [Co(HBSC)$_2$]

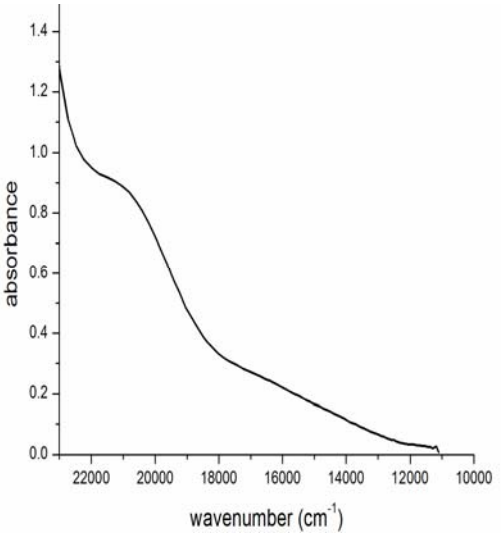

Fig. 5.17.6. [Co(BSC)bipy(N$_3$)]

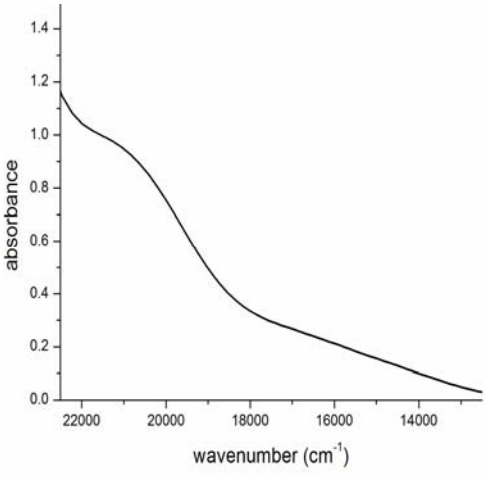

Fig. 5.17.7. [Co(BSC)dmbipy(N$_3$)]

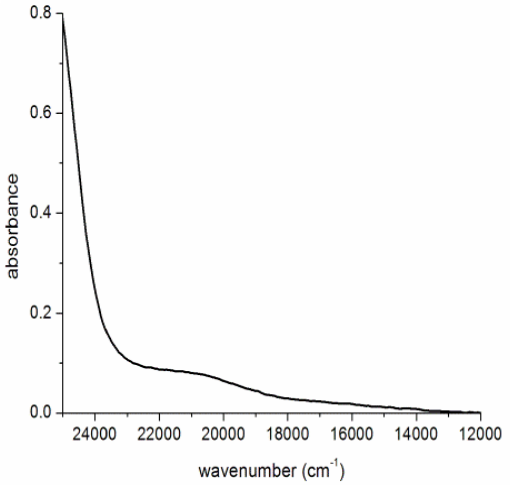

Fig. 5.17.8. [Co(HBSC)$_2$(NCS)]

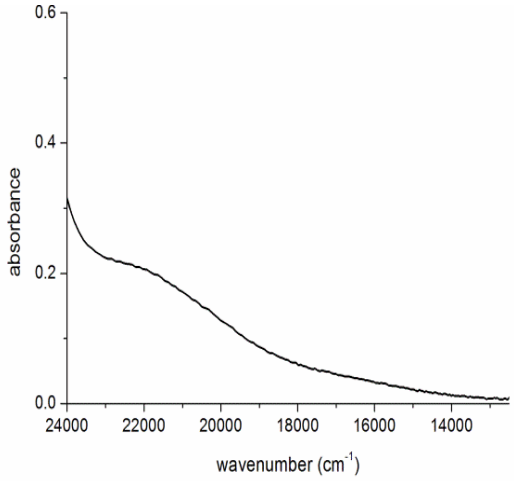

Fig. 5.17.9. [Co(BSC)phen(OAc)]

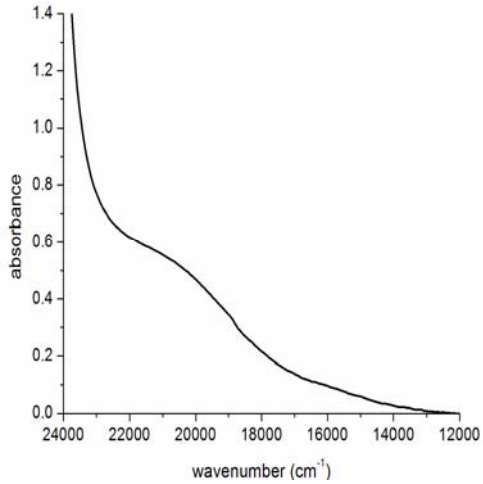

Fig.5.17.10. [Co(BSC)dmbipy(OAc)]

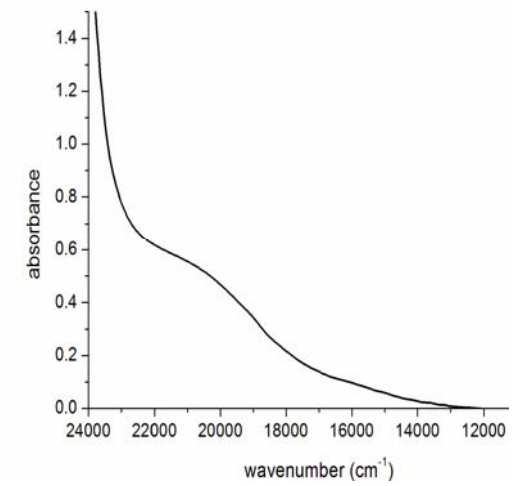

Fig.5.17.11. [Co(BSC)pic]

Fig. 5.17. Visible spectra of Co(II/III) complexes of H_2BSC.

5.3.6. Thermogravimetric analyses

Thermogravimetric analyses of complexes **15**, **26**, **27** and **28** have been done and mass losses observed below 180 °C indicate the water molecules present in these complexes are outside the coordination sphere [36]. Thermal behavior

of azido complexes have not been studied since they are potentially explosive. The thermograms of complexes **27** and **28** are presented in Figs. 5.18 and 5.19.

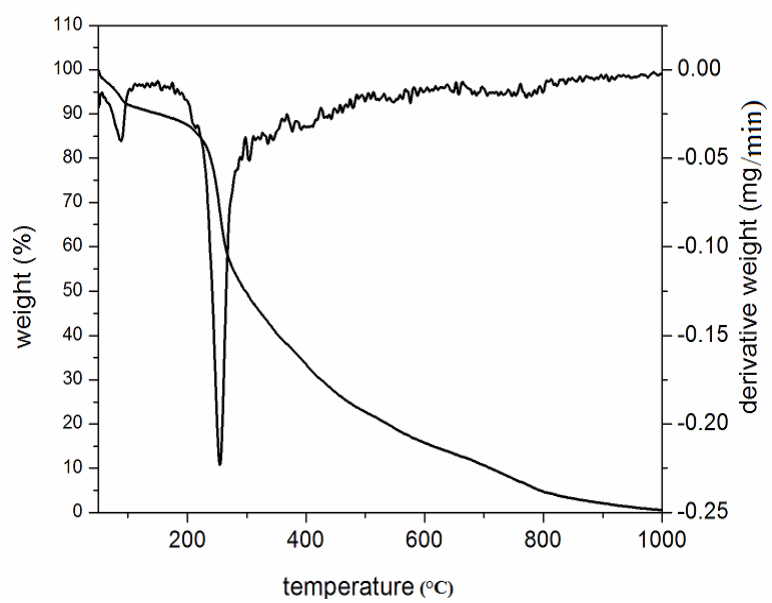

Fig. 5.18. Thermogram of [Co(BSC)dmbipy(OAc)]·3H_2O (27).

The thermogram of the complex **27** shows two well defined mass losses. The first mass loss of 7% below 90 °C (calcd. 7.5%) corresponds to the removal of three molecules of water. This suggests that water molecules are present outside the coordination sphere [35]. The second mass loss of 26.8% (calcd. 27.7%) *ca*. 250 °C is due to the decomposition of heterocyclic base, dimethylbipyridine. Weight losses due to the decomposition of ligand was found over 250 °C and degradation was found to be completed at 1000 °C.

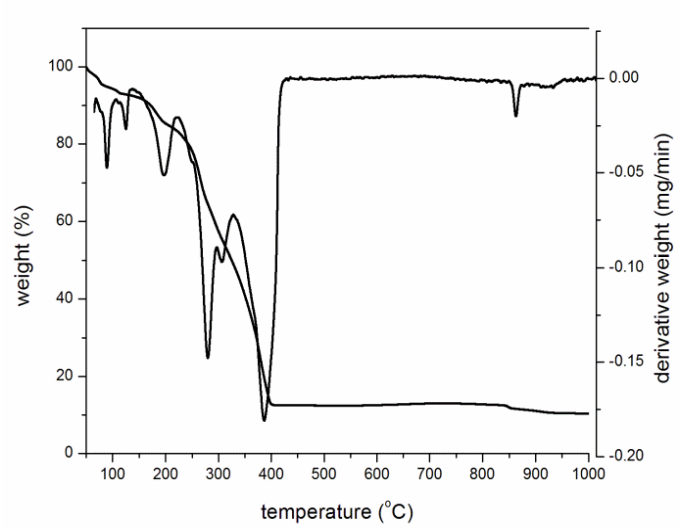

Fig. 5.19. Thermogram of [Co(BSC)pic]·3H_2O (28).

Thermogravimetric analysis shows that complex **28** undergoes three step degradation in the temperature range of 74-175 °C having a total mass loss of 9.5% (calcd.10%) corresponding to three molecules of water. The second weight loss of 17.2% (calcd. 18%) is due to the removal of the base, picoline and it occurs in 200-260 °C range and above 260 °C degradation of the ligand takes place.

In the light of the above physical methods discussed we have suggested octahedral geometry for all the complexes except compound **28** which is assumed to be square planar**.** The semicarbazones undergo double deprotonation to form dianions in all the complexes except **15** and **21** and act as tridentate ONO donors occupying the three positions of the octahedron. In compounds **15** and **21** the semicarbazones are in the amido form. In the case of complexes having the general formula [CoLBX], (B-Base and X-anion) base acts as a bidentate ligand and occupies the fourth and fifth positions. The azido, thiocyanato or acetato group occupies the sixth position as unidentate ligands in the octahedral geometry. The proposed structures of some compounds are presented here.

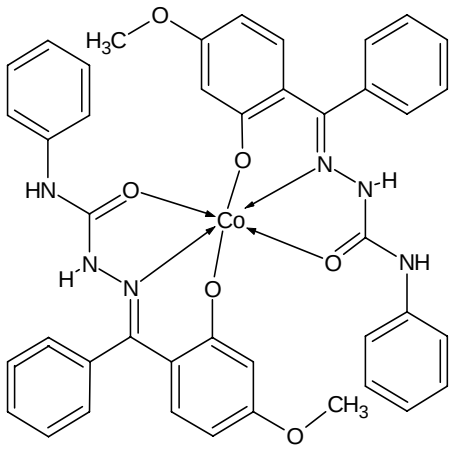

[Co(HBSC)$_2$] (21)

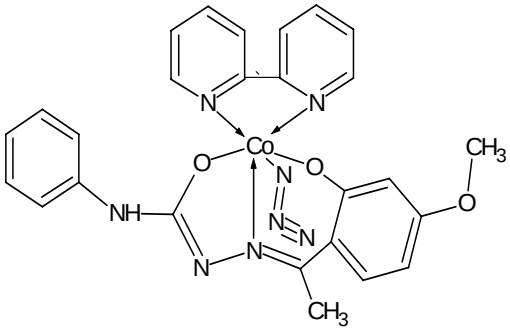

[Co(ASC)bipy(N$_3$)] (17)

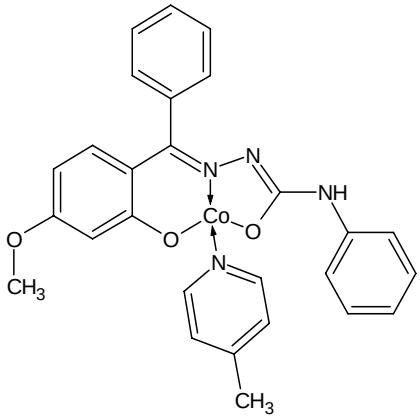

[Co(BSC)pic]·3H$_2$O (28)

References

[1] M. Amirnasr, K.J. Schenk, A. Gorji, R. Vafazadeh, Polyhedron 20 (2001) 298.

[2] M.M. Ali, J. Coord. Chem. 43 (1998) 89.

[3] S.M. Polson, R. Cini, C. Pifferi, L.G. Marzilli, Inorg. Chem. 36 (1997) 314.

[4] N.J. Henson, P.J. Hay, A. Redondo, Inorg. Chem. 38 (1999) 1618.

[5] C. Benchini, R.W. Zoeliner, Adv. Inorg. Chem. 44 (1997) 263.

[6] W.J. Geary, Coord. Chem. Rev. 7 (1971) 81.

[7] A. Sreekanth, U.L. Kala, C.R. Nair, M.R.P. Kurup, Polyhedron 23 (2004) 41.

[8] B.N. Figgis, R.S Nyholm, J. Chem. Soc. (1958) 4190.

[9] J.R. Anacona, Gladys Da Silva, J. Chil. Chem. Soc. 50 (N2) (2005) 447.

[10] J.C. Bailar, H.J. Emeleus, R.S. Nyholm, A.F. Trotman, Dickenson in Comprehensive Inorganic Chemistry, Pergamon Press, New York (1975).

[11] A.B.P. Lever, Inorganic Spectroscopy, Elsevier, Amsterdam (1984).

[12] M.S. Refat, S. Chandra, M. Tyagi, Therm. Anal. Calorim. 100 (2009) 261.

[13] M. Yamami, M. Tanaka, H. Sakiyama, T. Koga, K. Kobayashi, H. Miyasaka, M. Ohba, H. Okawa, J. Chem. Soc., Dalton Trans. (1997) 4595.

[14] P. Bindu, M.R.P. Kurup, Indian J. Chem. 38A (1999) 388.

[15] V.L. Siji, M.R. Sudarsanakumar, S. Suma, M.R.P. Kurup, Spectrochim. Acta Part A 76 (2010) 22.

[16] R.P. John, A. Sreekanth, M.R.P. Kurup, S.M. Mobin, Polyhedron 21 (2002) 2515.

[17] V. Suni, M.R.P. Kurup, M. Nethaji, Polyhedron 26 (2007) 5203.

[18] J.R Dimmock, K.K. Sidhu, S.D. Tumber, S.K. Basran, M. Chen, J.W. Quail, Eur. J. Med. Chem. 30 (1995) 287.

[19] D.X. West, J.K. Swearingen, J. Valde`s-Martın`ez, S. Herna`ndez-Ortega, A.K. El-Sawaf, F.V. Meurs, A. Castineiras, I. Garcia, E. Bermejo, Polyhedron 18 (1999) 2919.

[20] M. Joseph, V. Suni, M.R.P. Kurup, M. Nethaji, A. Kishore, S.G. Bhat, Polyhedron 23 (2004) 3069.

[21] N. Nakamoto, Infrared and Raman Spectra of Inorganic and Coordination Compounds, John Wiley & Sons, New York, USA, 3rd edition, 1978.

[22] K.B. Yatsimirskii, Pure and Appl. Chem. 49 (1977) 115.

[23] V.L. Siji, M.R. Sudarsanakumar, S. Suma, Transit. Met. Chem. 36 (2011) 417.

[24] M.S. Nair, R.S. Joseyphus, Spectrochim. Acta Part A 70 (2008) 749.

[25] P.K. Samal, A.K. Patra, M. Nethaji, A.R. Chakravarthy, Inorg. Chem. 46 (2007) 11112.

[26] S.S. Tandon, L.K. Thompson, M.E. Manuel, J.N. Bridson, Inorg. Chem. 22 (1994) 5555.

[27] M. Joseph, M. Kuriakose, M.R.P. Kurup, E. Suresh, A. Kishore, S.G. Bhat, Polyhedron 25 (2006) 61.

[28] N.R. Sangeetha, S. Pal, Polyhedron 19 (2000) 1593.

[29] R.A. Bailey, S.L. Kozak, T.W. Michelsen, W.N. Mills, Coord. Chem. Rev. 6 (1971) 407.

[30] S. Chandra, Sangeetika, V.P. Tyagi, S. Raizada, Synth. React. Inorg. Met. Org. Chem. 33 (2003) 147.

[31] S. Chandra, Sangeetika, S.D. Sharma, Spectrochim. Acta 59A (2003) 755.

[32] M.B. Ferrari, G.G. Fava, C. Pelizzi, P. Tarasconi, J. Chem. Soc., Dalton Trans. (1992) 2153.

[33] M.B. Ferrari, G.G. Fava, C. Pelosi, M.C. Rodriguez-Arguelles, P. Tarasconi, J. Chem. Soc., Dalton Trans. (1995) 3035.

[34] M.S. Refat, S. Chandra, M. Tyagi, J. Therm. Anal. Calorim. 100 (2010) 261.

[35] N.K. Singh, S.K. Kushawaha, Transit. Met. Chem 26 (2001) 140.

[36] H.J. Choi, M.P. Suh, Inorg. Chem. 38 (1999) 6309.

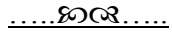

Chapter 6

SYNTHESES AND SPECTRAL CHARACTERIZATION OF NICKEL(II) COMPLEXES OF N^4-PHENYLSEMICARBAZONES

Contents

6.1. Introduction

Nickel is one of the four elements that are ferromagnetic around room temperature. Naturally occurring nickel is composed of five stable isotopes ^{58}Ni, ^{60}Ni, ^{61}Ni, ^{62}Ni and ^{64}Ni with ^{58}Ni being the most abundant (68.077% natural abundance). ^{62}Ni is the most stable nuclide of all the existing elements. Nickel is the earth's 22nd most abundant element and the 7th most abundant transition metal. Nickel is a transition element that is both siderophile (associates with iron) and chalcophile (associates with sulfur) having atomic number, 28 and atomic mass, 58.6934(2) g/mol. The most common oxidation state of nickel is +2, but compounds of Ni^0, Ni^{1+} and Ni^{3+} are well known. The ionic radius of divalent nickel is close to that of divalent iron and magnesium, allowing the three elements to substitute for one another in the crystal lattices of some silicates and oxides.

Nickel compounds have many applications. Nickel oxide is used in porcelain painting and in electrodes for fuel cells, nickel acetate as a mordant in textile industry, nickel carbonate in ceramic colors and glazes.

Some reports show that labile four-coordinated nickel(II) complexes with tridentate thiosemicarbazone and semicarbazone, semicarbazones exhibit antibacterial activities, whereas, six-coordinated nickel(II) complexes with thiosemicarbazone and semicarbazone, semicarbazones show no activities against the test microorganisms [1].

Ni(II) forms many stable four, five and six coordinate complexes. It can exist in a wide variety of C.N. (coordination number) which complicates its coordination chemistry. For C.N. = 4, both tetrahedral and square planar complexes can be found. For C.N. = 5, both square pyramidal and trigonal bipyramidal complexes are formed. The phrase '*anomalous nickel'* has been used to describe this behavior and the fact that equilibrium often exists between these forms.

This chapter deals with the syntheses and spectral investigation of five Ni(II) complexes derived from two semicarbazones, 2-hydroxy-4-methoxyacetophenone-N^4-phenylsemicarbazone (H_2ASC) and 2-hydroxy-4-methoxybenzophenone-N^4-phenylsemicarbazone (H_2BSC). The heterocyclic base, 1,10-phenanthroline and the pseudohalide $-N_3^-$ are used as coligands.

6.2. Experimental

6.2.1. Materials

Nickel(II) acetate tetrahydrate, 1,10-phenanthroline (Ranchem), and NaN_3 (Merck) were used as supplied. Solvents were purified by standard procedures before use.

6.2.2. Syntheses of semicarbazones

The semicarbazones $H_2ASC{\cdot}H_2O$ and H_2BSC were synthesized according to the procedure given in Chapter 2.

6.2.3. Syntheses of Ni(II) complexes of 2-hydroxy-4-methoxyacetophenone-N^4-phenylsemicarbazone

6.2.3.1. *[Ni(HASC)OAc]·3H$_2$O (29)*

It is prepared by refluxing methanolic solutions of nickel(II) acetate tetrahydrate (0.248 g, 1 mmol) and $H_2ASC{\cdot}H_2O$ (0.317 g, 1 mmol) for 3 h. and keeping overnight the resulting solution at room temperature. The green compound formed was filtered, washed with methanol and ether. It was then dried over P_4O_{10} in *vacuo*.

Elemental Anal. Found (Calcd.) (%): C: 45.77 (45.99); H: 5.69 (5.36); N: 8.32 (8.94)

6.2.3.2. *[Ni(ASC)phen(H$_2$O)]·H$_2$O (30)*

To a hot solution of 1 mmol of $H_2ASC{\cdot}H_2O$ (0.317 g, 1 mmol) in methanol, was added 1 mmol 1,10-phenanthroline (0.198 g) in methanol. Nickel(II) acetate tetrahydrate (0.248 g, 1 mmol) dissolved in methanol was added to the above mixture with constant stirring. The mixture was then refluxed for 4 h. and the resulting green solution was kept overnight at room temperature. The green complex formed was filtered, washed with methanol and ether. It was then dried over P_4O_{10} in *vacuo*.

Elemental Anal. Found (Calcd.) (%): C: 58.17 (58.77); H: 5.26 (4.76); N: 11.68 (12.24)

6.2.3.3. *[Ni(HASC)phen(N_3)] (31)*

A mixture of $H_2ASC{\cdot}H_2O$ (0.317 g, 1 mmol), nickel(II) acetate tetrahydrate (0.248 g, 1 mmol) and 1,10-phenanthroline (0.198 g, 1 mmol) in methanol was heated under reflux for 1 h. and to it sodium azide (0.065 g, 1 mmol) in methanolic medium was added in drops with constant stirring and further stirred for 3 h. and was kept at room temperature. The yellowish brown compound formed was filtered, washed with methanol followed by ether. It was then dried over P_4O_{10} in *vacuo*.

Elemental Anal. Found (Calcd.) (%): C: 58.61 (58.06); H: 4.32 (4.18); N: 19.71 (19.35)

Caution! Azide metal complexes with organic ligands are potentially explosive and should be handled with care.

6.2.4. Syntheses of Ni(II) complexes of 2-hydroxy-4-methoxybenzophenone-N^4-phenylsemicarbazone

6.2.4.1. *[Ni(HBSC)$_2$] (32)*

A hot solution of H_2BSC (0.361 g, 1 mmol) in methanol was mixed with a hot methanolic solution of nickel(II) acetate tetrahydrate (0.124, 0.5mmol) and was refluxed for 4 h. The resulting green solution was allowed to cool at room temperature. The green product compound formed was filtered, washed with methanol and ether and dried over P_4O_{10} in *vacuo*.

Elemental Anal. Found (Calcd.) (%):C: 59.96 (60.19); H: 4.94 (4.33); N: 10.34 (10.03)

6.2.4.2. *[Ni(HBSC)phen(OAc)] (33)*

To a hot methanolic solution of H_2BSC (0.361 g, 1 mmol), was added a hot methanolic solution of nickel(II) acetate tetrahydrate (0.248 g, 1 mmol) and 1,

10-phenanthroline (0.198 g, 1 mmol). The mixture was refluxed for 4 h. and kept overnight for cooling. The green compound formed was filtered, washed with methanol, followed by ether. It was then dried over P_4O_{10} in *vacuo*.

Elemental Anal. Found (Calcd.) (%): C: 63.65 (63.85); H: 4.79 (4.44); N: 10.34 (10.64)

6.3. Results and discussion

Five Ni(II) complexes reported here, have been synthesized by refluxing equimolar ratios of the semicarbazones and nickel acetate for complexes **29** and **30**, **31** and **33** while for complex **32** it is in 2:1 ratio. In compounds **30, 31** and **33**, 1,10-phenanthroline is coordinated, while in **31** the azido group is also coordinated to form hexacoordinate complexes. Compound **29** is tetracoordinate. All the complexes are green in color and are partially soluble in DMF, CH_3CN and DMSO. The complexes are characterized by the following physico-chemical methods.

6.3.1. Elemental analyses

Carbon, hydrogen and nitrogen analyses of all the five samples were tabulated in Sections 6.2.3 and 6.2.4.

6.3.2. Molar conductivity

The molar conductivities of the complexes in DMF (10^{-3} M) solutions were measured at 298 K with a Systronic model 303 direct reading conductivity bridge. It is observed that the values lie in the range of 2-20 ohm^{-1} cm^2 mol^{-1}, which are well below the range (65-90 ohm^{-1} cm^2 mol^{-1}) for uni-univalent electrolytes in the same solvent, indicating the nonelectrolytic nature of the complexes [2].

6.3.3. Magnetic susceptibility

The magnetic moments of the complexes were calculated from the magnetic susceptibility measurements at room temperature. The observed values of magnetic moment for complexes are generally diagnostic of the coordination geometry about the metal ion [3]. Out of the five complexes synthesized, $[Ni(HASC)(OAc)]\cdot 3H_2O$ (**29**) is tetracoordinate and the remaining four are hexacoordinate. All the complexes are paramagnetic with a high spin d^8 system and the effective magnetic moments for compounds **30**-**33** are found to be in the range 2.75-2.95 B.M., corresponding to two unpaired electrons, which are consistent with the octahedral geometry of the complexes. Complex **29** shows a magnetic moment of 3.28 B.M. which is slightly greater than the spin only value which may be due to orbital contribution. So it excludes the possibility of a square planar geometry, and suggests a tetrahedral geometry for compound **29** which corresponds to similar reports [4]. The magnetic moment and molar conductivity values of the complexes are given in Table 6.1.

Table 6.1. Molar conductivities and magnetic susceptibilities of Ni(II) complexes

Compound	λ_m*	μ_{eff} (B.M.)
$[Ni(HASC)(OAc)]\cdot 3H_2O$ (**29**)	6	3.28
$[Ni(ASC)\ phen(H_2O)]\cdot H_2O$ (**30**)	11	2.86
$[Ni(HASC)phen(N_3)]$ (**31**)	9	2.95
$[Ni(HBSC)_2]$ (**32**)	8.8	2.91
[Ni(HBSC)phen(OAc)] (**33**)	20	2.75

*Molar conductivity (mho cm^2 mol^{-1}) taken in 10^{-3} M DMF solution.

6.3.4. Infrared spectra

The bonding sites of the semicarbazones involved in coordination with the metal ions have been examined with careful comparison of the IR spectra of semicarbazones and their complexes and are tabulated in Table 6.2. In principle, the semicarbazone can exhibit amido-iminol tautomerism since it contains –NH–C=O functional group. In all the complexes synthesized for our present study, except in compound **30**, the semicarbazone exists in the amido form. In compound **30**, it is in the iminolate form.

Table 6.2. The important IR frequencies (cm^{-1}) of semicarbazones and their Ni(II) complexes

Compound	ν(C=O)	ν(C=N)	ν(N–N)	ν(C–O)	ν(^{2}NH)	ν(Ni–O)	ν(Ni–N)
$H_2ASC\cdot H_2O$	1692	1619	1020	1270	3295	----	----
[Ni(HASC)(OAc)]·$3H_2O$ (**29**)	1665	1597	1033	1236	3217	481	421
[Ni(ASC)phen(H_2O)]·H_2O (**30**)	----	1604	1030	1242	----	506	427
[Ni(HASC)phen(N_3)] (**31**)	1640	1605	1029	1240	3205	507	411
H_2BSC	1662	1631	1059	1294	3145	----	----
[Ni($HBSC)_2$] (**32**)	1653	1598	1101	1242	3136	509	426
[Ni(HBSC)phen(OAc)] (**33**)	1655	1601	1107	1232	3150	508	424

The strong band observed in the spectrum of $H_2ASC\cdot H_2O$ at 1692 cm^{-1} is assigned to *ν*(C=O) stretching vibration. A shift to lower frequency of this band by 27 cm^{-1} for complex **29** (Fig. 6.1) and 52 cm^{-1} for complex **31** (Fig. 6.3) suggests the involvement of the CO group in coordination to the metal ion in the amido form [5]. The medium band at *ca.* 3295 cm^{-1} assigned to ν(^{2}N–H) in the semicarbazone is not disappearing, but shifted slightly due to complexation, further confirms this argument. For complex **30** (Fig. 6.2), the *ν*(C=O) mode of the free ligand is not observed indicating enolisation of C=O followed by

deprotonation and and chelation with the metal ion [6]. Correspondingly ν(^{2}N–H) band disappears and an additional carbon-nitrogen double bond stretching frequency is formed at 1558 cm^{-1}. Similarly for complexes of H_2BSC, **32** and **33** (Figs. 6.4 and 6.5), the *ν*(C=O) stretching vibration suffers a shift to lower frequency by about 8 cm^{-1} from 1662 cm^{-1} confirming its coordination through carbonyl oxygen. The bands at 3535 and 3316 cm^{-1} ascribed to phenolic –OH group respectively for the semicarbazones $H_2ASC{\cdot}H_2O$ and H_2BSC have disappeared, giving evidence for deprotonation of phenolic –OH and its coordination to the central metal ion. The onset of new bands in the 1232-1242 cm^{-1} region is assigned for ν(C–O) band. This is further confirmed by the appearance of new bands in the 481-509 cm^{-1} range assigned to *ν*(Ni−O) [7].

The position of *ν*(C=N) band of the semicarbazones appeared at 1619 and 1631 cm^{-1} is shifted towards lower wave numbers (1597-1605 cm^{-1}) in the complexes indicating coordination via the azomethine [8,9]. This is confirmed by the appearance of bands in the range of 411–427 cm^{-1}, which has been assigned to the *ν*(Ni−N) [10]. A strong band found at 1020 cm^{-1} in $H_2ASC{\cdot}H_2O$ and at 1059 cm^{-1} in H_2BSC is due to the *ν*(N−N) group. The position of this band is shifted towards higher wave numbers in the spectra of complexes due to the increase in the bond strength, which again confirms the coordination via the azomethine nitrogen. Thus, it may be concluded that the semicarbazones behave as tridentate chelating agent coordinating through azomethine nitrogen, phenolate and iminolate oxygens. The broad bands at *ca.*3400 cm^{-1} in complexes **29** and **30** show the presence of water present. The presence of coordinated water is further confirmed by the appearance of a nonligand band at 840 and 727 cm^{-1}, assigned to the rocking and wagging modes of water respectively [11].

The IR spectra of Ni(II) acetato complexes, **29** and **33** show strong bands at 1567 and 1563 cm^{-1}, assigned to ν_a(C−O) and medium intensity bands at 1340 and 1320 cm^{-1} ascribed to ν_s(C−O), respectively. The difference between these two frequencies indicates that both acetate ions are coordinated to the metal ion in a unidentate fashion [12].

The azido complex **31** (Fig. 6.3) exhibits the antisymmetric ν(NNN) vibration as a sharp band at 2031 cm^{-1}, and a strong band at 1338 cm^{-1} which is assigned to ν_s(NNN) vibration. The δ(NNN) band is observed at 694 cm^{-1} for this complex [13]. In complexes containing phenanthroline, new bands are observed around 470 cm^{-1} which can be ascribed to coordination of this base to the Ni(II) centre.

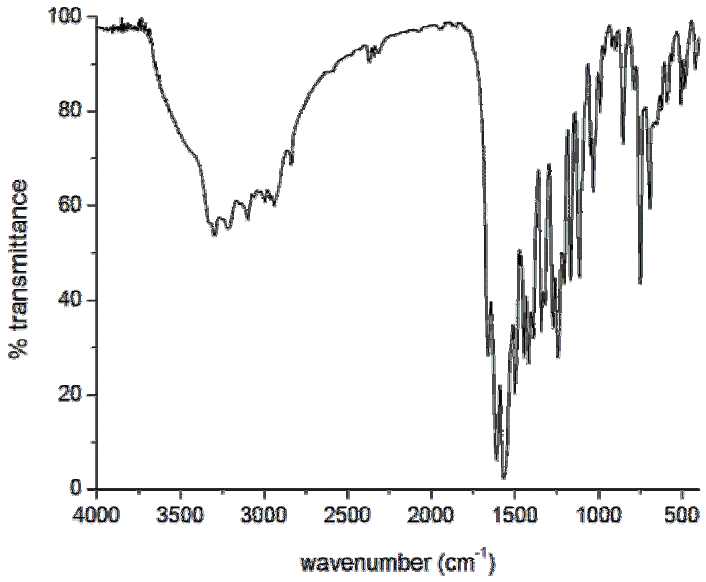

Fig. 6.1. IR spectrum of [Ni(HASC)(OAc)]·3H_2O (29).

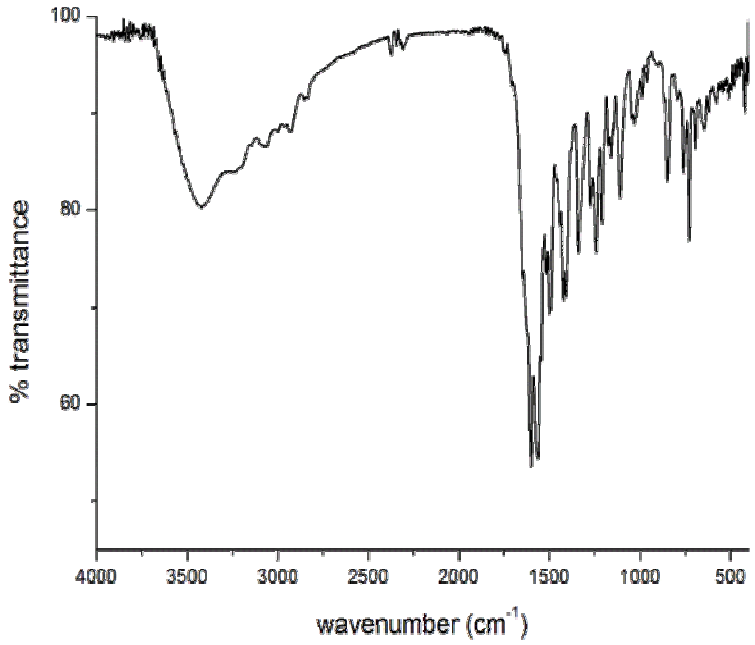

Fig. 6.2. IR spectrum of [Ni(ASC)phen(H_2O)]·H_2O (30).

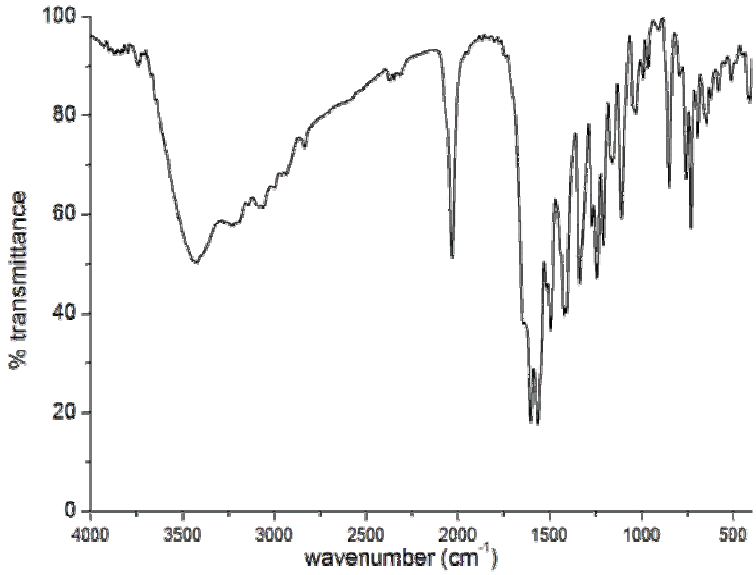

Fig. 6.3. IR spectrum of [Ni(HASC)phen(N_3)] (31).

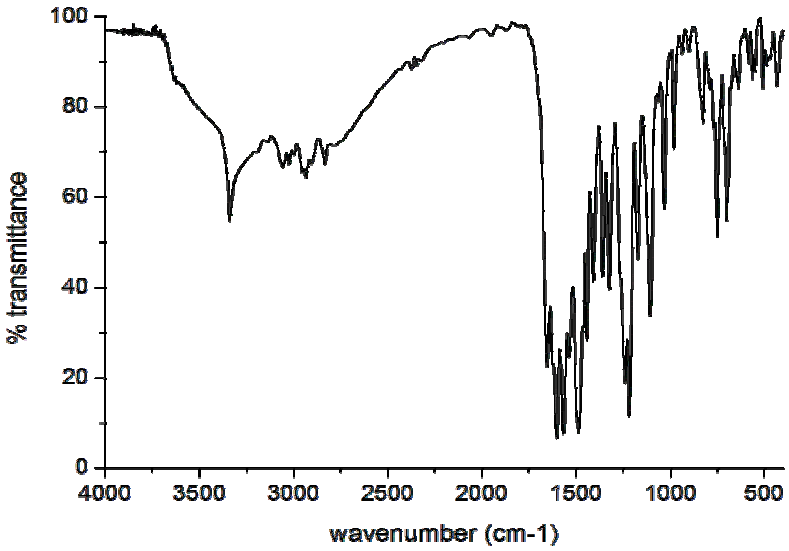

Fig. 6.4. IR spectrum of $[Ni(HBSC)_2]$ (32).

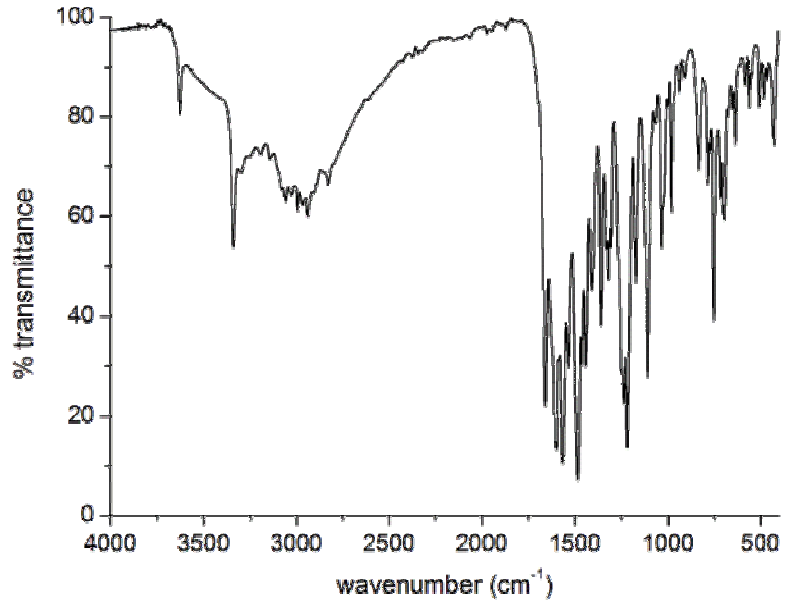

Fig. 6.5. IR spectrum of [Ni(HBSC)phen(OAc)] (33).

6.3.5. Electronic spectra

The UV spectra of the semicarbazones and complexes were recorded in acetonitrile solutions and the visible spectra in DMF. The intraligand transitions of semicarbazones H_2ASC and H_2BSC suffered considerable shift on complexation. In the complexes the bands in the region 29910-43960 cm^{-1} are attributed to the shifted intraligand transitions. The charge transfer transitions are observed as intense bands in the 25540-28600 cm^{-1} range, and are assigned to O→ Ni LMCT transitions confirming coordination to the metal ion (Figs. 6.6 and 6.7). The electronic spectral data of the semicarbazones and complexes are summarized in Table 6.3.

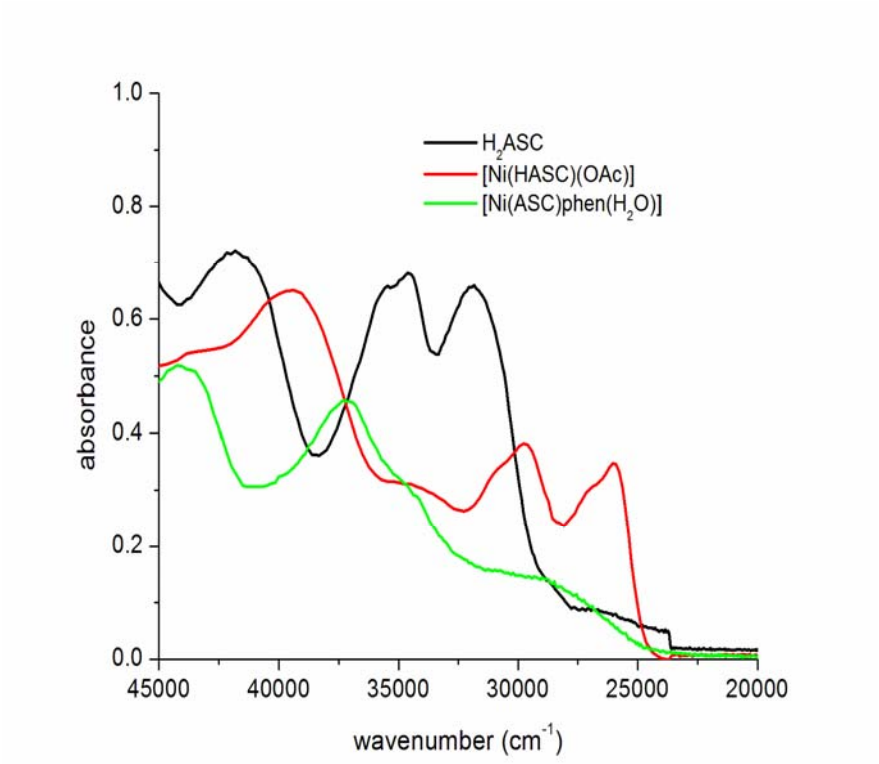

Fig. 6.6. Electronic spectra of H_2ASC, [Ni(HASC)(OAc)] and [Ni(ASC)phen(H_2O)].

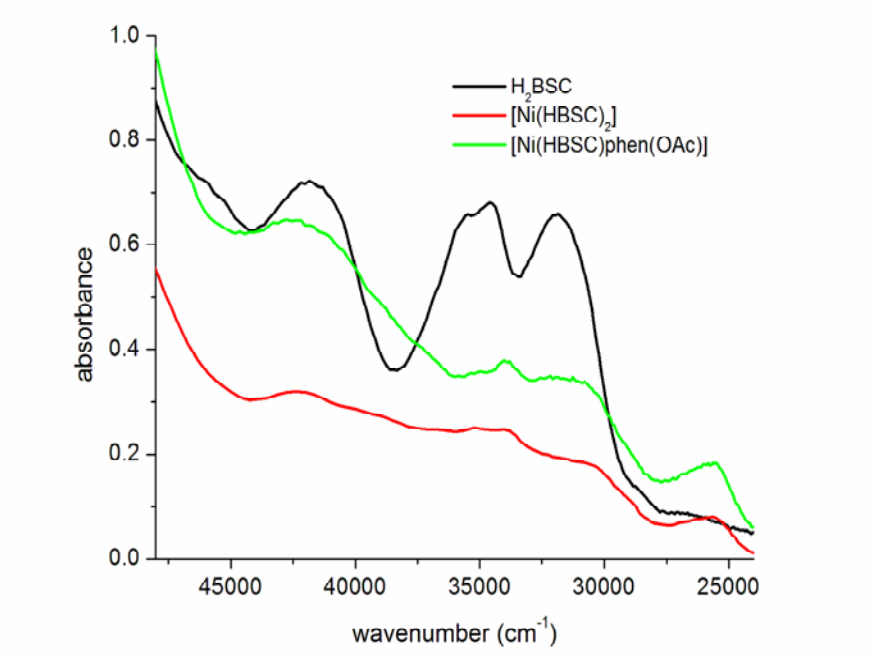

Fig. 6.7. UV spectra of H_2BSC, $[Ni(HBSC)_2]$ and [Ni(HBSC)phen(OAc)].

All the complexes synthesized except $[Ni(HASC)OAc]\cdot 3H_2O$ (**29**) have octahedral geometry as evidenced from their magnetic moments. The ground state of Ni(II) in an octahedral coordination is $^3A_{2g}$ and three expected spin allowed transitions are $^3T_{2g}(F) \leftarrow {}^3A_{2g}(F)$ (ν_1), $^3T_{1g}(F) \leftarrow {}^3A_{2g}(F)$ (ν_2) and $^3T_{1g}(P) \leftarrow {}^3A_{2g}(F)$ (ν_3) in the increasing order of energy [14]. In complexes **30** and **31** a weak absorption is observed at *ca.* 20000 cm^{-1} and it can be assigned to $^3T_{1g}(F) \leftarrow {}^3A_{2g}(F)$ (ν_2). However, these bands are not well resolved. In compounds **32** and **33,** the two weak bands observed around 17000 and 20000 cm^{-1} corresponding to the octahedral geometry and we have assigned these to $^3T_{2g}(F) \leftarrow {}^3A_{2g}(F)$ (ν_1) and $^3T_{1g}(F) \leftarrow {}^3A_{2g}(F)$ (ν_2) respectively. The ν_3 band is not located due to masking by the high-intensity charge transfer bands [15,16].

In nickel(II) complexes with tetrahedral stereochemistry also, we expect three transitions; $^3T_2(F) \leftarrow {}^3T_1(F)$, $^3A_2(F) \leftarrow {}^3T_1(F)$, $^3T_1(P) \leftarrow {}^3T_1(F)$. For the tetrahedral complex **29**, three bands are observed at 18490, 13450 and 12350 cm^{-1}. The absorption bands obtained for the complexes **29-33** in the visible region are shown in Figs. 6.8.1.-6.8.5.

Table 6.3. Electronic spectral assignments (cm^{-1}) of N^4-phenylsemicarbazones and their Ni(II) complexes.

Compound	Intraligand transitions	LMCT	*d-d*
H_2ASC	31780, 34540, 35600 (sh), 41750		
[Ni(HASC)(OAc)]·3H_2O (**29**)	29910, 30540 (sh), 34390, 39530, 43810	25920	18490,13450, 12350
[Ni(ASC) phen(H_2O)]·H_2O (**30**)	30920 (sh), 34390 (sh),37080, 43960	27350	20000
[Ni(HASC)phen(N_3)] (**31**)	30780, 39480, 43800	28600	20000
H_2BSC	31330, 33820, 35030, 41680	----	----
[Ni(HBSC)$_2$] (**32**)	30590, 33960, 42230	25540	17070, 20060
[Ni(HBSC)phen(OAc)]·2H_2O (**33**)	31260, 33900, 41940	25680	17000, 20730

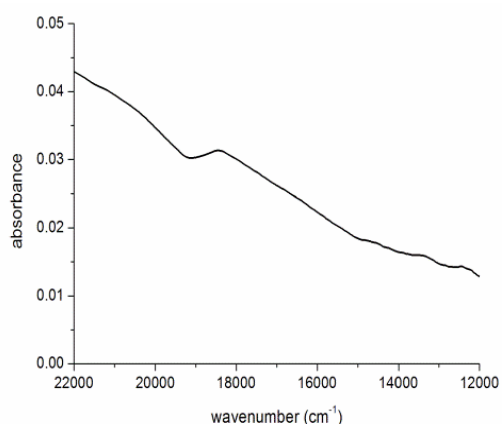

Fig. 6.8.1. [Ni(HASC)(OAc)]

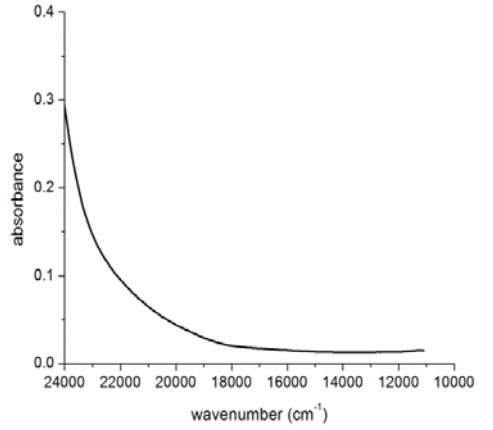

Fig. 6.8.2. [Ni(ASC)(phen)(H_2O)]

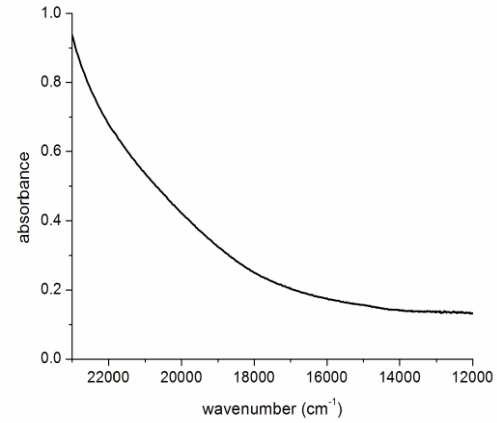

Fig. 6.8.3. [Ni(HASC)phen(N_3)]

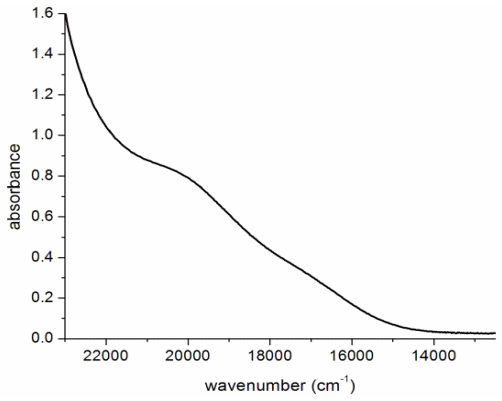

Fig. 6.8.4. [Ni(HBSC)$_2$]

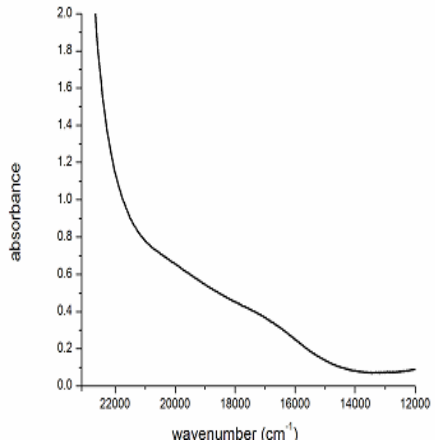

Fig. 6.8.5. [Ni(HBSC)phen(OAc)]

Fig. 6.8. Visible spectra of Ni(II) complexes.

6.3.6. Thermogravimetric analyses

Thermogravimetric analysis measures the amount and rate of change in the weight of a compound as a function of temperature or time in a controlled atmosphere. Measurements are used to predict the thermal stability at temperatures upto 1000 °C. By this technique we can predict the water present in a compound is inside or outside the coordination sphere. Reports show that weight losses for lattice water is below 200 °C and that for coordinated water molecules are in the range 200-350 °C [17,18]. Thermogravimetric analyses for the complexes **29**, **30** and **33** showed slight weight losses below 200 °C indicating the presence of lattice water. The thermogram of complex **30** is presented in Fig. 6.9.

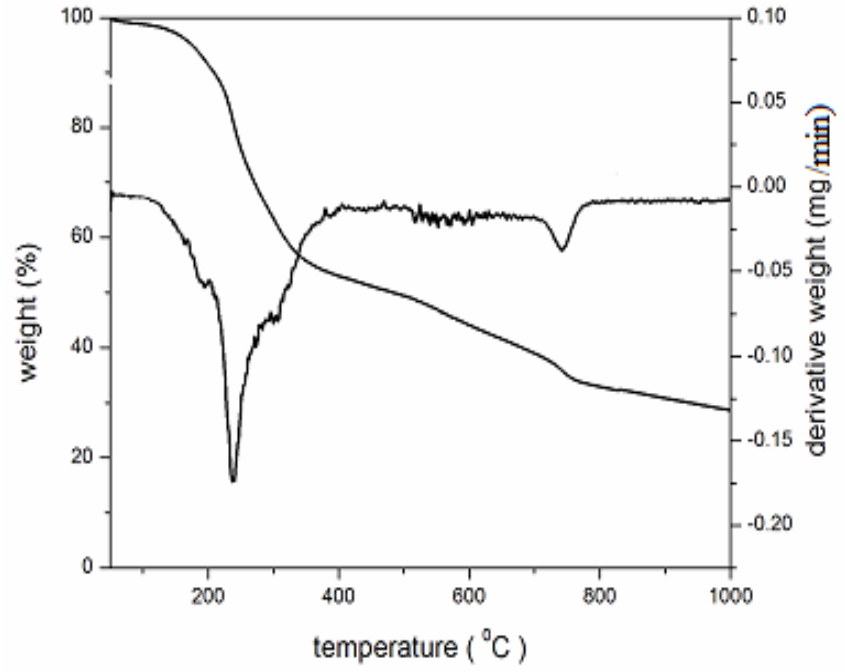

Fig. 6.9. Thermogram of [Ni(ASC)(phen)(H_2O)]·H_2O (30).

This TG-DTG plot shows two weight loss steps, with a first weight loss of 3.6% (calcd. 3.15%) around 160 °C, with the second loss of 3.3% (calcd. 3.25%) around 220 °C. So we can assume one molecule of water is inside and the other outside the coordination sphere. The total weight loss of 40.2% (calcd. 40.9%) in the temperature range of 150-320 °C corresponds to the removal of two molecules of water and one phenanthroline molecule. Above this temperature decomposition of the ligand takes place.

On the basis of the physico-chemical characterizations discussed above, the tentative structures proposed for some Ni(II) complexes are presented below. Out of the five Ni(II) complexes synthesized, compound **29** has got tetrahedral geometry, while all others have been assigned octahedral geometry. In all complexes except **30**, the semicarbazones exist in the amido form, while in **30** it is in the iminolate form. The lattice water molecules are omitted in the structures shown.

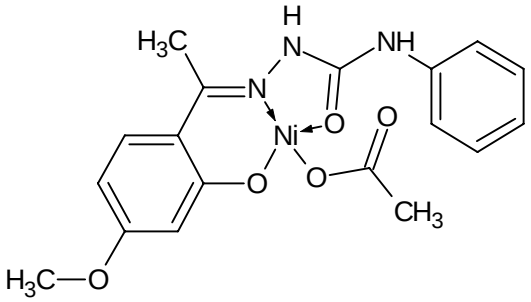

[Ni(HASC)(OAc)]·3H₂O (29)

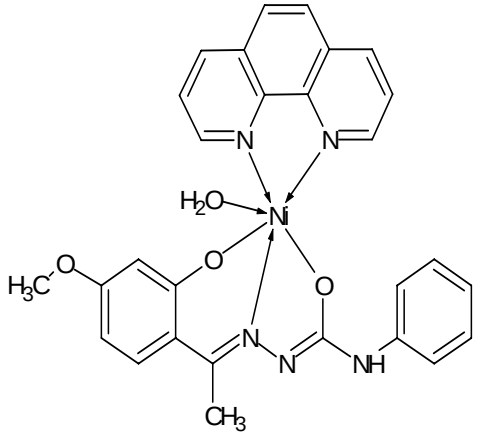

[Ni(ASC)(phen)(H_2O)]·H_2O (30)

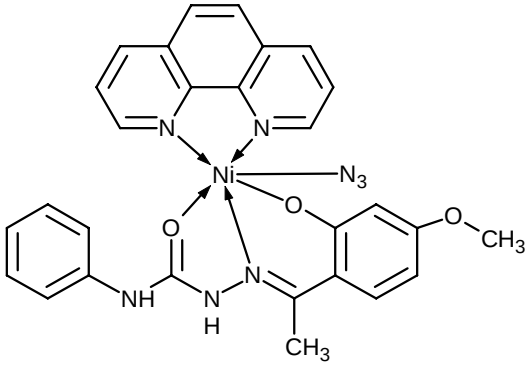

[Ni(HASC)phen(N_3)] (31)

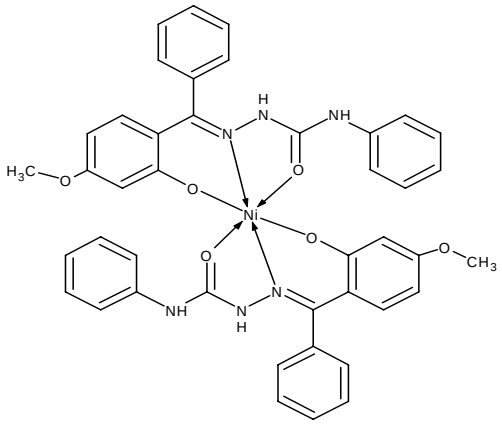

[Ni(HBSC)$_2$] (32)

References

[1] N.C. Kasuga, K. Sekino, M. Ishikawa, A. Honda, M. Yokoyama, S. Nakano, N. Shimada, C. Koumo, K. Nomiya, J. Inorg. Biochem. 96 (2003) 298.

[2] W.J. Geary, Coord. Chem. Rev. 7 (1971) 81.

[3] B.N. Figgis, R.S. Nyholm, J. Chem. Soc. (1958) 4190.

[4] A.A.A. Abu-Hussen, A.A.A. Emara, J. Coord. Chem. 57 (2004) 973.

[5] M.S. Refat, S. Chandra, M. Tyagi, J. Therm. Anal. Calorim 100 (2010) 267.

[6] V. Philip, V. Suni, M.R.P. Kurup, M. Nethaji, Spectrochim. Acta Part A 64 (2006) 171.

[7] M.F. Iskander, T.E. Khalil, R. Werner, W. Haase, I. Svoboda, H. Fuess, Polyhedron 19 (2000) 1181.

[8] M. Joseph, A. Sreekanth, V. Suni, M.R.P. Kurup, Spectrochimica Acta Part A 64 (2006) 637.

[9] R.K. Agarwal, I. Chakraborti, H. Agarwal, Synth. React. Inorg. Met.-Org. Chem. 34 (2004) 1431.

[10] S. Chandra, L.K. Gupta, Spectrochim. Acta Part A 61 (2005) 269.

[11] V. Stefov, V.M. Petrusevski, B. Soptrajanov, J. Mol. Struct. 293 (1993) 97.

[12] N. Nakamoto, Infrared and Raman Spectra of Inorganic and Coordination Compounds, John Wiley & Sons, New York, 3rd edition, 1978.

[13] M. Joseph, V. Suni, M.R.P. Kurup, M. Nethaji, A. Kishore, S.G. Bhat, Polyhedron 23 (2004) 3069.

[14] C.S. Kumar, J. Indian Chem. Soc. 84 (2007) 325.

[15] M.A. Ali, S.M.G. Hossain, S.M.M.H. Majumder, M. Nazimuddin, M.T.H. Tarafder, Polyhedron 6 (1987) 1653.

[16] A.B.P. Lever, Inorganic Spectroscopy, Elsevier, Amsterdam (1984) 513.

[17] H. Cesur, T.K. Yazicilar, B. Bati, V.T. Yilmaz, Synth. React. Inorg. Met.-Org. Chem. 31 (2001) 1271.

[18] S. Kavlak, H. Kaplan Can, Z.M.O. Rzaev, A. Guner, J. Appl. Polym. Sci. 100 (2006) 3926.

Chapter 7

SYNTHESES AND SPECTRAL CHARACTERIZATION OF COPPER(II)COMPLEXES OF N^4-PHENYLSEMICARBAZONES

Contents

7.1. Introduction

Transition metal complexes with potential biological activity are the focus of extensive investigation. Interestingly, complexation with copper enhances the biological activity of a wide variety of organic ligands [1,2]. Copper is the third most abundant transition metal element in biological systems, with an occurrence of 80-120 mg. in human body. Copper proteins have diverse roles in biological electron transport and oxygen transportation processes that exploit the easy interconversion of Cu(I) and Cu(II). Copper is also found in many superoxide dismutases, proteins that detoxify superoxides by converting it (disproportionation) to oxygen and hydrogen peroxide. Mixed ligand complexes play an important role in biological processes like activation of enzymes by metals [3]. Such complexes are useful in the storage and transport of active substances through membranes [4,5]. Semicarbazones constitute one of the most important class of oxygen and nitrogen donor ligands. The formation of a variety of metal complexes from these ligands indicates the spectacular progress in coordination and bioinorganic chemistry. These complexes have tetrahedral, octahedral, square planar and trigonal bipyramidal geometries [6].

This chapter deals with the syntheses and characterization of copper(II) complexes with potential ONO donor ligands, 2-hydroxy-4-methoxyacetophenone-N^4-phenylsemicarbazone (H_2ASC), 2-hydroxy-4-methoxybenzophenone-N^4-phenylsemicarbazone (H_2BSC). Out of the seven complexes prepared, two are binuclear and the remaining five are mixed ligand metal chelates incorporating some heterocyclic compounds like 1,10-phenanthroline, 2,2′-bipyridine and 4,4′-dimethyl-2,2′-bipyridine, besides the principal ligands.

7.2. Experimental

7.2.1. Materials

2-Hydroxy-4-methoxyacetophenone (Sigma-Aldrich), 2-hydroxy-4-methoxybenzophenone (Sigma-Aldrich), N^4-phenylsemicarbazide (Sigma-Aldrich), copper(II) acetate monohydrate (Qualigens), 1,10-phenanthroline (Ranchem), 2,2′-bipyridine (Qualigens) and 4,4′dimethyl-2,2′-bipyridine (Qualigens) were of analar grade and were used as received. Solvents used were methanol, ethanol, acetonitrile and N,N-dimethylformamide (all are Merck).

7.2.2. Syntheses of semicarbazones

The syntheses of the semicarbazones $H_2ASC{\cdot}H_2O$ and H_2BSC were done as described in Chapter 2.

7.2.3. Syntheses of Cu(II) complexes of 2-hydroxy-4-methoxyacetophenone-N^4-phenylsemicarbazone

7.2.3.1. *$[Cu_2(ASC)_2]$ (34)*

To a hot methanolic solution of $H_2ASC{\cdot}H_2O$ (0.317 g, 1 mmol), was added a methanolic solution of copper(II) acetate monohydrate (0.199 g, 1 mmol). The

solution was heated under reflux for 4 h. The product formed was green colored and it was filtered, washed with methanol, followed by ether and dried over P_4O_{10} in *vacuo*.

Elemental Anal. Found (Calcd.) (%): C: 53.01 (53.25); H: 4.20 (4.19); N: 11.70 (11.64)

7.2.3.2. *[Cu(ASC)phen] (35)*

This complex was synthesized by refluxing a hot methanolic solution of $H_2ASC{\cdot}H_2O$ (0.317 g, 1 mmol) and a solution of copper(II) acetate monohydrate (0.199 g, 1 mmol) in methanol for 4 h. The green complex formed was filtered and it was dissolved in acetonitrile and a little dimethylformamide and the solution was refluxed again for about 6 h. by adding 1,10-phenanthroline (0.198 g, 1 mmol) and the product separated was filtered, washed with ether and dried over P_4O_{10} in *vacuo*.

Elemental Anal. Found (Calcd.) (%): C: 61.72 (62.16); H: 4.36 (4.28); N: 12.82 (12.94)

7.2.3.3. *[Cu(ASC)bipy]·2.5H_2O (36)*

The complex **36** was synthesized by following the same procedure as that of complex **35** and using the base 2,2′-bipyridine (0.156 g, 1 mmol). The solution was heated under reflux for 6 h. The complex formed was collected, washed with ether and dried over P_4O_{10} in *vacuo*.

Elemental Anal. Found (Calcd.) (%): C: 55.04 (55.56); H: 4.43 (5.02); N: 11.96 (12.46)

7.2.4. Syntheses of Cu(II) complexes of 2-hydroxy-4-methoxybenzophenone-N^4-phenylsemicarbazone

7.2.4.1. *[Cu_2(BSC)$_2$] (37)*

A hot solution of H_2BSC (0.361 g, 1 mmol) in methanol was treated with a methanolic solution of copper(II) acetate monohydrate (0.199 g, 1 mmol). The

solution was refluxed for 4 h. and the resulting green solution was allowed to stand at room temperature and after slow evaporation the complex separated out was collected, washed with methanol followed by ether and dried over P_4O_{10} in *vacuo*.

Elemental Anal. Found (Calcd.) (%): C: 59.77 (59.64); H: 4.04 (4.05); N: 10.20 (9.94)

7.2.4.2. *[Cu(BSC)phen]·3H$_2$O (38)*

This complex was synthesized by refluxing a hot methanolic solution of the H_2BSC (0.361 g, 1 mmol), 1,10-phenanthroline (0.198 g, 1 mmol) and copper(II) acetate monohydrate (0.199 g, 1 mmol) for 4 h. The complex formed was filtered, washed with methanol, followed by ether and dried over P_4O_{10} in *vacuo.*

Elemental Anal. Found (Calcd.) (%): C: 59.96 (60.31); H: 5.04 (4.75); N: 10.26 (10.66)

7.2.4.3. *[Cu(BSC)dmbipy]·4H$_2$O (39)*

This complex was prepared by refluxing 1:1:1 ratio of copper(II) acetate monohydrate (0.199 g, 1 mmol), H_2BSC (0.361 g, 1 mmol), and 4,4′-dimethyl-2,2′-bipyridine (0.184 g, 1 mmol) in methanolic medium for 4 h. The complex formed was filtered, washed with methanol, followed by ether and dried over P_4O_{10} in *vacuo.*

Elemental Anal. Found (Calcd.) (%): C: 58.84 (58.35); H: 4.93 (5.49); N: 9.66 (10.31)

7.2.4.4. *[Cu(BSC)bipy]·2H$_2$O (40)*

A hot solution of H_2BSC (0.361 g, 1 mmol) in methanol was mixed with 2,2′-bipyridine (0.156 g, 1 mmol). To this a hot methanolic solution of copper(II) acetate monohydrate (0.199 g, 1 mmol) was added and refluxed for 2 h.

The complex formed was filtered, washed with methanol followed by ether and dried over P_4O_{10} in *vacuo*.

Elemental Anal. Found (Calcd.) (%): C: 60.76 (60.53); H: 4.16 (4.75); N: 10.45 (11.38)

7.3. Results and discussion

Seven copper complexes were synthesized. The compounds **34** and **37** were prepared by the reaction of the appropriate semicarbazone with copper acetate monohydrate in 1:1 ratio. Complexes **35**, **36**, **38**, **39** and **40** were synthesized by refluxing metal salt, corresponding heterocyclic bases, and semicarbazones in 1:1:1 ratio. In all the complexes semicarbazones exist in the iminolate forms and act as dideprotonated tridentate ligands, coordinating through phenolic and iminolic oxygens and azomethine nitrogen. All complexes are green in color and are soluble in solvents like DMSO, DMF and CH_3CN. Compounds **34** and **37** are dimeric in nature, while others are monomeric mixed ligand metal chelates. They are characterized by the following physico-chemical methods.

7.3.1. Elemental analyses

Elemental (C, H, N) analyses of all samples were carried out using a Vario EL III CHN analyzer at SAIF, Kochi, India and the values were given in Sections 7.2.3 and 7.2.4. These formulae of the complexes reveal that metal, semicarbazones and heterocyclic bases are present in the ratio 1:1:1.

7.3.2. Molar conductivity

The molar conductivity of the complexes were measured at 298 K with a Systronic model 303 direct reading conductivity bridge in DMF (10^{-3} M)

solutions and the observed values were found to be in the range 6-40 ohm^{-1} cm^2 mol^{-1} confirming the nonelectrolytic nature of the complexes [7].

7.3.3. Magnetic susceptibility

The room temperarure magnetic susceptibilities of the mononuclear complexes have normal magnetic moments in the polycrystalline state and are in the range 1.65-1.77 B.M. which are very close to the spin only value of 1.73 B.M. for d^9 copper system. Complexes **34** and **37** showed μ_{eff} values 1.34 and 1.42 B.M. respectively and this may be due to the considerable antiferromagnetic interaction between metal centres suggesting dimeric nature to this complex [8]. The magnetic moment and molar conductivity values of the complexes are given in Table 7.1.

Table 7.1. Molar conductivities and magnetic susceptibilities of Cu(II) complexes.

Compound	λ_m*	μ_{eff} (B.M.)
$[Cu_2(ASC)_2]$ (**34**)	8	1.34
[Cu(ASC)phen] (**35**)	10	1.74
[Cu(ASC)bipy]·$2H_2O$ (**36**)	4.8	1.76
$[Cu_2(BSC)_2]$ (**37**)	2.8	1.42
Cu(BSC)phen]·$3H_2O$ (**38**)	40	1.65
Cu(BSC)dmbipy]·$4H_2O$ (**39**)	2.6	1.74
[Cu(BSC)bipy]·$2H_2O$ (**40**)	9	1.72

*Molar conductivity (mho cm^2 mol^{-1}) taken in 10^{-3} M DMF solution.

7.3.4. Infrared spectra

The IR spectra of the copper complexes were recorded in the range 4000-400 cm^{-1} with KBr pellets. The significant changes in the group frequencies of complexes compared to their respective metal free ligands

attributed to ligand coordination to metal centres. Since IR spectra are rich with bands, tentative assignments of vibrational bands, useful for determining mode of coordination of semicarbazones are presented in Table 7.2.

Table 7.2. The important IR frequencies (cm^{-1}) of semicarbazones and their Cu(II) complexes.

Compound	ν(C=N)	ν(C=N)[a]	ν(N–N)	ν(C–O)	ν(^{2}N–H)	ν(Cu–O)	ν(Cu–N)
$H_2ASC{\cdot}H_2O$	1619	----	1020	1270	3295	----	----
$[Cu_2(ASC)_2]$ (**34**)	1605	1588	1082	1255	----	482	416
[Cu(ASC)phen] (**35**)	1604	1530	1099	1263	----	485	419
$[Cu(ASC)bipy]{\cdot}2.5H_2O$ (**36**)	1604	1540	1087	1241	----	512	429
H_2BSC	1629	----	1059	1294	3145	----	----
$[Cu_2(BSC)_2]$ (**37**)	1602	1529	1082	1243	----	495	418
$[Cu(BSC)phen]{\cdot}3H_2O$ (**38**)	1602	1524	1091	1247	----	549	428
$[Cu(BSC)dmbipy]{\cdot}4H_2O$ (**39**)	1603	1531	1086	1245	----	514	422
$[Cu(BSC)bipy]{\cdot}2H_2O$ (**40**)	1604	1542	1089	1242	----	495	414

[a] Newly formed C=N

Comparing the IR spectra of the semicarbazones, $H_2ASC{\cdot}H_2O$ and H_2BSC with that of the copper complexes, we observed that the strong bands assigned to ν(C=O) stretching vibrations at 1692 and 1662 cm^{-1} respectively, disappeared in their complexes, which showed that the H–N–C=O has transformed to N=C–O–H, coordinating to copper in the enolate form. This is further supported by the disappearance of the stretching frequencies attributed to N^2H at 3295 and 3145 cm^{-1} and the appearance of bands in the range 1524-1588 cm^{-1} for the newly formed –C=N–N=C moiety. The ν(C=N) band of the semicarbazones at 1619 and 1631 cm^{-1} undergo a negative shift of wavenumber (14-27 cm^{-1}) in the complexes indicating coordination via

azomethine nitrogen [9,10]. This has been confirmed by the bands in the 414-429 cm^{-1} range and it is assignable to the ν(Cu–N) band [11]. The positive shift of the frequency assigned to the ν(N–N) band in the spectra of the complexes is owing to the increase in double bond character, off-setting the loss of electron density via donation to the metal [12]. The broad absorption bands at 3335 and 3316 cm^{-1} assigned to phenolic –OH for the semicarbazones have disappeared in the complexes, thereby indicating the coordination of the phenolic oxygen to the copper atom [13]. The appearance of new peaks in the range 482-549 cm^{-1} again confirms Cu–O coordination [14]. Bands in the region 950-550 cm^{-1} are due to the substituted benzene ring. The broad bands observed around 3400 cm^{-1} in all the complexes except **34**, **35** and **37** indicate the presence of water in their lattice. In compounds **35**, **36**, **38**, **39** and **40** bands due to heterocyclic breathing are observed in the region 740-1450 cm^{-1}.

Thus it is seen that semicarbazones act as a dianionic tridentate chelating agents in the complexes. The fourth and fifth coordination sites in complexes **35**, **36**, **38**, **39** and **40** are occupied by N atoms of the heterocyclic bases. The IR spectra of the compounds are shown in Figs. 7.1-7.7.

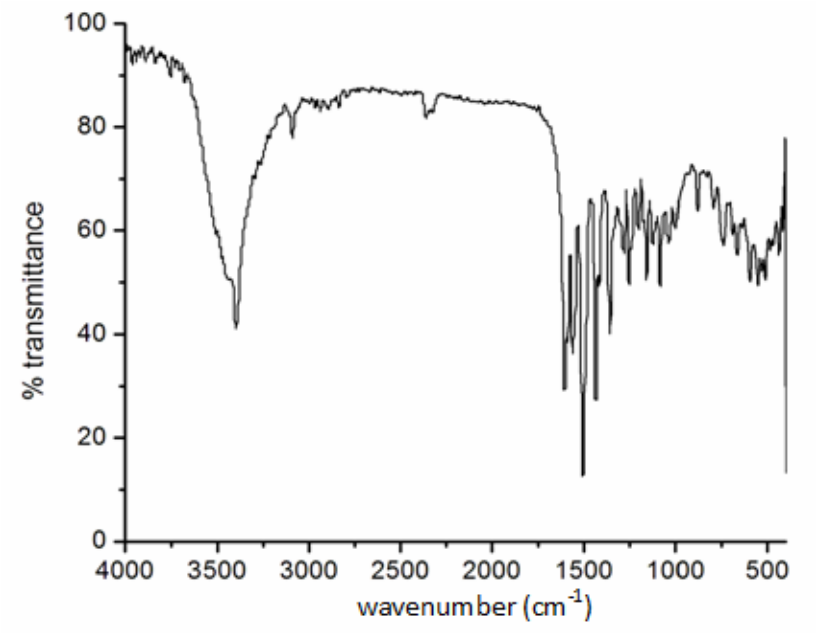

Fig. 7.1. Infrared spectrum of $[Cu_2(ASC)_2]$ (34).

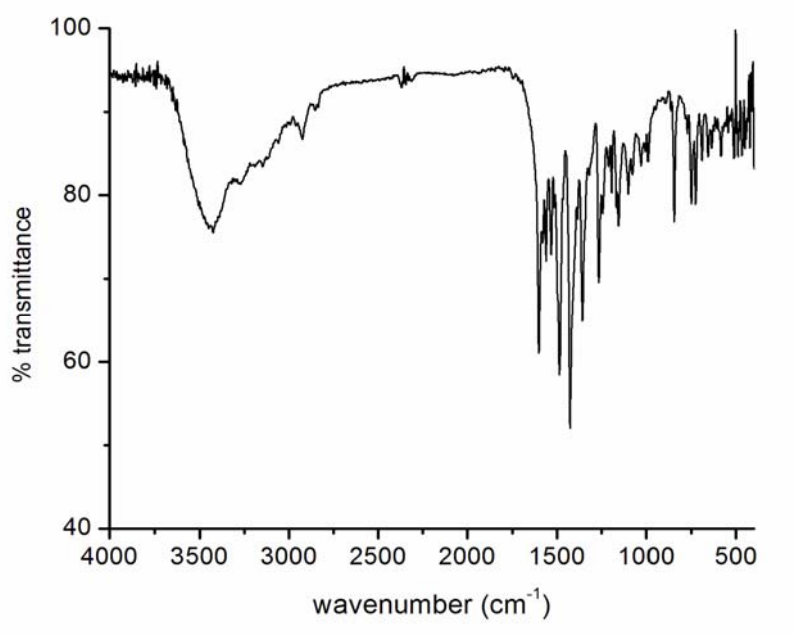

Fig. 7.2. Infrared spectrum of [Cu(ASC)phen] (35).

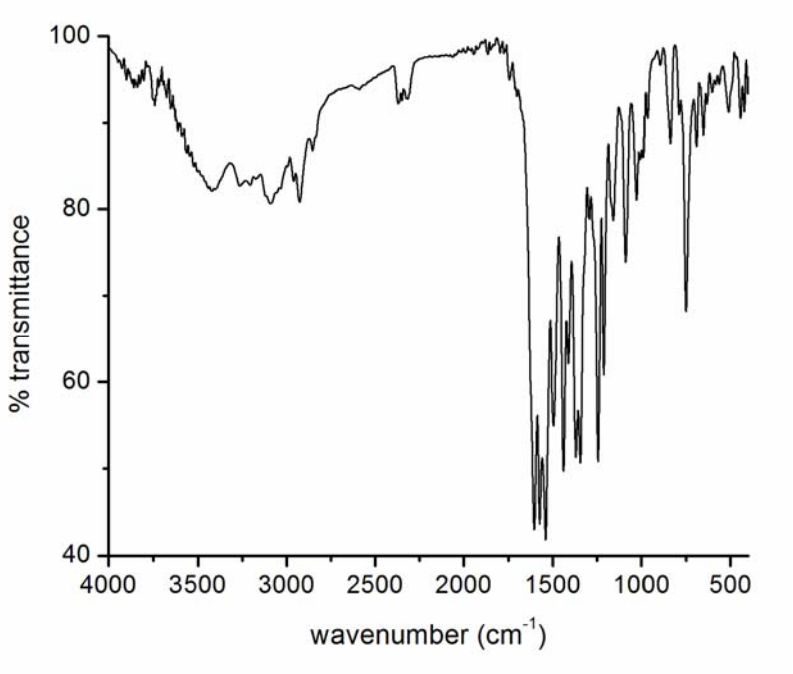

Fig. 7.3. Infrared spectrum of [Cu(ASC)bipy]·2.5H_2O (36).

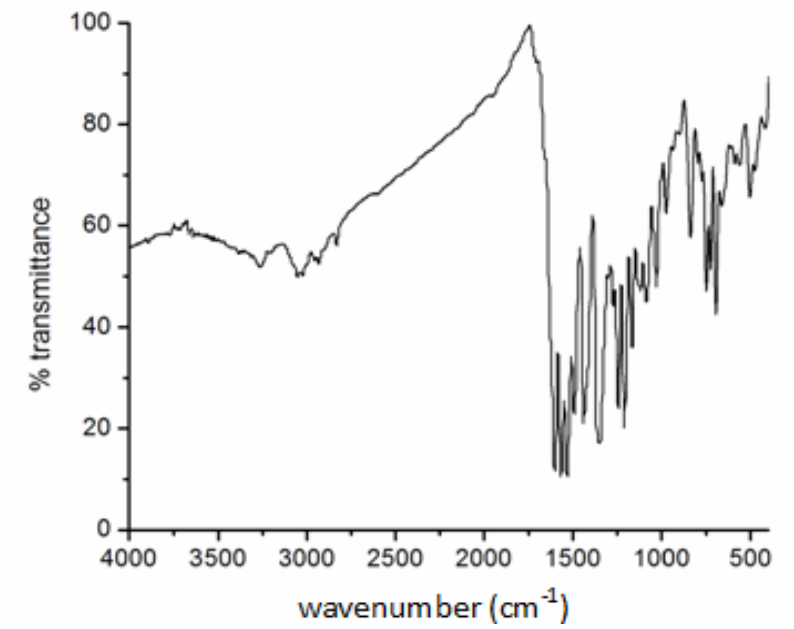

Fig. 7.4. Infrared spectrum of [$Cu_2(BSC)_2$] (37).

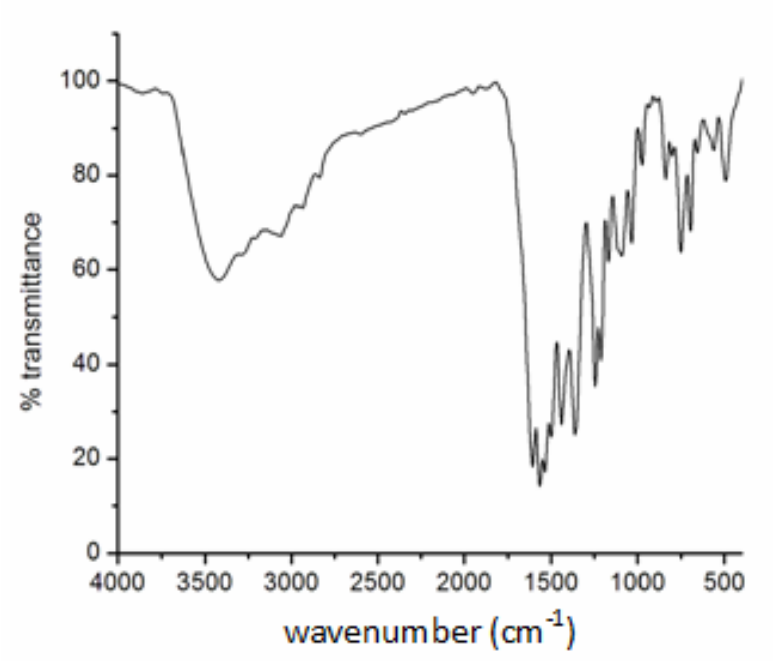

Fig. 7.5. Infrared spectrum of [Cu(BSC) phen]·3H$_2$O (38).

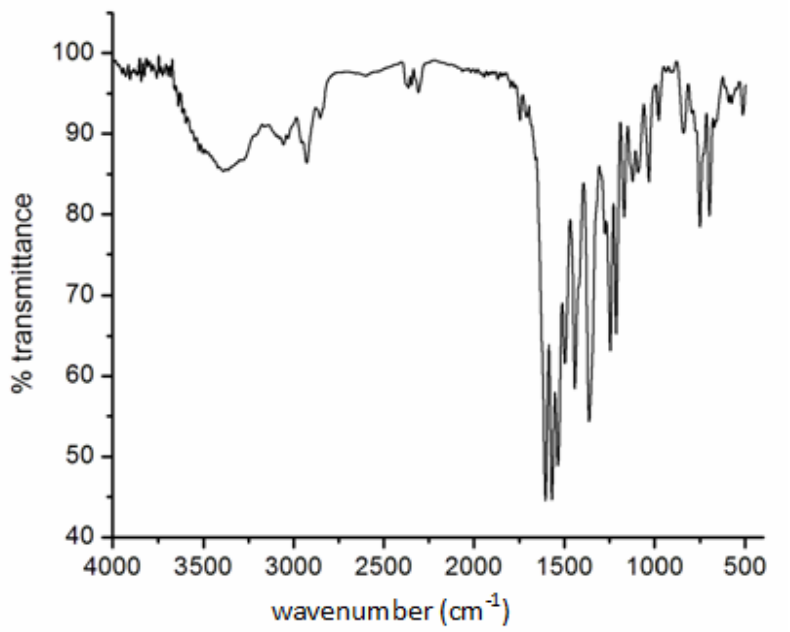

Fig. 7.6. Infrared spectrum of [Cu(BSC) dmbipy]·4H$_2$O (39).

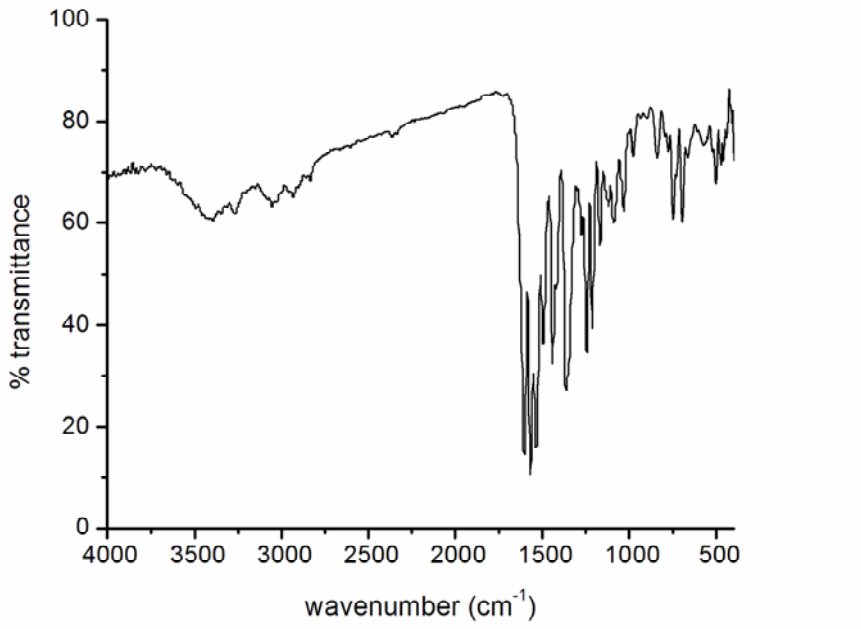

Fig. 7.7. Infrared spectrum of [Cu(BSC)bipy]·2H_2O (40).

7.3.5. Electronic spectra

The UV-Vis spectra give much insight into the coordination geometry around copper(II) ion. For complexes, **35**, **36**, **37**, **38** and **40** UV spectra were recorded in acetonitrile solution (Figs. 7.9 & 7.10) and for complexes **34** and **39** in DMF solution (Figs. 7.8 & 7.11). The intraligand transitions n→π* and π→π* of phenyl rings and semicarbazide moiety are assigned to the bands in the range 31780-41750 cm^{-1} for the semicarbazone H_2ASC and in the range 31330-41680 cm^{-1} for H_2BSC [15]. These bands undergo shift to longer wavelength region on complexation indicating coordination. The intense ligand to metal charge transfer (LMCT) transitions are observed at high energy region. The intensity of these transitions reflects the overlap of the ligand and metal orbitals involved in the charge transfer. For all the complexes **34-40**, LMCT transitions are observed in the 25950-27250 cm^{-1} range, and its broadness can

be explained as due to the combination of O→Cu and N→Cu LMCT transitions [16].

Copper(II) has the spectroscopic ground state term ^2D which will be split by an octahedral field into two levels, $^2T_{2g}$ and ^2E_g. However, if the geometry around copper(II) complex is of lower symmetry, the energy levels again split resulting in more transitions and its electronic spectrum is somewhat more complicated. For a square planar complex with $d_{x^2-y^2}$ ground state, three transitions are possible *viz*, $d_{x^2-y^2} \rightarrow d_{z^2}$, $d_{x^2-y^2} \rightarrow d_{xy}$ and $d_{x^2-y^2} \rightarrow d_{xz}$, d_{yz} ($^2A_{1g} \leftarrow {}^2B_{1g}$, $^2B_{2g} \leftarrow {}^2B_{1g}$ and $^2E_g \leftarrow {}^2B_{1g}$) and square pyramidal complexes have the $d_{x^2-y^2} \rightarrow d_{xz}$, d_{yz} and $d_{x^2-y^2} \rightarrow d_{z^2}$ transitions [17,18]. The visible spectra of all the complexes were recorded in DMF solutions and exhibit *d-d* bands centered around 16000 cm^{-1} (Figs. 7.12.1-7.12.7). Since the four *d* orbitals lie very close together, each transition cannot be distinguished by their energy and hence it is very difficult to resolve the bands into separate components. EPR studies are found very consistent with a $d_{x^2-y^2}$ ground state and is the most common ground state for Cu(II) complexes. However, results obtained from electronic spectra do not permit a structural diagnosis free of uncertainty. The electronic spectral bands of the ligand and the complexes are presented in Table 7.3.

Table 7.3. Electronic spectral assignments (cm^{-1}) of N^4-phenylsemicarbazones and their Cu(II) complexes.

Compound	Solvent	Intraligand transitions	LMCT	*d-d*
H_2ASC	CH_3CN	31780, 34540, 35600(sh), 41750	----	----
H_2ASC	DMF	31590, 34250, 35300	----	----
$[Cu_2(ASC)_2]$ (**34**)	DMF	31950, 33270, 36900	27250, 26480 (sh)	16630
[Cu(ASC)phen] (**35**)	CH_3CN	32020 (sh), 34590 (sh), 37290, 43690	27330, 26450 (sh)	16230
[Cu(ASC)bipy]·2.5H_2O (**36**)	CH_3CN	31600, 35150, 42270, 46970(sh)	26300	15280
H_2BSC	CH_3CN	31330, 33820, 35030, 41680	----	----
H_2BSC	DMF	31030, 32070 (sh), 33610, 34890	----	----
$[Cu_2(BSC)_2]$ (**37**)	CH_3CN	31590, 38790	26320(sh), 26980	16120
[Cu(BSC)phen]·3H_2O (**38**)	CH_3CN	31480, 33930, 37000, 43110	25960(sh), 26960	16350
[Cu(BSC)dmbipy]·4H_2O (**39**)	DMF	31110, 32280, 36390	26020(sh), 26610	16280
[Cu(BSC)bipy]·2H_2O (**40**)	CH_3CN	31400, 34000, 35100,42300	25950(sh), 26660	16180

sh = shoulder

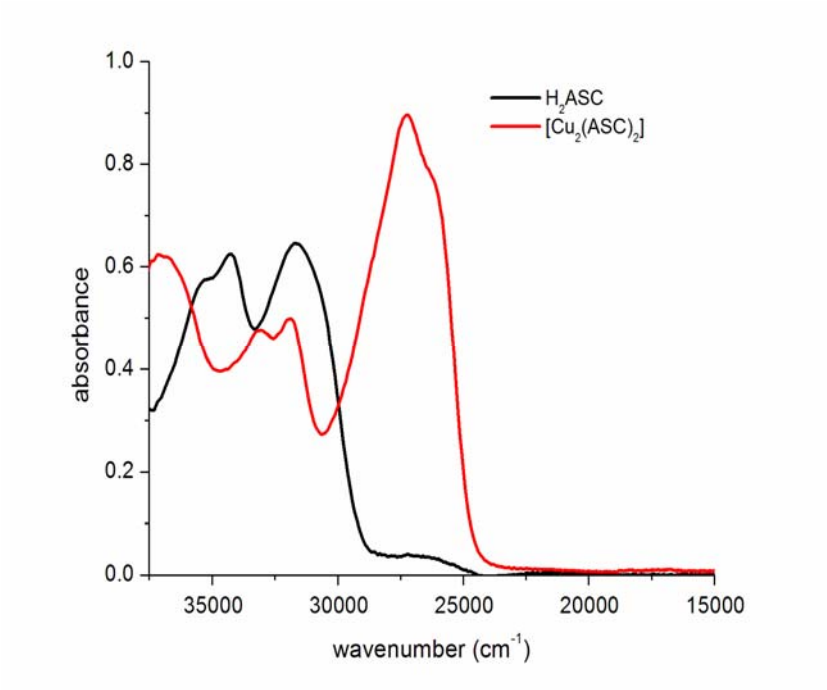

Fig.7.8. UV spectra of H_2ASC and $[Cu_2(ASC)_2]$.

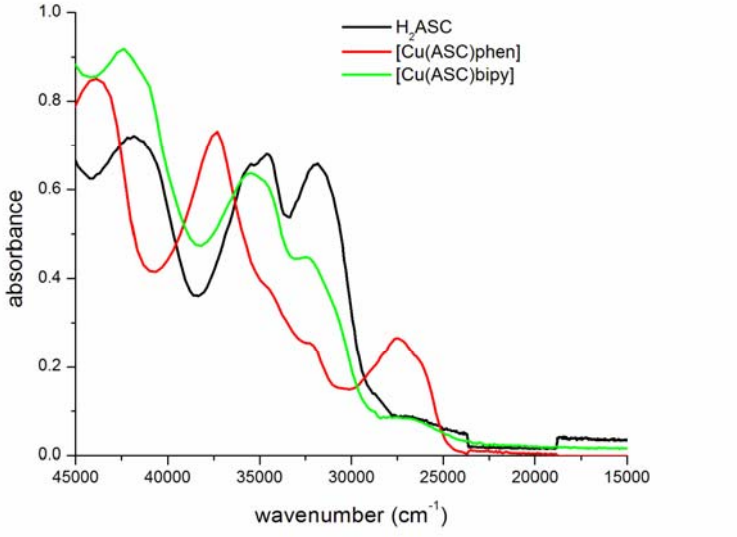

Fig.7.9. UV spectra of H_2ASC, [Cu(ASC)phen] and [Cu(ASC)bipy].

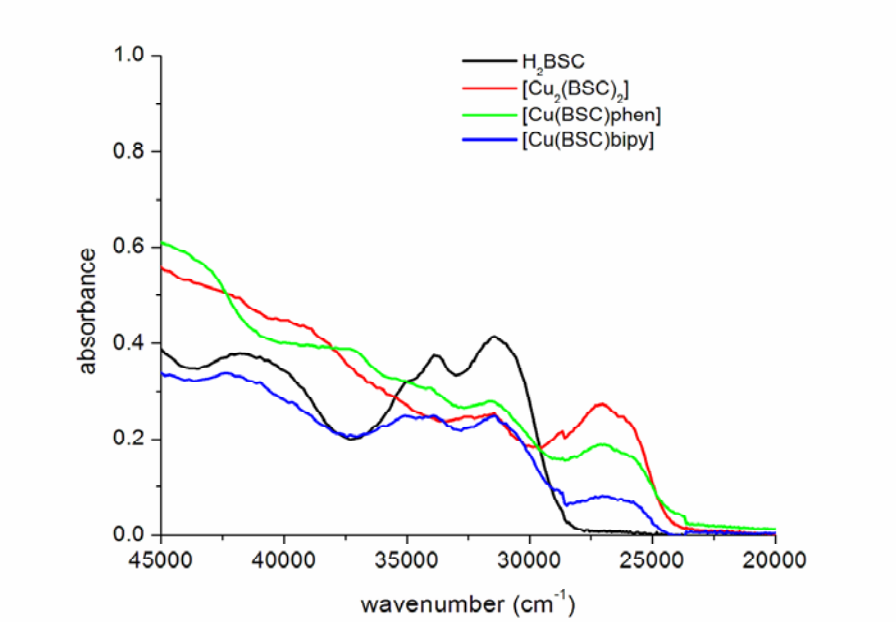

Fig.7.10. UV spectra of H_2BSC, $[Cu_2(BSC)_2]$, [Cu(BSC)phen] and [Cu(BSC)bipy].

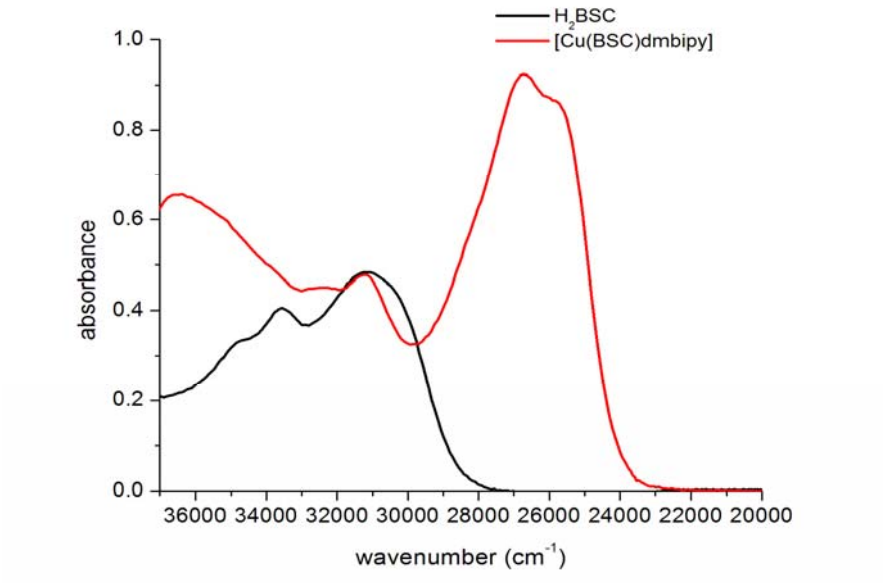

Fig. 7.11. UV spectra of H_2BSC and [Cu(BSC)dmbipy].

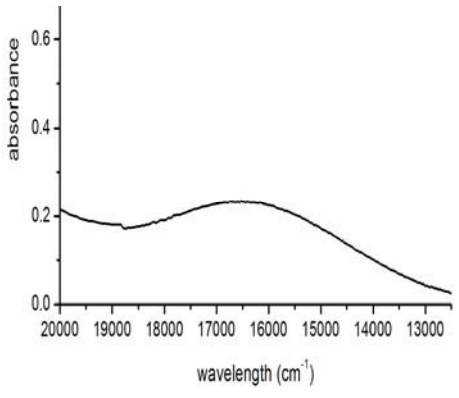

Fig.7.12.1. [$Cu_2(ASC)_2$]

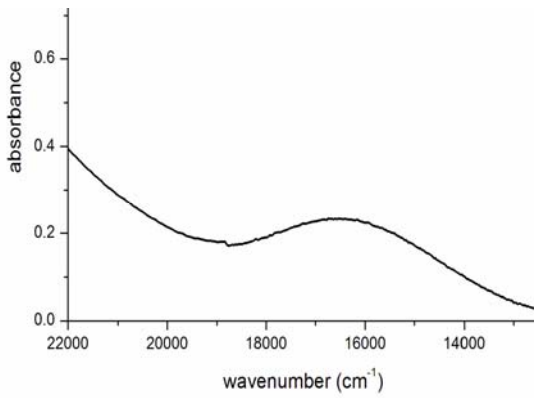

Fig.7.12.2. [Cu(ASC)phen]

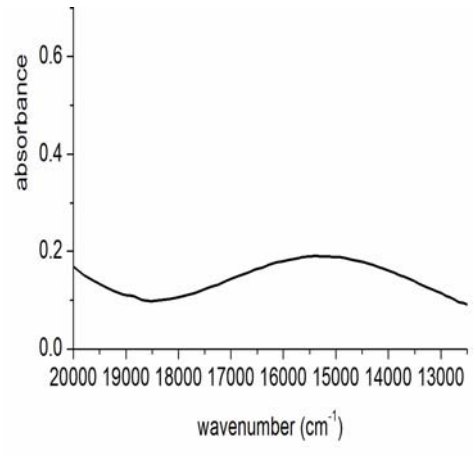

Fig.7.12.3. [Cu(ASC)bipy]

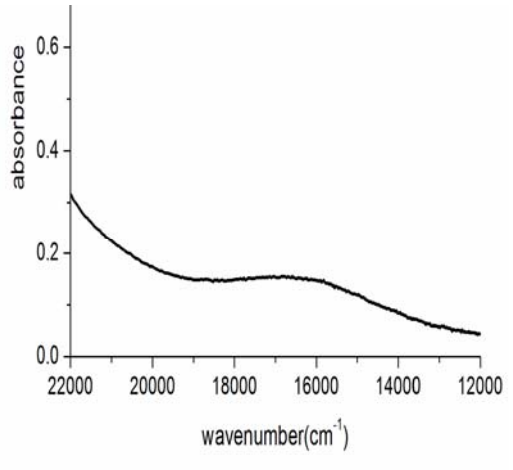

Fig.7.12.4. [$Cu_2(BSC)_2$]

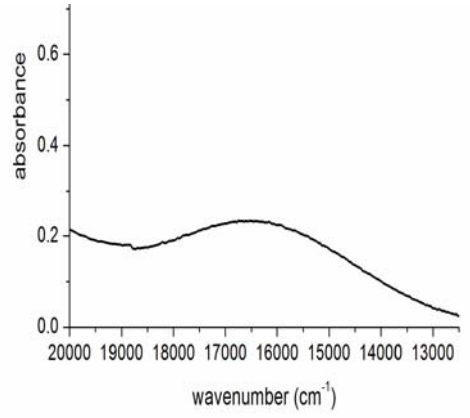

Fig.7.12.5. [Cu(BSC)phen]

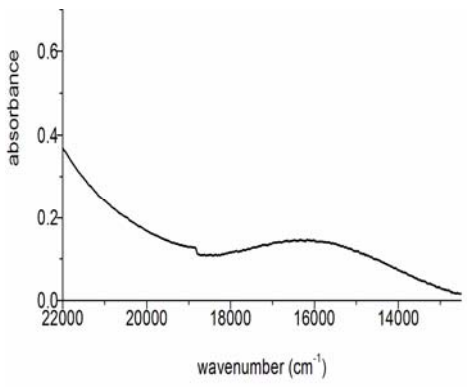

Fig.7.12.6. [Cu(BSC)dmbipy]

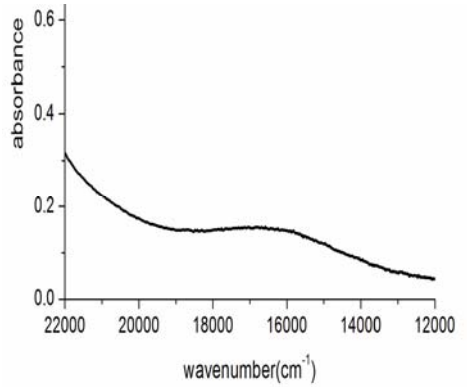

Fig. 7.12.7. [Cu(BSC)bipy]

Fig.7.12. Visible spectra of Cu(II) complexes.

7.3.6. Electron paramagnetic resonance spectra

The EPR spectra of complexes in polycrystalline state at 298 K and in frozen DMF at 77 K were recorded in the X band, using 100 kHz field modulation and 9.4 GHz microwave frequency; *g* factors were quoted relative to the standard marker TCNE (g =2.00277). Some of the EPR spectra are simulated and the experimental (blue) and simulated (black) best fits are included [19]. The EPR spectral parameters of the copper(II) complexes are presented in the Table 7.4.

The copper(II) ion, with a d^9 configuration, has an effective spin of S = 1/2 and is associated with a spin angular momentum $m_s = \pm 1/2$, leading to a doubly degenerate spin state in the absence of a magnetic field. In a magnetic field this degeneracy is lifted and the energy difference between these states is given by $\Delta E = h\nu = g\beta B$ where h is the Planck's constant, ν is the frequency, g is the Lande splitting factor (equal to 2.0023 for a free electron), β is the electronic Bohr magneton and B is the magnetic field. For the case of a $3d^9$

copper(II) ion the appropriate spin Hamiltonian assuming a B_{1g} ground state is given by

$$\hat{H} = \beta[g_{\parallel} B_z S_z + g_{\perp} (B_x S_x + B_y S_y)] + A_{\parallel} I_z S_z + A_{\perp} (I_x S_x + I_y S_y)$$

An easy application of EPR spectroscopy uses the Cu(II) ion, a particularly favorable example of a metal ion that exhibits a wide range of stereochemistry with a variety of intermediate situations. For coordination geometries corresponding to an elongated octahedron, a square pyramid or square planar, the ground state is $d_{x^2-y^2}$. When the coordination around Cu(II) ion is a compressed octahedron or a trigonal bipyramid, the ground state is d_z^2. EPR spectroscopy can distinguish the ground states $d_{x^2-y^2}$ and d_z^2 on the basis of the principal values of the *g* tensor in the anisotropic spectra [20].

The EPR spectra of all the compounds **34-40** were recorded. All these complexes except **35** and **37** show only one broad signal in the polycrystalline state at 298 K. For complexes **35** and **37** the spectra are axial. Such isotropic spectrum, consisting of only one broad signal and hence only one *g* value (g_{iso}), arises from extensive exchange coupling through misalignment of the local molecular axes between different molecules in the unit cell (dipolar broadening) and enhanced spin lattice relaxation. This type of spectra unfortunately give no information on the electronic ground state of copper(II) ions present in the complexes.

The complex $[Cu_2(ASC)_2]$ **(34)** in polycrystalline state displayed an isotropic spectrum with g_{iso} = 2.103 (Fig. 7.13).

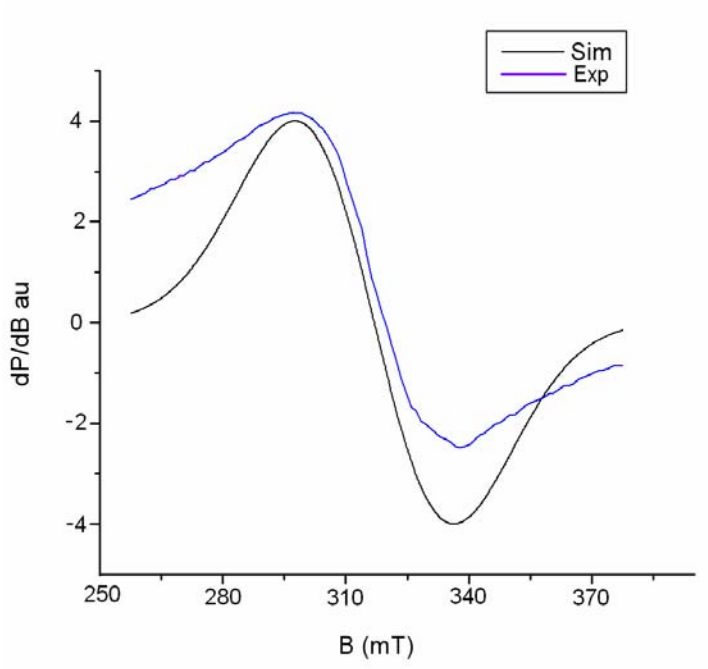

Fig.7.13. EPR spectrum of $[Cu_2(ASC)_2]$ (34) in polycrystalline state at 298K.

However in frozen DMF at 77 K, we got an axial spectrum with hyperfine splitting into four lines both in the perpendicular and parallel regions ($g_{\|} = 2.210$, $g_{\perp} = 2.047$) and ($A_{\|} = 175 \times 10^{-4}$ cm^{-1}, $A_{\perp} = 43 \times 10^{-4}$ cm^{-1}) and is presented in Fig. 7.14. The hyperfine splitting is due to the interaction of the electron spin with the copper nuclear spin (I=3/2). In addition to these, the high field signal is split into three lines with an average spacing of 16×10^{-4} cm^{-1} by the coordination of azomethine nitrogen to the copper nucleus. The most important aspect found in the spectrum is a half field signal at g = 4.37 indicating dimeric species [21] which arises due to the $\Delta m_s = \pm 2$ transitions.

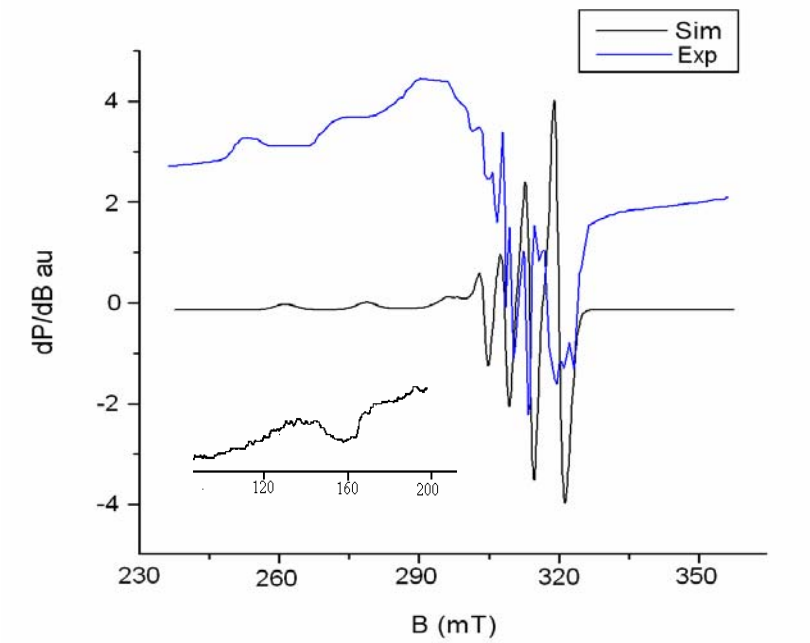

Fig.7.14. EPR spectrum of $[Cu_2(ASC)_2]$ (34) in DMF at 77 K.

The EPR spectrum of complex **35** is axial both in the polycrystalline state (Fig.7.15) and in frozen DMF (Fig.7.16) with four hyperfine splittings due to the interaction of the electron spin with the nuclear spin (I=3/2) of copper. In the polycrystalline state $g_{\|}$ = 2.244, $g_{\perp}$ = 2.060 and $A_{\|}$ = 221x $10^{-4}cm^{-1}$, $A_{\perp}$ = 22x10^{-4} cm^{-1}. The geometric parameter G for axial spectrum, which is a measure of exchange interaction between copper centres, is calculated using the equation, and it is found to be 4.188, indicating its monomeric nature having no exchange interaction in the complex.

$$G = (g_{\|} - 2.0023) / (g_{\perp} - 2.0023)$$

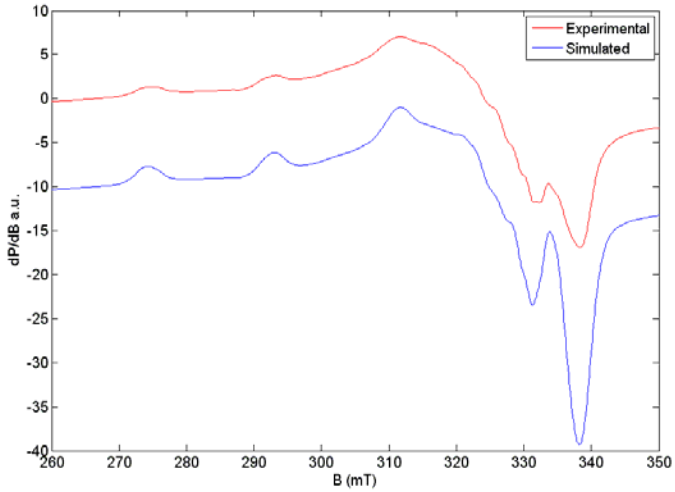

Fig. 7.15. EPR spectrum of [Cu(ASC)phen] (35)in polycrystalline state at 298 K.

In frozen DMF the same parameters are obtained. $g_{\|} = 2.240$, $g_{\perp} = 2.060$ and $A_{\|} = 221\text{x}10^{-4}$ cm^{-1}, $A_{\perp} = 22\text{x}10^{-4}$ cm^{-1}. Moreover, both in the perpendicular and parallel regions superhyperfine splittings are seen, with $A_{N\|} = 25\text{x}10^{-4}$ and $A_{N\perp} = 29\text{x}10^{-4}$ which give an evidence for the coordination of phenanthroline and azomethine nitrogens.

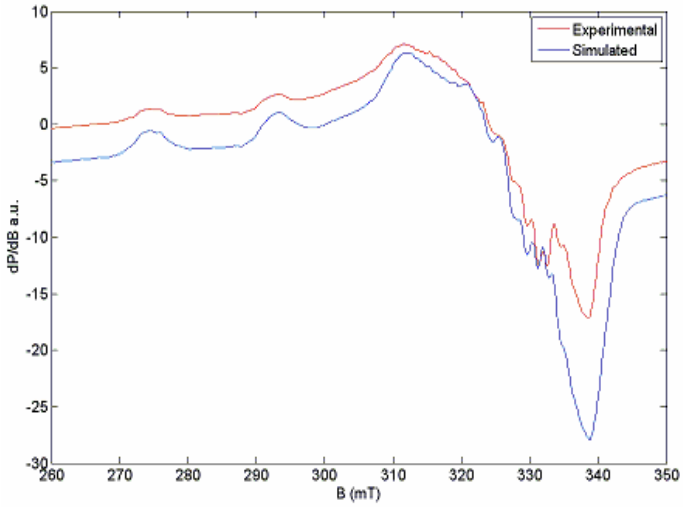

Fig. 7.16. EPR spectrum of [Cu(ASC)phen] (35) in DMF at 77 K.

The complex **36** exhibited an isotropic spectrum (g_{iso} = 2.116) (Fig. 7.17) in polycrystalline state and a well defined axial spectrum ($g_{\|}$ = 2.199, $g_{\perp}$ = 2.047 $A_{\|}$ = 227x10^{-4} cm^{-1}, $A_{\perp}$ = 23 x10^{-4} cm^{-1}) with four hyperfine splittings in frozen DMF at 77 K.

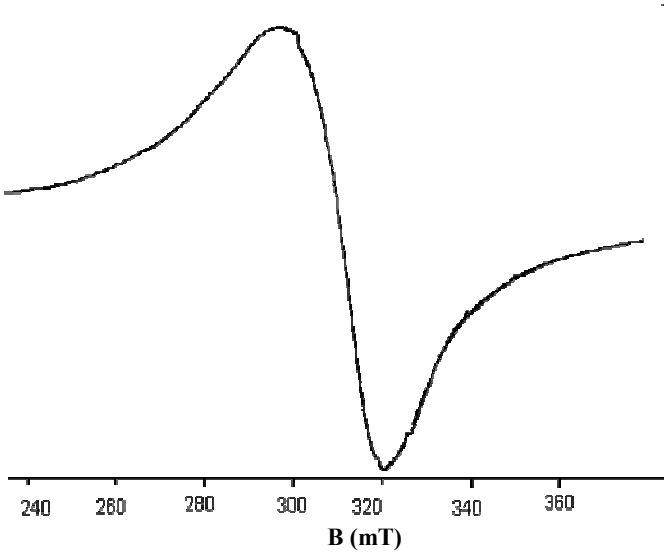

Fig. 7.17. EPR spectrum of [Cu(ASC)bipy]·2.5H$_2$O (36) in polycrystalline state at 298 K.

Moreover, both in the perpendicular and parallel regions, five splittings are seen with an average spacing of 15x10^{-4} cm^{-1} which corresponds to the interaction of the electron with nuclear spin of two nitrogens (2x2x1+1=5), which gives an evidence for the coordination of bipyridyl and azomethine nitrogens (Fig. 7.18).

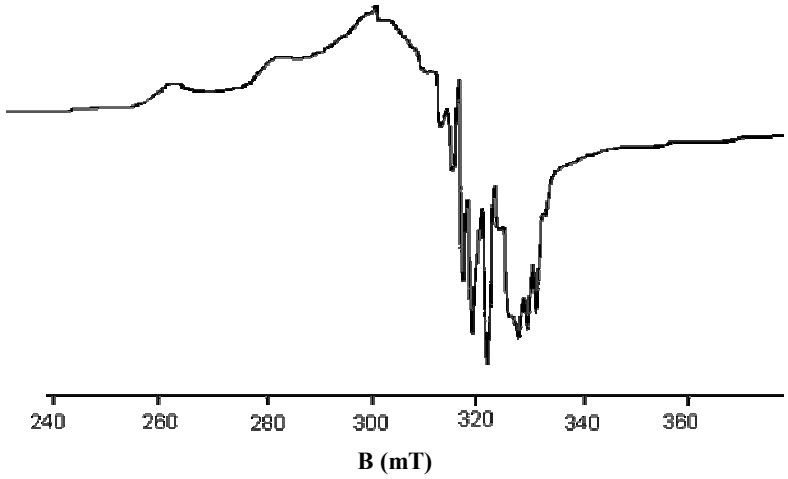

Fig. 7.18. EPR spectrum of [Cu(ASC)bipy] in DMF at 77 K.

For these pentacoordinate complexes **35** and **36** the fact that $g_{\|}$ is greater than $g_{\perp}$ suggests a distorted square-pyramidal structure and rules out the possibility of a trigonal bipyramidal structure, which would be expected to have $g_{\perp} > g_{\|}$. Here the expected superhyperfine splittings of all three nitrogen atoms (one azomethine nitrogen and two nitrogens from phenanthroline / bipyridine) are not observed. Thus the coordination polyhedron comprises one phenanthroline / bipyridyl nitrogen, the azomethine nitrogen, the enolate and the phenolate oxygens of the semicarbazone (which form the base of the pyramid) and the remaining phenanthroline/bipyridyl nitrogen [22] (which occupies the axial position); as shown in the proposed structures at the end of this chapter.

In polycrystalline state the EPR spectrum of $[Cu_2(BSC)_2]$ (**37**) is axial with $g_{\|} = 2.311$ and $g_{\perp} = 2.066$. Here a half field signal is obtained (Fig. 7.19) due to transitions corresponding to $\Delta m_s = \pm 2$. In X-band spectra, transitions due to $\Delta m_s = \pm 1$ are associated with magnetic fields of *ca*. 300 mT, while transitions due to $\Delta m_s = \pm 2$ generate an absorption at half of this field *ie. ca.* 150 mT.

The spectrum of compound **37** showed an additional absorption *ca*. 150 mT with g = 4.29, both in polycrystalline state and in frozen DMF, for a spin coupled Cu(II) dimer, and the copper-copper distance is likely to be less than 3.5 Å [21,23].

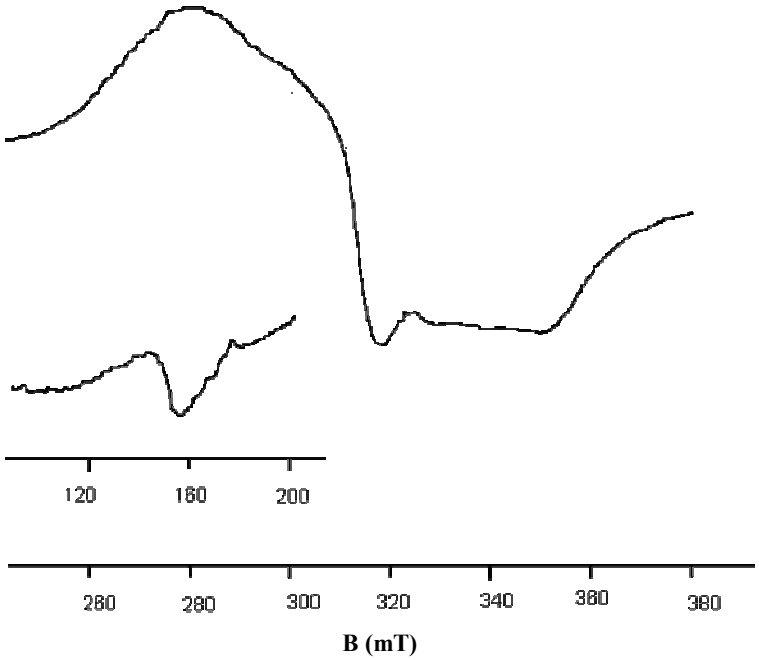

Fig. 7.19. EPR spectrum of $[Cu(BSC)]_2$ (37) in polycrystalline state at 298 K.

In frozen DMF compound **37** displayed an axial spectrum with four hyperfine splittings in the parallel region. But the expected superhyperfine splittings due to azomethine nitrogen are missing in this compound. The peculiar feature of this spectrum is that the presence of seven hyperfine splittings for the half field signal, due to the coupling of the electron spin with the nuclear spin of the two Cu centers (2nI+1 = 2x2x3/2+1). It is a good evidence for the dimeric species (Fig.7.20).

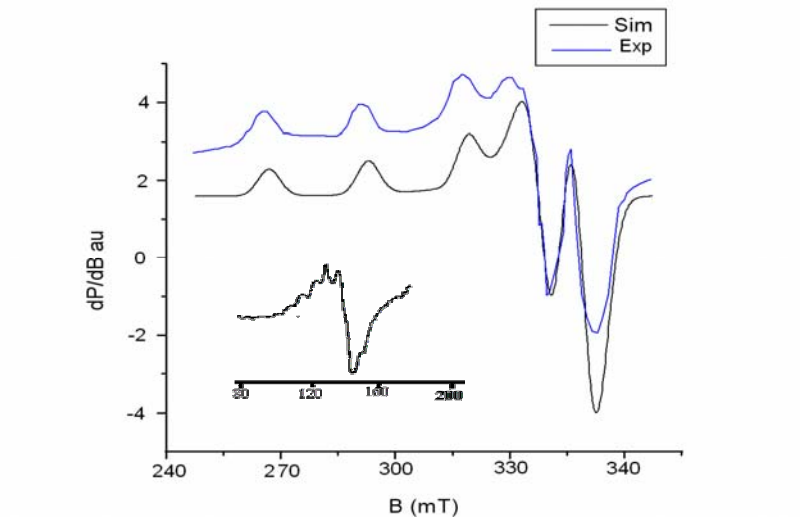

Fig. 7.20. EPR spectrum of $[Cu_2(BSC)_2]$(37) in DMF at 77 K.

Compound **38** displayed an isotropic spectrum in polycrystalline state (Fig. 7.21) with g_{iso} = 2.120.

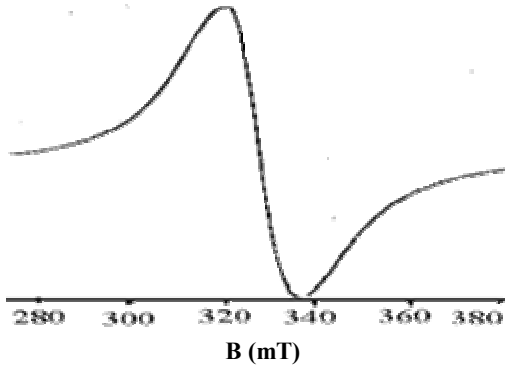

Fig. 7.21. EPR spectrum of [Cu(BSC) phen]·$3H_2O$ (38) in polycrystalline state at 298 K.

In frozen DMF compound **38** exhibits an axial spectrum with $g_{\|}$ = 2.23 and $g_{\perp}$ = 2.09 and $A_{\|}$ = 192x10^{-4} cm^{-1}. In this compound also superhyperfine splittings are missing.

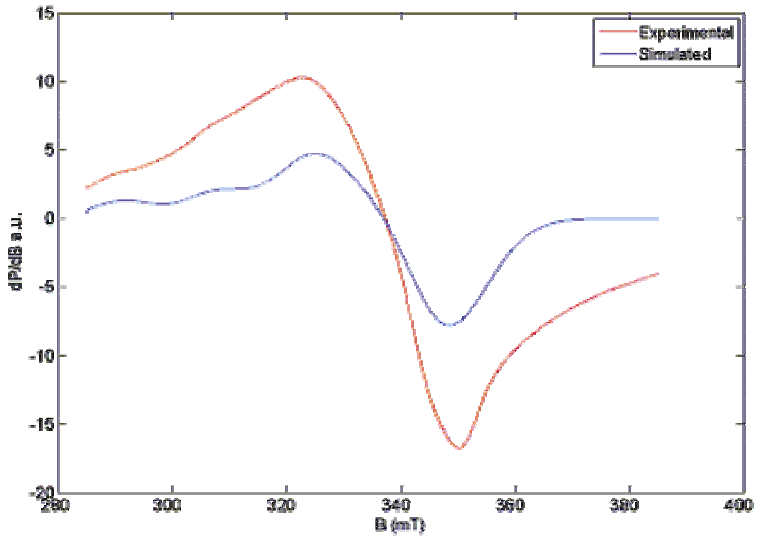

Fig. 7.22. EPR spectrum of [Cu(BSC)phen] in DMF at 77 K.

The compound **39** shows one broad signal at g_{iso} = 2.086 in the polycrystalline state at 298 K (Fig. 7.23) arising from dipolar broadening and enhanced spin lattice relaxation. This type of spectrum does not give any information on the electronic ground state of the Cu(II) ion present in the complex.

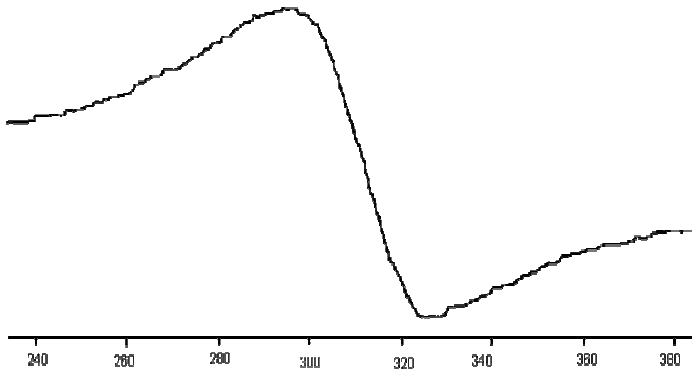

Fig. 7.23. EPR spectrum of [Cu(BSC)dmbipy]·4H$_2$O (39) in polycrystalline state at 298 K.

But its spectrum in DMF at 77 K is axial with four hyperfine lines ($g_{\|}$ = 2.197, $g_{\perp}$ = 2.055, $A_{\|}$ = 209 x10^{-4} cm^{-1}, $A_{\perp}$ = 48 x10^{-4} cm^{-1}). In addition, it shows superhyperfine lines in the high field components as expected from the coordination of two nitrogen atoms (one azomethine and the other from 4,4′-dimethylbipyridyl ring) (Fig. 7.24) with an average spacing of 23x10^{-4} cm^{-1}.

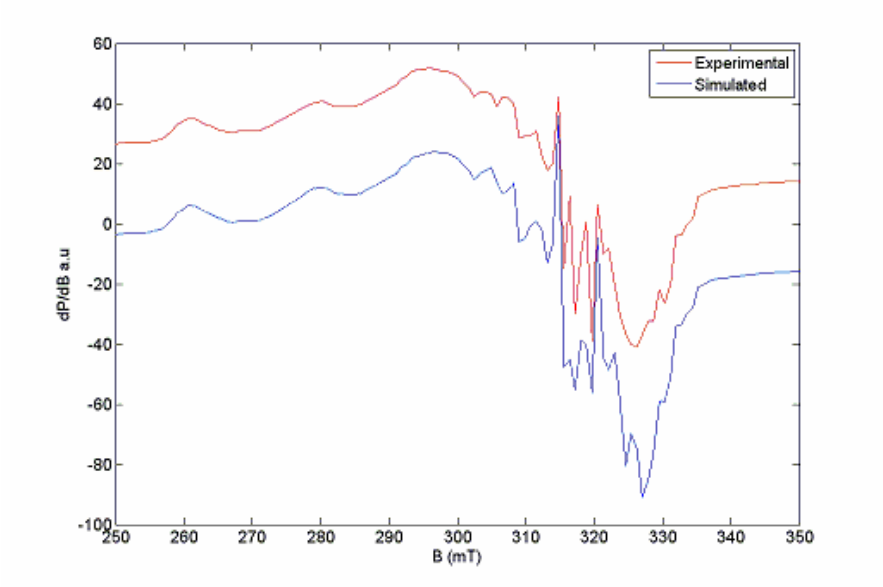

Fig. 7.24. EPR spectrum of [Cu(BSC)dmbipy] in DMF at 77 K.

The complex [Cu(BSC)bipy]·2H_2O (**40**) exhibited an isotropic spectrum (g_{iso} = 2.110) (Fig. 7.25) in polycrystalline state.

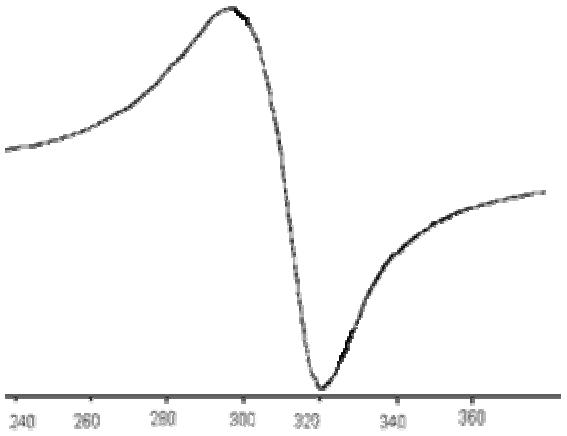

Fig.7.25. EPR spectrum of [Cu(BSC)bipy]·2H_2O (40) in polycrystalline state at 298 K.

But the spectrum of the compound [Cu(BSC)bipy]·2H_2O (**40**) in DMF at 77 K shows an axial spectrum with four hyperfine lines ($g_{\|}$ = 2.232, $g_{\perp}$ = 2.050, $A_{\|}$ = 213x10^{-4} cm^{-1} and $A_{\perp}$= 24x10^{-4} cm^{-1}) as expected due to the interaction of the electron spin with the nuclear spin (I=3/2) of copper (Fig.7.26).

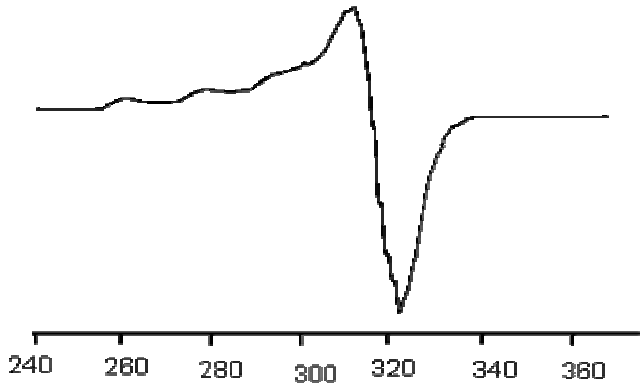

Fig. 7.26. EPR spectrum of [Cu(BSC)bipy] in DMF at 77 K.

In all the pentacoordinate systems as $g_{\|} > g_{\perp}$, a square pyramidal geometry with unpaired electron in $d_{x^2-y^2}$ orbital, can be assigned and rules out the possibility of a trigonal bipyramidal structure which would be expected to have $g_{\perp} > g_{\|}$.

Table 7.4. EPR spectral data for Cu(II) complexes in polycrystalline state at 298 K and in DMF at 77 K.

Compound	Polycrystalline state (298 K)	DMF solution (77 K)										
	g_{iso}	$g_{\parallel}$	$g_{\perp}$	g_{av}	$A_{\parallel}$ [a]	$A_{\perp}$ [a]	A_{av} [a]	α^2	β^2	γ^2	$K_{\parallel}$	$K_{\perp}$
$[Cu_2(ASC)_2]$ (**34**)	2.103	2.210	2.047	2.101	175	43	87	0.753	0.958	0.889	0.7221	0.69
[Cu(ASC)phen] (**35**)	2.244/2.060 ($g_{\parallel}$ / $g_{\perp}$)	2.240	2.060	2.120	221	22	88	0.917	0.832	0.819	0.763	0.752
[Cu(ASC)bipy]·2.5H_2O (**36**)	2.116	2.199	2.047	2.097	227	23	91	0.885	0.761	0.725	0.673	0.642
$[Cu_2(BSC)_2]$ (**37**)	2.310/2.067 ($g_{\parallel}$ / $g_{\perp}$)	2.226	2.060	2.128	201	---	--	0.848	0.870	0.883	0.737	0.749
Cu(BSC)phen]·3H_2O (**38**)	2.120	2.230	2.090	2.136	192	---	--	0.839	0.892	1.108	0.750	0.930
[Cu(BSC)dmbipy]·4H_2O (**39**)	2.086	2.196	2.055	2.102	208	30	89	0.834	0.828	0.862	0.690	0.719
[Cu(BSC)bipy]·2H_2O (**40**)	2.110	2.232	2.050	2.111	213	24		0.8829	0.8483	0.7732	0.749	0.683

[a] Expressed in units of cm^{-1} multiplied by a factor of 10^{-4}.

From the EPR spectral data for these complexes we can infer that the $g_{\|}$ values are nearly the same for all the complexes indicating that the bonding is dominated by the semicarbazone moiety. In all the complexes, $g_{\|} > g_{\perp} > 2.0023$. The fact that $g_{\|}$ values are less than 2.3 is an indication of significant covalent character to the M–L bond [24,25]. The g_{av} values of all the complexes in the solution state are consistent with the g_{iso} values suggesting that they are not undergoing any kind of dissociation in the solution state.

The EPR parameters $g_{\|}$, $g_{\perp}$, $A_{\|}$ and the energies of *d-d* transitions were used to evaluate the bonding parameters α^2, β^2 and γ^2 for the Cu(II) ion in various ligand field environments which may be regarded as measures of the covalence of the in-plane σ-bonds (α^2), in-plane π-bonds (β^2) and out-of-plane π-bonds (γ^2) respectively. The fraction of the unpaired electron density located on the copper ion *i.e.*, value of in-plane σ-bonding parameter α^2 estimated from the expression,

$$\alpha^2 = -A_{\|} / 0.036+(g_{\|}-2.0023)+ 3/7(g_{\perp}- 2.0023)+ 0.04$$

The metal-ligand bond is purely ionic, if the value of α^2 is unity and it is completely covalent, if α^2 =0.5 [24,26]. Here α^2 values calculated for the complexes lie in between 0.5 and 1, which means that the metal-ligand bonds in the complexes under investigation are partially ionic and partially covalent in nature.

The following simplified parameters were used to evaluate the bonding parameters, $K_{\|}$ and $K_{\perp}$ [27,28].

$$K_{\|}^{2} = (g_{\|} - 2.0023)\, E_{d\text{-}d}/8\lambda_o$$

$$K_{\perp}^{2} = (g_{\perp} - 2.0023)\, E_{d\text{-}d}/2\lambda_o$$

Where $K_{\|}^2 = \alpha^2\beta^2$ and $K_{\perp}^2 = \alpha^2\gamma^2$, $K_{\|}$ and $K_{\perp}$ are orbital reduction factors and λ_o represents the one electron spin orbit coupling constant which equals -828 cm^{-1}.

Hathaway has pointed out that, for pure σ bonding, $K_{\|} \approx K_{\perp} \approx 0.77$, and for in plane π-bonding, $K_{\|} < K_{\perp}$, while for out-of-plane π-bonding, $K_{\perp} < K_{\|}$. Here in compounds **34**, **35**, **36** and **40** it is observed that $K_{\perp} < K_{\|}$ indicates the presence of out of plane π bonding. In all other complexes, $K_{\|} < K_{\perp}$, *i.e.*, in plane π bonding is significant.

7.3.7. Thermogravimetric analyses

Thermal techniques, such as thermogravimetric analyses (TG and DTG), have been successfully employed for the study of thermal stability and nature of water molecules in complexes. Reports show that the weight losses for lattice water are below 200 °C and due to coordinated water are in the range of 200-350 °C [29,30]. Here the copper complexes **36**, **38**, **39** and **40** were studied from ambient temperature to 1000 °C in nitrogen atmosphere. The weight loss profiles are analyzed. The percent of weight loss at any given temperature and the temperature ranges of the degradation process were determined. The thermograms are presented below.

In complex **36** the observed mass loss of 35% in the temperature range 190-240 °C is consistent with the removal of bipyridine and two and half molecules of lattice water present (calcd. 35.8%) (Fig. 7.27).

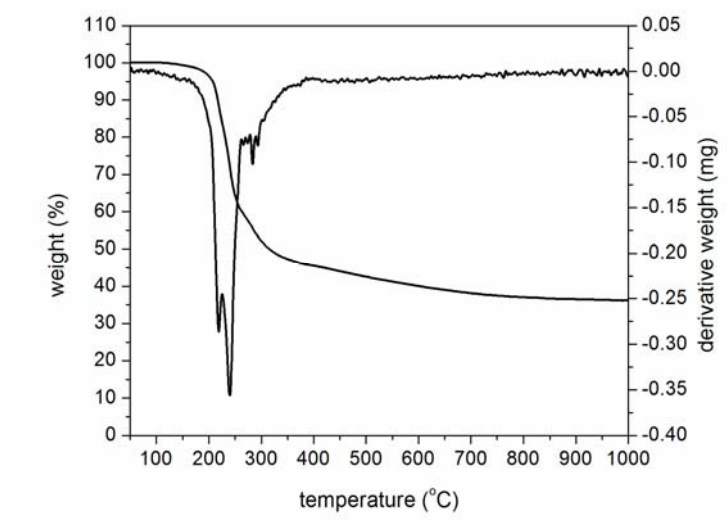

Fig. 7.27. Thermogram of [Cu(ASC)bipy]·2.5H_2O (36).

For complex **38** (Fig. 7.28) the decomposition is not so sharp and a total mass loss of 37.4% is observed in the temperature range 153-220 °C due to the removal of three molecules of water and one phenanthroline molecule (calcd. 38.3%). The approximate mass loss for the three consecutive steps in the range of 153-190 °C is 8% and it attributes to three molecules of lattice water present in the compound.

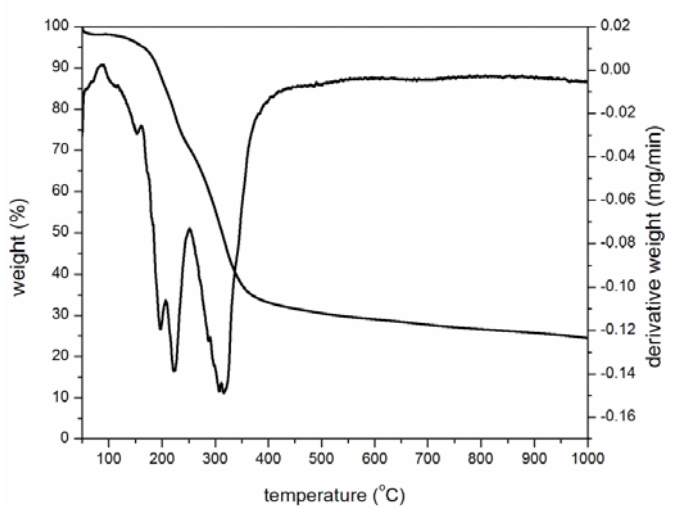

Fig. 7.28. Thermogram of [Cu(BSc)phen]·3H_2O (38).

The complex [Cu(BSC)dmbipy]·4H_2O (**39**) clearly shows a mass loss of 10% (calcd. 10.6%) at 165 °C indicating the presence of four molecules of lattice water (Fig. 7.29).

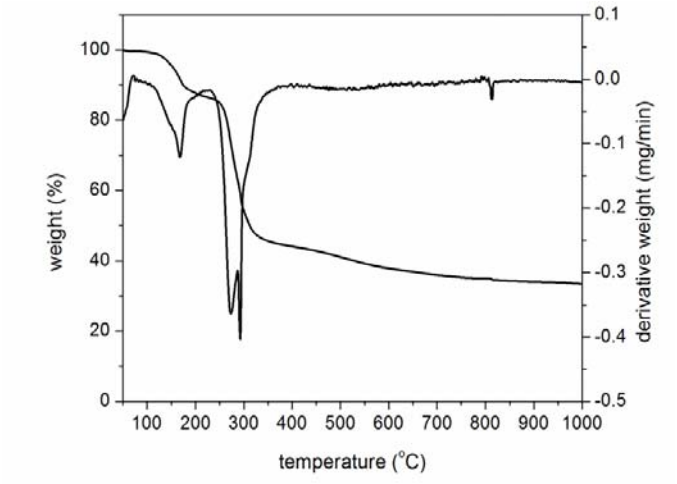

Fig. 7.29. Thermogram of [Cu(BSC)dmbipy]·4H_2O (39).

A peak observed at 87 °C for the complex **40** indicates the presence of lattice water. The mass loss of 30% observed (calcd. 30.6%) in the range of 87-235 °C can be assigned to the removal of bipyridine and two molecules of water **(**Fig. 7.30**).**

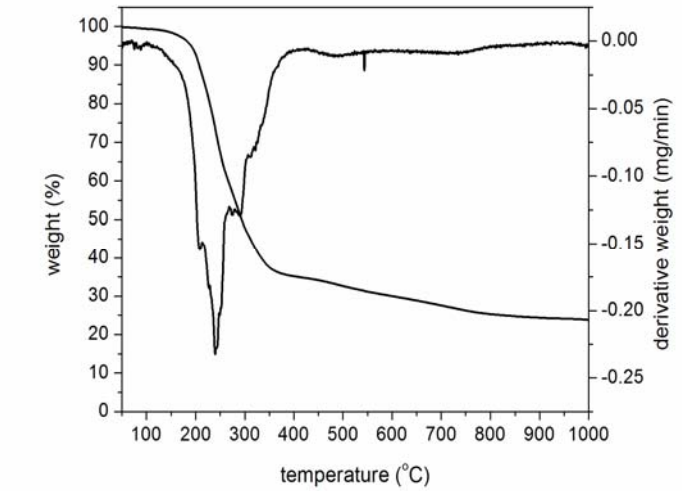

Fig. 7.30. Thermogram of [Cu(BSC)bipy]·2H_2O (40).

7.3.8. Cyclic voltammetric studies

Cyclic voltammetry is a simple and direct method for measuring the formal potential of a half reaction when both oxidized and reduced forms are stable during the time required to obtain the voltammogram. The electrochemical behavior of Cu(II) complexes were investigated by cyclic voltammetry using DMF solutions of the complexes. Cyclic voltammograms were recorded on a CHI 608 D electrochemical analyzer with a three electrode compartment consisting of platinum disc working electrode, platinum wire counter electrode and Ag/Ag^{+} reference electrode. Tetraethylammonium phosphate was the supporting electrolyte. All these redox processes are not reversible as indicated by the non-equivalent current intensity of cathodic and anodic peaks [22]. The voltammogram is run between the potentials of +2 and -2 V at a scan speed of 100 mV/s. The cyclic voltammetric data for the Cu(II) complexes are summarized in Table 7.5.

Table 7.5. Electrochemical data of the Cu(II) complexes in DMF.

Compound	Epc (V)	Ipc (μA)	Epa (V)	Ipa (μA)
$[Cu_2(ASC)_2]$ (**34**)	0.182	6.0	-1.384	5.72
	-0.129	5.17	-0.185	4.96
	-1.621	23.5	0.606	-7.69
$[Cu(ASC)bipy]\cdot 2H_2O$ (**36**)	0.920	0.712	-0.925	-3.05
	-0.148	3.72	0.956	-7.82
$[Cu(BSC)]_2$ (**37**)	0.1943	5.61	-1.295	6.33
	-0.110	5.30	-0.391	-3.59
	-1.476	20.2	0.576	-7.59
$Cu(BSC)phen]\cdot 3H_2O$ (**38**)	0.185	2.91	-0.254	-2.95
	-0.149	3.0	0.728	-5.28
$Cu(BSC)dmbipy]\cdot 4H_2O$ (**39**)	0.165	3.12	-0.406	-1.17
	-0.185	2.94	0.846	-5.44

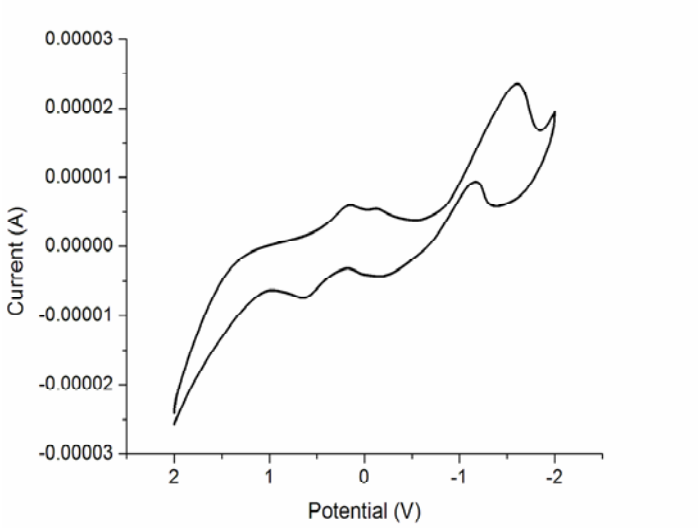

Fig. 7.31. Cyclic voltammograms of $[Cu_2(ASC)_2]$ (34) in DMF.

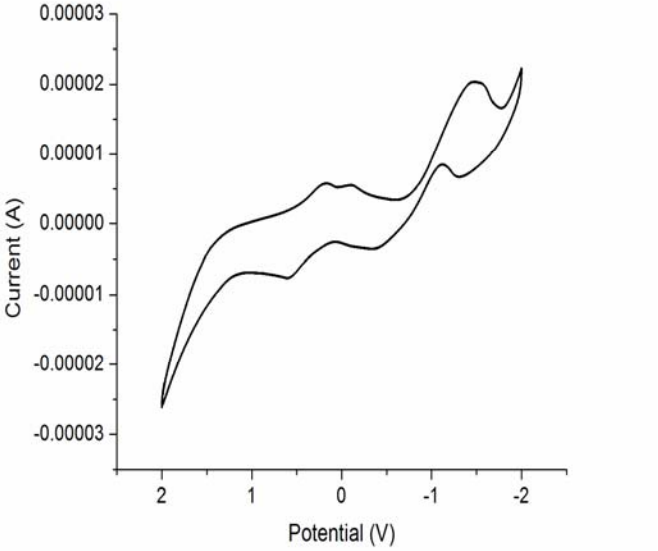

Fig. 7.32. Cyclic voltammograms of $[Cu_2(BSC)_2]$ (37) in DMF.

The binuclear copper complexes **34** and **37** (Figs. 7.31 and 7.32) showed similar features in the investigated potential range. They displayed three well defined reduction waves in the regions 0.182 to 0.194, -0.129 to -0.110 and -

1.62 to -1.476 V coupled with three anodic waves in the regions -1.384 to -1.295, -0.185 to -0.391, 0.606 to 0.576 V respectively. For binuclear copper complexes a sequential one electron transfer reactions has been reported as shown below [31].

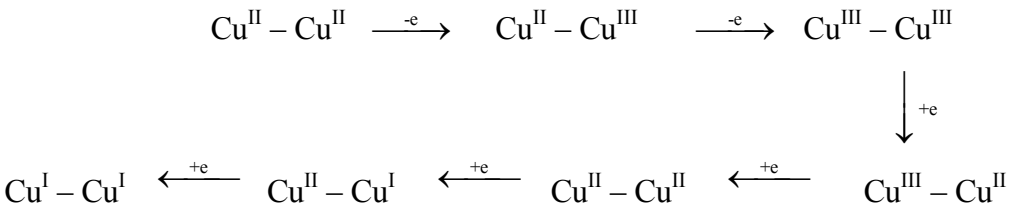

The mixed ligand mononuclear copper complexes **36**, **38** and **39** showed two redox processes in all cases. Two cyclic voltammograms are shown in Figs.7.33 and 7.34. In compound **38** the peaks at 0.185 V, -0.149 V correspond to successive copper(II) reduction processes, Cu(II)/Cu(I) and Cu(I)/Cu(0) couple respectively [32] and corresponding oxidation peaks at 0.728 V and -0.254 V are obtained in the reverse scan (Fig. 7.33). The voltammogram of complex **39** (Fig.7.34**)** displays a reduction peak at E_{pc}= 0.165 V with an associated oxidation peak at E_{pa}= 0.846 V and another weak reductive response at -0.185 V with an oxidative response at -0.046 V. These redox processes are influenced by the coordination number, stereochemistry and the hard / soft character of the ligand's donor atoms. Additional weak cathodic and anodic waves are observed for these complexes which may be due to the presence of heterocyclic bases as coligands.

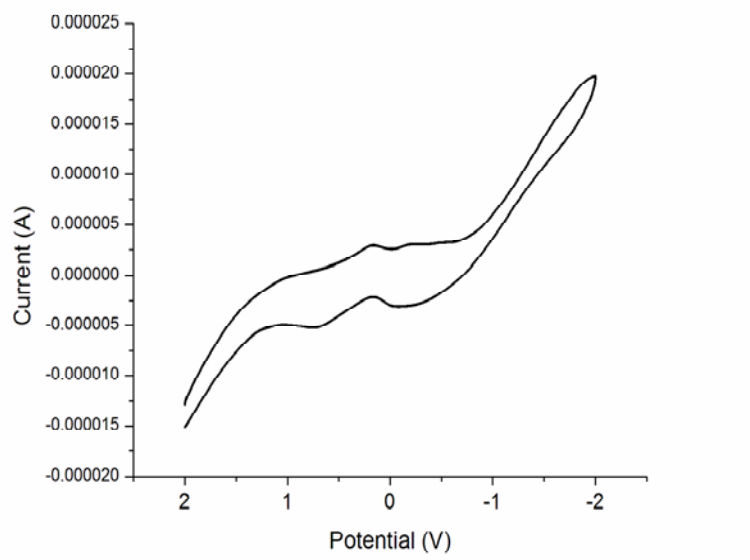

Fig. 7.33. Cyclic voltammograms of [Cu(BSC)phen] $3H_2O$ (38) in DMF.

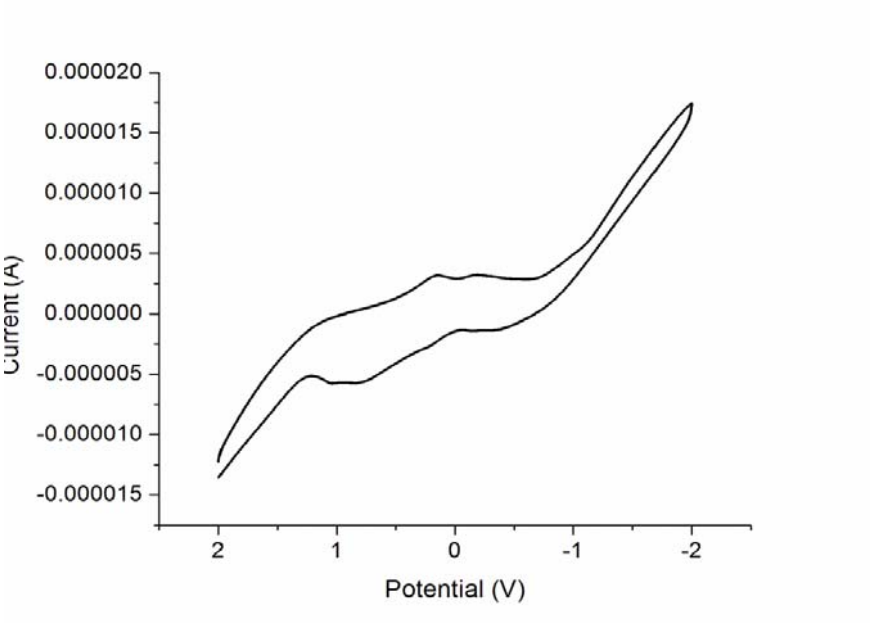

Fig. 7.34. Cyclic voltammograms of Cu(BSC)dmbipy]·$4H_2O$ (39) in DMF.

The results of spectral, magnetic and EPR studies of the copper(II) complexes suggest that the N^4-phenylsemicarbazones chosen for our investigation act as tridentate ONO donor ligands. Out of the seven complexes synthesized compounds **34** and **37** are binuclear and the remaining five (**35, 36, 38, 39 and 40**) are mononuclear pentacoordinate systems with the fourth and fifth coordination sites are occupied by the nitrogen atoms of the heterocyclic bases. EPR study suggests a distorted square-pyramidal structure for these complexes and rules out the possibility of a trigonal bipyramidal structure. Some proposed structures are presented. Lattice water molecules are omitted in complex **38.**

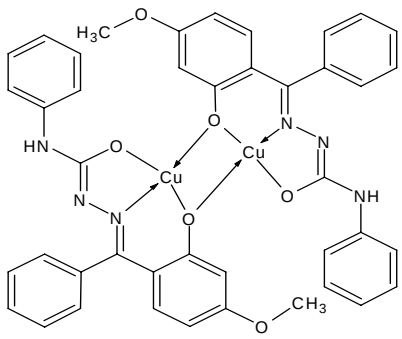

[Cu₂(BSC)₂] (37)

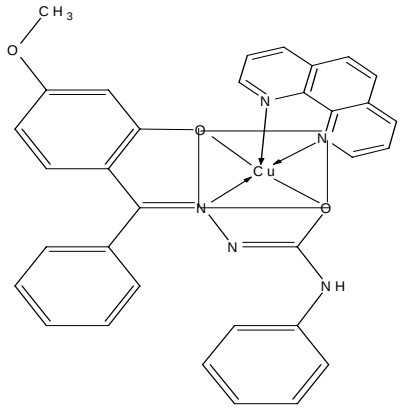

[Cu(BSC)phen]·3H₂O (38)

References

[1] J.D. Ranford, P.J. Sadler, D.A. Toucher, J. Chem. Soc., Dalton Trans. (1993) 3393.

[2] E.W. Ainscough, A.M. Brodie, A. Dobbs, J.D. Ranford, J.M. Waters, Inorg. Chim. Acta 236 (1995) 83.

[3] P.K. Panda, B.K. Mohaptra, J. Indian Chem. Soc. 61 (1984) 365.

[4] S. Chandra, M. Tyagi, J. Indian Chem. Soc., 85 (2008) 42.

[5] R.N. Prasad, K.M. Sharma, A. Agrawal, J. Indian Chem. Soc. 46A (2007) 600.

[6] T.S. Lobana, R. Sharma, G. Bawa, S. Khanna, Coord. Chem. Rev. 253 (2009) 977.

[7] W.J. Geary, Coord. Chem. Rev. 7 (1971) 81.

[8] D.X. West, J.K. Swearingen, Transit. Met. Chem. 26 (2001) 260.

[9] B.S. Garg, M.R.P. Kurup, S.K. Jain, Y.K. Bhoon, Transit. Met. Chem. 13 (1988) 92.

[10] V.L. Siji, M.R. Sudarsanakumar, S. Suma, M.R.P. Kurup, Spectrochim. Acta Part A 76 (2010) 22.

[11] K. Nakamoto, Infrared and Raman Spectra of Inorganic and Coordination Compounds, Part B, 5th edition, Wiley, New York, 1997.

[12] R.C. Maurya, S. Rajput, J. Mol. Struct. 833 (2007) 133.

[13] A. Sreekanth, U.L. Kala, C.R. Nayar, M.R.P. Kurup, Polyhedron 23 (2004) 41.

[14] V. Ramesh, P. Umasundari, K.K. Das, Spectrochim. Acta Part A 54 (1998) 225.

[15] C.R.K. Rao, P.S. Zacharias, Polyhedron 16 (1997) 1201.

[16] R.P. John, A. Sreekanth, V. Rajakannan, T.A. Ajith, M.R.P. Kurup, Polyhedron 23 (2004) 2549.

[17] A.B.P. Lever, Inorganic Electronic Spectroscopy, 2nd ed., Elsevier Amsterdam (1984).

[18] B.J. Hathaway, A.A.G. Tomlinson, Coord. Chem. Rev. 5 (1970) 24.

[19] G. Swarnabala, M.V. Rajasekharan, Inorg. Chem. 28 (1989) 662.

[20] E. Garribba, G. Micera, J. Chem. Educ. 83 (2006) 1229.

[21] A.H. Maki, B.R. McGarvey, J. Chem. Phys. 29 (1958) 31.

[22] P. Bindu, M.R.P. Kurup, T.R. Satyakeerty, Polyhedron 18 (1999) 321.

[23] U.L. Kala, S. Suma, M.R.P. Kurup, S. Krishnan, R.P. John, Polyhedron 26 (2007) 1427.

[24] J.R. Wasson, C. Trapp. J. Phys. Chem. 73 (1969) 3763.

[25] D. Kivelson, R. Neiman, J. Chem. Soc. Dalton Trans. (1961) 49.

[26] B.J. Hathaway, Structure and Bonding, Springer Verlag, Heidelberg (1973) 60.

[27] B.N. Figgis, Introduction to Ligand Fields Interscience, New York (1966) 295.

[28] D.X. West, J. Inorg. Nucl. Chem 43 (1984) 3169.

[29] S. Kavlak, H. Kaplan Can, Z.M.O. Rzaev, A. Guner, J. Appl. Polym. Sci. 100 (2006) 3926.

[30] G.A. Nazri, C. Julien, Solid State Ionics 80 (1995) 271.

[31] G.A.A Al-Hazmi, M.S. El-Shahawi, I.M. Gabr, A.A. El-Asmi, J. Coord. Chem., 58 (2005) 713.

[32] R.P. John, A. Sreekanth, V. Rajakannan, T.A. Ajith, M.R.P. Kurup, Polyhedron 23 (2004) 2549.

.....ooo.....

Chapter 8

SYNTHESES AND SPECTRAL CHARACTERIZATION OF ZINC(II) COMPLEXES OF N^4-PHENYLSEMICARBAZONES

Contents

8.1. Introduction

The coordination chemistry of zinc in both nonbiological and biological areas has been the subject of intensive researches. Zinc plays multifaceted roles in biological system. The second most abundant transition element in biological systems after iron, zinc is essential for life. With closed *d*-shell, unlike iron and copper, zinc(II) finds biological relevance as a redox-stable element in metalloprotein structures. In proteins, zinc ions are often coordinated to the amino acid side chains of aspartic acid, glutamic acid, cysteine and histidine. The metal also has a flexible coordination geometry, which allows proteins using it to rapidly shift conformations to perform biological reactions. It has been recognized as an important cofactor in biological molecules, either as a structural template in protein folding or as a Lewis acid catalyst that can readily adopt 4-, 5- or 6-coordination [1]. Based on homology based searches of human genome, Andreini *et al*. [2] concluded that ~ 2800, i.e., ~10%, of the proteins could be zinc proteins, encompassing all the six International Union of Biochemistry recognized classes of enzymes; in fact zinc is the only metal so widespread in the distribution. The zinc-finger type transcription regulators, comprising more than 4% of human proteome,

call upon zinc as a tetra-coordinating element; involvements of zinc as catalytic element, on the other hand, call upon its electrophilic character, in stabilizing anionic intermediates, and dynamic coordination geometry, in facilitating bond rearrangements. In protein engineering and design applications, zinc could be an aid in control of both conformation and function [2,3]. The currently known zinc centers could provide the structural consensus for characterization of the newer zinc-binding sequences, as well as serve as the guidelines for protein engineering and design applications. Two examples of zinc-containing enzymes are carbonic anhydrase and carboxy peptidase which are vital to the processes of carbon dioxide regulation and digestion of proteins, respectively. Mononuclear zinc complexes may serve as model compounds for zinc enzymes such as phospholipase C, bovine lens leucine aminopeptidase, ATPases, carbonic anhydrases and peptide defomylase. Binuclear cores are versatile at active sites of many metalloenzymes and play essential role in biological systems. Zinc deficiency can result in alterations in iron transport, storage and regulatory proteins, which facilitate iron accumulation in cells [4].

Five isotopes of zinc occur in nature. ^{64}Zn is the most abundant isotope. Zinc element has a $d^{10}s^2$ electronic arrangement and they typically form M^{2+} ions. However, many of their compounds are appreciably covalent. In view of the stability of the filled *d* sublevel, the element shows a few of the characteristics of transition metals despite its position in the *d*-block of the periodic table. It resembles other transition metals in the formation of stable complexes with O, N and S-donor ligands and with ions like cyanide, halide etc. Complexes of zinc are mostly 4- or 6- coordinate although 5-coordinate complexes are reported. Among these complexes, some have attracted special attention as model compounds for the active sites

of zinc-containing enzymes [5] and their functions strongly depend upon the coordination environment around the zinc ion. Therefore, for understanding or creating functional zinc complexes, it is important to consider the relationship of the coordination characteristics peculiar to zinc ion.

Biological activity of thiosemicarbazones and semicarbazones are found to increase on complexation with transition metals [6], higher activity being incorporated with substitution at N^4-position [7]. This chapter deals with the syntheses and characterization of three zinc complexes of H_2ASC and H_2BSC.

8.2. Experimental

8.2.1. Materials

Zinc(II) acetate dihydrate (Aldrich) and 1,10-phenanthroline (Ranchem) were commercial products of higher grade and were used without further purification. Solvents used were methanol and DMF.

8.2.2. Syntheses of semicarbazones

Details regarding the syntheses of $H_2ASC{\cdot}H_2O$ and H_2BSC are described in Chapter 2.

8.2.3. Syntheses of Zn(II) complexes of 2-hydroxy-4-methoxyacetophenone-N^4-phenylsemicarbazone

8.2.3.1. *[Zn(HASC)(OAc)] (41)*

A solution of $H_2ASC{\cdot}H_2O$ (0.317 g, 1 mmol) in methanol was treated with a methanolic solution of zinc(II) acetate dihydrate (0.218 g, 1 mmol). 1 mL DMF is also added. The solution was heated under reflux for 4 h. The resulting solution was allowed to stand at room temperature and after slow

evaporation colorless complex separated out was filtered washed with methanol followed by ether and dried over P_4O_{10} in *vacuo*.

Elemental Anal. Found (Calcd.) (%): C: 51.38 (51.14); H: 4.99 (4.53); N: 9.91 (9.94)

8.2.4. Syntheses of Zn(II) complexes of 2-hydroxy-4-methoxybenzophenone-N^4-phenylsemicarbazone

8.2.4.1. *[Zn(HBSC)(OAc)] (42)*

A hot methanolic solution of H_2BSC(0.361 g, 1 mmol) was treated with a methanolic solution of zinc(II) acetate dihydrate (0.218 g, 1 mmol) and 1 mL of DMF and the mixture was heated under reflux for 3 h. and cooled. The pale yellow colored complex separated was filtered, washed thoroughly with methanol followed by ether and dried over P_4O_{10} in *vacuo.*

Elemental Anal. Found (Calcd.) (%): C: 56.62 (56.98); H: 4.44 (4.37); N: 8.62 (8.67)

8.2.4.2. *[Zn(HBSC)phen(OAc)]·H_2O (43)*

A hot methanolic solution of H_2BSC (0.361 g, 1 mmol) was treated with a methanolic solution of zinc(II) acetate dihydrate (0.218 g, 1 mmol), 1,10-phenanthroline (0.198 g, 1 mmol) and 1 mL of DMF and the resulting solution was refluxed for 5 h. It was allowed to stand at room temperature and upon slow evaporation the light yellow colored complex separated out was filtered, washed with methanol followed by ether and dried over P_4O_{10} in *vacuo*.

Elemental Anal. Found (Calcd.) (%): C: 61.64 (61.54); H: 4.79 (4.57); N: 10.29 (10.25)

8.3. Results and discussion

Equimolar ratios of the semicarbazones and the metal acetate yielded the light yellow colored complexes **42** and **43**, while complex **41** was colorless. In compound **43**, 1,10-phenanthroline is used as the coligand and we got a hexacoordinate complex. We tried to prepare complexes using other heterocyclic bases like bipyridine and γ-picoline with both the semicarbazones H_2ASC and H_2BSC. Unfortunately these bases are not getting coordinated with Zn^{2+} and we got compounds with the same stoichiometry as that of **41** and **42**. They are partially soluble in DMF, CH_3CN and DMSO. The complexes are characterized by the following physico-chemical methods.

8.3.1. Elemental analyses

Elemental (C, H, N) analyses of all samples were carried out using a Vario EL III CHNS analyzer at SAIF, Kochi, India and the values were given in Section 8.2.3 and 8.2.4. From the observed C, H, N values the above stoichiometry for the complexes were proposed.

8.3.2. Molar conductivity

The molar conductivities of the complexes in DMF (10^{-3} M) solutions were measured at 298 K with a Systronic model 303 direct reading conductivity bridge. The molar conductivity measurements showed that all the three complexes are non-electrolytic in nature as evidenced from the very low range of 2-8 ohm^{-1} cm^2 mol^{-1}. For a 1:1 electrolyte the range lies 65-90 ohm^{-1} cm^2 mol^{-1} in the same solvent [8].

8.3.3. Infrared spectra

The characteristic IR bands of the complexes differ from their free ligands, and provide significant indications regarding the coordination and bonding sites of the semicarbazones. Table 8.1 lists the relevant bands of all the three complexes and corresponding semicarbazones. In these three complexes the ligands exist in the amido form as proven from the following data. The spectrum of the free ligands exhibit medium bands at 3295 and 3145 cm^{-1} which are assigned to $\nu(^2N–H)$ vibration and the bands at 3408 and 3249 cm^{-1} are due to $\nu(^4N–H)$, respectively for $H_2ASC{\cdot}H_2O$ and H_2BSC [9]. These indicate that the semicarbazones remain in the amido form in the solid state [10]. In the compounds **41**, **42** and **43** the peaks due to $\nu(^2N–H)$ are shifted slightly, but is indicative of their presence and we can assume that there is no enolization and deprotonation of the ligand, confirming its coordination to the central metal ion in the amido form itself. This is further confirmed from the shift of ν(C=O) to lower frequencies in the complexes [11,12]. In complex **41**, ν(C=O) is shifted to 1657 cm^{-1} from 1692 cm^{-1} of the free ligand (Fig. 8.1). The shift is to 1655 and 1633 cm^{-1} respectively for the compounds **42** and **43** (Figs. 8.2 and 8.3) from 1662 cm^{-1} assigned to ν(C=O) of H_2BSC. On coordination of azomethine nitrogen, ν(C=N) shifts to lower wavenumbers by 15-31 cm^{-1} [13,14]. The band due to ν(C=N) shifts from 1619 cm^{-1} in the metal free $H_2ASC{\cdot}H_2O$ to 1604 cm^{-1} in compound **41**. Similarly the band at 1629 cm^{-1} in the uncomplexed semicarbazone H_2BSC, suffers shift to 1610 and 1598 cm^{-1} respectively for compounds **42** and **43**. The shift of ν(C=N) towards a lower frequency on coordination is due to the decrease of the bond order as a result of metal nitrogen bond formation. This azomethine coordination is confirmed by the presence of new bands in the range 427-432 cm^{-1} assignable to ν(Zn–N) in all the complexes [15]. The bands due to

ν(N−N) of the semicarbazones found at 1020 and 1059 cm^{-1} are shifted to increased frequency region in complexes, owing to increased bond strength, again confirms the coordination *via* the azomethine nitrogen.

The IR spectra of the complexes do not exhibit the absorption bands due to the –OH stretching mode of phenolic oxygen, giving evidence for deprotonation during coordination. The band present at 3535 cm^{-1} in $H_2ASC{\cdot}H_2O$ and at 3316 cm^{-1} in H_2BSC ascribed to phenolic –OH are not seen in complexes. The appearance of weak bands in the region 461-506 cm^{-1} indicates the presence of Zn–O bond, resulting from the coordination of phenolate oxygen [16]. Besides, the shifting of the band due to the Ar–O group to lower frequencies as listed in Table 8.1 indicates the weakening of Ar–O group due to coordination. The IR absorption band at *ca.* 3400 cm^{-1} in the complex **43** confirms the presence of lattice water which is further supported by the weight loss in thermogravimetry.

Table 8.1. The important IR frequencies (cm^{-1}) of semicarbazones and their Zn(II) complexes.

Compound	ν(C=O)	ν(C=N)	ν(N–N)	ν(C–O)	ν(^{2}N–H)	ν(^{4}N–H)	ν(Zn–O)	ν(Zn–N)
$H_2ASC{\cdot}H_2O$	1692	1619	1020	1270	3295	3408	----	----
[Zn(HASC)(OAc)] (**41**)	1657	1604	1043	1245	3260	3303	461	432
H_2BSC	1662	1629	1059	1292	3145	3249	----	----
[Zn(HBSC)(OAc)] (**42**)	1655	1610	1065	1286	3089	3217	506	427
[Zn(HBSC)phen(OAc)] ·H_2O (**43**)	1633	1598	1068	1286	3199	3322	484	430

The three zinc complexes synthesized here are acetato complexes. The asymmetric and symmetric stretching bands corresponding to the unidentate types of acetate groups are present in all the complexes. The asymmetric stretching bands are present at 1577, 1580 and 1573 cm^{-1} respectively for the

complexes **41**, **42** and **43** and their symmetric stretching modes occur at 1329, 1324 and at 1328 cm^{-1} [17].

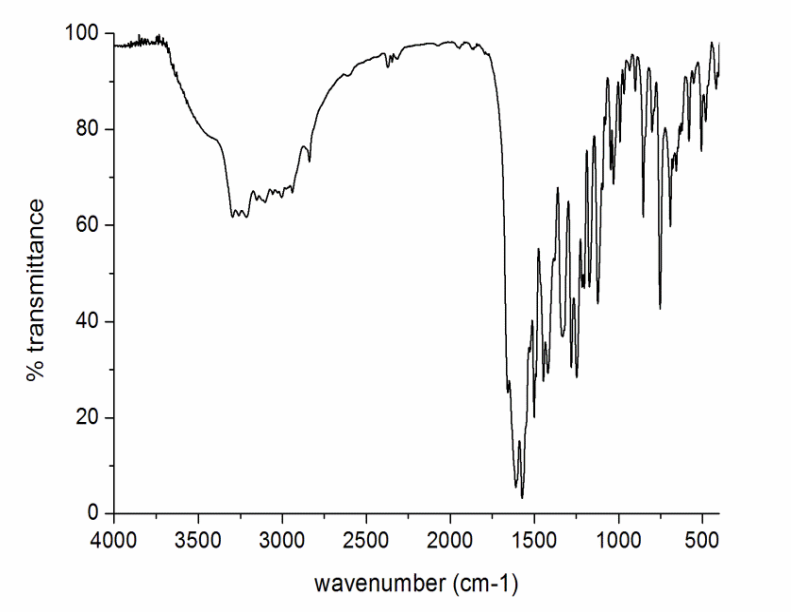

Fig. 8.1. IR spectrum of [Zn(HASC)(OAc)] (41).

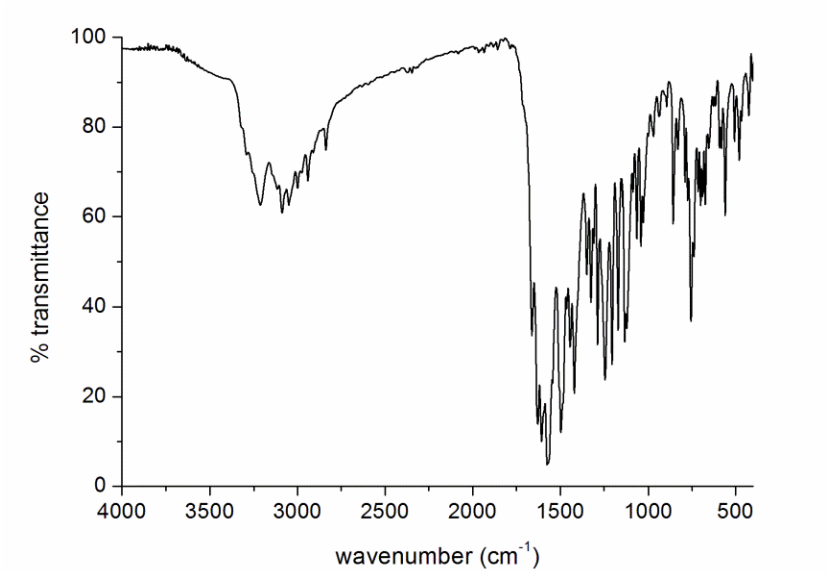

Fig. 8.2. IR spectrum of [Zn(HBSC)(OAc)] (42).

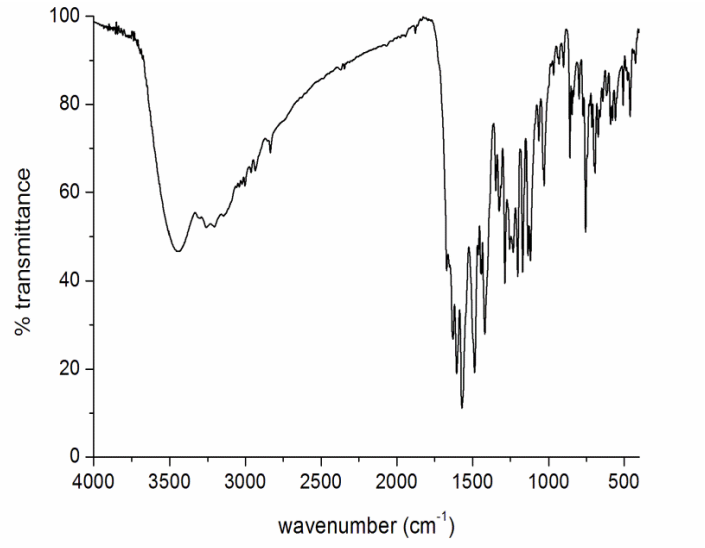

Fig. 8.3. IR spectrum of [Zn(HBSC)phen(OAc)]·H_2O (43).

8.3.4. Electronic spectra

The electronic spectral data of zinc(II) complexes are given in Table 8.2. The semicarbazone H_2ASC, shows absorption bands in the region 31590-35300 cm^{-1} in DMF due to intraligand transitions of the semicarbazone moiety. These intraligand transitions are shifted in the range 31750-35560 cm^{-1} for the complex [Zn(HASC)(OAc)] (**41**) (Fig. 8.4) on complexation. Similarly for compound [Zn(HBSC)(OAc)] (**42**) the shifted intraligand transitions are in the range 31350-41170 cm^{-1} compared to those transitions of H_2BSC in CH_3CN (31330-41680 cm^{-1}) (Fig. 8.5). For complex [Zn(HBSC)phen(OAc)]·H_2O (**43**), spectrum is recorded in DMF and these transitions are seen in 31270-34880 cm^{-1} range compared to those of H_2BSC in DMF (31030-34890 cm^{-1}) (Fig. 8.6). This shift is caused by metal-ligand electron interaction during chelation, indicating coordination *via* azomethine nitrogen and carbonyl oxygen. It can also be explained due to the weakening of C=O bond and the conjugation system being enhanced upon complexation [18,19].

A new band is observed in the spectra of complexes in the range 26230-27840 cm^{-1}. We have assigned these intense broad bands to Zn→O charge transfer transitions and this confirms the coordination of amido oxygen to the metal ion. The light yellow color for these complexes arises due to these charge transfer transitions. The MLCT band is shown separately for the complex **42** on the right of Fig. 8.5.

Table 8.2. Electronic spectral assignments (cm^{-1}) of N^4-phenylsemicarbazones and their Zn(II) complexes.

Compound	Solvent	Intraligand transitions	MLCT
H_2ASC	DMF	31590, 34250, 35300	
[Zn(HASC)(OAc)] (**41**)	DMF	30640 (sh), 31750, 34260, 35560	27840
H_2BSC	CH_3CN	31330, 33820, 35030, 41680	-----
Zn(HBSC)(OAc)] (**42**)	CH_3CN	31350, 41170	26280
H_2BSC	DMF	31030, 32070 (sh), 33610, 34890	
[Zn(HBSC)phen(OAc)]·H_2O (**43**)	DMF	31270, 33640, 34880	26230

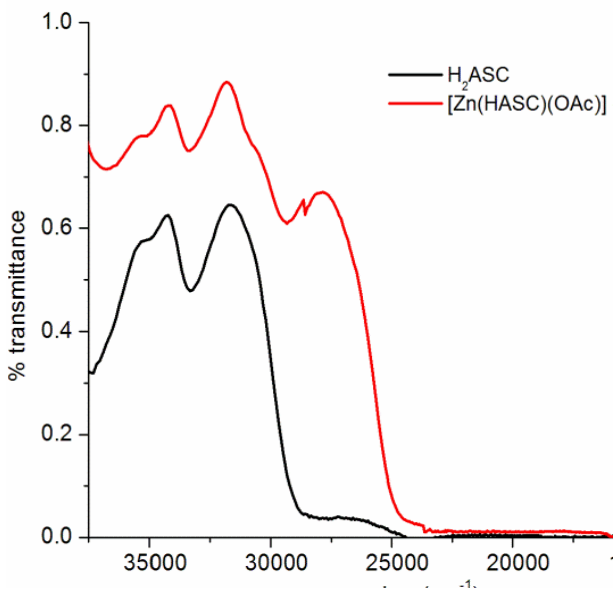

Fig. 8.4. UV spectra of H_2ASC and [Zn(HASC)(OAc)].

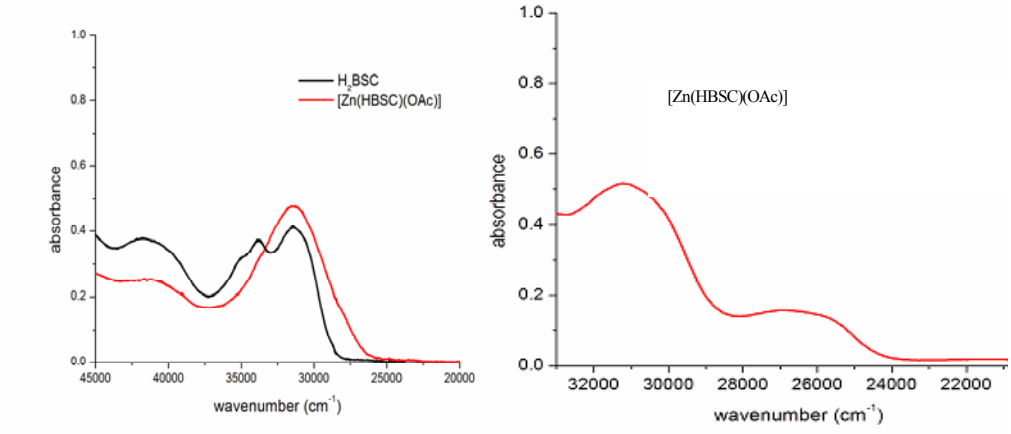

Fig. 8.5. UV spectra of H_2BSC and [Zn(HBSC)(OAc)].

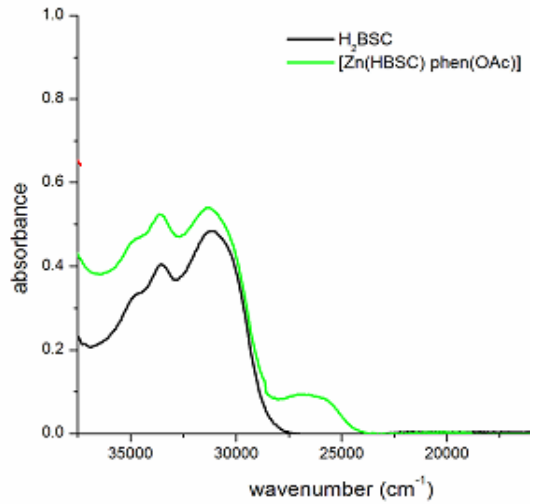

Fig. 8.6. UV spectra of H_2BSC and [Zn(HBSC)phen(OAc)].

8.3.5. Thermogravimetric analyses

The thermogravimetric analyses were undertaken for all these three complexes in the temperature range of 50-1000 °C in an atmosphere of nitrogen. The thermogram of complex **41** (Fig. 8.7**)** does not show a weight loss below 200 °C, indicating the absence of lattice water. The complex is stable upto 300 °C. Then it shows two weight loss steps due to the pyrolysis of semicarbazone moiety and acetato group.

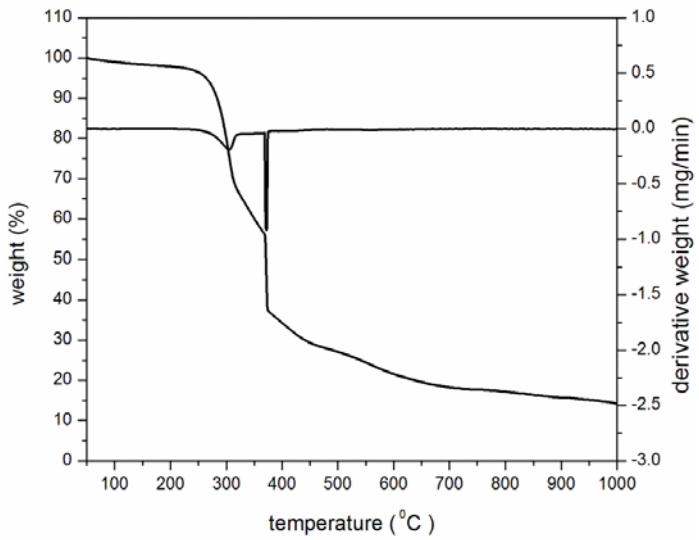

Fig. 8.7. Thermogram of [Zn(HASC)(OAc)] (41).

The thermogram of compound **42** does not show the presence of water molecules (Fig. 8.8), either in or out of the coordination sphere. It is stable upto 250 °C. After this temperature decomposition of the complex occurs with the removal of ligand and the acetato group as indicated by two weight losses.

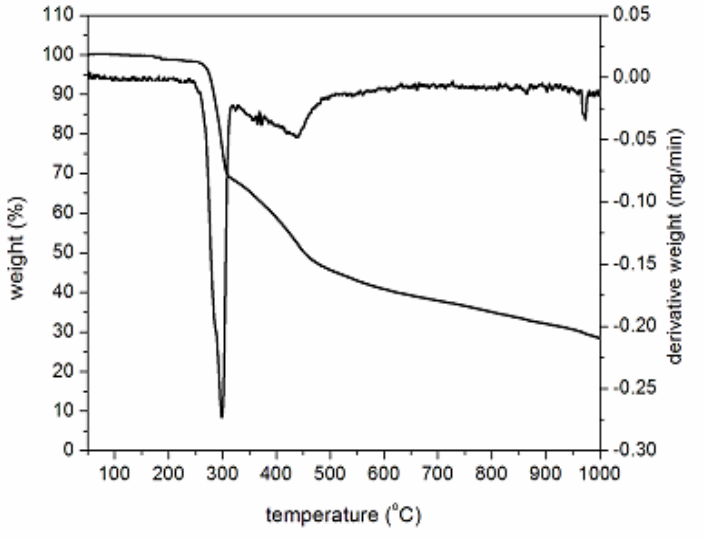

Fig. 8.8. Thermogram of [Zn(HBSC)(OAc)] (42).

The thermogravimetric analysis of complex [Zn(HBSC)phen(OAc)]·H_2O (**43**) clearly shows a weight loss of 2.4% (calcd. 2.6%) below 200 °C confirming the presence of one molecule of water outside the coordination sphere [20]. Then a weight loss of 27.5% is observed (calcd. 27.06%) in the temperature range of 255-280 °C and can be assigned to the dissociation of one molecule of the base, phenanthroline. Above 300 °C degradation of the ligand and acetato group takes place.

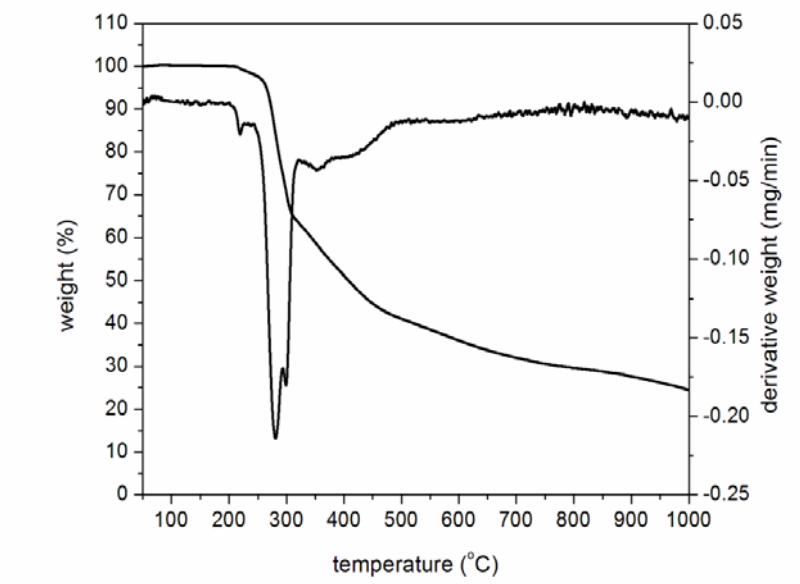

Fig. 8.9. Thermogram of [Zn(HBSC)phen(OAc)]·H_2O (43).

On the basis of the physico-chemical characterizations discussed above the tentative structures proposed for the Zn(II) complexes are given below. The compounds **41** and **42** are tetracoordinate and compound **43** is hexacoordinate**.** The lattice water is omitted in compound **43**.

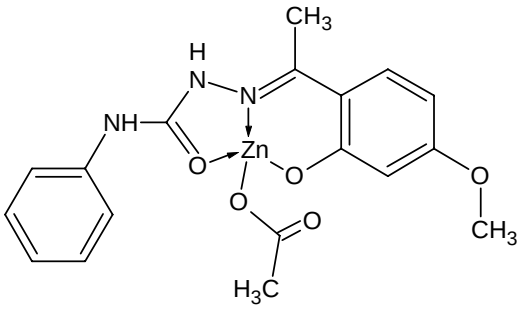

[Zn(HASC)(OAc)] (41)

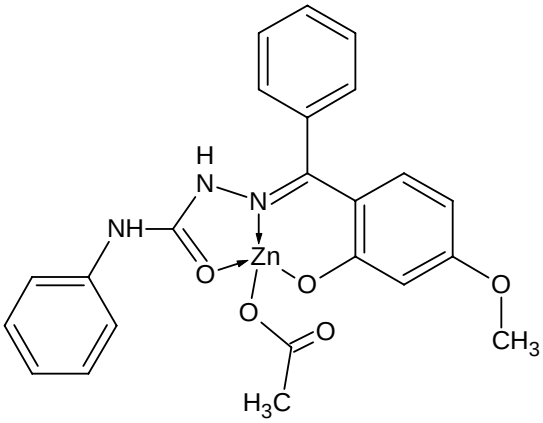

[Zn(HBSC)(OAc)] (42)

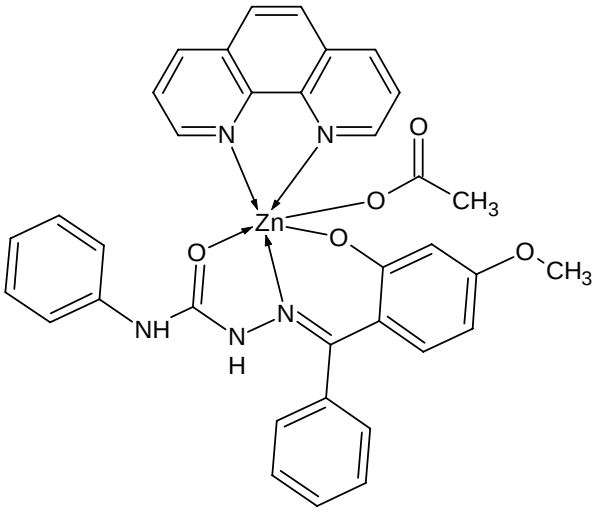

[Zn(HBSC)phen(OAc)]·H_2O (43)

References

[1] K. Peariso, C.W. Goulding, S. Huang, R.G. Mathews, J.E. Penner-Hahn, J. Am. Chem. Soc. 120 (1998) 8410.

[2] C. Andreini, L. Banci, I. Bertini, A. Rosato, J. Proteome Res. 5 (2006) 196.

[3] L. Regan, Trends Biochem. Sci. 20 (1995) 280.

[4] B.J. Niles, M.S. Clegg, L.A. Hanna, S.S. Chou, T.Y. Momma, H. Hong, C.L. Keen, J. Biol. Chem. 283 (2008) 5168.

[5] G. Parkin, Chem. Commun. 1971 (2000).

[6] D.X. West, A.E. Liberta, S.B. Padhye, R.C. Chikate, P.B. Sonawane, A.S. Kumbhar, R.G. Yerande, Coord. Chem. Rev. 123 (1993) 49.

[7] D.L. Klayman, J.F. Bartosevich, T.S. Griffin, C.J. Manson, J.P. Scovill, J. Med. Chem. 22 (1979) 885.

[8] W.J. Geary, Coord. Chem. Rev. 7 (1971) 81.

[9] A.K. El-Sawaf, D.X. West, F.A. El-Saied, R.M. El-Babnasawy, Transit. Met. Chem. 23 (1998) 649.

[10] Y.-P. Tian, W.-T. Yu, C.-Y. Zhao, M.-H. Jiang, Z.-G. Cai, H.-K. Fun, Polyhedron 21 (2002) 1217.

[11] T.A. Reena, E.B. Seena, M.R.P. Kurup, Polyhedron 27 (2008) 1825.

[12] V.L. Siji, M.R. Sudarsanakumar, S. Suma, Polyhedron 29 (2010) 2035.

[13] E.B. Seena, M.R.P. Kurup, Spectrochim. Acta Part A 69 (2008) 726.

[14] L. Singh, U.P. Singh, I. Chakraborti, Asian J. Chem. 13 (2001) 1618.

[15] E. Bermejo, A. Castineiras, L.M. Fostiak, I.G. Santos, J.K. Swearingen, D.X. West, Polyhedron 23 (2004) 2303.

[16] J.R. Dimmock, K.K. Sidhu, S.D. Tumber, S.K. Basran, M. Chen, J.W. Quail, Eur. J. Med. Chem. 30 (1995) 287.

[17] M.R.P. Kurup, S.V. Chandra, K. Muraleedharan, J. Therm Anal. Calorim. 61 (2000) 909.

[18] L. Latheef, M.R.P. Kurup, Polyhedron 27 (2008) 35.

[19] I.-X. Li, H.-Tang, Yi-Zhi Li, M. Wang, L.-F. Wang, C.-G. Xia, J. Inorg. Biochem 78 (2000) 167.

[20] M.R. Maurya, N. Bharti, Transit. Met. Chem. 24 (1999) 389.

SUMMARY AND CONCLUSION

Coordination chemistry, the chemistry of metal complexes, is one of the most active areas of research in inorganic chemistry. Werner's basic ideas remain unchallenged even today despite all the advanced technical developments which have taken place since his days. However the advent of sophisticated physicochemical techniques of high precision and capability has considerably enriched our understanding of the nature of the metal-ligand bond, the structure and stereochemistry of metal complexes, their stability and other properties. Semicarbazones are promising ligands in coordination chemistry because of their excellent metal binding capability. The formation of a variety of metal complexes from these ligands speaks for their spectacular progress in coordination and bioinorganic chemistry. They are the condenzation products of semicarbazide with suitable aldehyde or ketone and are generally represented as $R^1R^2C{=}N{-}NH{-}CO{-}NH_2$.

Semicarbazones are compounds with versatile structural features and can coordinate to the metal atom either as a neutral ligand or as a deprotonated anion due to their facile amido iminol tautomerism. In solid state they predominantly exist in amido form, whereas in solution iminol form predominates. Coordination possibilities deriving from the many potential donor atoms in the semicarbazone backbone are increased if the substituents R^1 and or R^2 include additional donor atoms. The π-delocalization and the configurational flexibility of their molecular chain can give rise to a great variety of coordination modes.

Semicarbazones are well known due to their wide spectrum of biological potential. The biological applications of these compounds are due to their ability to form metal complexes. It was reported that arylsemicarbazones were devoid of sedative hypnotic activity and exhibited anticonvulsant activity with less neurotoxicity. Another important application of semicarbazones is in the nonlinear optics. The wide transparency window in the entire visible region, make them ideal candidates for NLO device applications. They have a great place in analysis and can be used in selective and sensitive determination of metal ions. They are widely used as spectrophotometric agents for the analysis of metal ions.

Our work includes two ligand systems with the following abbreviations

1) 2-hydroxy-4-methoxyacetophenone-N^4-phenylsemicarbazone (H_2ASC)
2) 2-hydroxy-4-methoxybenzophenone-N^4-phenylsemicarbazone (H_2BSC)

and the synthesis of some metal complexes of vanadium(IV), manganese(II), cobalt(II/III), nickel(II), copper(II) and zinc(II) including some mixed ligand metal chelates incorporating heterocyclic bases and some pseudohalogens.

The work presented in this thesis is divided into eight chapters.

Chapter1

Chapter 1 involves a general introduction to semicarbazones, their binding modes, biological importance and applications in different areas like non linear optics and in spectrofluorimetric analysis. The scope of the present work, different analytical and spectroscopic techniques employed for the characterization of semicarbazones and their metal complexes are also included in this chapter.

Chapter 2

This chapter contains details regarding the synthesis of two new ONO donor semicarbazones and their characterization by elemental analysis, mass, IR, ^{1}H NMR and UV-Vis spectroscopy including single crystal X-ray diffraction studies.

The N^4-phenylsemicarbazones synthesized are

1) 2-hydroxy-4-methoxyacetophenone-N^4-phenylsemicarbazone monohydrate (H_2ASC)·H_2O
2) 2-hydroxy-4-methoxybenzophenone-N^4-phenylsemicarbazone (H_2BSC)

Single crystal X-ray diffraction studies elucidate the structures for H_2ASC·H_2O & H_2BSC. The compound H_2ASC·H_2O crystallizes in monoclinic $P2_1/c$ space group from its ethanolic solution. The presence of one water molecule in the lattice leads to a supramolecular chain stabilized by hydrogen bonding. H_2BSC crystallizes in orthorhombic $P2_1/c$ space group from its methanolic solution and monoclinic $P2_1/c$ space group from a mixture of methanol and DMF with one molecule of DMF as solvent of crystallization. The dimethylformamide solvent molecule is disordered with site occupancies of 0.684 (3) and 0.316 (3).

Chapter 3

This chapter discusses the syntheses and characterization of seven oxidovanadium (IV) complexes with potential ONO donor ligands. These include two binuclear vanadium (IV) complexes and the remaining five are mononuclear complexes with heterocyclic bases like phenanthroline, 2,2′-bipyridine, 4,4′-dimethyl-2,2′-bipyridine and 4-picoline as coligands. All the

complexes are characterized by various techniques such as elemental analysis, conductance, magnetic susceptibility measurements, IR, EPR, electronic spectral studies, and thermogravimetric analysis. In all the complexes, semicarbazones are coordinated to the metal centre in the iminol form and hence act as dideprotonated tridentate ligands as evidenced from the shift of characteristic IR bands of the complexes from the metal free phenylsemicarbazones. The observed molar conductances in 10^{-3} M DMF solution reveal that all the complexes are non-electrolytic in nature. The magnetic susceptibility measurements reveal that all the complexes are paramagnetic with lower values of 1.2 & 1.27 BM for binuclear complexes. In the EPR spectra, the *g* values are typically less than the free electron value. In polycrystalline state at 298 K, EPR spectra of all complexes are isotropic in nature, while in DMF at 77 K, show two sets of eight-line pattern, characteristic of an unpaired electron being coupled to the vanadium nuclear spin. The thermal studies indicate the presence of lattice water in all the complexes.

Chapter 4

This chapter describes the syntheses and characterization of seven Mn(II) complexes using elemental analyses, magnetic susceptibility measurements, IR, EPR, electronic spectral studies, cyclic voltammetry and thermogravimetric analyses. From the magnetic susceptibility measurements all are found to be high spin d^5 system. In one complex the semicarbazone coordinates in the neutral form as evidenced from the IR spectral data and its molar conductivity proves to be a 2:1 electrolyte. In all other complexes semicarbazone exists in the amido form and coordinates monoanionically as HASC and HBSC by the deprotonation of phenolic oxygen atom. In the perchlorate complexes, the perchlorate ion enters as a counterion outside the

coordination sphere of (Mn^{2+}) and behaves as 1:1 electrolytes. EPR spectra of the complexes were recorded in polycrystalline state at 298 K and in frozen DMF at 77 K. In frozen DMF, a hyperfine sextet is observed with a pair of low intensity forbidden lines lying between each of the two main hyperfine lines in some complexes. One complex appears to be a dimer with eleven hyperfine splittings in the polycrystalline state due to the coupling of the electron spin with the nuclear spin of the two manganese centres. The *g* value is very close to the free electron spin value of 2.0023 which is consistent with the typical Mn(II) system.

Thermal behaviour of the complexes was investigated by TG-DTG plots and presence of lattice ethanol molecules is confirmed in one complex.

Chapter 5

Chapter 5 explains the syntheses of fourteen cobalt(II/III) complexes along with their characterization using various physicochemical techniques including IR spectroscopy, electronic spectral studies and thermal analyses. The coligands used here are heterocyclic bases and anions like azide and thiocyanate. The molar conductivity measurements in DMF indicate that all the complexes are nonelectrolytes. Magnetic susceptibility measurements indicate that three of the complexes are paramagnetic with cobalt in the (+2) oxidation state while all others are found to be diamagnetic with (+3) oxidation state with a spin paired octahedral configuration. In two complexes semicarbazone is in the amido form and coordinates monoanionically while in all others enolization takes place during complexation. The thermal behaviour of complexes shows that the hydrated complexes lose water molecules in the first step, followed by the decomposition of ligand molecules in the subsequent steps.

Chapter 6

This chapter deals with the syntheses and characterization of five nickel(II) complexes by CHN analyses, conductivity and magnetic susceptibility measurements, IR, electronic spectral studies and thermogravimetric analyses. All the complexes are found to be paramagnetic excluding the possibility of square planar geometry. In one of the complexes the semicarbazone moiety is coordinated in the enolate form while in all others it is in the amido form as evidenced from IR spectral data.

Chapter 7

This chapter deals with the syntheses and characterization of seven copper(II) complexes. The heterocyclic bases like 1,10-phenanthroline, 2,2′-bipyridine and 4,4′-dimethyl-2,2′-bipyridine are used as coligands. The characterization is done by various techniques such as elemental analyses, magnetic susceptibility measurements, IR, EPR, electronic spectral studies, cyclic voltammetry and thermogravimetric analyses. In all the complexes the semicarbazone exists in iminol form and gets coordinated through azomethine nitrogen, phenolate and iminol oxygens. All the complexes are nonelectrolytic in nature. The effective magnetic moment (μ_{eff}) values for the mononuclear copper(II) complexes were found to be close to the spin only value, which corresponds to a single unpaired electron. The low magnetic moment values for two complexes may be due to some interaction between metal centers. EPR spectra of the complexes were recorded in polycrystalline state at 298 K and in frozen DMF at 77 K. All spectra except one in polycrystalline state are isotropic in nature. In frozen DMF they are found to be axial with hyperfine lines in the parallel and perpendicular regions and superhyperfine splittings give clear evidence for the coordination of azomethine nitrogen and that of

heterocyclic bases. Two complexes were found to be dimeric as is evident from the half field signals. In one of the complexes a half field signal with seven hyperfine splittings was observed due to coupling of the electron spin with nuclear spin of two copper atoms. The $g_{\|} > g_{\perp} > 2.0023$ indicate that the unpaired electron in Cu(II) resides in the ground state $d_{x^2-y^2}$ orbital. The EPR spectra of five coordinate copper(II) complexes in which $g_{\|} > g_{\perp}$ value suggest a distorted square pyramidal structure and rules out the possibility of a trigonal bipyramidal structure which would be expected to have $g_{\perp} > g_{\|}$. Thermal stability of the complexes can be obtained from thermograms of the complexes.

Chapter 8

This chapter describes the syntheses and characterization of three zinc(II) complexes. The characterization techniques include elemental analyses, conductance and magnetic susceptibility measurements, IR, electronic spectral studies and thermogravimetric analyses. All the three complexes are nonelectrolytic and diamagnetic. In all the complexes the semicarbazone is in the amido form as evidenced from the shift of carbonyl stretching frequency and acts as monoanionic tridentate ONO donor by deprotonation of phenolic oxygen. The thermal analyses show that one complex has one molecule of water in its lattice.

List of Abbreviations

H_2ASC	2-Hydroxy-4-methoxyacetophenone-N^4-phenylsemicarbazone
H_2BSC	2-Hydroxy-4-methoxybenzophenone-N^4-phenylsemicarbazone

Complexes

1	$[VO(ASC)]_2 \cdot 2H_2O$
2	$[VO(ASC)(bipy)] \cdot 2H_2O$
3	$[VO(ASC)(dmbipy)] \cdot 3H_2O$
4	$[VO(BSC)]_2 \cdot 2H_2O$
5	$[VO(BSC)(phen)] \cdot 2H_2O$
6	$[VO(BSC)(dmbipy)] \cdot 2H_2O$
7	$[VO(BSC)(pic)] \cdot 0.5H_2O$
8	$[Mn(HASC)(OAc)]$
9	$[Mn(H_2ASC)(H_2O)]Cl_2$
10	$[Mn(HASC)(phen)]ClO_4$
11	$[Mn(HBSC)_2]$
12	$[Mn(HBSC)Cl]_2 \cdot 2EtOH$
13	$[Mn(HBSC)(phen)]ClO_4 \cdot H_2O$
14	$[Mn(HBSC)(phen)(OAc)]$
15	$[Co(HASC)_2] \cdot 3H_2O$
16	$[Co(ASC)phen(N_3)]$
17	$[Co(ASC)bipy(N_3)]$
18	$[Co(ASC)dmbipy(N_3)]$
19	$[Co(ASC)phen(NCS)] \cdot 2H_2O$
20	$[Co(ASC)pic(N_3)]$
21	$[Co(HBSC)_2]$
22	$[Co(BSC)phen(N_3)] \cdot 2H_2O$
23	$[Co(BSC)bipy(N_3)]$
24	$[Co(BSC)dmbipy(N_3)]$
25	$[Co(HBSC)_2(NCS)]$
26	$[Co(BSC)phen(OAc)] \cdot 1.5\ H_2O$

27 $[Co(BSC)dmbipy(OAc)]\cdot 3H_2O$

28 $[Co(BSC)pic]\cdot 3H_2O$

29 $[Ni(HASC)OAc]\cdot 3H_2O$

30 $[Ni(ASC)phen(H_2O)]\cdot H_2O$

31 $[Ni(HASC)phen(N_3)]$

32 $[Ni(HBSC)_2]$

33 $[Ni(HBSC)phen(OAc)]$

34 $[Cu_2(ASC)_2]$

35 $[Cu(ASC)phen]$

36 $[Cu(ASC)bipy]\cdot 2.5H_2O$

37 $[Cu_2(BSC)_2]$

38 $[Cu(BSC)phen]\cdot 3H_2O$

39 $[Cu(BSC)dmbipy]\cdot 4H_2O$

40 $[Cu(BSC)bipy]\cdot 2H_2O$

41 $[Zn(HASC)(OAc)]$

42 $[Zn(HBSC)(OAc)]$

43 $[Zn(HBSC)phen(OAc)]\cdot H_2O$

DMF	Dimethyl formamide
DMSO	Dimethyl sulphoxide
phen	1,10-phenanthroline
bipy	2,2′-bipyridine
dmbipy	4,4′-dimethyl-2,2′-bipyridine
pic	4-picoline

.....ജോ.....

Research Publications

1). (2E)-2-[(2-Hydroxy-4-methoxyphenyl)(phenyl)methylidene]-N-phenylhydrazinecarboxamide dimethylformamide monosolvate

C.F. Annie, J.M. Jacob, M. Sithambaresan, M.R. Prathapachandra Kurup, Acta Cryst. E68 (2012) o1519-o1520.

2). (2E)-2-[1-(2-Hydroxy-4-methoxyphenyl)ethylidene]-N-phenylhydrazinecarboxamide monohydrate

C.F. Annie, J.M. Jacob, M. Sithambaresan, M.R. Prathapachandra Kurup, Acta Cryst. E68 (2012) o2985-o2986.

.....ꕥ.....